Fluorescent Probes of Conformational Signal Relay in Membrane Environments

A thesis submitted to The University of Manchester for the degree of

Doctor of Philosophy

In the faculty of Engineering and Physical Sciences

2015

Francis George Alexander Lister

School of Chemistry

Contents

Word Count 53,756

Fluorescent Probes of Conformational Signal Relay in Membrane Environments

Francis George Alexander Lister

2015

A thesis submitted to The University of Manchester for the degree of
Doctor of Philosophy
In the faculty of Engineering and Physical Sciences

G-Protein Coupled Receptors (GPCRs) are a class of membrane-bound receptor proteins capable of relaying a biological signal across a cell membrane through a solely conformational change in their transmembrane domain. Previous work has shown that helical foldamers composed of achiral monomeric units can be used in an analogous manner to relay stereochemical information on the nano-scale through the conformational control of screw-sense preference. While this work has produced some highly successful examples of signal relay, mimicking the function of GPCRs, its reliance on screw-sense responsive NMR probes has restricted further development into membrane environments.

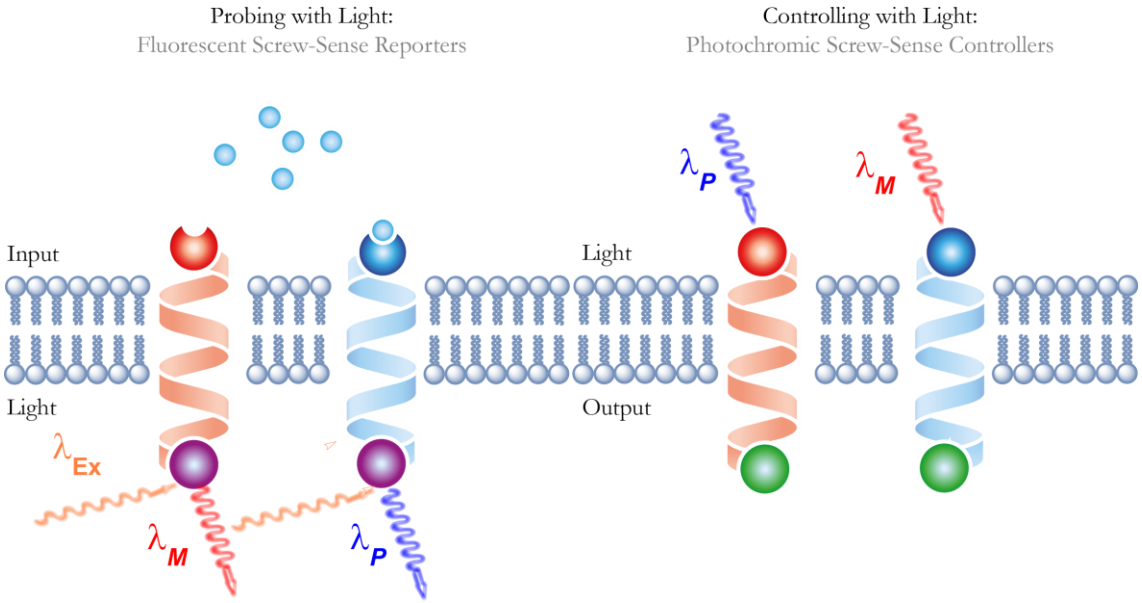

This thesis describes the successful development of a pyrene based screw-sense responsive fluorescence probe and its subsequent use in the development of a series of membrane-based GPCR mimics.

This thesis has also details the preliminary steps towards the development of light-responsive controllers of screw-sense preference for nano-scale signal relay devices.

Declaration

No portion of the work referred to in the thesis has been submitted in support of an application for another degree or qualification of this or any other university or other institute of learning.

Copyright Statement

i. The author of this thesis (including any appendices and/or schedules to this thesis) owns certain copyright or related rights in it (the "Copyright") and s/he has given The University of Manchester certain rights to use such Copyright, including for administrative purposes.

ii. Copies of this thesis, either in full or in extracts and whether in hard or electronic copy, may be made **only** in accordance with the Copyright, Designs and Patents Act 1988 (as amended) and regulations issued under it or, where appropriate, in accordance with licensing agreements which the University has from time to time. This page must form part of any such copies made.

iii. The ownership of certain Copyright, patents, designs, trade marks and other intellectual property (the "Intellectual Property") and any reproductions of copyright works in the thesis, for example graphs and tables ("Reproductions"), which may be described in this thesis, may not be owned by the author and may be owned by third parties. Such Intellectual Property and Reproductions cannot and must not be made available for use without the prior written permission of the owner(s) of the relevant Intellectual Property and/or Reproductions.

iv. Further information on the conditions under which disclosure, publication and commercialisation of this thesis, the Copyright and any Intellectual Property and/or Reproductions described in it may take place is available in the University IP Policy (see http://documents.manchester.ac.uk/DocuInfo.aspx?DocID=487), in any relevant Thesis restriction declarations deposited in the University Library, The University Library's regulations (see http://www.manchester.ac.uk/library/aboutus/regulations) and in The University's policy on Presentation of Theses

Acknowledgements

Firstly, I'd like to thank Jonathan for giving me the opportunity to work in his group. The project has been really interesting and the support and guidance throughout was fantastic. I'd also like to thank Simon who has given excellent support and advice on all things membrane throughout the project

Thank to all of the members of the Clayden Group, past and present who I have worked with, it's been a great four years: Anne, Beatrice, Bryden Cath, Dan, Dan, Daniele, Edmund, Fernando, Gaëlle, Jemma, Jenn, John, Josep, Juliens, Katharina, Liam, Matteo, Mike, Mike, Nadia, Nicole, Rachel, Rob, Romain, Romina, Sam, Sarah, Vincent and Wojciech.

A large number of you have helped me but, in particular, I would like to thank three excellent Post-Docs who have tirelessly helped me throughout the project: Jenn, Matteo and Liam.

I would like to thank all of my proofreaders: Jonathan, Simon, Jenn, Bryden, Liam, Matteo, Wojciech, Mike. In the latter stages of writing I would like to thank Sam; my usual write-up buddy, Dan and Wojciech who have kept me going through a mixture of positive support and, in Wojciech's case, calculated mental assault. All of which was greatly appreciated. Thanks also to Rick for showing how to use illustrator properly − I hope you like the schemes.

I would also like to thank the member of the department without whom this work wouldn't have been possible: Ralph and Carlo and for greatly improving the NMR department. Gareth, Iyla and Mohammed in the mass spec department, Carole and Rehana for help with HPLC and Jim for the crystal structures.

Thanks of course to my friends and family. I'm indebted to my mother who has tirelessly encouraged me, despite numerous challenges: a great inspiration for doing a PhD. Special thanks also to my brother Harry, who kept me from quitting multiple times and my girlfriend Laura, who has disrupted the writing of this thesis at all of its key stages.

Abbreviations

Ac	Acetyl
Aib	α-Amino isobutyric acid
Ala	Alanine
ArC	Aromatic C
ArCH	Aromatic CH
ATR	Attenuated total reflection
Boc	*tertiary*-butyloxycarbonyl
BQPA	*N,N*-bis(2-quinolyl)methyl-*N*-(2-pyridyl)methylamine
Cbz	Carboxybenzyl
CD	Circular Dichroism
DCM	Dichloromethane
DIPEA	*N,N*-Diisopropylethylamine
DMF	Dimethylformamide
DMPC	2-dimyristoyl-sn-glycero-3-phosphocholine
DNA	Deoxyribonucleic acid
DOPC	1,2-dioleoyl-sn-glycero-3-phosphocholine
DPoPC	1,2-dipalmitoleoyl-sn-glycero-3-phosphocholine
DPPC	1,2-dipalmitoyl-sn-glycero-3-phosphocholine
E	Excimer Emission
E	Entgegen
E/M	Ratio of Excimer to Monomer fluorescence emission
EDC	1-Ethyl-3-(3-dimethylaminopropyl)carbodiimide
EDC.HCl	1-Ethyl-3-(3-dimethylaminopropyl)carbodiimide hydrochloride
ES	Electrospray Ionisation
Et_2O	Diethyl Ether
EtOAc	Ethyl Acetate
EtOH	Ethanol
EYPC	L-α-lysophosphatidylcholine
FRET	Fluorescence Resonance Energy Transfer
GDP	Guanosine-5'-diphosphate
GFP	Green Fluorescent Protein
Gly	Glycine
GPCR	G-Protein Coupled Receptor
GTP	Guanosine-5'-triphosphate
GUV	Giant Unilamellar Vesicle
HMQC	Heteronuclear Multiple-Quantum Correlation
HOBt	Hydroxybenzotriazole
HOMO	Highest Occupied Molecular Orbital
HPLC	High Performance Liquid Chromatography
HRMS	High Resolution Mass Spectrometry
i-Bz	*Ipso* Position, Benzyl Group
IPA	Isopropyl Alcohol
IR	Infrared
LUMO	Lowest Unoccupied Molecular Orbital

LUV	Large Unilamellar Vesicle
M `	Monomer Emission; Molar Concentration
m-Bz	*Meta* Position, Benzyl Group
Me	Methyl
MeOH	Methanol
mL	Millilitres
mM	Millimolar Concentration
mmol	millimoles
MOPS	3-(N-morpholino)propanesulfonic acid
mp	Melting Point
NMR	Nuclear Magnetic Resonance
PET	Photoinduced Electron Transfer
PHA	Perhydroanthracene
Phe	Phenylalanine
POPC	1-palmitoyl-2-oleoyl-sn-glycero-3-phosphocholine
ppb	Parts Per Billion
ppm	Parts Per Million
Py	Pyridine
Pya	Pyrenylalanine
PyC	Pyridine Aromatic C
PyCH	Pyridine Aromatic CH
Pyr	Pyrene
PyrC	Pyrene Aromatic C
PyrCH	Pyrene Aromatic CH
QuinC	Quinoline Aromatic C
QuinCH	Quinoline Aromatic CH
RNA	Ribonucleic acid
RT	Room Temperature
s	Singlet
S,S-BisPhenPyrEt	(1*S*,2*S*)-1,2-bis(4-(pyren-1-ylmethoxy)phenyl)ethane-1,2-diamine
S,*S*-BisPyrEt	(1*S*,2*S*)-1,2-(1-pyrene)ethylenediamine
SUV	Small Unilamellar Vesicle
t	Triplet
*t*Bu	*tertiary*-butyl
TFA	Trifluoro Acetic Acid
THF	Tetrahydrofuran
TLC	Thin Layer Chromatography
TOF	Time of Flight
Tyr	Tyrosine
UV	Ultraviolet
Val	Valine
VT	Variable temperature
Z	Zusammen
αMv	α-methylvaline
Δ	Heat to reflux
δ	Chemical Shift

Preface

The author graduated from the University of Bristol in 2011 with a Masters degree in Chemistry (1st class hons). Under the supervision of Dr. M. Carmen Galan, he investigated the development of a cleavable linker for use with ionic liquid tags to aid in the synthesis and purification of complex carbohydrate fragments.

In 2011, he moved to Manchester to undertake a PhD in the research group of Prof. Jonathan Clayden. The project has investigated the use of light in the probing and control of helical foldamers, towards the development of a biomimetic G-Protein Coupled Receptors. The findings of this research are presented in this thesis.

1.0 Introduction

1.1 Foldamers

Biological function depends on the interactions of proteins and other biomolecules at the molecular level. Biosynthesis, cell-signalling and immune response are but a few of the many complex functions that depend entirely on the dynamic solution architectures of proteins. Chemically speaking, these architectures are a global *conformation* that is the result of non-covalent interactions between the monomeric units from which they are constructed. Biology achieves the synthesis of its vast array of complex biomolecules from three main building blocks: α-amino acids, ribonucleic acids, and carbohydrates. (Figure 1).

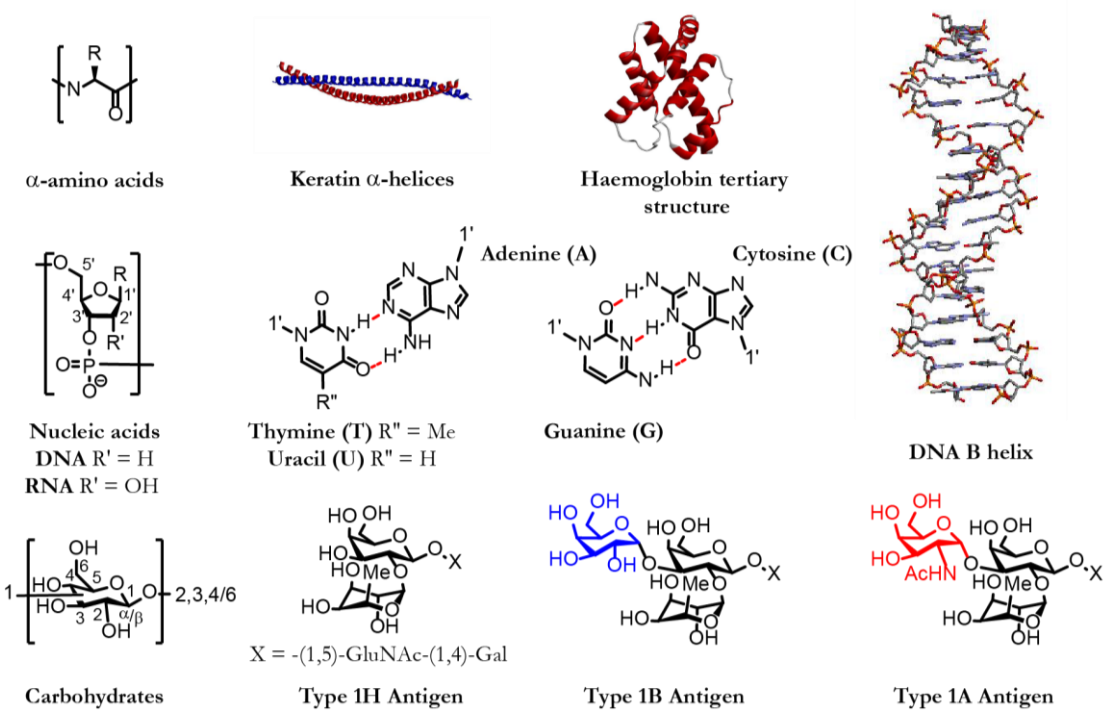

Figure 1 - Key biological building blocks.

Proteins are constructed through the peptidic linkage of α-amino acids. In the aqueous environments of living organisms the non-covalent interactions of the peptidic chain and the surrounding water molecules (hydrogen-bonding, steric repulsion, hydrophobic stacking) cause it to fold into a defined secondary structure.

The interactions of these secondary structures, the most prevalent of which are α-helices and β-sheets, lead to the formation of tertiary structure. Individual proteins can also aggregate to form larger quaternary structures[1]

Hydrogen-bonding in nucleic acids is highly selective, inducing double helix formation in DNA and RNA strands. The structural complexity achievable through the variation of both building block and linkage in carbohydrates has been utilised by biology for cellular communication. Complex carbohydrates, expressed on the outside of the cell, provide a structural language for other organisms or cells within an organism to read and interact with. The human blood groups, for example are identified at the molecular level by a specific set of carbohydrate structures expressed at the cell surface.[2]

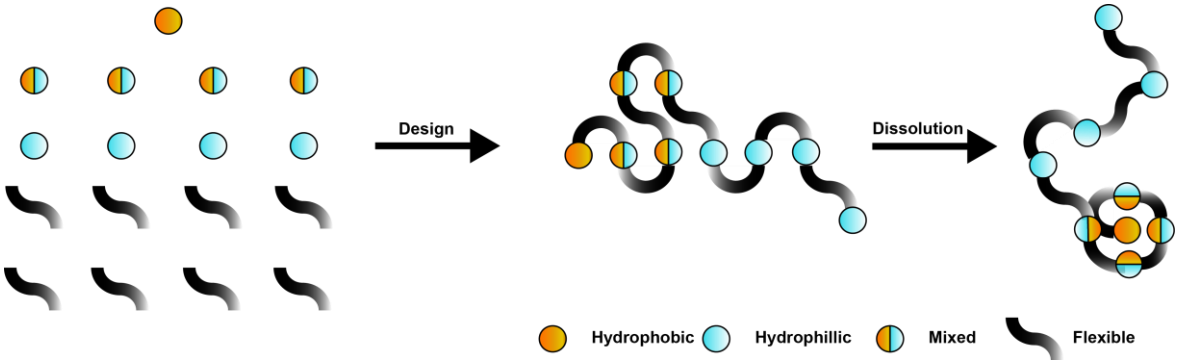

Figure 2 - The principles of solution-based foldamer design.

Foldamers[3,4] are a broad class of synthetic oligomers and polymers, constructed from both biological and abiotic monomeric units. These units are chosen to induce defined conformations in the resulting macromolecules they construct. Like their biological counterparts, certain foldamers are designed to adopt secondary structures in solution (Figure 2). In water the priciples that lead to the folding of peptides in biology can be used to develop foldameric analogues from synthetic materials. If designed correctly these foldamers have the potential for biological activity[5] and are of high interest in the development of therapeutics that block protein-protein interactions[6]

The synthetic building blocks used in construction of foldamers are outside the structural library of biology and offer improved stability to proteolysis and metabolism *in vivo*. The potential for foldameric therapeutics is particularly apparent amongst the β-peptide class of foldamers. β-peptides mimic the structure of biological α-peptides, but possess an extra carbon between the α-carbon and the nitrogen.[7] They are known to form a variety of helical structures in solution and have improved stability against proteases.[8]

While the selective inhibition of protein-protein interaction is challenging for small molecules, the larger secondary structures of oligomeric foldamers offer improved targeting and selectivity.[6] Some highly interesting examples of β-peptide use in potential antimicrobial,[9–12] antiviral[13,14]and anti-cancer[15] therapeutics have been published.

In cancer therapy, disrupting the interactions between proteins within a cancer cell can provide a selective trigger for cell death.[15,16] The interaction between hDM2, a human oncogene and P53, a transcription factor that controls cell response to stress is of particular interest for therapy (Figure 3).[17] A series of β-peptide analogues, known to form 14-helices decorated with key residues from the p53 α-helical fragment responsible for binding were synthesised. These were found to adopt a solution conformation closely matching that of the biological α-helical fragment, with one analogue having nanomolar affinity for the hDM2 groove.[15]

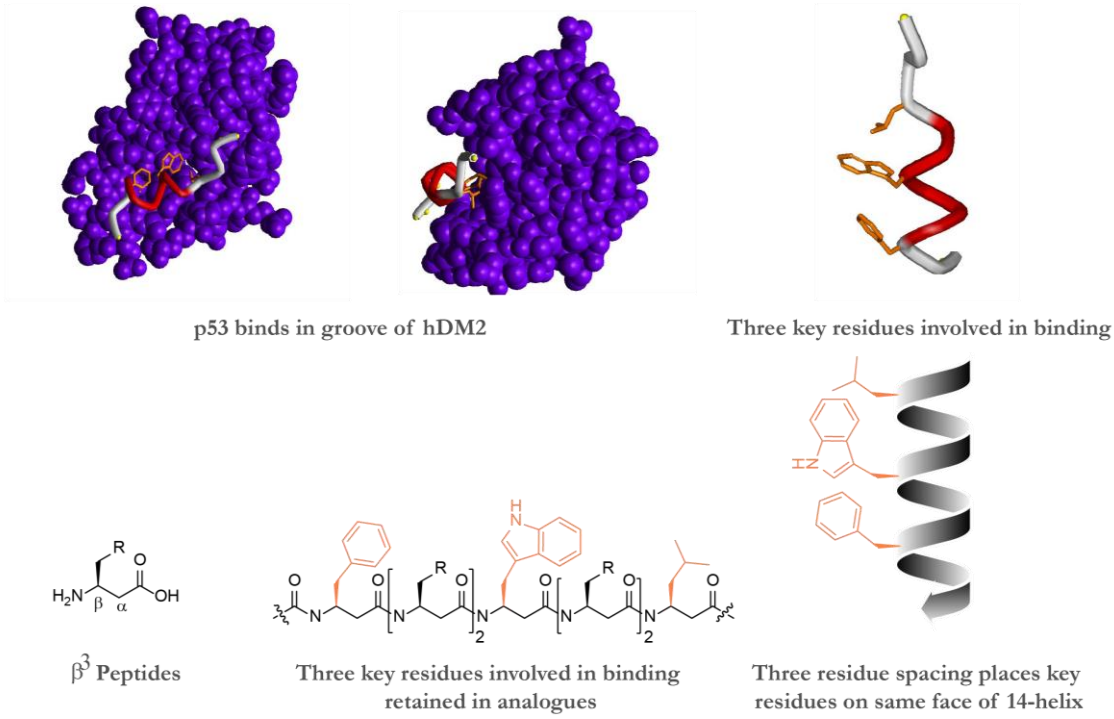

Figure 3 – β-peptide foldamers as potential anti-cancer therapeutics.

1.2 Biomimetic Structures

The examples of foldamers in the previous section highlight the potential for designed structures to operate on a biological level, disrupt biological events and provide novel therapeutics by replicating the function of protein structure. While they are highly impressive and their potential uses clear, their design process mirrors the design process of small molecule drug design. The foldameric structures described are an enhanced form of highly selective peptide ligand replicating the binding interaction of protein molecules.

The development of biomimetic structures, operating above the level of secondary architecture, capable of performing the whole function of more complex proteins in vivo is a great challenge for chemists.

A recent publication by the Leigh group (Figure 4) points towards the development of these systems, with attempts to make a biomimetic version of the ribosome,[18] the biological peptide synthesiser. In biology, the sequence-specific synthesis of peptide structure is critical to the formation of working proteins. While the ribosome achieves this effortlessly, creating a molecular system with similar properties is highly challenging.

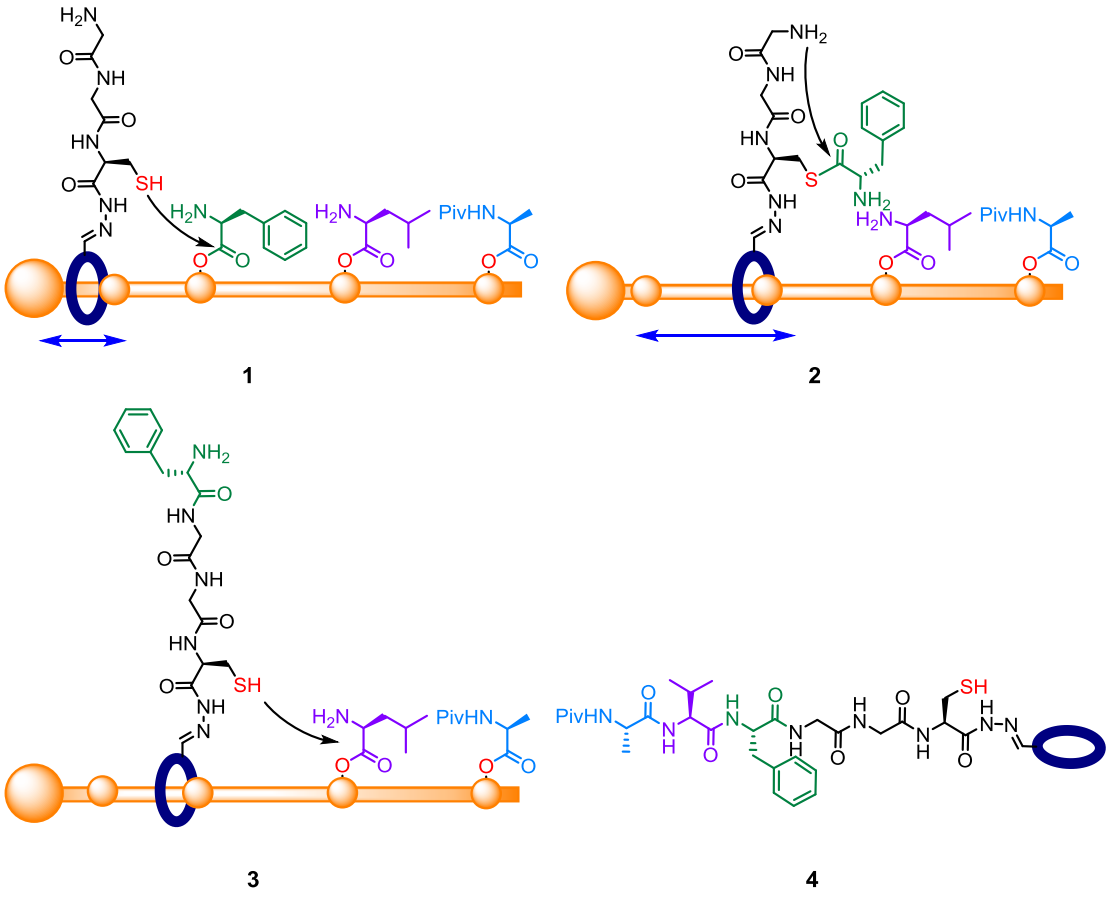

Figure 4 - A biomimetic peptide synthesiser.[19]

In their system Leigh and co-workers used the unthreading of a rotaxane to drive the sequence-specific synthesis of a peptide chain. The biomimetic ribosome consists of a ring with a reactive arm threaded on to a rod that is blocked at one terminus. The ring is free to oscillate along the rod but complete unthreading is obstructed by a sequence of peptide fragments (Phe, Val, Ala) **1**. As the ring oscillates along the rod, its reactive thiol arm can remove a peptide fragment from the rod **2**, adding it to the growing peptide sequence on the ring **3**. As each peptide is removed from the rod the ring is free to move further along it, reacting with the next peptide in sequence along the rod. The rigidity and size of the rod prevents the reactive arm interacting with other peptide fragments further along the rod ensuring a sequence-specific synthesis as the ring unthreads **4**.

The study of highly complex biological systems by the synthesis of biomimetic structures offers two key advantages:

Firstly a simplified system is easier to understand and can provide key information on comparison with the original biological target.

Secondly, the versatility of these systems and the possibility for straightforward elaboration allows the development of multiple functional structures applicable to a number of research fields including materials, biology, synthesis and medicine.

1.3 The G-Protein Coupled Receptor

The ability of one cell to coordinate biochemical events in other cells in an organism has allowed rising evolutionary complexity across the eukaryotic domain and is at the heart of key biological processes including cell division, regulation and differentiation, processes the organism depends on for development and survival. Throughout the complex signalling pathways that exist in biology, information transmission across the cell membrane is of utmost importance. Transmembrane signalling is equally important in single cell organisms where signal transmission across the cell membrane allows the organism to respond to its surroundings.[20]

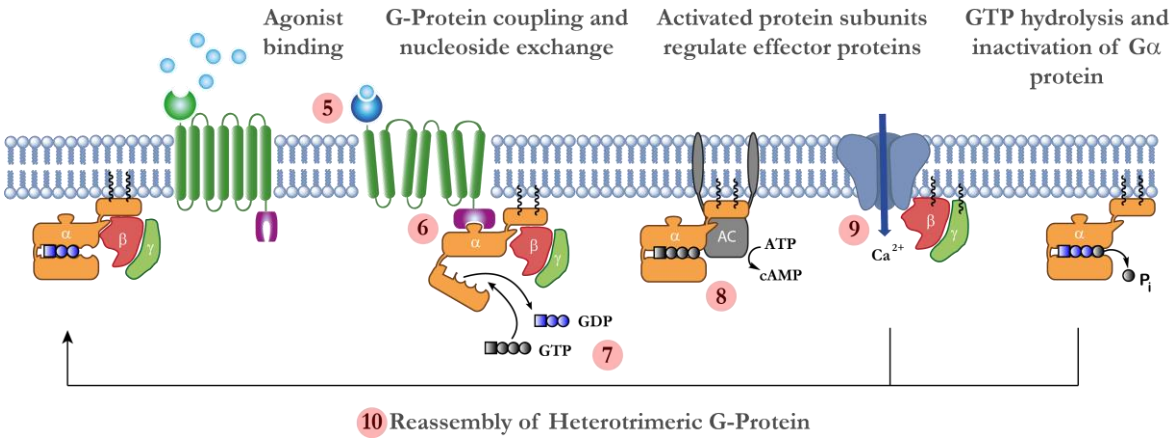

Figure 5 - The G-Protein Coupled Receptor and its function in the cell membrane.[21]

G-Protein coupled receptors[21–25] (GPCRs) are a specific type of transmembrane receptor that mediate signal transduction across a cell membrane through a *conformational* change in protein structure. They are characterised by membrane spanning domain composed of 7 α-helical units each 20-25 amino acids in length, connected in a serpentine fashion by head to tail loops with an extracellular N-terminus and intracellular C-terminus.

The mode of GPCR action (Figure 5) is as follows: binding of an agonist, such as a hormone or other protein **5**, leads to a conformational change in the helical domain inducing intracellular binding of the membrane bound G-protein trimer **6**. On formation of the G protein-receptor complex GDP is released from the α–subunit of the G protein trimer **7.** Complexation of GTP into the vacated α–subunit binding site leads to dissociation of the α and βγ subunits. These dissociated subunits proceed to regulate their respective effector proteins: the adenylyl cyclase (AC) **8** and Ca^{2+} ion channels **9**. Subsequent hydrolysis of the GTP bound in the α–unit to GDP allows for the reformation of the G-protein trimer **10**, completing the cycle.[21,25]

The superfamily of GPCRs are responsible for wide range of different signalling processes An estimated 80% of known hormone and neurotransmitter signalling pathways depend on GPCRs at transmembrane.[26] GPCRs are of particular interest to pharmaceutical industry as inhibition of a specific GPCR will have a pronounced effect on the downstream signalling of G-proteins, effectors and subsequent biological processes. As of 2002 an estimated 30% of marketable small-molecule drugs targeted GPCRs.[27]

1.4 Conformational Control of Helical Foldamers

If the monomeric units of a foldamer weakly induce helicity it may exist as a mixture of helical and random coil conformations in solution. As the helicogenic potential of the monomeric units increases the foldamer will adopt a fully helical conformation in solution. If the monomeric units are also achiral, the resulting helix will have no inherent screw-sense preference (*M*/*P*) and assuming a low barrier to helical inversion, will rapidly interconvert between left (*M*) and right handed (*P*) helical forms (Figure 6A).

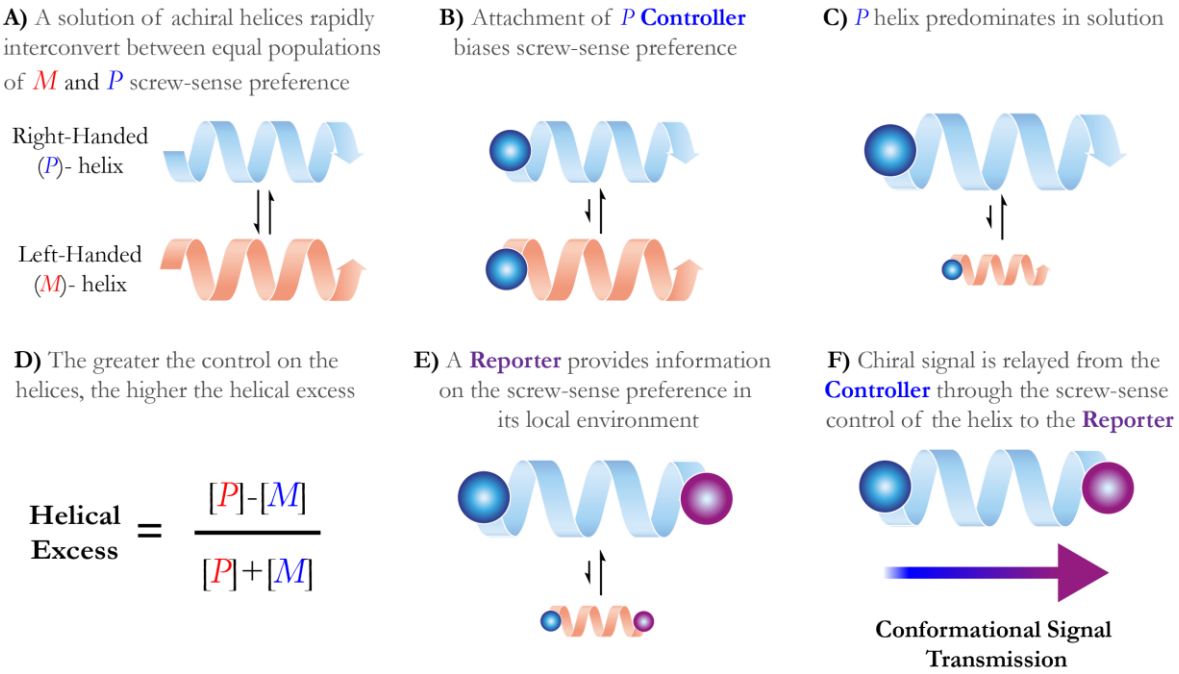

Figure 6 - The principles of screw-sense preference control

A **Controller** is any chiral fragment placed within an otherwise achiral helix that induces a conformational preference throughout the whole helix. Providing the structure is completely helical, a **Controller** placed at one terminus of the helix can bias the screw-sense preference of the entire helix (Figure 6B) leading to one helical configuration predominating in solution (Figure 6C). The helical excess, analogous to

enantiomeric excess, is a measure of the degree to which one screw-sense preference predominates in solution (Figure 6D). A **Reporter** is any chemical fragment that provides a localised read-out of screw-sense preference (*M*/*P*) from its position within the helix (Figure 6E).

The strength of control placed on the helix by a **Controller** at one terminus can be detected at the distal terminus using a **Reporter** group (Figure 6F). This is in effect a relay of binary information (*M*/*P*) from the **Controller** to the **Reporter** through the conformational control of the helix screw-sense preference. The strength of signal relay is the net result of the combined properties of **Controller** efficacy, the propensity for a particular helical foldamer to relay information and total length of the helix (Figure 6F).

1.5 Choosing the Helix

Judicious choice is required in the selection of the helical fragment required for signal relay. The helix must be constructed from achiral monomers and possess a barrier of inversion sufficiently low enough to allow rapid screw-sense inversion relative to the time scale of signal transmission. The configuration of nature's peptidic building blocks induce the formation of right-handed α-helices[1] These naturally occurring helices are unsuitable for use in signal relay due to the large thermodynamic preference for the right-handed screw-sense. Inversion to the left-handed helix would be highly unfavourable. Helices constructed from achiral blocks have no thermodynamically induced screw-sense preference and have the potential to switch between and left and right handed screw-sense preference.

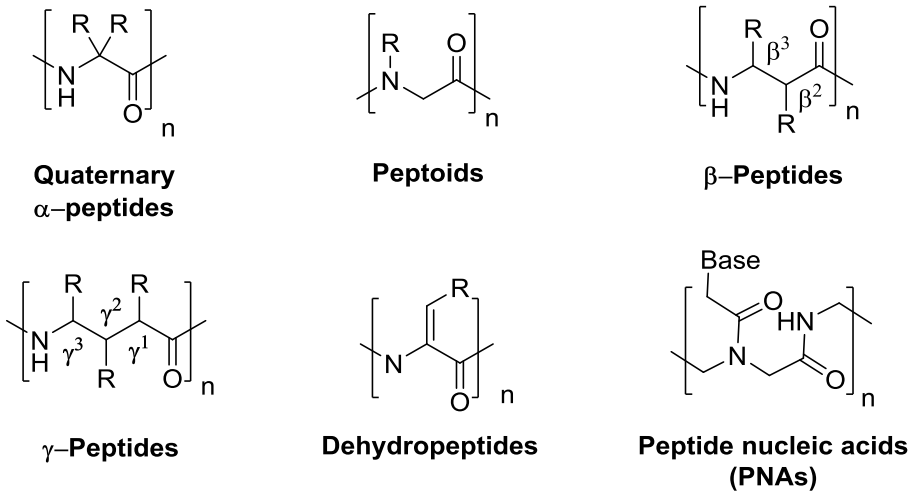

Figure 7 – Helicogenic foldameric monomers.

Examples of helical structures can be found amongst foldameric analogues of peptides and DNA, namely quaternary α-peptides,[28] peptoids,[29,30] β-peptides,[5,7,16] γ-peptides,[7] de-hydro peptides,[31] and peptide nucleic acids (PNAs).[32–37] The physical interactions between the achiral building blocks that lead to helix formation (steric, hydrogen-bonding, hydrophobic) are highly advantageuous for the relay of chiral information.

The hydrogen-bonding interaction and steric congestion of quaternary α-amino acids, the building blocks of quaternary α-peptides, lead to strong, helicogenic interactions directly between monomeric units $(i \rightarrow i_{\pm 1})$ and at residues spaced $(i \rightarrow i_{\pm 3})$ along the peptide chain. The ability to supply and study chiral influence from a variety of readily available amino acids, easily attached by peptidic coupling reactions along with the biological compatibility of α-amino acids makes them a highly suitable candidate for use in biomimetic signal relay devices.

1.6 α-Aminoisobutyric Acid and the 3_{10} helix

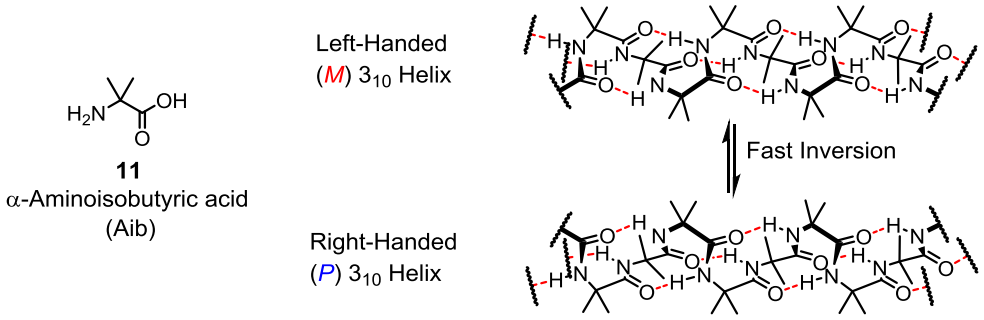

Figure 8 - The 3_{10} helical structures of α-Aminoisobutyric acid.

Peptides containing α-Aminoisobutyric acid (Aib) **11**, the simplest of quaternary α-amino acids[38] predominantly adopt helical structures due to the conformational restraint placed on their secondary structures at the geminal dimethyl substituted C_α positions. Ramachandran plots of glycine, alanine and Aib (Figure 9) highlight this. Differing only in degree of substitution at the C_α position, increasing methyl substitution leads to a large decrease in rotational freedom available to the residue when part of a peptide chain.

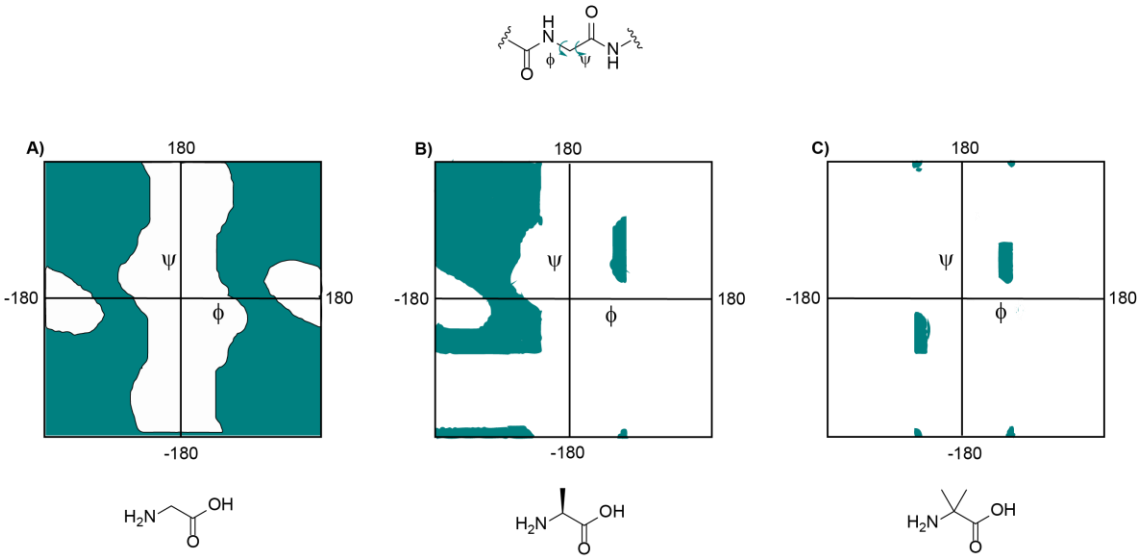

Figure 9 – Ramachandran plots of glycine (A) alanine (B) and α-Aminoisobutyric. Coloured areas show allowed values for ϕ and ψ torsional angles when incorporated into a peptide chain.

This steric "Thorpe-Ingold" effect is so pronounced that peptides with greater than 50% Aib content, particularly those containing segments of $(Aib)_{n\geq 2}$ form a tightly twisted 3_{10} helical structure[39] consisting of 3 residues per turn, forming a 10 atom hydrogen-bonded ring. The 3_{10} helix is longer and narrower than the more stable α-helix and is much rarer in nature.[40] It is characterised by a hydrogen bond network of $(i \rightarrow i_{\pm 3})$ *cf.* α-helix $(i \rightarrow i_{\pm 4})$.

For the homologous $(Aib)_n$ series even the trimer $(Aib)_3$, which is only just long enough to form a complete helical turn, exists in helical form as a type III/III' *β*–turn[41] with the larger homologues adopting a 3_{10} helical structure.[42]

$(Aib)_n$ helices exist in solution as a rapidly inverting racemic mixture of *M* and *P* 3_{10} helical enantiomers. Using series of Boc-Aib_n-OMe homologues and variable temperature ^{13}C NMR, Hummel *et al.* calculated a $\Delta G^{\ddagger}$ of inversion of 4.6 kJ mol^{-1} per Aib residue based on the Boc-Aib_{10}-OMe helix in DCM.[39]

The interconversion between enantiomeric *M* and *P* helical conformations is thought to occur via a "zipper-like" mechanism, with a stepwise breaking of H-bond interactions proceeding along the chain length.[43]

1.7 Reporting on Helicity

Understanding the behaviour of a helix in solution is very important in the development of dynamic helical systems. X-ray crystallography (Figure 10A) can provide detailed structural information but is limited to the solid state structure of the helix which can differ from that in solution. X-ray crystallography is further limited by the requirement of a crystallisable helix.

Circular dichroism (CD) provides detailed information on chirality in solution, measuring the absorbance of a circularly polarised light source over a wavelength range. For helical structures, particular repeating interactions in the helix lead to signature absorbances at set wavelengths. The type of helix (α, 3_{10}, 12-helix) can be identified by these absorbances with opposite screw-sense preference observable as opposing signs in the absorbance (Figure 10B).[44] While CD provides information on the global conformation of a helix it typically cannot provide localised information on screw-sense preference from points within the helix.[31] The groups of Inai,[31,45] and Clayden[46] have designed CD reporter structures compatible with Aib helices; these are discussed in context later. Crucial to their function is an absorbance profile that differs from that of the peptide helix.

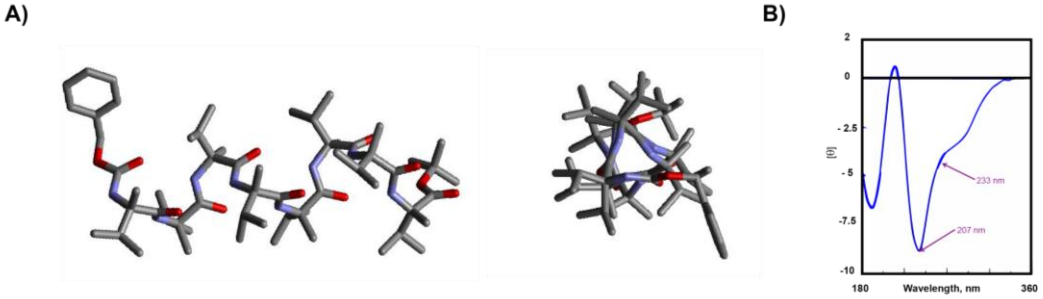

Figure 10 - The crystal structure of a right-handed (*P*) 3_{10} helix, Cbz-Aib_8-OtBu (**A**) and accompanying CD spectra (**B**).[47] The negative band at 207 nm and shoulder centered at 222 nm indicative of 3_{10} *P*-helix.

1.8 Diastereotopic NMR Probes

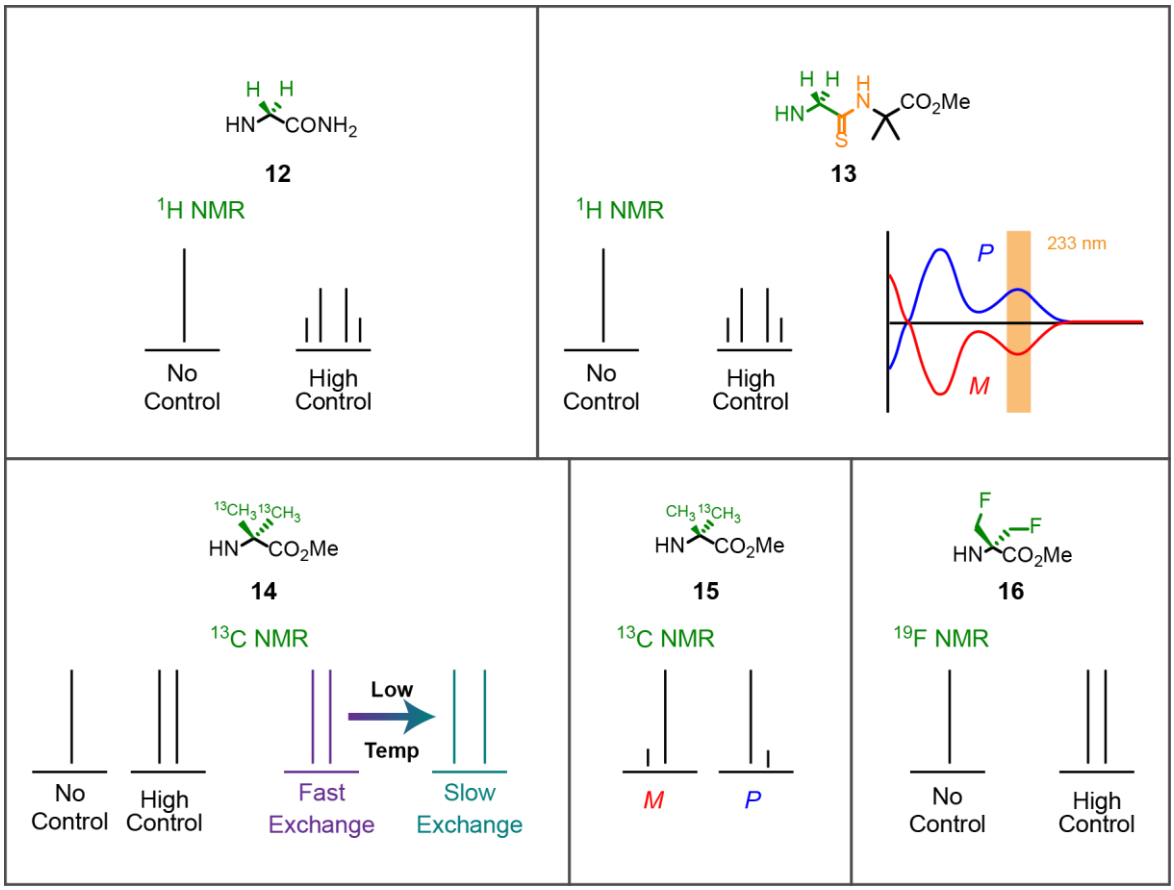

Figure 11 - NMR probes developed and used by the Clayden group as screw-sense reporters.

NMR probes using ^{1}H (**12**,[48] **13**[46]) ^{13}C (**14**,[49] **15**[50,51]) and ^{19}F (**16**[52]) nuclei have been developed for Aib helices within the group. They can be inserted at any position in the helical backbone and provide quantitative information on helicity *via* observable differences in the NMR spectrum. A pair of geminal spin active nuclei (**A** and **B**, Figure 12) placed on the backbone of a helix will experience differing magnetic environments in either the *M* or *P* conformation. The observed NMR signal arising from this conformational magnetic inequivalence is dependent on the rate of inversion, $\boldsymbol{k}$ between the *M* and *P* helices.

If $\boldsymbol{k}$ is slow with respect to the NMR timescale $\left(\boldsymbol{k} \ll \boldsymbol{\pi\Delta\nu/\sqrt{2}}\right)$ the nuclei are rendered diastereotopic and the signal observed in the NMR will be split, with the signal from each nuclei separated by a chemical shift $\boldsymbol{\Delta\delta_{Slow}}$

If $\boldsymbol{k}$ is fast with respect to the NMR timescale $\left(\boldsymbol{k} \gg \boldsymbol{\pi\Delta\nu/\sqrt{2}}\right)$ the magnetic inequivalence is removed and the splitting of the signal between the two nuclei $\boldsymbol{\Delta\delta}$ is removed.

If a chiral controller is attached to the helix at a remote position to the NMR probe it will bias the screw-sense preference of the helix, rendering the geminal nuclei of the probe diastereotopic. As the chiral influence of the controller is remote from the probe structure, separated by the achiral helix, the arising diastereotopicity of the probe nuclei provides a measure of the quality of signal relay from controller to reporter.

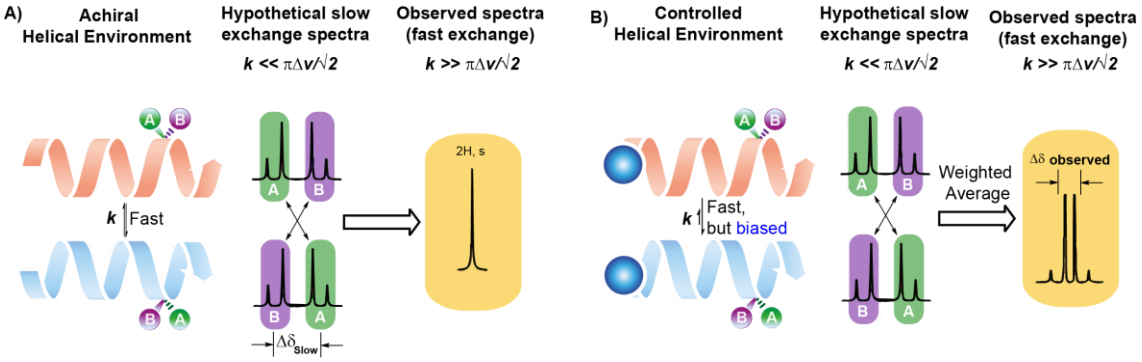

Figure 12 – Principles of diastereotopic NMR probes.

Increasing signal quality is a combined measure of the efficacy of the chiral controller, the fidelity of signal relay through the achiral helix and the length of the helix through which the signal relayed. It is apparent as an increase in the observed diastereotopic splitting of the probe nuclei $\Delta\delta$ up to the maximum observable splitting at slow exchange $\Delta\delta_{Slow}$. The degree of control placed on an achiral helix in fast exchange by a remote chiral influence can be quantified by dividing the observed splitting at fast exchange $\Delta\delta_{Observed}$ by the maximum splitting achievable for the same helix at slow exchange $\Delta\delta_{Slow}$.

The use of the ^{13}C reporter structure **14** in conjunction with variable temperature ^{13}C NMR has allowed the determination of $\Delta\delta_{Slow}$ and the subsequent quantification of transmission quality in Aib helical systems.[49] Clayden and co-workers have determined the range of control possible (peptide length)[53] and the fidelity of signal transmission across a range of solvents. They observed very high signal fidelity in non-polar solvents (<1% signal loss per Aib)[54] In polar solvents the high signal fidelity is lower but still very reasonable (2.5% per Aib residue, MeOH).[49]

1.9 Covalent Control of Screw-Sense Preference

Early work by Inai *et al.* highlighted the controlling effect of a single chiral amino acid on helical oligomers composed of a mixture of Aib and Z-dehydrophenylalanine (Δ Phe). The presence of the achiral Δ Phe chromophore allowed the handedness of the helix to be studied by circular dichroism (CD) and exciton couplet experiments.[45]

Further work showed that placement of single chiral amino acids at either terminus led to a strong preference in handedness (*M*/*P*) in the helices. Opposing chiral influences (D- vs. L-amino acids) at either end led to the disruption of this helical preference.[55]

Further work by the group also highlighted the possibility of non-covalent control of the achiral helical system in the presence of excess Boc-L-Proline.[56,57]

Intrigued by the nature of this non-covalent control, they proposed a three point covalent interaction between the chiral Boc-L-Proline and the N-terminus of the peptide.[58] To investigate further they attached a C-terminal (*Z*)-Δ-(4,4′-biphenyl)-*α,β*-didehydroalanine probe to determine, using CD, the extent to which the chiral influence was transmitted through the helical system[31] (Figure 13)

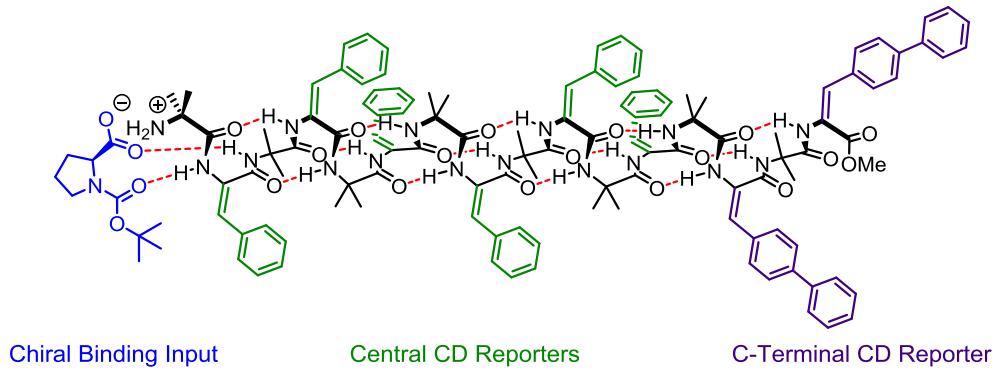

Figure 13 - The use of a central and terminal CD reporters of helicity.

The absorption difference in central Δ Phe groups and terminal CD reporters allowed the determination of helicity both of the peptide as a whole and more specifically with the localised screw-sense preference of the C-terminus.

While these CD reporters gave a good indication of screw-sense induction, a more accurate method is required to quantify the strength of the signal.

1.10 Optimising Covalent Control of Screw-Sense Preference

Utilising their NMR reporter structures **13**-**16**, Clayden and co-workers have studied the magnitude of screw-sense control exerted on achiral Aib helices by library of chiral amino acid derivatives.

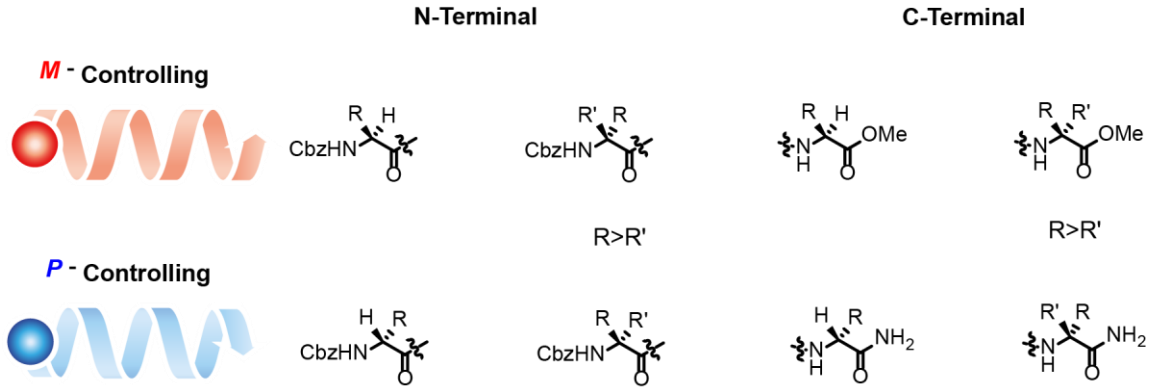

Figure 14 - Controllers of Aib screw-sense preference.

Investigating control at the N-terminus, they found that N-protected tertiary acids gave an *M*-helical screw-sense preference for L-controllers and *P* for D-controllers. Quaternary amino acids were found to give the opposite control of screw-sense preference with L- control giving *P*-helices and D control giving *M*-helices.[48]

Interested in comparative strength of control from an N or C terminal position, Clayden *et al.* synthesised a set of X-Aib$_8$GlyAib$_8$-Y oligomers (Figure 15) varying the presence and stereochemistry of N terminal controller (X) and C-terminal controller (Y) moieties. Using the observed splitting in the central Gly probe as a measure of screw-sense control, they found that a single chiral amino acid residue, for example phenylalanine, attached to either to N- or the C- terminus of the helix imparted greater control on the helical screw-sense preference when attached to the N-terminus. This suggested that a greater measure of helical preference control could be achieved from an N-terminal position.[59]

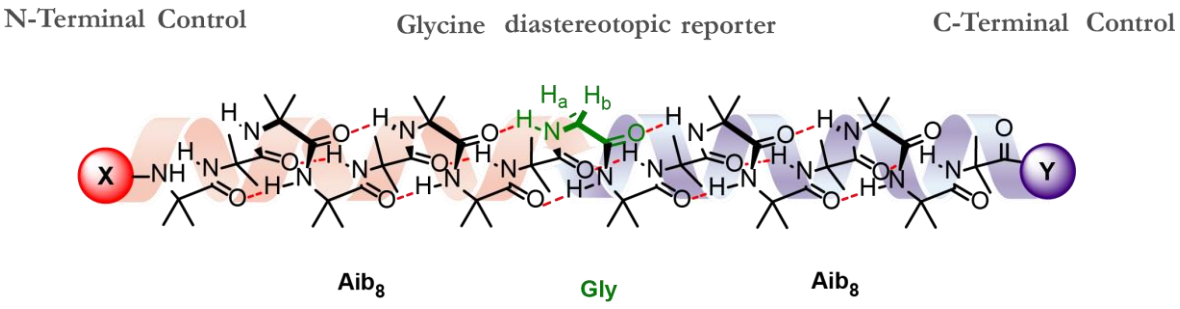

Figure 15 – The use of a central glycine NMR reporter to determine the strength of control from an N or C terminal position.[59]

Control of screw-sense preference induced at the C-terminus was found to depend not on the substitution of the amino acid α-centre but the C-terminal capping fragment. Secondary amides of both tertiary and quaternary L-amino acids gave a *P*-screw-sense preference. Equivalent C-terminal esters or tertiary amides, which lacked the final C-terminal NH bond interact differently with the helix, inducing and *M*-preference

1.11 Insulators and Amplifiers

The controller-reporter strategy was further used to investigate the relay potential of other amino acids residues when inserted within Aib helices. Various linkers were inserted at the centre of an Aib_9 helix controlled at the N-terminus with a single **Cbz-L-Phe** residue. The relay of chiral information is detected at the C-terminus using a glycinamide **$GlyNH_2$** reporter. Replacing the central Aib residue with a variety of amino acid linkers and comparing against the level of control for the Aib_9 helix Boddaert *et al.*[60] were able to determine the propensity of a variety of residues to relay or insulate the chiral signal. They found comparable signal fidelity for cyclic residue similar to Aib, (**Ac_5c**, **Ac_6c**, **Thp**) with the 6-member ring analogues (**Ac_6c**, **Thp**) found to slightly amplify signal relay. Introducing flexibility into the middle of the helix (**Gly, β-Ala**) led to a reduced signal. Further flexibility (**GlyGly**) or additional steric bulk at the quaternary centre (**Dpg**) was found to insulate signal transmission.

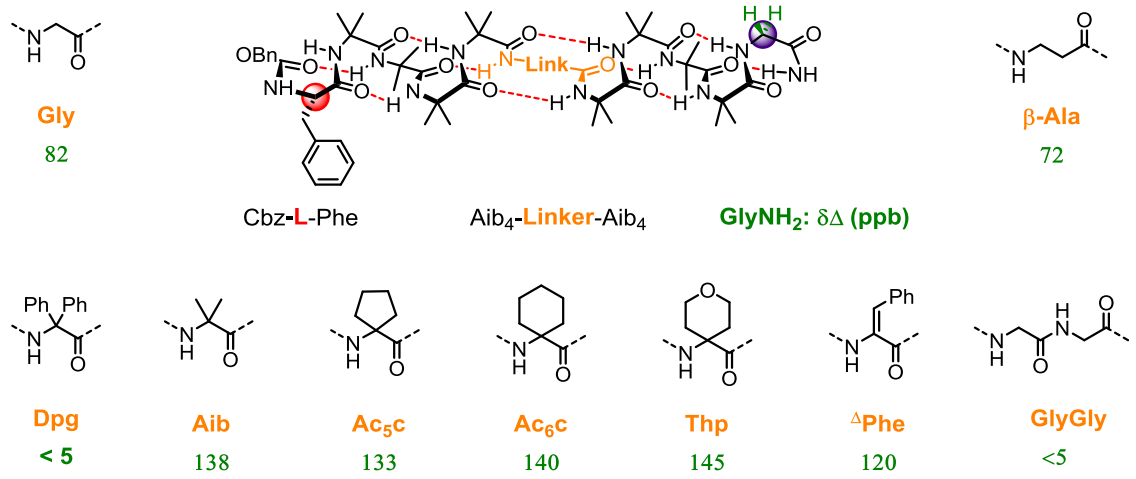

Figure 16 - Insulators and conductors of chiral relay in Aib helices.[60]

1.12 Remote Asymmetric Induction

Complete control of the helix screw-sense preference was found for the dipeptidic α-methylvaline $(\alpha Mv)_2$ **17** structure at both the N and C terminus. Byrne *et al.*[61] used this controlling fragment to induce a right handed screw-sense preference in a 4 nm long achiral helix comprised of Aib and Ac_6c fragments **18**. The quality of signal relay through the controlled achiral helix was great enough to induce asymmetry in an achiral reaction site located at the C-terminus, separated from the nearest chiral centre by 60 bonds of achiral helix **19**. This impressive result not only exemplifies the quality of signal really achievable in achiral helices but represents the first step towards more complex systems, where the reporter is replaced with a new structure, capable of further function.

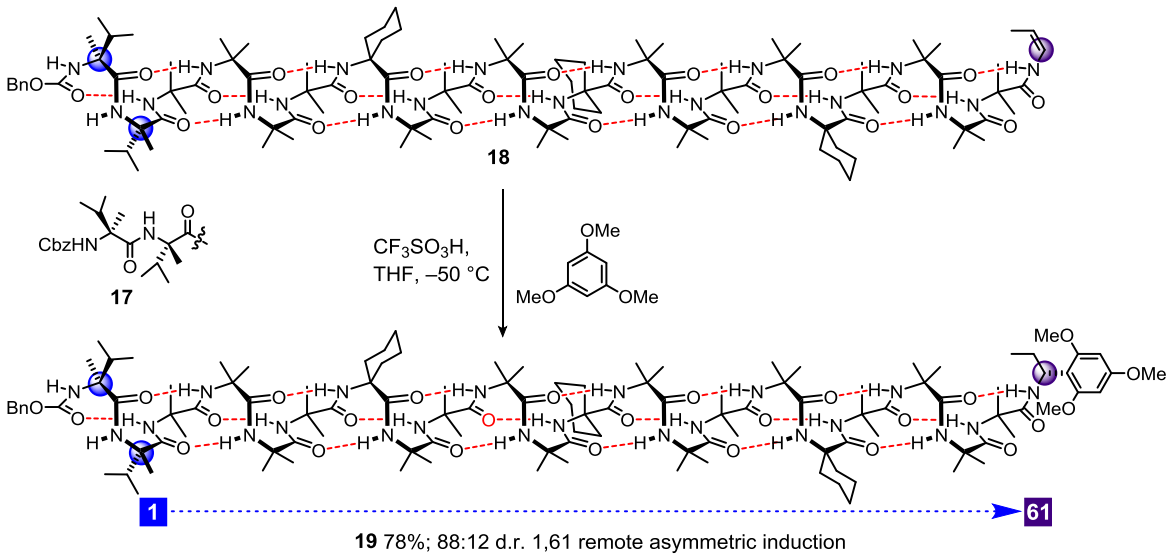

Scheme 1 - Signal relay through achiral helix induces asymmetry in remote reaction site.[61]

1.13 Switchable Control of Helicity

Developing a helical structure that can respond to external stimuli is essential to creating signal relay or biomimetic structures. A switchable controller placed at one terminus of the helix can therefore be controlled externally by a chemical input. Signal relay through the helix can then be detected at the distal terminus using a reporter structure.

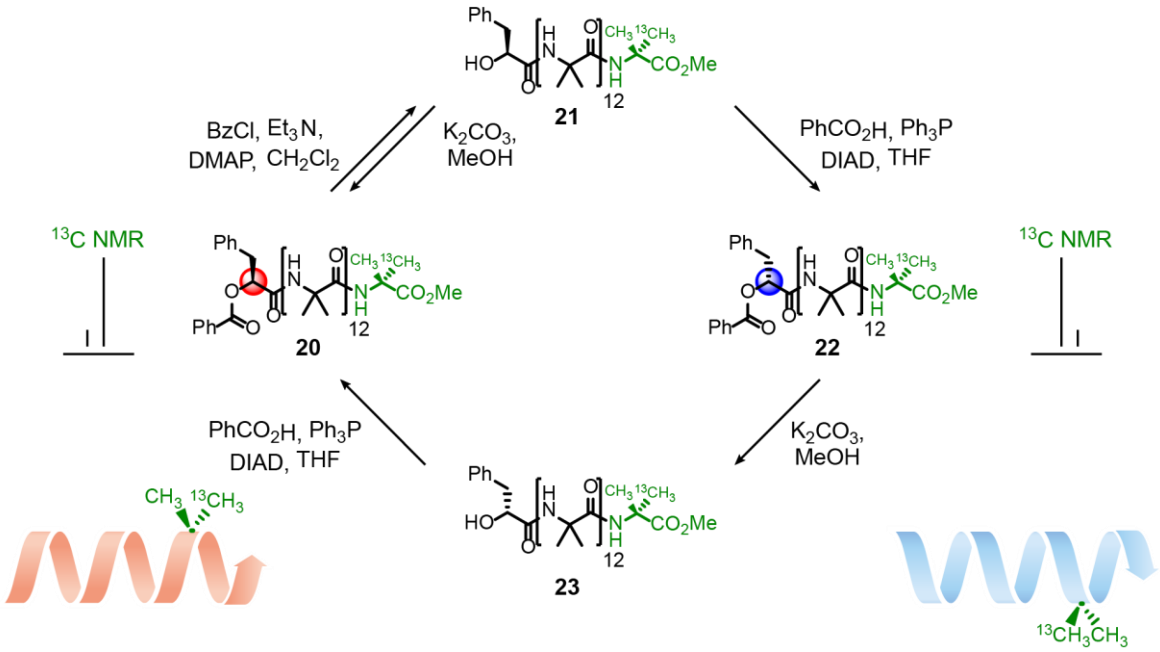

Scheme 2 – Reversible control of helix conformation through mitsunobu inversion of chiral controller.[51]

The earliest example of switchable control developed within the Clayden group used Mitsunobu conditions to invert the chirality of a 3-phenyllactate controller a between the *S*-**20**,**21** and *R*-**22**,**23** configuration. This change in chiral input was relayed from the N-terminus through the achiral Aib_{12} helix, 2.5 nm in length to the C-terminus. The switching signal could be detected at the C-terminus using an enantiomerically enriched ^{13}C labelled reporter.[50] The ^{13}C enrichment of the probe is greatest in the pro-*R* methyl group, which appears as the more intense of two peaks in the ^{13}C NMR spectrum. When placed in an *M*-helix the larger signal is upfield. Inversion of the helicity to *P* shifts the position of the pro-*R* peak so that it is downfield relative to the pro-*S*.

1.14 Early Receptor Mimics

More recent work within the group[62] has investigated the replacement of the N-terminal chiral controller with an achiral binding site. Closer in function to a biological receptor, a chiral signal is delivered to the N-terminus of the helix through the binding of a chiral messenger molecule.

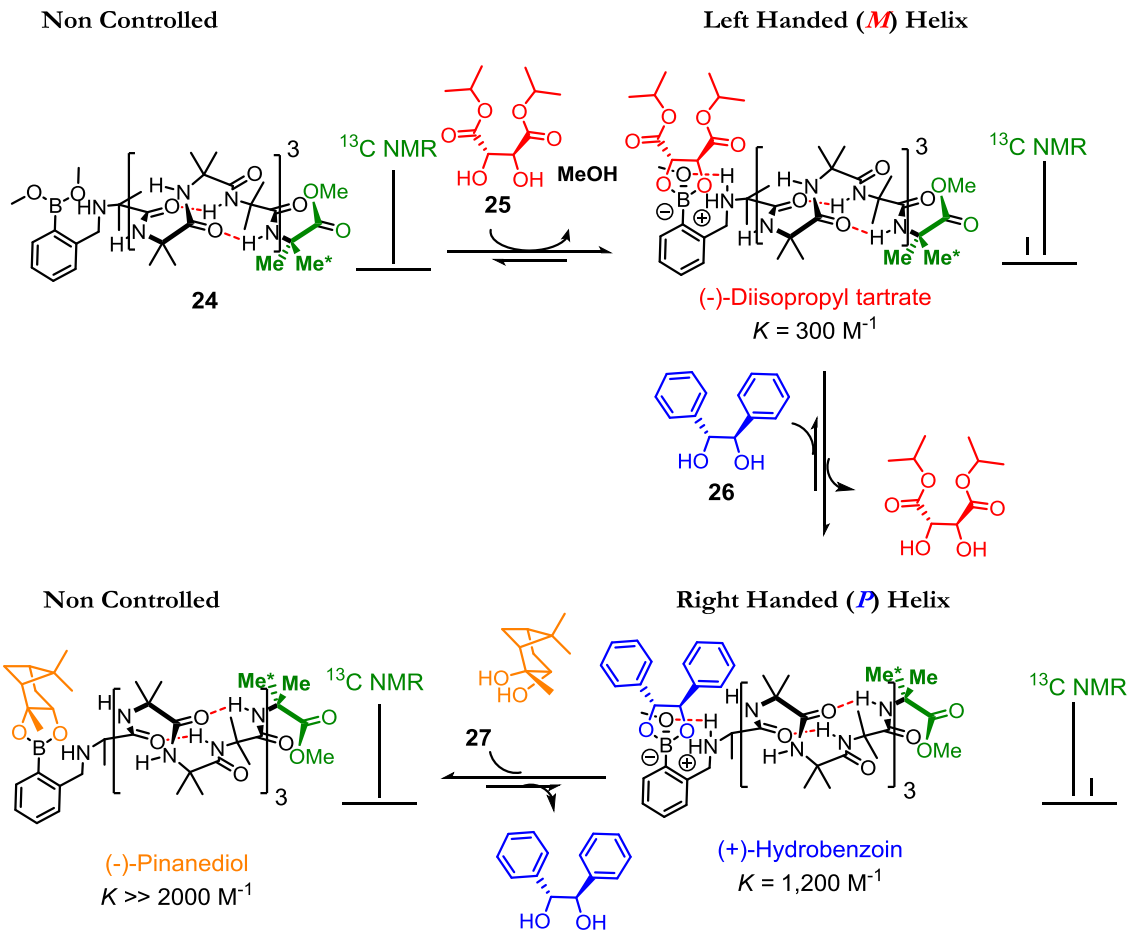

Scheme 3 - Achiral boronic ester binding site allows switchable signal relay through achiral Aib helix.[62]

A boronic ester attached to the N-terminus of an Aib oligomer provided a binding site capable of binding chiral diol agonists. The addition of chiral diols to a solution of the synthetic receptor **24** induces a screw-sense preference in the helix that can be detected at the C-terminus using a ^{13}C NMR probe. The different binding affinities and controlling ability of individual chiral diols was exploited to develop a switchable system. Initially the receptor is dormant with no chiral influence resulting in a singlet for the ^{13}C probe. Addition of (−)-diisopropyl tartrate **25** induces a left-handed helix with signal relay through the helix apparent as upfield positioning of the ^{13}C label. Further addition to the system of (+)-hydrobenzoin **26** displaces the tartrate inducing

a right-handed helix, with a downfield inversion of the ^{13}C label. Finally, the receptor can be switched off with the addition of (−)-pinanediol **27** which displaces both of the other diols in solution. (−)-pinanediol places no control on the helix, resulting in a return to the singlet signal for the ^{13}C probe. The biomimetic nature of this system was further exemplified in the binding of the ribonucleosides adenosine, guanosine, uridine and cytidine. Subtle differences in the ligand structure could be detected by the receptor and relayed to the reporter more than 2 nm away from the binding site.

1.15 pH Controlled Helix Inversion

Clayden and coworkers have also developed a pH responsive signal relay system through the development of an N-terminal basic binding site. The binding site **28** binds chiral acids in solution and through this non-covalent interaction, the chirality of the acid is relayed through the achiral peptidic helix to a remote NMR reporter. Chiral acids with different pKa values (Figure 17) preferentially bind at the N-terminal site at varying pH. Selection of two opposite screw-sense directing chiral acids with different pKa values allows a system where at a low pH one acid binds, inducing a screw-sense preference **29** with the second acid binding and inducing the opposite screw-sense at high pH **30.**

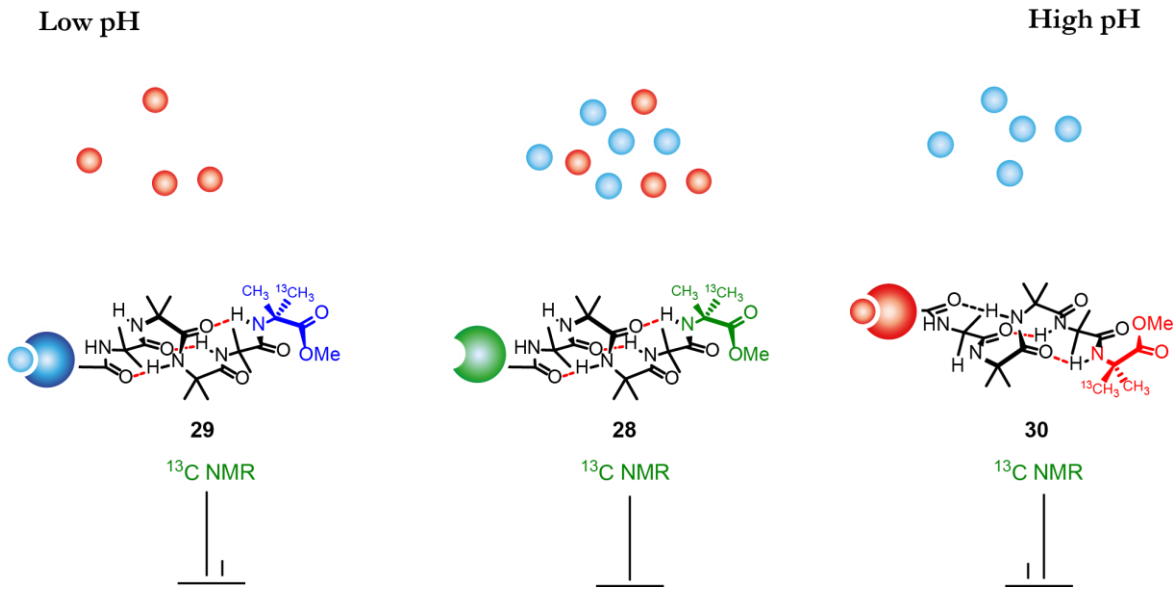

Figure 17 - pH responsive binding site concept. *P*-directing chiral acid binds at low pH, *M*-directing chiral acid binds at high pH.

A variety of binding sites **31a-j** and chiral acids **32a-h** were investigated within the study with **31e** proving to be the most successful binding site. Once the basic binding site was optimised on the shorter Aib_4 helix a longer Aib_8 foldamer **33e** was mixed with (*S*)-**32f,** (*S*)-**32d** and (*R*)-**32a** creating a multicomponent mixture that, on modulation of the pH induced either *M* or *P* helicity in the foldamer **33e.**

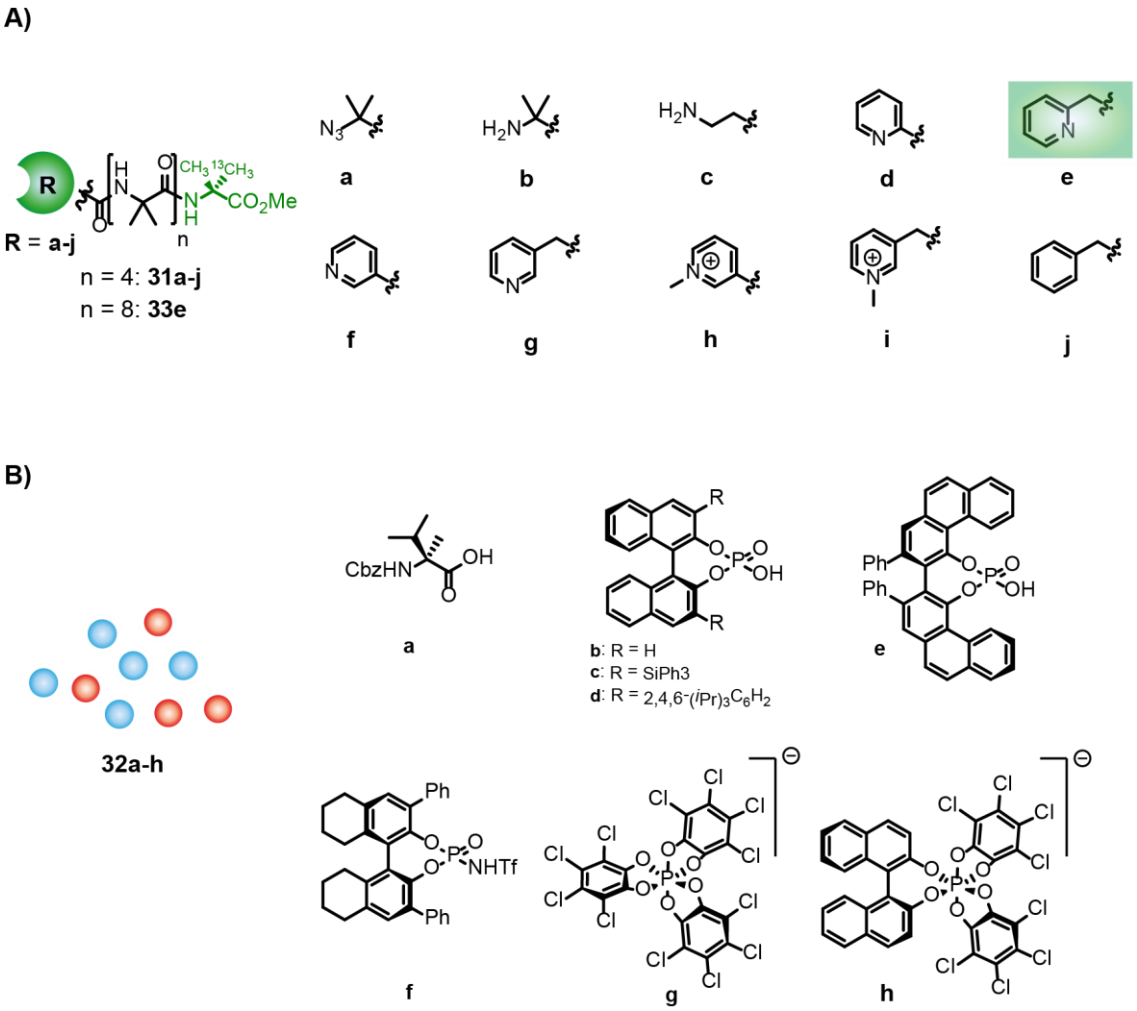

Figure 18 - Lewis acidic binding sites **(A)** and chiral amino acids **(B)** investigated by the Clayden group.[63]

1.16 Mimicing the GPCR in Membrane Environments

The development of switchable, receptor-like systems using an NMR compatible probe (Sections 1.14 & 1.15) and the induction of asymmetry at a remote reaction site 60 bonds away, a distance of 4 nm; roughly the thickness of a cell membrane (Section 1.12) has been discussed in detail earlier.

This work highlights the versatility of Aib helices for conformational signal relay in biomimetic devices. The possibility for straightforward elaboration through the replacement of controller and reporter units with more complex inputs (e.g. photochromic controllers, enzyme responsive switchable controllers) and outputs (e.g. reactive and catalytic sites) is clear, but their reliance on NMR limits them to homogeneous solution phase systems.

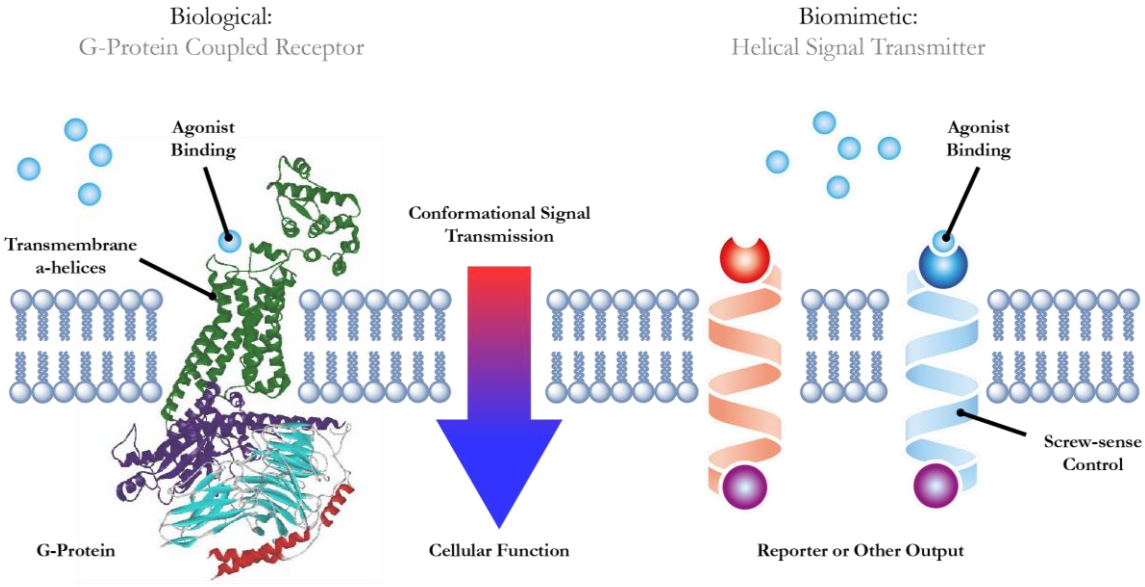

Figure 19 - Helical transducers as biomimetic G-Protein Coupled Receptors.

The use of Aib helices in the creation of a fully functioning mimic of a G-Protein Coupled Receptor (GPCR) has high potential (Figure 19). An Aib helix with switchable controller located at the outer surface of a cell membrane could, on binding an agonist, relay the signal through conformational control of helix screw-sense preference to a reporter located at the other terminus of the helix. Developing the earlier systems towards this aim requires their translation into membrane environments.

The compatibility of Aib helices with the membrane environment was a key design feature in the earlier work by Clayden *et al.*[53] It is best exemplified by the peptaibols, a class of membrane active fungal metabolites rich in Aib. Due to their ampithatic nature, naturally occurring peptaibols are known to self-associate to form ion channels, spanning the width of lipid bilayer membranes.[64]

The membrane insertion properties of peptaibols are highly studied[65–68] due to the antibiotic function arising from their pore-forming ability. Alamethicin is arguably the most studied, the presence of the Aib units strongly inducing an α-helical structure[69,70]

While the membrane spanning potential of Aib residues is ideal for the development of a GPCR mimic, the formation of pores, an alternative method of transmembrane communication[71] is less desirable.

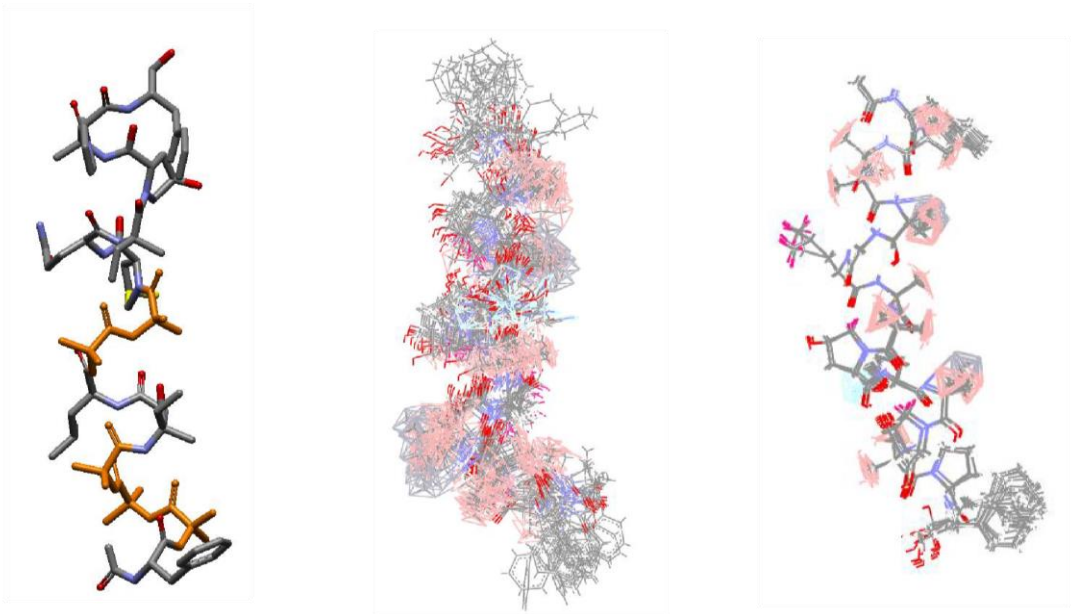

Figure 20 - Antiamoebin 1: Xray crystal structure showing Aib residues in orange[64] (**A**). Solution structure in MeOH indicates greatest movement in Aib regions[72] (**B**). NMR solution structure in DMPC/DHPC bicelles shows more movement in lower Aib region[73] (**C**)

Observations of the peptaibol Antiamoebin 1 further support the potential for Aib helices in conformational signalling systems that avoid pore formation. Antiamoebin 1[74] interconverts rapidly between *M* and *P* helicity and possesses low biological activity when compared to other peptaibols of equal length. This reduced activity is thought[75] to be the result of rapid interconversion between *M* and *P* screw-sense in an Aib rich segment of the peptaibol preventing aggregation and channel forming in membrane environments.

1.17 Membrane Environments

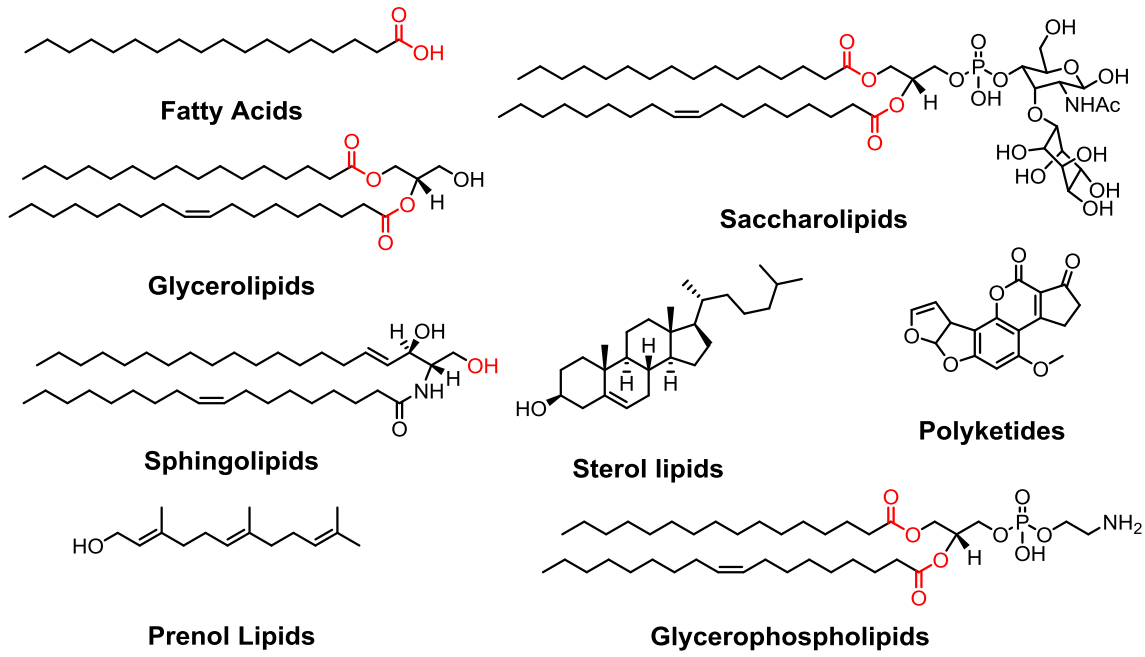

Figure 21 - Main classes of lipid found in the cell membrane.[76,77]

The membrane of a cell is essential for its function, providing a selectively permeable barrier that protects the cell's internal machinery from the outside world. The main constituents of a cell membrane are its lipids. There are 8 distinct classes of lipid as defined by the 2005 LIPID MAPS classification system.[76,77] Of these **Glycerophospholipids** are the most prevalent class in mammalian membranes and a major constituent of the membranes in all eukariotic life.[78]

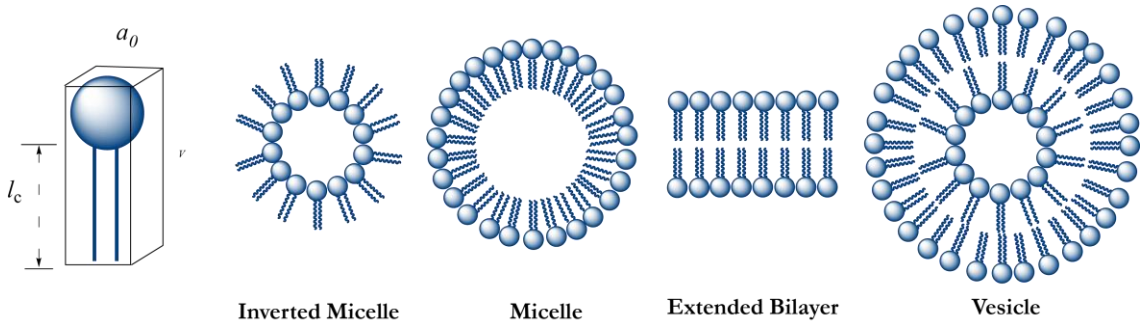

Figure 22 - Extended structure of lipids and other amphiphilic molecules.

In aqueous environments these amphiphilic compounds self-assemble into a variety of supramolecular structures (Figure 22). The type of structure formed is dependent on the geometric properties of the amphiphile and can be predicted using the equation developed by Israelachvili *et al.* [79]

The key geometric parameters involved are:

v, The volume of the hydrocarbon core.

$\mathbf{a_0}$, The optimal surface area per amphiphile

$\mathbf{l_c}$, The fully extended length of the hydrocarbon tail

The relationship of these parameters ($\boldsymbol{v} / \mathbf{a_0 l_c}$) varies and is dependant largely on the size of the head group and the degree of unsaturation in the tail. For phospholipids in general $\boldsymbol{V} / \mathbf{a_0 l_c} > 2/3$ and the formation of globular and cylindrical micelles is prevented**.** As this relationship tends to infinity the favourability of extended bilayer formation increases. These extended bilayers can fold into lamellae or encapsulate the surrounding solvent to form vesicles.

1.18 The Dynamics of Membrane Environments

Owing to the flexible nature of phospholipids from which the lipid bilayers are constructed and their dynamic nature membranes can adopt a variety of phase structures (Figure 23) These phases have a pronounced effect on the properties for the membrane influencing thickness, fluidity, flexibility, permeability and the motility of proteins embedded in the membrane layer.

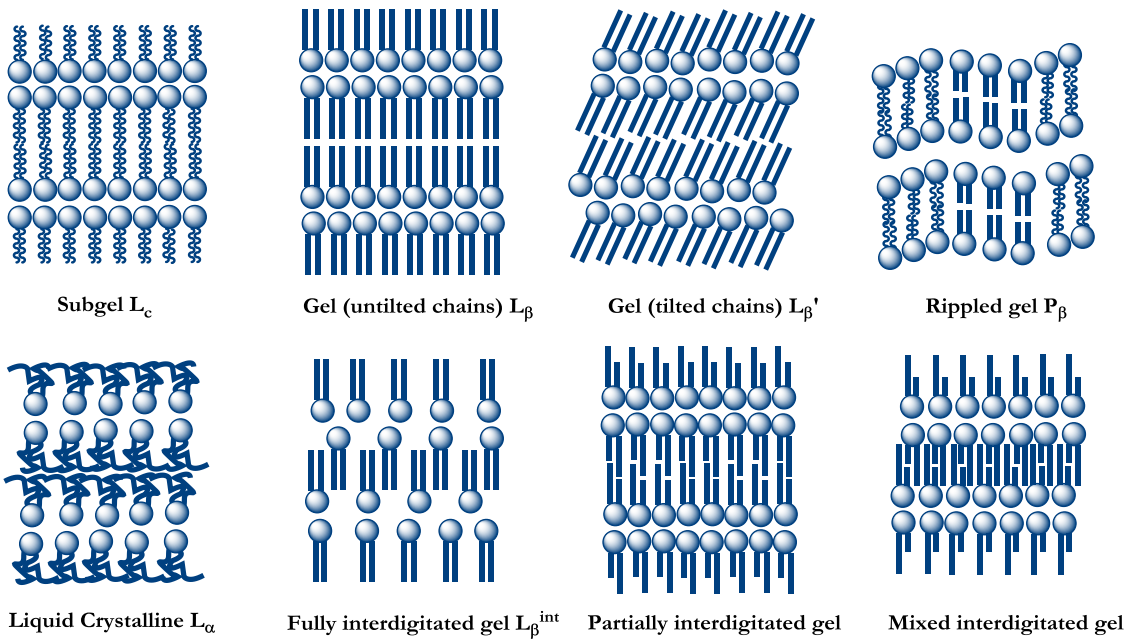

Figure 23 - The phase types of lipid bilayers.[78]

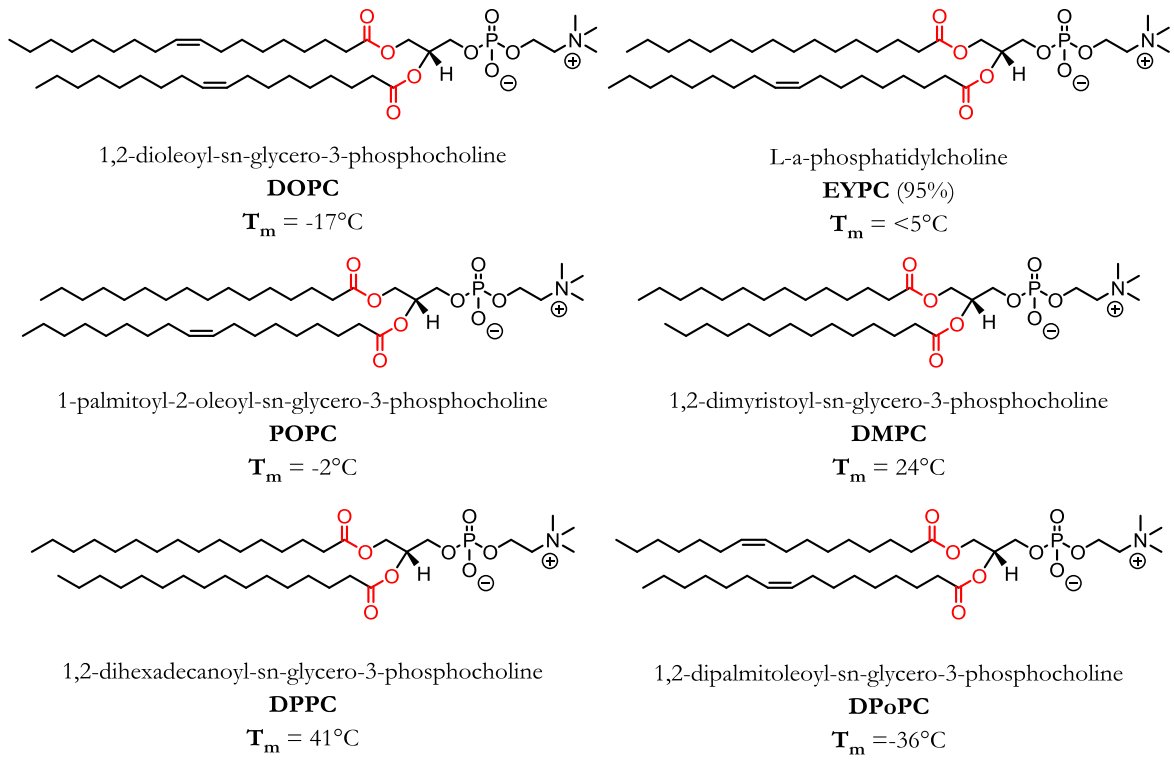

Figure 24 - Commercially available phospholipids (Avanti) and their phase transition temperatures[80]. EYPC is an extract from hen's egg and has variable composition and transition temperature.

The resultant phase of a membrane depends on the composition of its phospholipids: phospholipids with unsaturated hydrocarbon tails pack less effectively than saturated ones (Figure 24) resulting in more fluid phases.

Temperature also has a large effect on the properties of a membrane. A membrane composed of 100% phosphatidylcholine with fully saturated tails will exist as a gel in the solid ordered phase $\mathbf{L_\beta}$, below its transition temperature $\mathbf{T_m}$ (Figure 25A). Each lipid type has an associated transition temperature and can vary greatly depending on the structure of the lipid. If a membrane is heated above its $\mathbf{T_m}$ it forms a liquid crystal $\mathbf{L_\alpha}$ phase (Figure 25B). The mobility of constituent lipids varies greatly across the two phases.

In the $\mathbf{L_\beta}$ phase interactions between the lipid and the surrounding bilayer are high, resulting in low lateral mobility of constituent lipids (Diffusion coefficients: Lipid ~10^{-10} cm^{-2} s^{-1})[81]

The liquid crystal phase has much weaker interactions between lipids resulting in significantly higher lateral mobility (~10^{-7} cm^{-2} s^{-1})[81]. Larger proteins embedded in the membrane, like GPCRs move more slowly (2-5 × 10^{-8} cm^{-2} s^{-1})[77] as they can also be affected by crowding in the membrane.

The transmembrane "flip-flop" of lipids between the inner and outer leaflets (Figure 25C) is far slower due to the repulsive forces that need to be overcome passing a polar head group through the hydrophobic tail region. This movement is still possible but occurs on the order of hours.

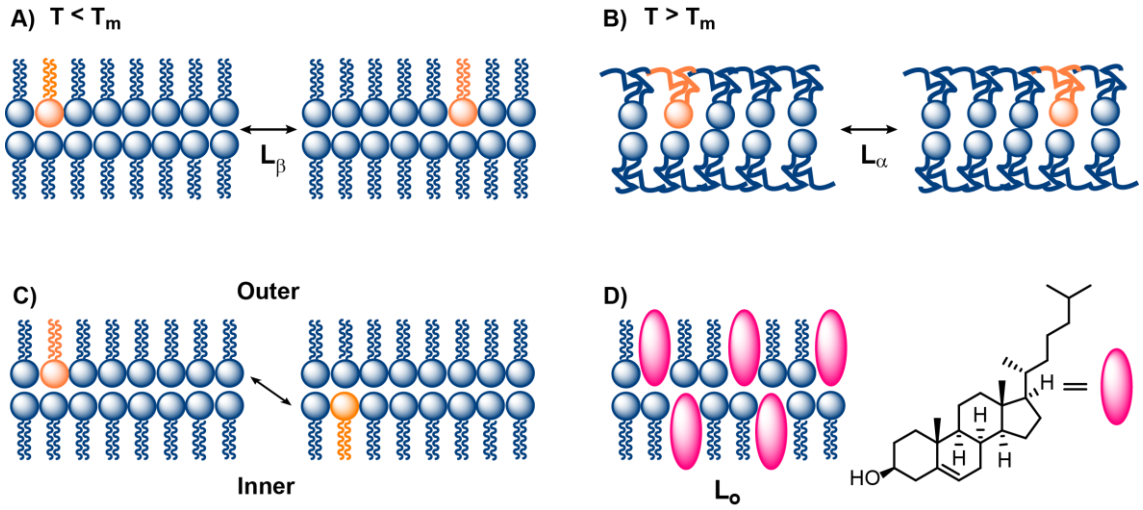

Figure 25 - Motion in membranes: lateral motion in the solid-ordered phase (**A**) lateral motion in the liquid crystalline phase (**B**) transmembrane motion between membrane leaflets (**C**) the liquid ordered phase (**D**).

Cholesterol is a sterol lipid that can be found in concentrations of up to 40% in animal cell membranes.[82] Its presence in bilayers can produce a further phase, the liquid-ordered $\mathbf{L_o}$ phase, similar to the fluid $\mathbf{L_\alpha}$ phase (Figure 25D).

In this phase interactions between the lipid components are enhanced, and the resulting bilayers are significantly stronger. If the fraction of cholesterol exceeds 30% mol/mol, the endotherm corresponding to $\mathbf{T_m}$ disappears[83]

Cholesterol improves both membrane fluidity and strength and can also influence the bilayer thickness. Membrane thickness depends on lipid composition: longer acyl chains give thicker bilayers. Cholesterol can either increase or decrease bilayer width depending on phase and chain length of the phospholipids.

1.19 Vesicles

To fully develop a biomimetic system it will be necessary to investigate the properties of Aib helices within a membrane environment. A variety of methods exist for the synthesis of vesicles from lipids that recreate the environment of the cell membrane while removing the complexity of the living cell. These synthetic vesicles, which are also known as liposomes, are classed depending on size.

Typically, the lipid constituents of the vesicle are first formed into a film (Figure 26). The film is then rehydrated in water or buffer solution. The method used for rehydration has a large effect on the resultant size of the vesicle. Throughout the process, the formation of vesicles should be performed above the $\mathbf{T_m}$ of the constituent lipids. This is because the shear forces required to form the vesicles are far lower for lipids in the liquid crystalline $\mathbf{L_\alpha}$ phase[84]

Small unilamellar vesicles (SUVs; ≤ 100nm) can be formed by the sonication of the lipid film into the surrounding solvent. Large Unilamellar Vesicles (LUVs; 100nm - 1μm) are first vortexed into solution to give a complex mixture of solvated structures. Subsequent extrusion of this mixture through a polycarbonate membrane allows the formation of LUVs of a set size, dependant on the pore size of the polycarbonate membrane.[85]

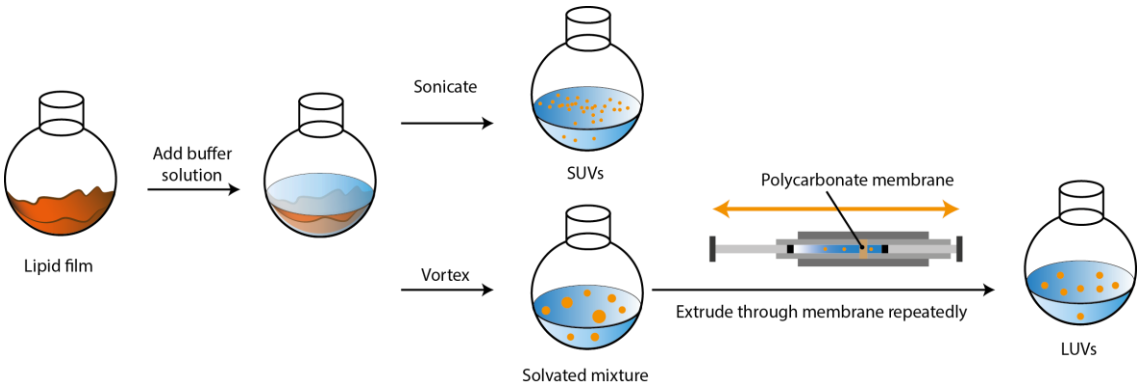

Figure 26 - Formation of small unilamellar vesicles (SUVs) and large unilamellar vesicles (LUVs) from lipid films.

Giant Unilamellar Vesicles (GUVs; 1 - 100μm can be formed in eight principal ways. Of these the most common[86] is the electroswelling method developed by Angelova and Dimitrov.[87] The lipid film is formed on a conducting surface (Figure 27). Once submerged in a bath solvent with a second electrode, a cyclic voltage is supplied to the surface at a temperature above the transition temperature $\mathbf{T_m}$ of the lipid. The power output of the cyclic voltage is increased gradually leading to the formation of GUVs on the electrode surface. Finally a square-waved step voltage is supplied to the surface releasing them into solution.

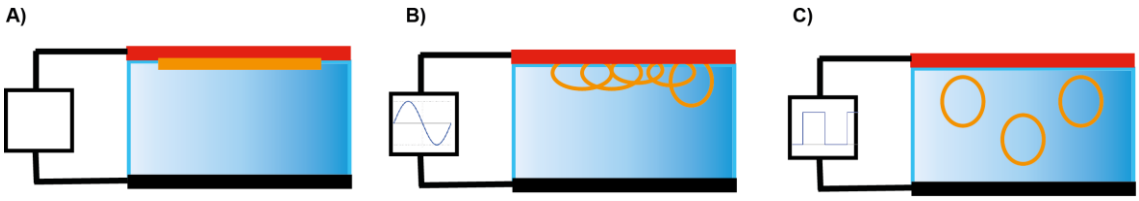

Figure 27 - Electroformation of GUVs. **A**) A lipid film (—) is prepared on a conducting slide (—) and placed in solution. **B**) Application of cyclic voltage to the solution at a temperature above the lipids T_m causes the film to swell. **C**) A square wave at the end of the process releases the GUVs from the conducting surface.

Owing to their larger size, comparable with that of living cells, GUVs offer an excellent cellular model that is easily viewable under a microscope. The original electroswelling method is limited by the requirement for low ionic strength bath solutions during the swelling process, preventing the incorporation of charged species into the GUV or the production of GUVs under physiological conditions. Work by Pott *et al.*[88] improved on the original method, allowing for the use of bath solutions with salinities up to 250mM NaCl or $CaCl_2$, opening the door for the production of GUVs under physiological conditions.

2.0 Overview of Projects

While the developed NMR reporters have proven to be highly effective in probing the conformational state of Aib helices in isotropic NMR solvents a new reporter design is required to probe the helical conformational state of the receptor mimic in a membrane bound situation.

This is due to (1) The masking of the NMR signals from the overlapping micelle lipid signals. (2) Broadening of NMR signals due to slow relaxation times in a membrane environment (3) The relatively low concentration of the receptor mimic within the cell, its signals not only masked but drowned out by the intensity of the micelles own NMR signals.[89]

The design of a fluorometric conformational probe, where a conformational change in the probe is detectable in its fluorescent spectra would offer a solution to these challenges. Providing both the high sensitivity of fluorescent spectroscopy and a greater compatibility with translucent membrane systems. The development of a fluorescent reporter structure is discussed in **Project 1.**

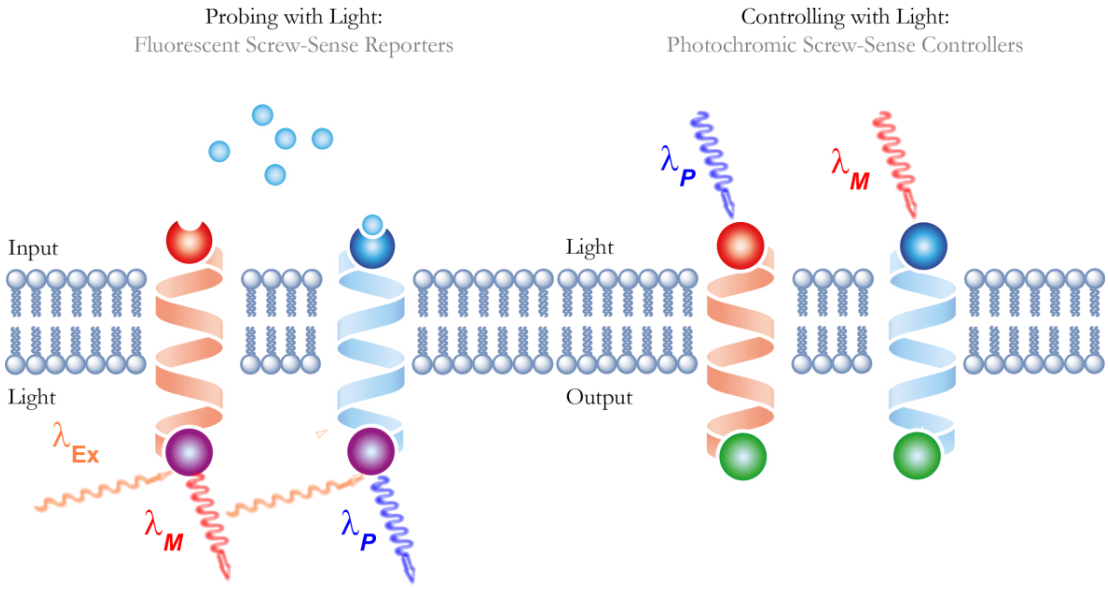

Figure 28 - The probing and control of Aib-based helical systems in membrane environments with light.

The use of a photochemical signal as an input is also highly advantageous in the development of more complex systems. Photochromic controllers can be designed so that their switching behaviour is orthogonal to surrounding biological triggers allowing for the development of bio-orthogonal switching devices in living systems. Work toward the development of a photo-responsive screw-sense controller is further discussed in **Project 2.**

3.0 Project 1 Introduction

3.1 Photophysical Properties of Fluorescent Molecules.

When a molecule in the ground state **F** absorbs a photon of light $h\nu_1$ it forms an excited state **F*.** The energy of a photo-excited molecule can dissipate through a variety of pathways as the molecule relaxes from excited to ground state **F**.

Fluorescence is the observed emission of light that occurs if **F*** relaxes to **F** with the release of a second photon of light $h\nu_2$. Prior to emission the excited state **F*** can relax to lower energy vibrational state. The energy of emitted light $h\nu_2$ is equal to the energy gap between the vibrational energy level of **F*** and **F**.[90]

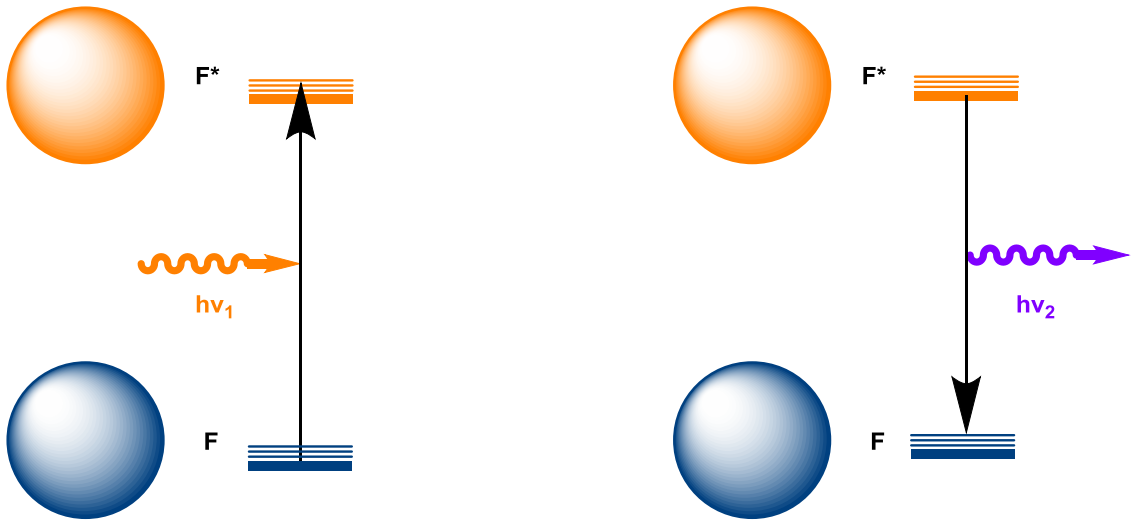

Figure 29 - The photophysics of fluorescent molecules.

The term *fluorescence* was first introduced by G.G. Stokes in 1852[91] to describe light that had been emitted following the absorption of light. In a remarkably simple experiment performed the year earlier he split light into its fractions using a prism. Passing a solution of quinine sulphate through the resulting spectrum he observed that the solution, which remained unchanged in the visible spectrum, glowed when it was placed outside the fringes of the violet visible spectrum.

A fluorophore is a molecule that on excitation to an excited state (for example HOMO-LUMO, nπ-nπ*) undergoes a radiative relaxation back to its ground state. Relaxation of the excited state vibrational levels can led to a Stokes shifted fluorescence signal at a longer wavelength than the excitation wavelength.

In the excited state however a variety of further processes can occur that are specific to chemical attributes within the fluorophore or the local environment in which the fluorophore resides. The presence of a lone pair within or adjacent to a fluorophore

can quench fluorescence by Photoinduced Electron Transfer (PET). Trapping of the lone pair prevents this quenching mechanism, switching on fluorescence. PET systems can be useful in chelation based probing systems, where for example chelation of a metal ion prevents this quenching effect and can be detected by an increase in fluorescence[92] (Figure 30A).

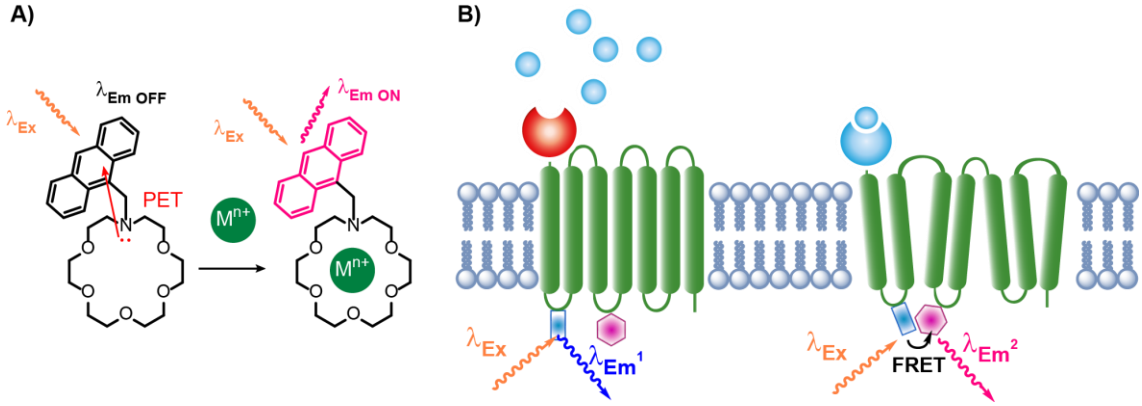

Figure 30A) - The use of PET (Photoinduced Electron Transfer) and **B)** FRET (Fluorescence Resonance Energy Transfer) systems in the fluorescent detection of structural change.

Fluorescence Resonance Energy Transfer (FRET) systems (Figure 30B) make use of two differing fluorophores. Excitation of the first donor fluorophore leads to a radiationless energy transfer to a second acceptor fluorophore with subsequent fluorescence relaxation of the acceptor to the ground state. FRET based systems are governed by: (1) The separation between the donor and acceptor pair. (2) The extent of overlap between the emission spectra of the donor and the absorption spectra of the acceptor. (3) The relative orientation of the respective emission dipole and acceptor moments.

The change in protein conformation and structure can be probed very effectively with a variety of FRET systems. The use of a FRET reporter of protein conformation is depicted in Figure 28B. Binding of a ligand induces a conformational change in the protein structure switching on a FRET system indicated by suppression of fluorescent emission from the donor and a new fluorescent signal from the acceptor fluorophore.[93]

The use of FRET based fluorescence probing systems has had much application in cell biology in cases where the popular green fluorescent protein (GFP) is too large that it disrupts the function of the protein of interest. The protein of interest can be labeled with a far smaller fluorescent dye and investigated with a FRET type interaction between the GFP and non-disruptive dye.[94]

3.2 Excimeric Conformational Probes

Certain fluorophores exhibit an excimeric fluorescence spectrum in addition to fluorescence of the excited momoner. This occurs when an excited state monomer interacts in a specific way with a ground state monomer to form an exited dimer (Excimer). Excimer fluorescence is characterised by a broad peak lacking vibrational structure, with a wavelength of maximum intensity that is red-shifted in comparison to the maximum intensity of the monomer fluorescence.

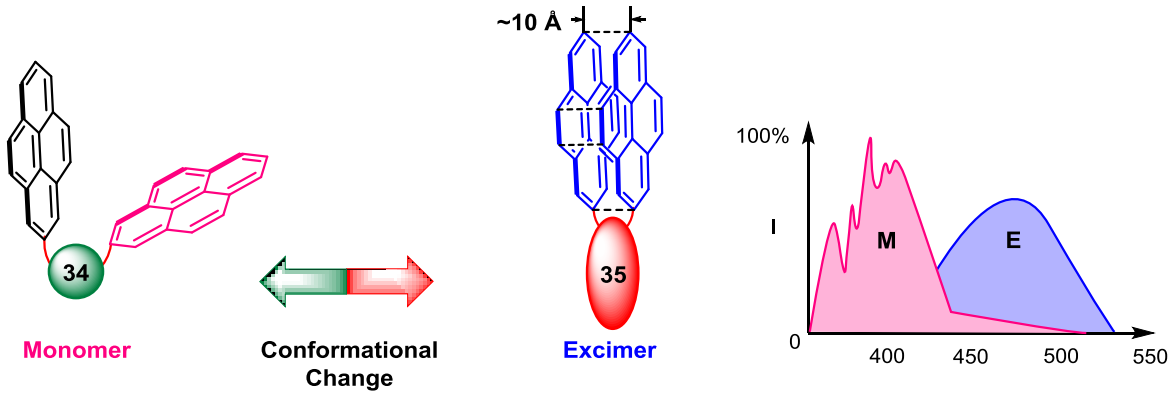

Figure 31 – Photophysical properties of pyrene.

Of the known excimer systems pyrene and its derivatives have been found to be the most effective.[95] The photophysical behavior of pyrene**,** forming an excimer when spatially close to a second pyrene, can be used in a doubly labelled reporter where conformational changes in the reporter (**34** to **35**) are observable as a change in the intensity ratio of excimer (E) to monomer (M) fluorescence: E/M.

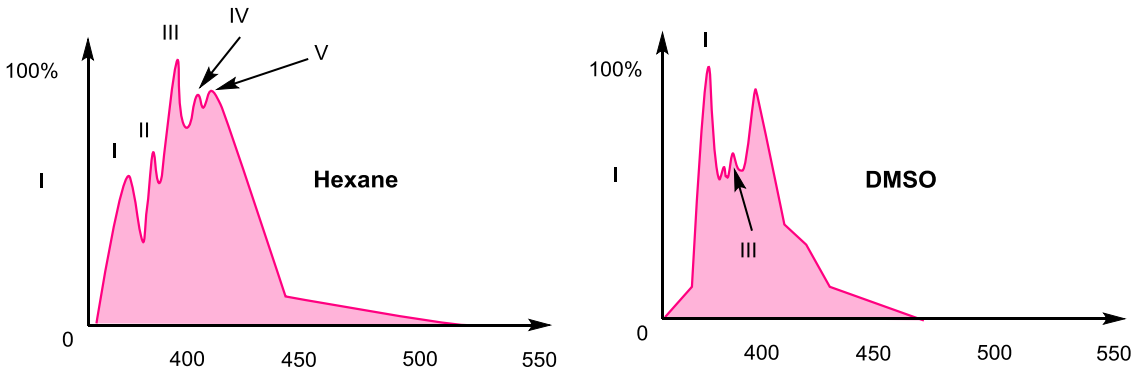

Figure 32 – Photophysical properties of pyrene.[96]

A further advantage to the use of pyrene reporters is their ability to determine the local electrostatic environment of the probes, as changes in local polarity are reflected in changes in the relative intensity of the I and III vibronic bands, the "Py value".[96]

The versatility of pyrene, providing information on both conformation and local polarity has made it highly suitable in a variety of probing systems: In the investigation of enzymatic conformational change.[96] In the functionalisation of oligonucleotide structures, allowing for the probing of DNA conformation, interaction and function.[97,98] In the development of biosensors, where the attachment of pyrene probes to a binding enzyme, couples the high substrate specificity of the enzyme to the high sensitivity of the pyrene label. This allows for a highly sensitive biosensor, indicating the presence of a particular substrate in a complex mixture.[99]

In the membrane environment pyrene has been used to accurately determine critical micelle concentrations and the extent of water penetration in lipid bilayers.[100] Its use in biological membranes[101,102] has provided information on the phase transition and microviscosity. It has also been used to probe lateral diffusion in the hydrophobic region of membranes.[103] Pyrene labelled analogues of phosphatidyl choline lipids have also been designed to probe the dynamics of phosphatidylcholine membranes.[104]

Two exemplary uses of a pyrene *conformational* reporter can be found in the work of Krauss *et al.*[105–107] and the work of Wu *et al.*[108]

Krauss and co-workers attached two pyrene probes with allyl ester linkers in the equatorial positions at one end of a perhydroanthracene (PHA) ring system. To the other end in the axial positions were attached two bis(pyridine) groups. Considering the bis(pyridine) groups as a metal chelate receptor, the system aimed to replicate *conformational* signal transduction via a triple ring flipping of the PHA system

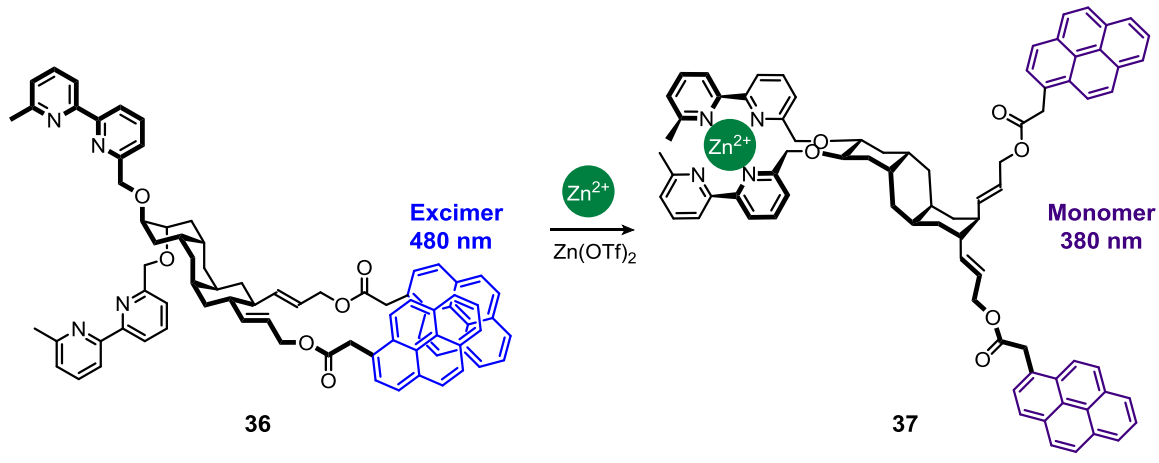

Scheme 4 - Photophysical properties of pyrene.

In solution the isolated structure adopts a conformation **36** with the bipyridine groups axial and the pyrene groups equatorial, their close proximity resulting in substantial excimer fluorescence.

In the presence of a Zn^{II} source complexation by the bispyridine groups led to the triple ring flip in the PHA system. This in turn led to a change in the proximity of the pyrene groups. Increasing Zn^{II} concentration resulted in complete suppression of excimer fluorescence as the chelated conformation **37** predominated.

Wu and co-workers developed the doubly pyrene labelled peptidic probe **38** for the ratiometric sensing of AT vs. GT sequences in a DNA strand. The free probe exists in a folded conformation that promotes excimer formation **39.** On binding to site specific regions in a DNA strand **40** this undergoes a conformational change to an extended structure. This conformational change is reflected in the probes fluorescence spectra, with a change from excimer to monomer fluorescence.

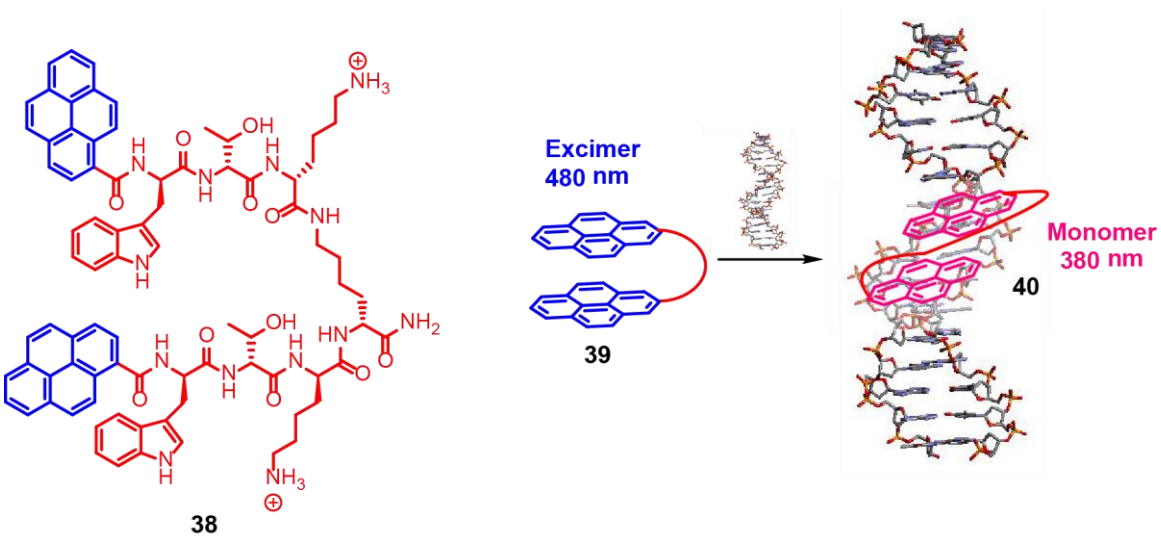

Scheme 5 - Photophysical properties of pyrene.

The ready uptake of the probe by cells and the ability to image DNA strands within cells using the probe in conjunction with fluorescence microscopy further highlights the compatibility and potential of a pyrene based fluorescence probe.[108]

A further advantage in choosing a hydrophobic fluorometric probe is that it may aid in the control of orientation of the receptor mimic, through a self-assembly process if used in conjunction with a polar controlling group.

3.3 Pyrenylalanine

The unnatural amino acid pyrenylalanine (Pya) **41** is an ideal component in the design of a fluorescent conformational probe. Analogous to phenylalanine, the amino acid structure is expected to interact closely with the peptidic backbone of Aib helices.

Synthetic methods for the synthesis of Pya are fairly limited with earliest synthesis of racemic Pya reported in 1941 by Lettre *et al.*[109] and later by the groups of Sisido. De Schryver and Mihara. Sisido *et al.* resolved Bz-Pya-OH **42** by co-crystalisation with optically pure samples of (+)-**43** or (−)-1-phenylethylamine **44** isolating the L-**45** or D-**46** enantiomer respectively.[110] De Schryer and co-workers coupled racemic *N*-Ac-Pya-OH **47** and PyaOMe **48** to form a dipeptide, seperating the erythreo **49** and threo **50** diastereomers of *N*-acetyl bis(pyrenylalanine) methyl ester.[111] Mihara *et al.* isolated enantiomerically pure L-Pya through the enzymatic de-acetylation of racemic *N*-Ac-Pya-OH **47**[112] and by the assymetric catalytic hydrogenation of a dehydro precursor (**51** → **52**).[113] More recent advances report the improvement of the assymetric hydrogenation method[114] and a new route to L-Pya via the nickel complex of a chiral schiff base (**53**→**54**).[115]

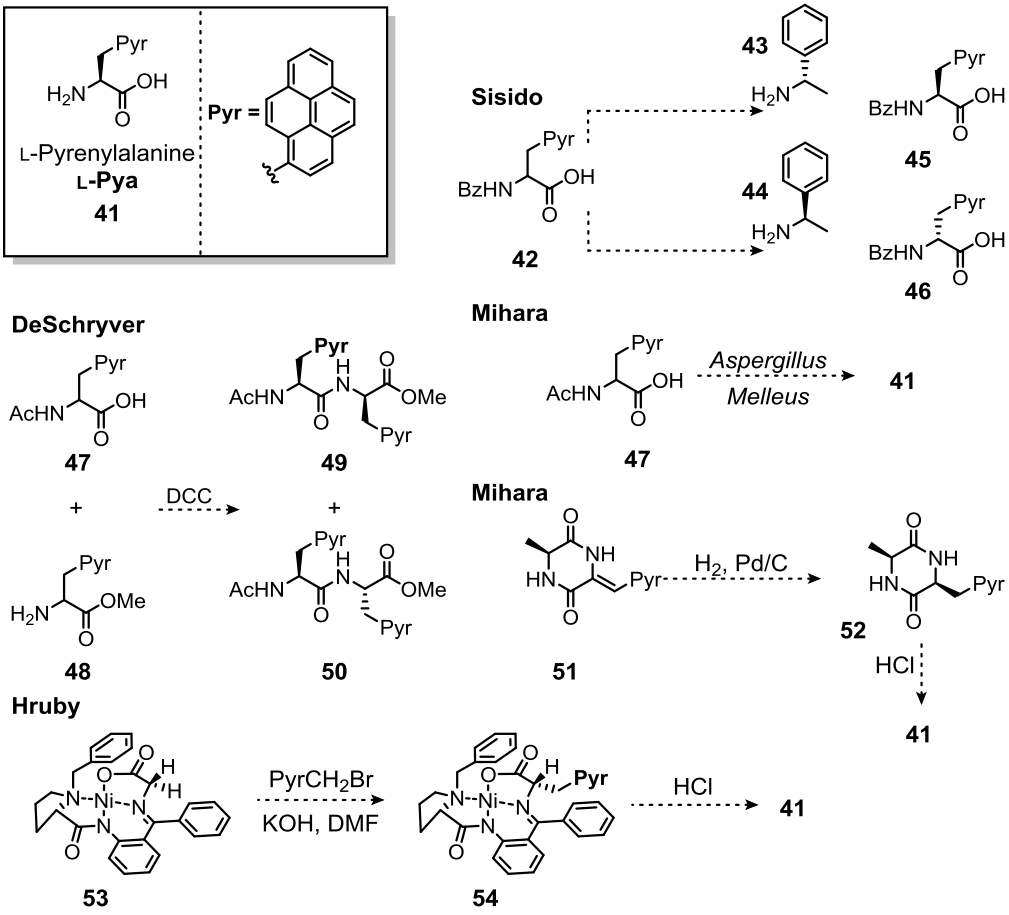

Scheme 6 - Synthetic routes to pyrenylalanine.

The incorporation of two spatially close Pya units into the Aib helix may provide a structure capable of reporting changes in screw-sense preference via changes in E/M fluorescent ratio. Pyrenylalanine has been incorporated into ligands for opiod, cholecystokinin and melanotropin receptors[115] and in synthesis of fluorescent enkephalin analogues.[113] Pya was also incorporated into α-helical segments of a 2-helix[112] and 4-helix[116] synthetic protein bundle highlighting changes in helix proximity with changing solvent composition. It has also been used to monitor protein dynamics through its introduction into a reductase peptide backbone.[117]

Work by Sisido *et al.* investigated the incorporation of Pya into helical structures both as helices poly(1-Pya)[118] and as a bis-Pya label in the backbone of a short α-helical polymer.[119,120] Due to solubility issues, the poly(L-1-Pya) helices were formed as a block copolymer with poly(γ-benzyl-DL-glutamate). They compared helices of poly(1-Pya) with a random co-polymer of poly(LD-1-Pya) using fluorescence, CD and circularly polarized fluorescence (CPF).[120] They found the E/M of the poly(L-1-Pya) to be significantly lower than that of the poly(LD-1-Pya). CD and CPF identified two types of excimer, one at 420-480 nm that they associate with random coil conformations and one at >500 nm the associate with slightly perturbed regions of the helix.[110,118]

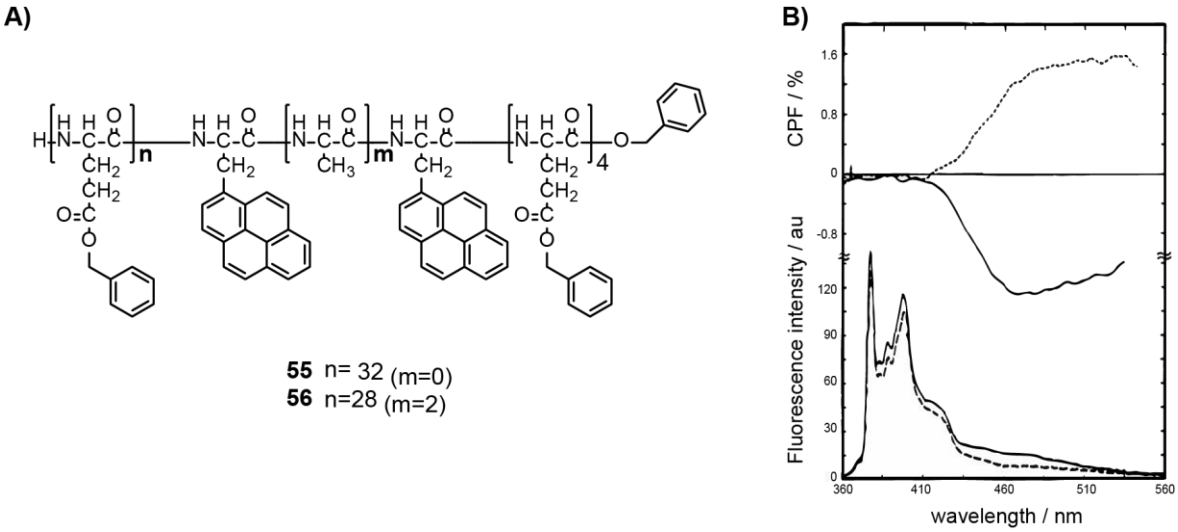

Figure 33 - Probing the dynamics of helical polymers using pyrene.[121]

Sisido and coworkers also used two probe structures incorporating two Pya units at the C-terminus of a polymer of γ-benzyl-L-glutamate in an attempt to probe deformation modes of helical structures (Figure 33). In the first helices the Pya units were adjacent **55** and in the second they were separated by two L-alanine residues **56**. The C-termini of both helices were capped with a $(\gamma\text{-benzyl-L-glutamate})_4$-OBz fragment to stabilise the helix at either side of the probe structure. In both cases a low

excimer was observed, suggesting that the Pya units did not deform the helices and the peptide chain was rigid enough to fix the side chain positions of the pyrene units.[121] This result bodes well for Pya based probes as the residues are controlled by the right-handed α-helix around them. If the screw-sense of the helix could be inverted, as in the Aib helix, perhaps the proximity of the pyrene units would increase leading to greater excimer. A further highly relevant observation by Sisido *et al.* used the helices to investigate the screw-sense of the pyrene excimer using CPF. They found that, while both helices are right handed, the changing proximity of the pyrene units in polymers **55** and **56** gave excimers of differing screw-sense preference. Helix **55** with adjacent Pya units had a negative CPF signal which they assigned as a right-handed excimer whereas **56** with the Ala_2 spacer gave the mirror-image positive signal, a left-handed excimer.[119]

3.4 Bis(pyrenylalanine) Conformational Probes

De Schryver *et al.* have investigated the relationship between intramolecular excimer formation and conformation in their studies of erythreo **49** and threo **50** diastereomers of N-acetyl bis(pyrenylalanine) methyl ester.[111]

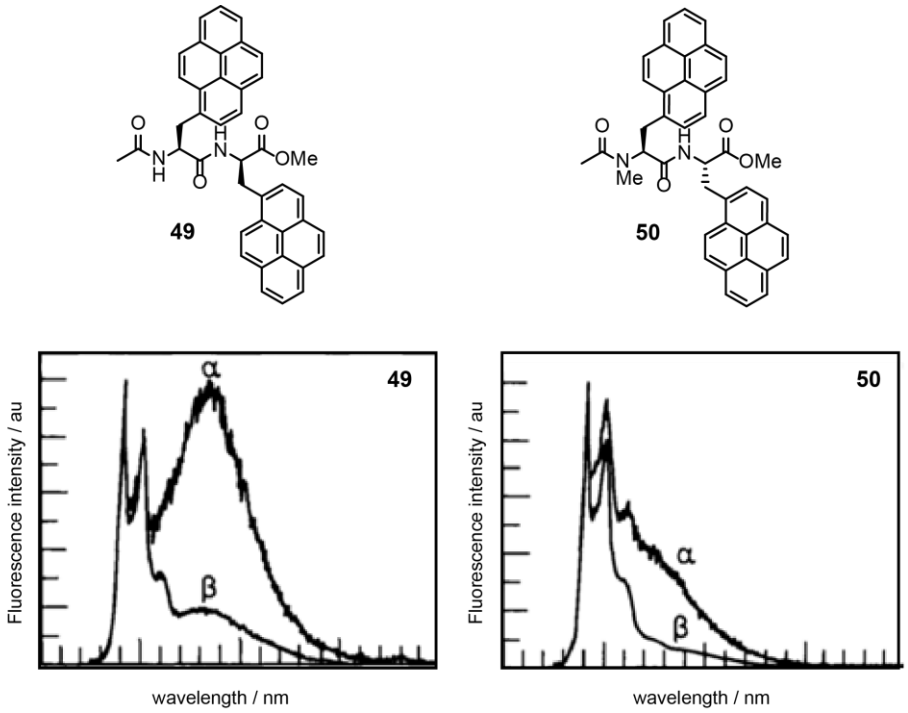

Figure 34 - Observed excimer monomer fluorescence for **49** and **50** in DCM (α) and N,N-dimethyl-acetamide. De Schryvver *et al.* 1984.[111]

Comparing the E/M fluorescence across a range of solvents they found two notable observations. Firstly, a higher E/M ratio was always observed for **49**. Comparing E/M ratios in DCM for example gave E/M = 3 and E/M = 1 for **49** and **50** respectively.

Secondly, they found that the E/M ratio were highly dependent on the hydrogen-bonding properties of the solvent. Hydrogen-bond accepting solvents were found to give lower E/M ratios when compared to non-bonding solvents.

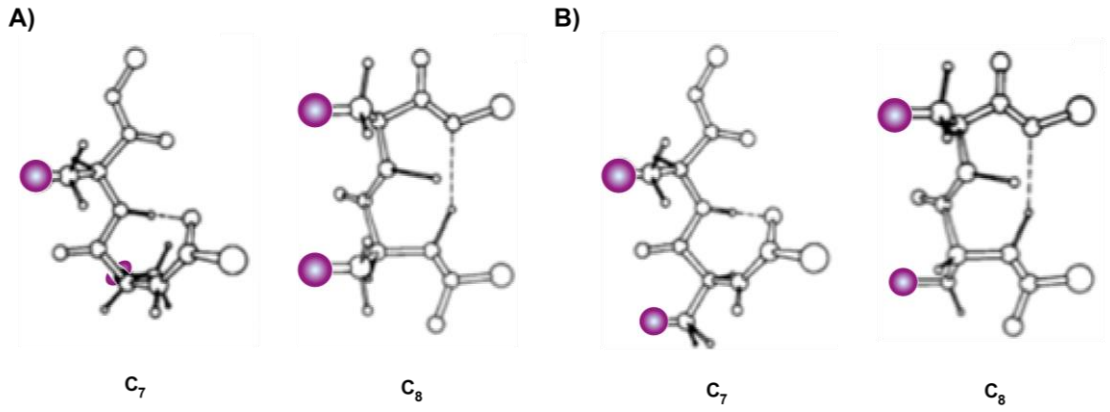

Figure 35 - Proposed excimer forming conformations for **49** (**A**) and **50** (**B**). De Schryver *et al.* 1984.[111]

The proposed explanation for this effect is related to the conformation of the molecule in solution, in non-bonding solvents the molecules are expected to adopt the folded $\mathbf{C_7}$ or $\mathbf{C_8}$ conformations, the $\mathbf{C_8}$ similar to a β-turn (the repeating turn structure of the 3_{10} helix)

These conformations, supported by an intramolecular H-bond, allow the pyrene side chain units, shown in purple, to align to form the excimer. In hydrogen-bond accepting solvents, this intramolecular hydrogen bond is disrupted and random coil conformations, which are not conducive to excimer conformation, predominate.

The observance across all solvents of a higher E/M ratio for the **49** is due to a higher proportion of the molecules adopting a folded state. This greater population of the folded conformation observed in **49** is due to a higher level of unfavourable steric interactions between the bulky pyrene side units in the erythreo random coil conformations.

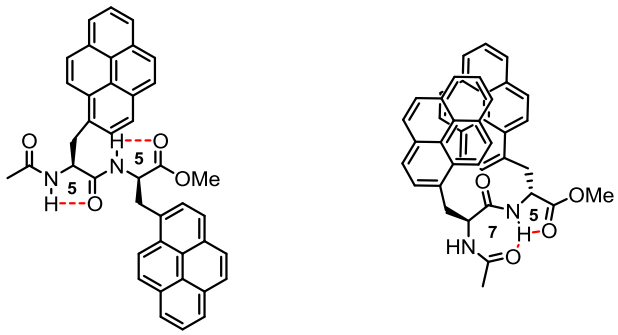

Figure 36 - C_5 and C_7 conformations of **49.**

Further investigation by the group indicated that the *N*-acetyl bis(pyrenylalanine) methyl ester compounds exist in conformational equilibrium between an extended C_5 and folded C_7 states. Of these only the C_7 state placed the two pyrene units in an orientation that permitted excimer formation.

In the C_5 conformation, the distance between the two pyrenyl groups (~7.0 Å) is too large for excimer formation to occur. In the C_7 conformation the distance between the groups is equal to the distance between the two α-carbons which is fixed at 4.5 Å. They note that this is also too large for other aromatic groups capable of excimer interaction that had been the subject of previous studies (3.5 Å) but the long life time of the pyrene excimer allows for the formation of an excimer in this geometry for pyrene side groups. The inability of the pyrene units to form a perfect sandwich geometry results in a hypsochromic shift of the excimer emission maxima to 465 nm for **49** and 455 nm for **50** when compared to the position of excimer maxima observed for intermolecular pyrene excimer interactions at 485 nm.[122]

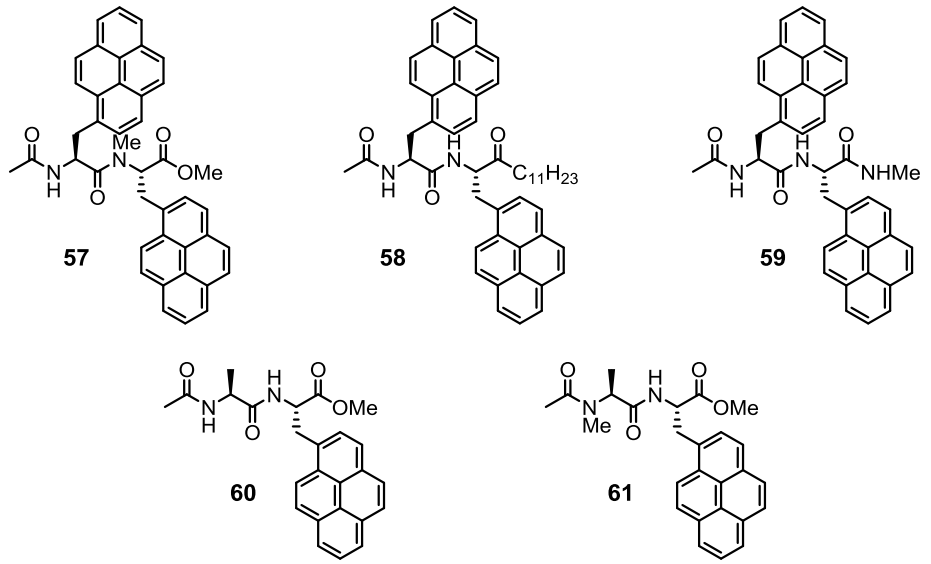

Figure 37 - Pyrenylalanine containing compounds investigated by De Schryver *et al.* 1987.[123]

Having extensively investigated the solvent effects, fluorescent properties and conformational states of *N*-acetyl bis(pyrenylalanine) methyl ester structures **49** and **50** the group proceeded to study more complex structures.[123]

They chose to investigate: the effects of the removal of intramolecular hydrogen bonding interactions, in the synthesis of N-methylated compound **57**, the relationship between main chain and side chain interactions in the synthesis of **58**; the addition of further hydrogen-bonding interactions with in the addition of a C-terminal methyl amide with **59** and the investigation of chain chirality on excimer formation with **60** and **61.**

Of these, the investigation of **59** was of particular interest, as it possessed the hydrogen-bonding network required to form the C_{10} or β turn geometry present in the 3_{10} structure of Aib_n helices.

For the erythro diastereomer they observed a shift in the emission maxima from 450 nm to 465 nm using time resolved fluorescent spectroscopy (Figure 38B) Having previously assigned the peak at 465 to emission from the C_7 excimer, this led them to assign the 450 nm emmision to the C_{10} excimer geometry.

This effect was not observed for the N-terminal amide threo diastereomer presumably because the steric repulsion between side groups prevents the formation of a β-turn.

With their proven ability to form excimer interactions in a variety of compatible solvents, the probe structures developed by De Schryver *et al.* provide ideal targets for the development of fluorescent reporters of conformational helicity.

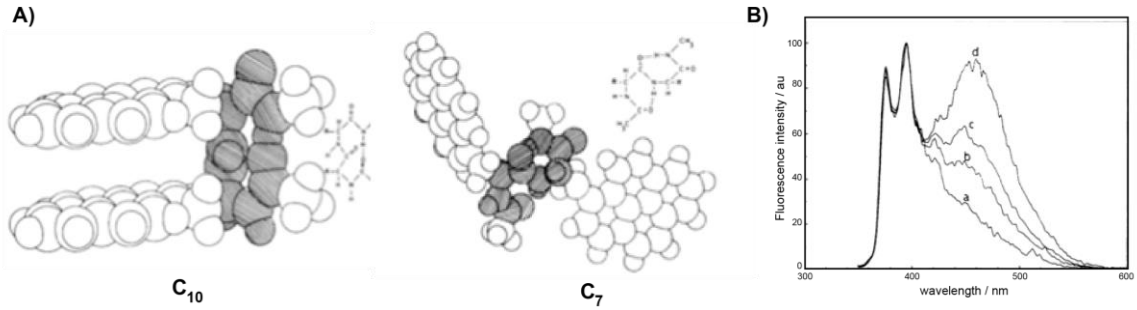

Figure 38A) The C_{10} and C_7 conformations of **59 B**) The time resolved fluorescence spectra of **53** DeSchryver and co-workers 1987.[123]

4.0 Project 1 Aims

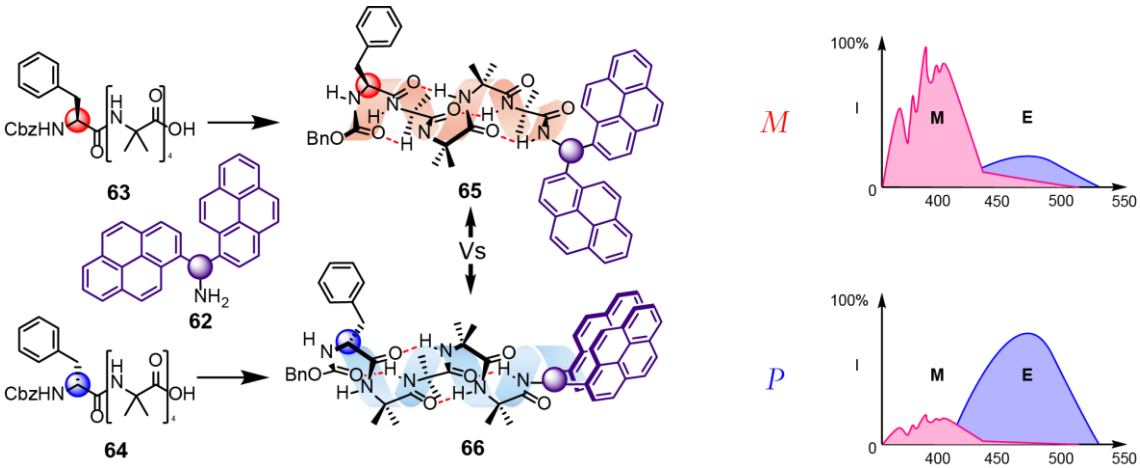

Scheme 7 - Synthetic strategy for the development of screw-sense responsive fluorescent probes.

The main focus of project 1 will look at the development of pyrene based screw-sense responsive fluorescence probes **62**.

To allow direct comparison of other probes previously synthesised in the group the probes **62** will be attached to both L-**63** and D-**64** phenylalanine controlled Aib_4 helical foldamers, which form opposing *M* and *P* helices in solution.[48] Comparing the L-**65** and D-**66** controlled structures, the greater the difference between the E/M fluorescence ratios for **65** and **66**, the better the probe.

The probe needs to be chiral to give different fluorescent responses to the enantiomeric *M*/*P* helices, but the control placed on the screw-sense preference by its own chirality must be minimised, allowing the probe to respond to a secondary chiral influence.

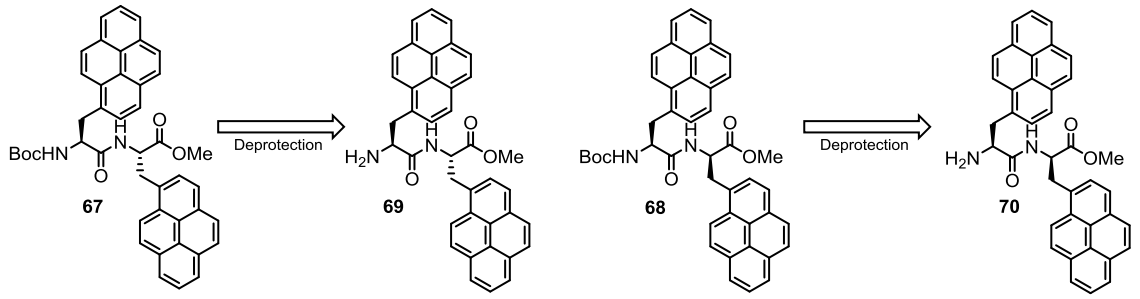

Scheme 8 - Bis(pyrenylalanine) probe targets

The primary synthetic targets for the first generation of probe structures are the Boc protected bispyrenylalanine structures **67** and **68** which, when deprotected to **69** and **70** respectively can be directly coupled to the Phe controlled Aib_4 helical structure. Critical to the synthesis of these structures will be the development of a synthetic route to enantiomerically pure samples of both L-Pya and D-Pya.

5.0 Development of screw-sense responsive fluorescent probes

5.1 Synthesis of Pyrenylalanine

Initial attempts to synthesise pyrenylalanine (Pya) **41** followed the method developed by Sisido and co-workers.[118] This was of particular interest as both the L- and D- enantiomers could be obtained by chiral resolution of a racemic mixture. However, the early stages of their procedure proved challenging due to solubility problems throughout the reaction. The Knoevenagel condensation of 1-pyrenyl aldehyde **71** and hippuric acid **72** lead to the formation of the crude oxazolone **73** as a crude red precipitate. The poor solubility of this precipitate in a range of solvents hindered analysis of reaction completion and purity. Therefore, the crude material was taken forward with the aim of purifying at a later stage.

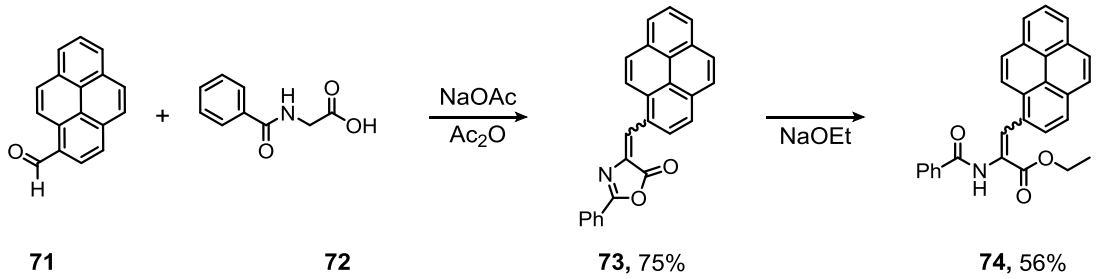

71 **72** **73,** 75% **74,** 56%

Scheme 9 - Synthesis of pyrenylalanine precursors.

The opening of the oxazolone **65** with sodium ethoxide resulted in low yields of the ethyl ester **74** contaminated with unknown aromatic impurities. The problems of both reactions were thought to arise from the unsatisfactory completion of the Knoevenagel reaction. The reaction mixture was highly viscous and maintaining homogeneity in the reaction was particularly challenging. Returning to an earlier method for the synthesis of **73**[109] the starting materials were finely ground together prior to the reaction, Furthermore, increasing the number of equivalents of NaOAc to 10, prolonging the reaction time to 3 days, and leaving the vessel open to air to allow loss of water resulted in a good yield of oxazolone **73**.

Ethoxide cleavage of the crude oxazolone formed from this method proceeded smoothly to give the ethyl ester **74** in 56% yield. An impurity formed in the hydrogenation step (Scheme 10) particularly hampered progress of the synthesis of **75**. Its co-elution in a wide range of solvent systems prevented purification by flash chromatography. Crystallisation in a variety of solvent systems was also attempted but found to be unsuccessful. Eventually, it was found that performing the hydrogenation at room temperature, in a 1:1 mixture of EtOH:EtOAc led to the lowest ratio of impurity to product. Repeated precipitation of the crude mixture from DCM using 40-60% petroleum ether was found to remove the impurity, affording the pure *N*-benzoyl-DL-1-pyrenylalanine ethyl ester **75** in 79% yield. Finally, cleavage of the ester in sodium hydroxide gave the free acid **42** in quantitative yield.

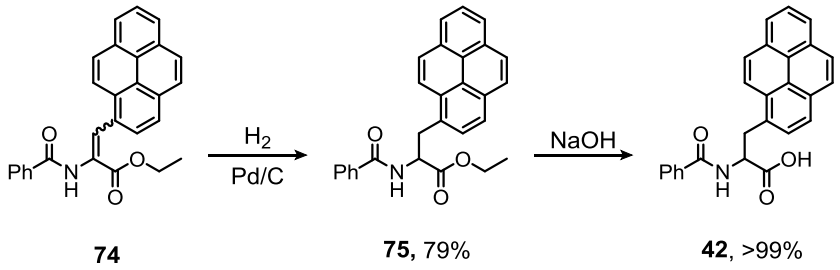

Scheme 10 - Synthesis of N-benzoyl-DL-pyrenylalanine.

With *N*-benzoyl-DL-1-pyrenylalanine **42** in hand, the next step was the separation of the enantiomers **45** and **46** by chiral resolution with optically pure α-methyl benzylamine.

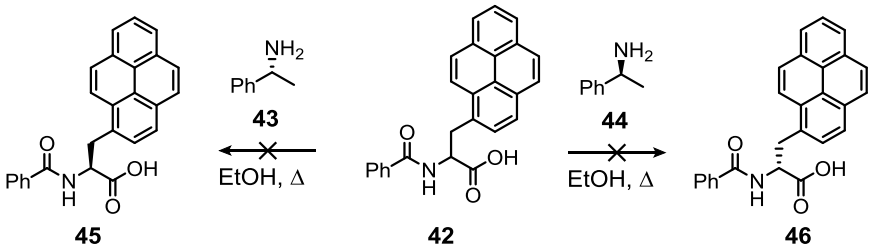

Scheme 11 - Chiral resolution of pyrenylalanine.

The crystallisation did not proceed smoothly, the quality of crystals obtained was poor and long waiting times were required for appreciable crops of crystals to be formed. $[\alpha]_D$ values obtained for the crystals indicated the resolution was unsuccessful. The unsatisfactory nature of the crystallisation method lead to its abandonment and prompted further investigations into the alternative methods for the synthesis of pyrenylalanine.

5.2 Enzymatic Route to Pyrenylalanine

Helpful discussion with the authors* of the crystallisation method[110] highlighted an enzymatic method for the synthesis of L-pyrenylalanine that could be further developed to give D-pyrenylalanine

1-pyrenemethanol **76** was converted to 1-bromomethylpyrene **77** in good yield using phosphourous tribromide. Subsequent reaction with diethyl acetamidomalonate **78**, followed by a 1-pot ester cleavage and decarboxylation gave *N*-acetyl pyrenylalanine **79** in 78% yield over three steps. The use of the acylase enzyme was critical in the isolation of unprotected L-pyrenylalanine **41** giving the target compound as a precipitate in 30% yield. It was found that the D enriched mother liquor of the reaction could be acidified and extracted with DCM to give the D enriched *N*-acetyl-pyrenylalanine, Column chromatography returned 33% of the pure *N*-acetyl-D-pyrenylalanine **80** which was de-acetylated under acidic conditions to give D-Pya.HCL **81** in 95% yield

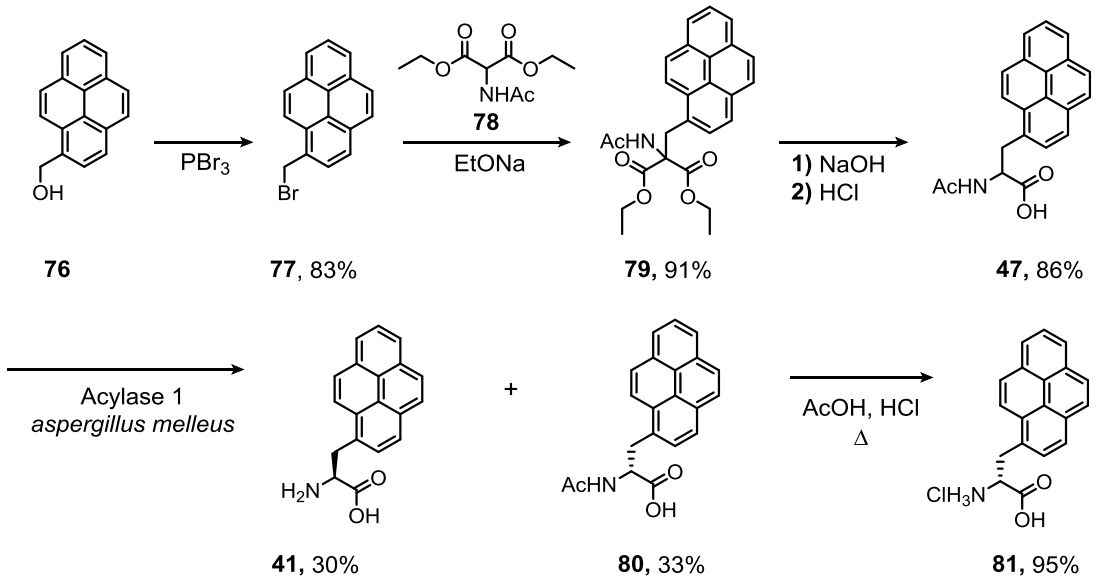

Scheme 12 - Enzymatic route to pyrenylalanine.

* Private Communication, Prof. Masahiko Sisido, Okayama University

5.3 Synthesis of Pyrenylalanine Derivatives

With samples of L- and D-pyrenylalanine in hand, the next stage of the strategy involved the preparation of suitably protected derivatives, to allow the synthesis of the desired pyrenylalanine dimers **67** and **68**. L-Pya **41** was converted to both Boc-L-Pya-OH **82** and L-Pya-OMe **83**, both in good yield. The HCl salt of D-Pya **81** was converted to the methyl ester **84** in reasonable yield.

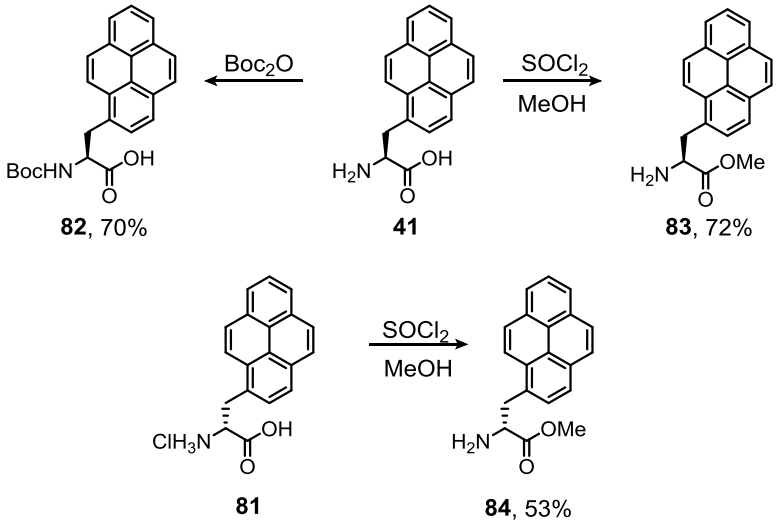

Scheme 13 - Synthesis of pyrenylalanine coupling partners.

5.4 Development of HPLC Method

An HPLC method was sought to determine the enantiopurity of the pyrenylalanine produced in the enzymatic reaction. The racemic *N*-acetyl pyrenylalanine used as a feed stock for the reaction was chosen as a starting point for method development. However, poor peak separation was observed for the racemate on the Whelk, ADH and ODH columns eluting with a solvent gradient of 10-30% IPA in hexane over 30 minutes.

Protection of the racemic acid as its methyl ester resulted in an improvement of peak separation. It was found that when eluting with a solvent ramp of 1-25% IPA in hexane over 40 minutes using the ADH column allowed for baseline separation of the D- and L- enantiomers

Analytical samples of the methyl esters **83** and **84** were acetylated and analysed using the developed HPLC method. The enantiopurity of the *N*-acetyl pyrenylalanine methyl ester samples was found to be 97:3 and 90:10 for the L- and D- derivatives respectively (Figure 39).

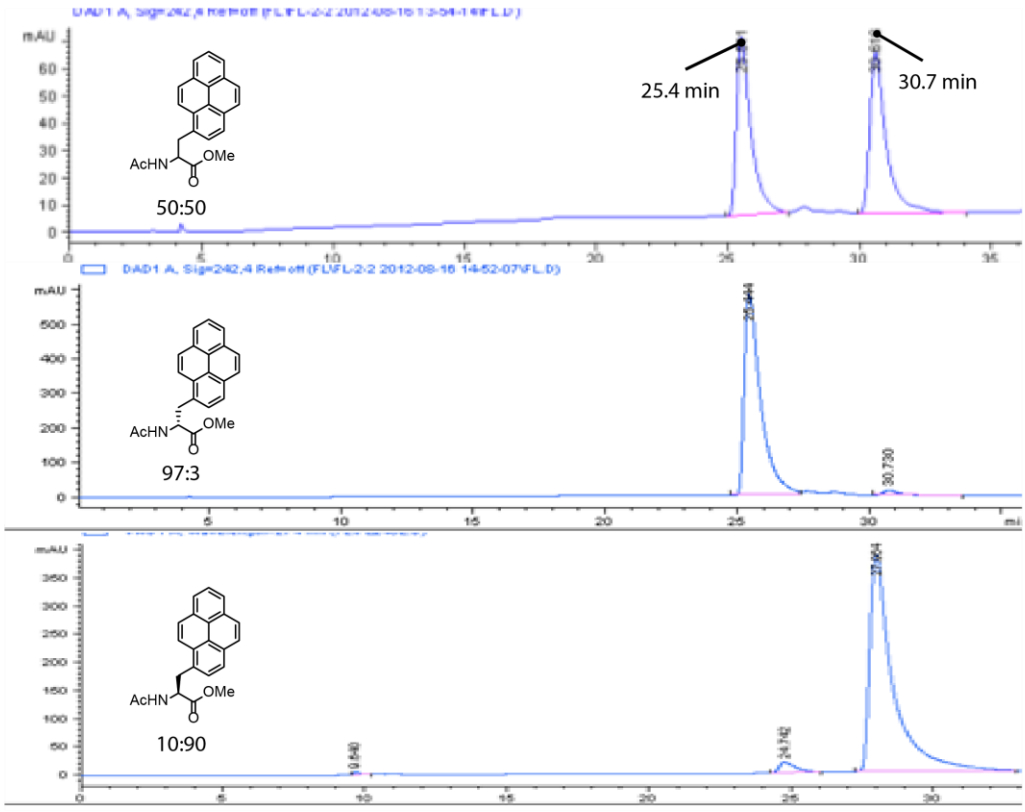

Figure 39 - HPLC analysis of racemic and chiral samples of *N*-acetyl-L-pyrenylalanine methyl ester: 1-25% IPA in Hexane over 40 minutes; flow rate 1 mL/min; ADH column; 242 nm.

5.5 Synthesis of 1st Generation Probes

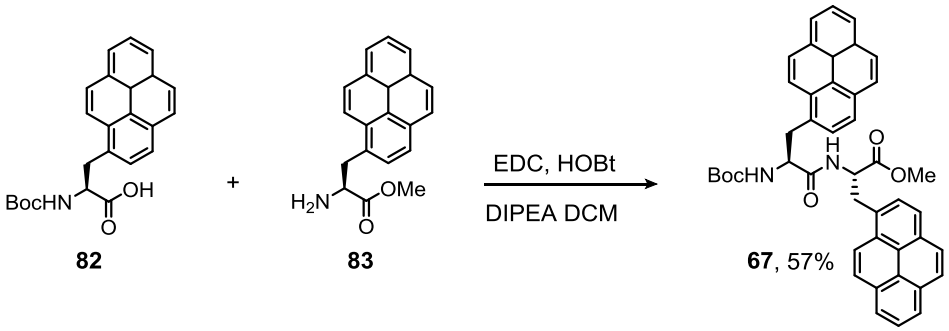

Scheme 14 - Synthesis of *N*-Boc-L-Pya-L-Pya-OMe.

Having confirmed the enantiopurity of the pyrene monomers, *N*-Boc-L-Pya-OH **82** was coupled to L-Pya-OMe **83** to give *N*-Boc-L-Pya-L-Pya-OMe **67** in a 57% yield after repeated purification by column chromatography was required to remove a close-running impurity.

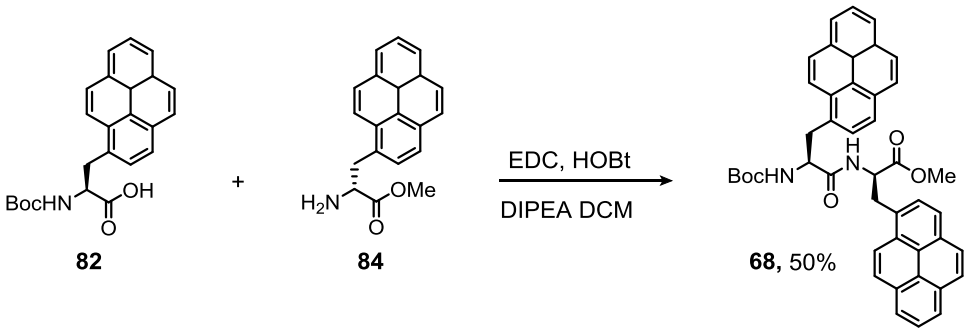

Scheme 15 - Synthesis of *N*-Boc-L-Pya-D-Pya-OMe..

Coupling of *N*-Boc-L-Pya **82** with D-Pya-OMe **84** gave 50% of *N*-Boc-L-Pya-D-Pya-OMe **68**. A crude fluorescence analysis of the Boc protected **67** and **68** (Figure 40) showed promising results, particularly for the L,D probe structure **68**.

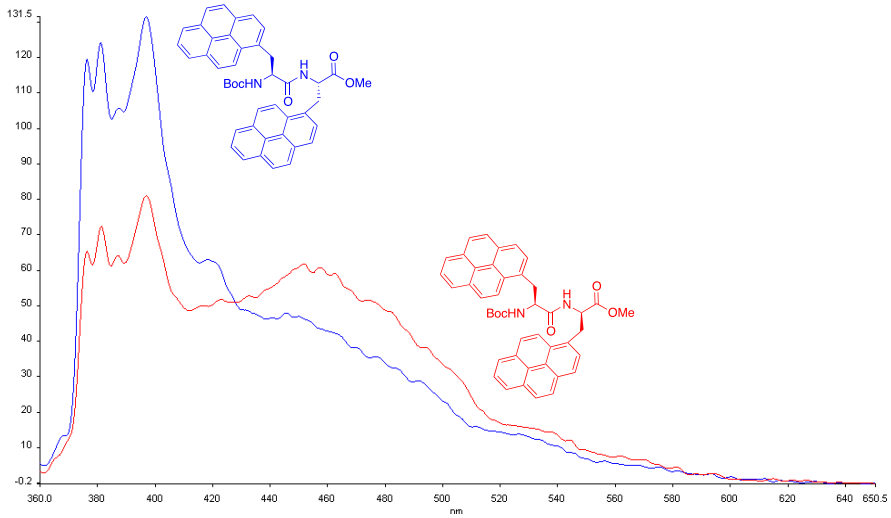

Figure 40 - Fluorescence analysis of **67** (Blue) and **68** (Red).

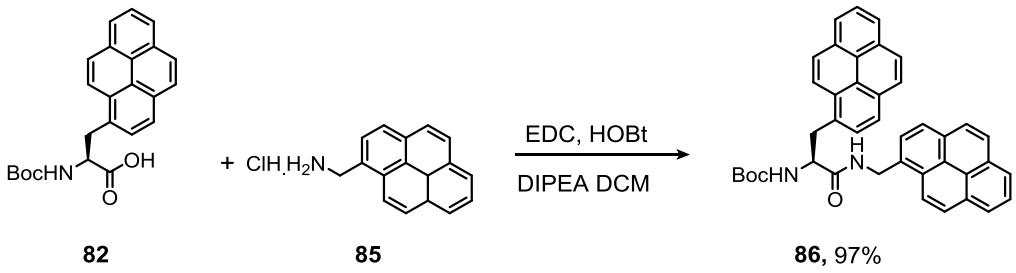

Scheme 16 - Synthesis N-Boc-Pya-CH_2-Pyr.

During the development of probes **67** and **68** a third, structurally related probe structure was designed incorporating the chiral fragment of Boc-L-Pya **82** and commercially available pyrenylamine hydrochloride **85.** Coupling these fragments with EDC gave *N*-Boc pyrenylalanine pyrenyl amide (*N*-Boc-Pya-CH_2-Pyr) **86** in excellent yield.

5.6 Synthesis of Aib Helices.

The next stage of the project was to investigate the fluorescence behaviour of the first generation probe structures when attached to the C-terminus of Aib oligomers. A successful probe structure should, on attachment to Aib helices of different screw-sense preference produce an observable difference between the E/M fluorescence ratios for the *M* and *P* screw-sense helix. An achiral unit comprised of four Aib residues was chosen, as it is the shortest length required to form a complete helical turn. Carboxybenzyl phenylalanine (Cbz-Phe) was used as the N-terminal controlling residue as optically pure samples of both enantiomers are commercially available and the controlling effect of the Phe residue on the Aib_4 helix is known from previous research using NMR probes.[48]

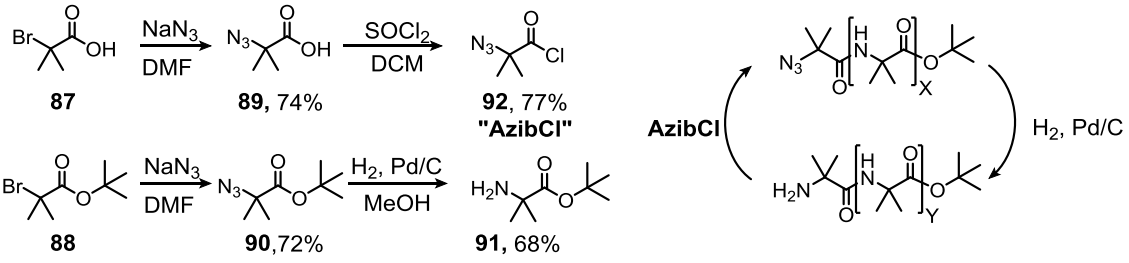

Scheme 17 - Synthesis of the Aib helix building block and iterative synthetic cycle used to build helices.

The synthesis of the Aib_4 fragment began with the conversion of α-bromo isobutyric acid **87** and tert-butyl 2-bromoisobutyrate **88** to their azido analogues **89** and **90**. Reduction of α-azido tertiary butyl isobutyrate **90** gave the C-terminal

building block of Aib oligomers, α-amino tertiary butyl isobutyrate **91**, in good yield. α-Bromo azido acid was converted to the reactive acid chloride (AzibCl) **92** and used immediately with **91** to form **93** in a satisfactory yield. Iterative reductive (X⟶Y;**94**, **96**) and coupling with freshly prepared AzibCl **84** (Y⟶X; **95, 97**) gave the reduced H-Aib$_4$-OtBu fragment **98**

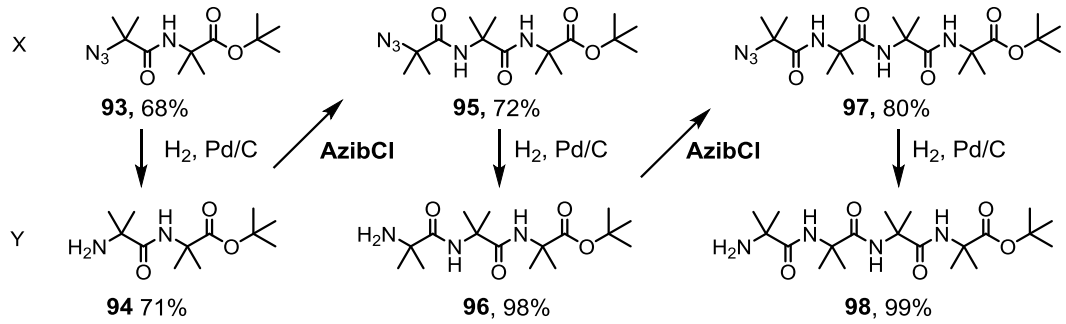

Scheme 18 - Synthesis of the Aib$_4$ tetramer

5.7 Synthesis and Analysis of 1st Generation Probes

The controlled peptides required for the analysis of the probe structure were obtained through the coupling of Cbz protected L-**99** or D-**100** phenylalanine with the tetrameric amine **98** to give the L-**101** and D-**102** controlled pentameric fragments respectively. Trifluoroacetic acid deprotection gave the L-**63** and D-**64** Cbz-Phe-Aib$_4$-OH helices required for coupling to the probe structures.

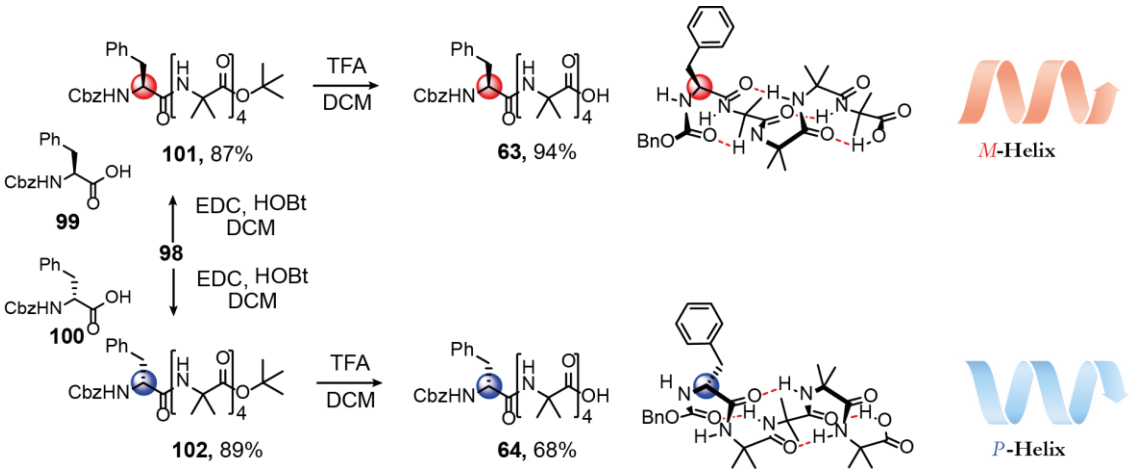

Scheme 19 - Synthesis of L- and D- of phenylalanine controlled helices.

In preparation for their attachment to Aib helices (Scheme 20), the Boc protecting groups of the probe structures **67**, **68** and **86** were removed using TFA. The solubility of the corresponding TFA salts and the neutralised amines were found to be very poor in useful solvents, with impurities detected by TLC. After attempting to isolate and purify the free amines of **67**, **68** and **86** it was decided to couple them directly to the helix, purifying after a two-step de-protection and coupling protocol.

For the Boc-L-Pya-L-Pya-OMe probe **67** coupling to the helical peptides **63** and **64** proceeded smoothly giving Cbz-L-Phe-Aib$_4$-L-Pya-L-Pya-OMe **103** and Cbz-D-Phe-Aib$_4$-L-Pya-L-Pya-OMe **104** in 74% and 84% yields respectively. On de-protection, the trifluoroacetic acid salt of NH-L-Pya-D-Pya-OMe probe **68** was particularly insoluble. A mixture of DCM/DMF basified with DIPEA was required for its dissolution. Adding the amine solution to the activated samples of L-**63** and D-PheAib$_4$OH **64** gave the desired structures **105** and **106** in moderate to good yields. Finally, the L-pyrenylalanine pyrenyl amide probe **86** was also de-protected and coupled in an identical fashion to the L-Pya-D-Pya-OMe probe giving the structures **107** and **108**, ready for fluorescence analysis.

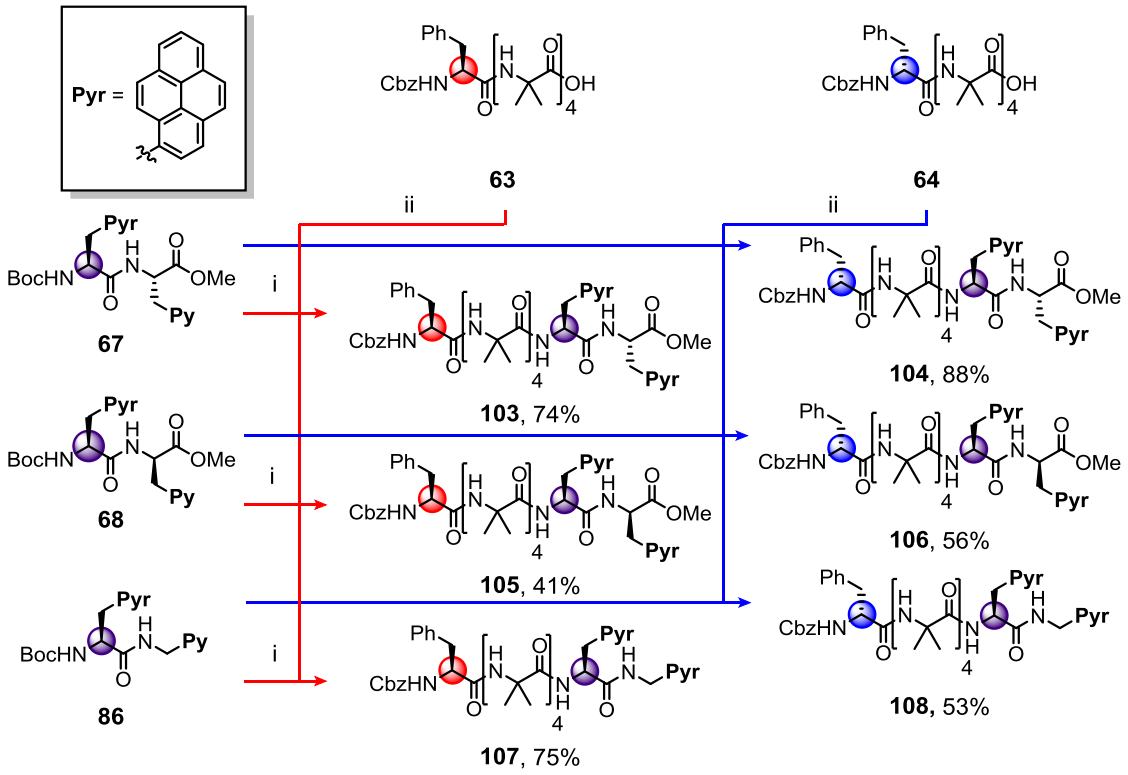

Scheme 20 - Coupling of 1st Generation probes to phenylalanine controlled helices. i, TFA/DCM. ii, EDC, HOBT, DIPEA, DCM

5.8 Fluorescence Analysis of 1st Generation Probes

The fluorescence spectra of the first generation probes (Figure 41) lacked any observable excimer fluorescence preventing the comparison of excimer to monomer ratio for each set of L vs. D controlled peptides. The lack of excimer implies that the distance between the two pyrene groups is too great to form an excimer. Both this and the controlling influence of the chiral probe structure were investigated in the development of further probe structures.

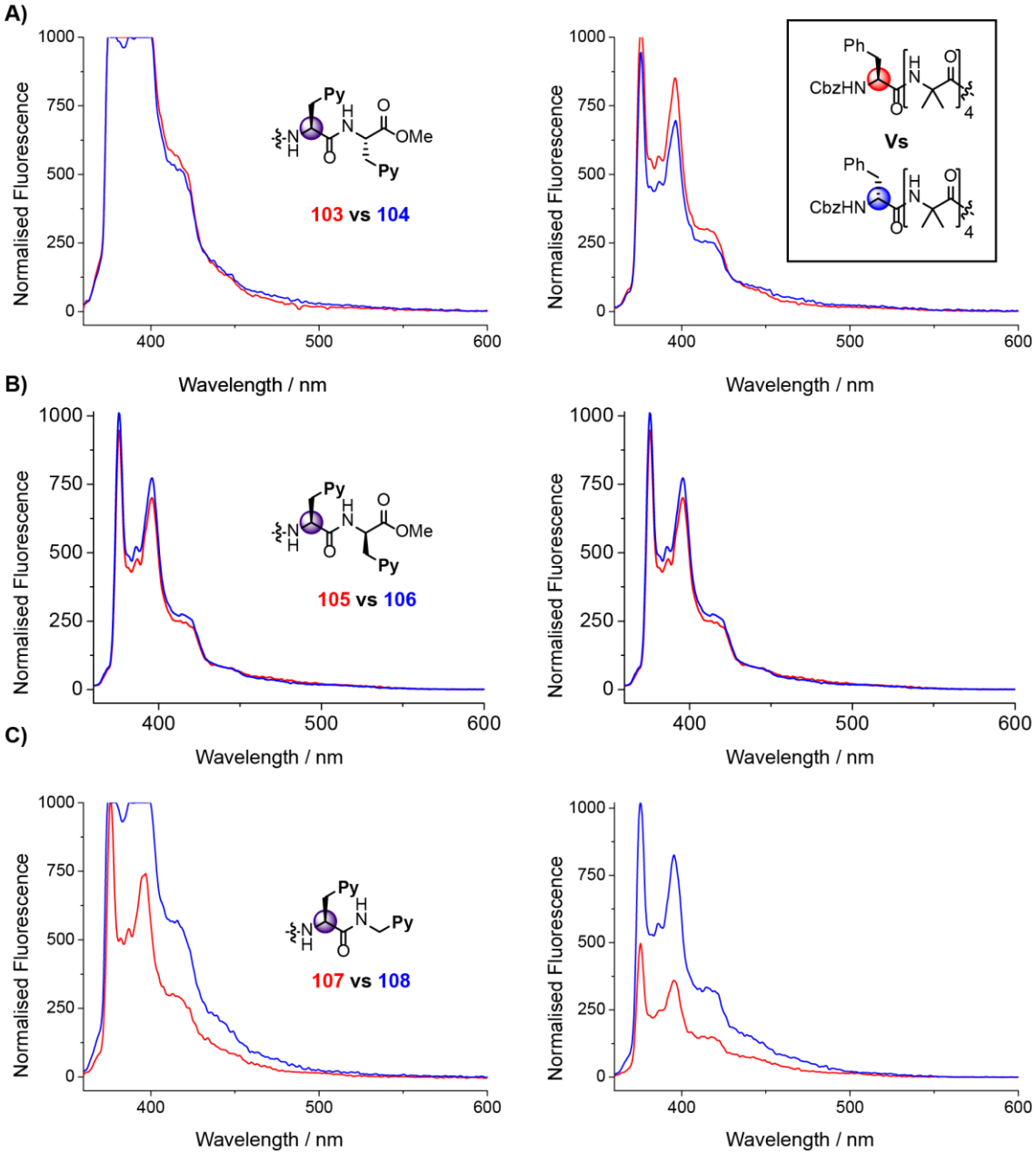

Figure 41 - Comparative fluorescence of probe structures **67, 68** and **86** attached to Cbz-L-PheAib$_4$-(**103**,**105**,**107**) or Cbz-D-PheAib$_4$-(**104**, **106**, **108**) scaffolds. Measurements performed at 20μM concentration in DCM (LHS) and MeCN (RHS).

5.9 A Problem of Control: 2nd Generation Probes

At this stage it was apparent that the pyrenylalanine structures were not successful candidates as fluorescence C-terminal screw-sense reporters. It was thought that the most likely reason for this is that the chiral influence of the probe was out-weighing any controlling influence delivered from the N-terminus by the Phe residue.

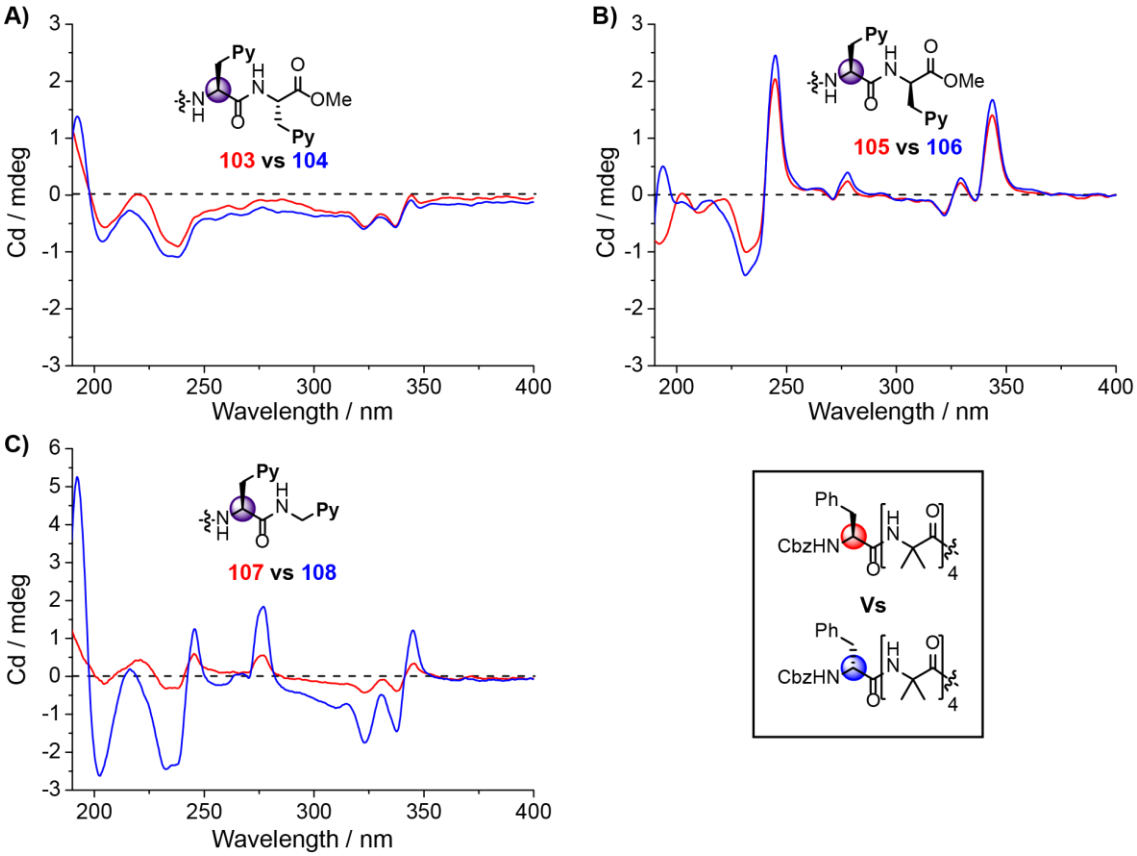

Figure 42 - CD spectra for compounds **103** vs **104** (**A**) **105** vs **106** (**B**) and **107** vs **108** (**C**) (20 μM) MeCN.

Circular dichroism spectra observed for the first generation probe structures were found to match in sign for a particular probe structure rather than the expected screw-sense of the helix to which they were attached. (Figure 42). As helices of opposing screw-sense preference should give mirror image CD spectra, this suggests that screw-sense preference control delivered to the helix is being dominated by the chiral influence of the probe structures.

The CD spectra for bis-Pya probe structures **67** and **68** were near identical despite differing control from the N-terminus. This suggests that the C-terminal amide structure with two chiral residues was greatly overpowering the control delivered from the N-terminus.

5.10 Crystal structure of Cbz-L-Phe-Aib$_4$-L-Pya-NHCH$_2$Pyr

An X-ray crystal structure obtained for L-Phe-Aib$_4$-L-Pya-NHCH$_2$Pyr **107** supports the findings from the CD data indicating that even the probes containing only one pyrenylalanine residue as the C-terminus enforce enough C-terminal control on the helix to overpower N-terminal control from the phenylalanine residue.

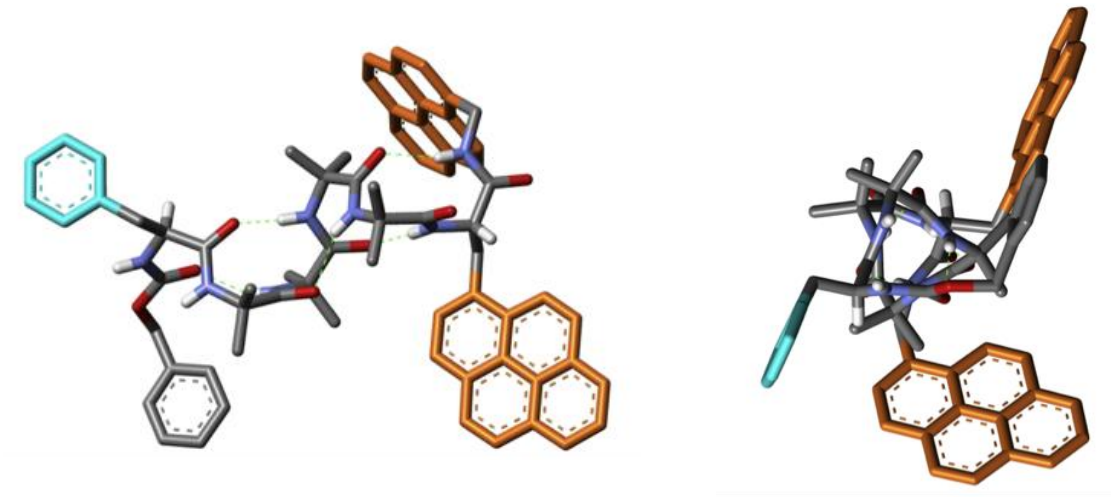

Figure 43 - X-ray crystal structure of L-Phe-Aib$_4$-L-Pya-NHCH$_2$Pyr **107** showing side on right handed helix (obtained from $CDCl_3$). Expected screw-sense for L-Phe controller is left handed.

As the Cbz-L-Phe residue is known to induce a left-handed screw-sense preference when placed at the N-terminus of an Aib helix[48] the crystal structure of Cbz-L-Phe-Aib$_4$-L-Pya-NHCH$_2$Pyr **107** was expected to be left-handed. Observation of the opposite, right-handed screw-sense preference indicates that even a single Pya residue is sufficient to dictate screw-sense preference.

The hydrogen-bonding interaction between the amide linkage of the probe structure and the carbonyl of the third Aib residue is of particular note. This interaction is likely to exist for all three of the first generation probe structures and is highly likely to contribute to the controlling nature of the probes by rigidifying the final turn and reinforcing control on the helix.[124]

The crystal structure also offers an explanation for the lack of excimer fluorescence observed. If the conformation of the peptide in solution resembles that in the solid state, the pyrene groups are too far apart for an excimer forming interaction to occur.

5.11 Synthesis of 2nd Generation Probes

As both CD and X-ray data obtained from the first generation probes indicated the probe structures were dominating control of screw-sense preference efforts were made to design a probe structure that exerted a lower level of control on the conformational preference of the helix.

It was thought that removal of the C-terminal NH bond (Figure 44; yellow highlight) present in all of the first generation probe structures might reduce the control on the helix induced by the probe.

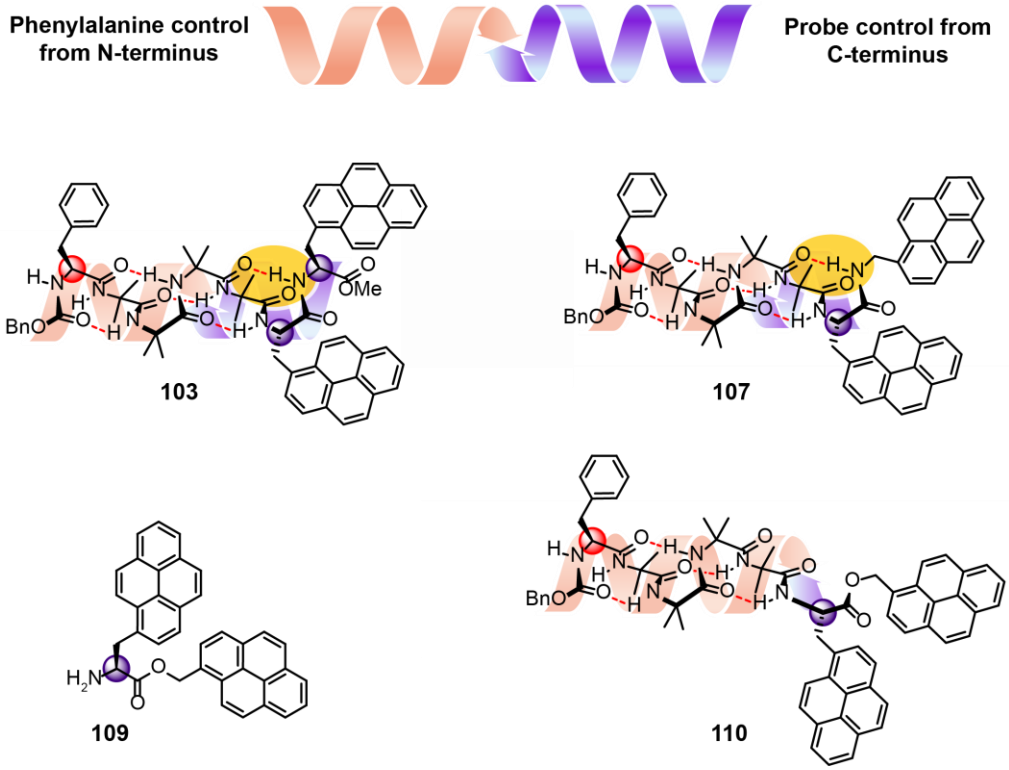

Figure 44 - Considerations in the development of 3rd Generation probe. The response of the probe is the result of competing chiral influences from the controller (red) and the probe (purple) Removal of the C-terminal NH (yellow) present in 1st and 2nd generation probes may reduce the control delivered by the probe.

The pyrenylalanine pyrenyl ester target **109** was of high interest as it was structurally analagous to the Pya-NH-Pyr probe **86** yet lacked the NH bond **110**, allowing for a direct structural comparison with the 1st generation probes.

Coupling of Boc-Pya-OH **82** to commercially 1-pyrenemethanol **77** was performed using standard peptide coupling conditions to give the ester **110** in 81% yield.

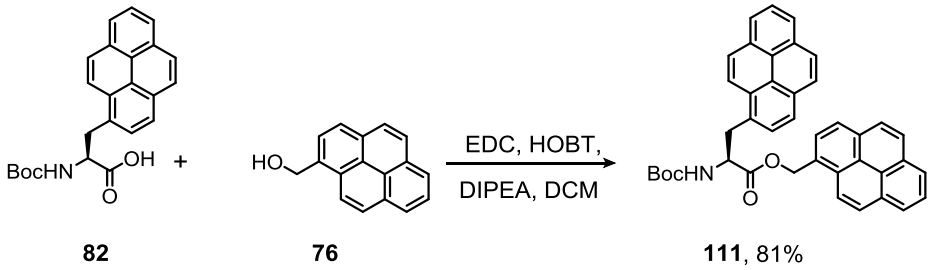

82 **76** **111**, 81%

Scheme 21 - Synthesis of pyrenylalanine pyrenyl ester probe.

Initial attempts to couple **111** with L-**63** and D-**64** were unsatisfactory, with poor yields and purity. Additionally, preliminary fluorescence on the crude products **113** and **112** gave no excimer. In light of the superior results of the 3rd generation probes, attempts to resynthesize and confirm the negative fluorescence results were abandoned.

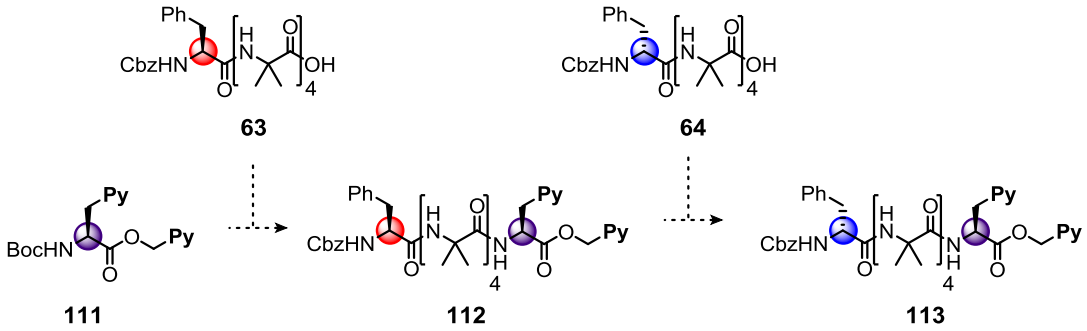

Scheme 22 - Abandoned route to test pyrenylalanine pyrenyl ester probe.

5.12 Development and Synthesis of 3rd Generation Probes

A methodology developed by Jik Chin and co-workers provided a straightforward synthetic route to a new core structure for a potential 3rd generation pyrene probe.[125] Their research made use of a parent diamine **114** that, on mixing with 2 equivalents of aldehyde **115** forms a diimine **116** which undergoes a [3,3]-sigmatropic rearrangement to **117**. The driving force of this reaction is the H-bond interactions between the hydroxyl groups of the parent diamine **114** and the nitrogens of the rearranged imine **117**, which stabilise the rearranged product. Cleavage with aqueous HCl in THF gives a new pure *S,S* diamine structure **118** in high purity as a dihydrochloride salt. Both *R,R* and *S,S* parent diamines are commercially available and can be used in the synthesis of a variety of desirable amine structures. The parent diamine structures give daughter amines of inverted stereochemistry (*R,R*→*S,S*; *S,S*→*R,R*), which occurs during chair transition state **119** of the [3,3] sigmatropic rearrangement (Scheme 23).

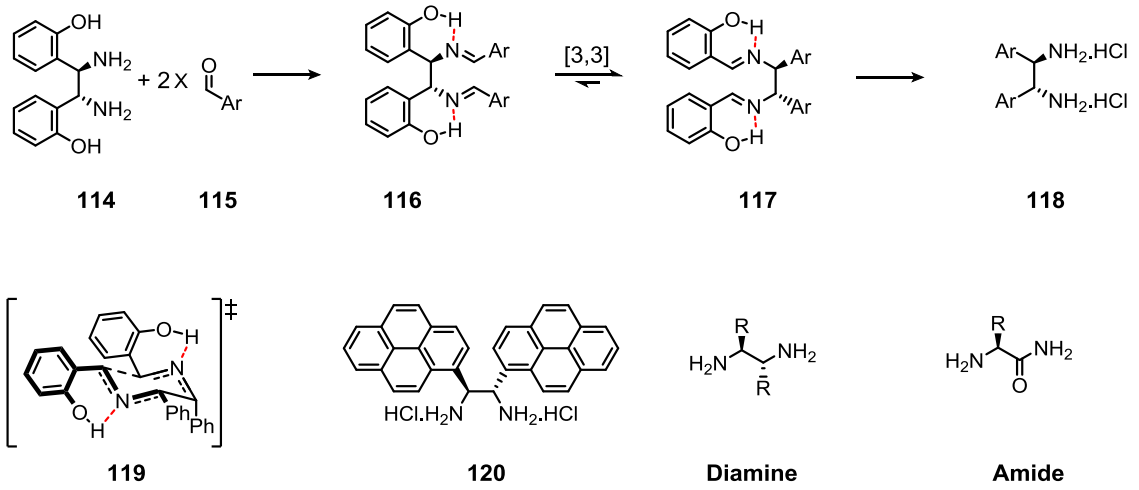

Scheme 23 - *S,S* diamine synthesis developed by Jik Chin and co-workers. Chair transition state of [3,3] sigmatropic rearrangement. Target probe structure and structural comparison with earlier amid probes.

The potential advantages of the new target diamine probe structure **120** are apparent when compared to the amide structure of the pyrenylalanine probes. Firstly, the chance of intramolecular excimer is increased by the closer proximity of the pyrene groups. Secondly, the loss of the hydrogen-bonding carbonyl and the altered configuration both have the potential to reduce control delivered to the C-terminus from the probe.

Following the method outlined by *Chin et al.*[125] 1-pyrenylaldehyde **71** was mixed with (1*R*,2*R*)-1,2-Bis(2-hydroxyphenyl)ethylenediamine **114** in DMSO. After three hours the solution is poured into water, causing the crude diimine to precipitate. This is dissolved in THF and reacted with HCl to give analytically pure (1*S*,2*S*)-1,2-(1-pyrene)ethylenediamine dihydrochloride "*S*,*S*-BisPyrEt" **120** in an 85% yield.

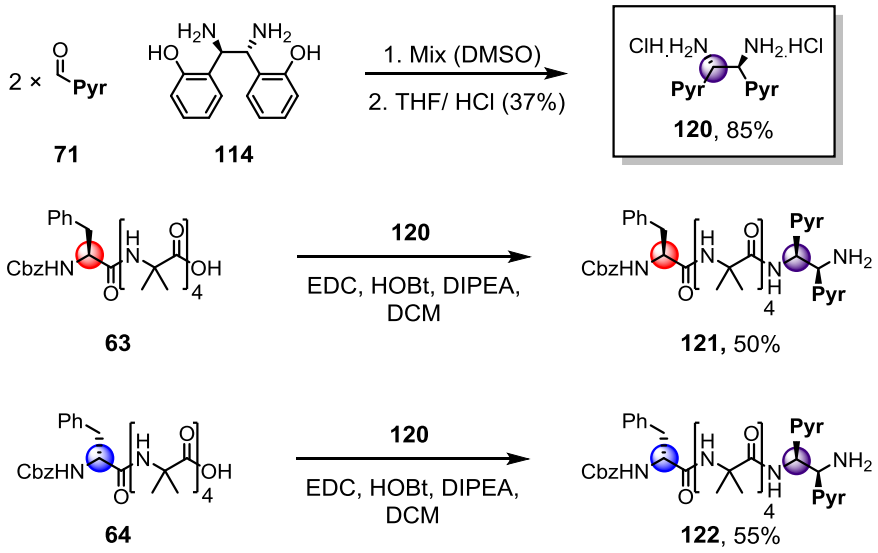

Scheme 24 - Coupling of diamine probes.

With the new *S*,*S*, bis-pyrene structure ready for use, it was coupled to L-Phe **63** and D-Phe **64** controlled Aib_4 helices following the protocol used for the earlier generations of pyrene probes. As the diamine **120** has two amine positions, there was a possibility that a second Cbz-Phe-Aib_4-OH helix could attach to the second amine. This was thought to be unlikely due to the steric bulk of the first helix after attachment. Excess probe **120** (1.5 equivalents) was used in the initial experiments to further reduce the possibility of secondary coupling of the acid. This strategy was successful giving **121** and **122** in 50 and 55% yields respectively. It should be noted that previous attempts to synthesise **121** and **122** had resulted in decomposition. Therefore, care was taken to store these and related compounds in the dark at −5 °C when not in use.

5.13 Fluorescence Spectra of 3rd Generation Probes in Solution

Fluorescence measurements of structures **121** and **122** were obtained over a range of concentrations (10, 5, 2.5 1.25 µM). The observed excimer fluorescence had the potential to arise from either an intermolecular or intramolecular interaction of pyrene groups. Only the intramolecular excimer relates to conformational changes in the bis-pyrene probe. Observation of concentration independent E/M ratios for both **121** and **122** indicate that both ratios are related to the intramolecular interactions of the bis-pyrene probe and therefore the screw-sense preference of the helix.

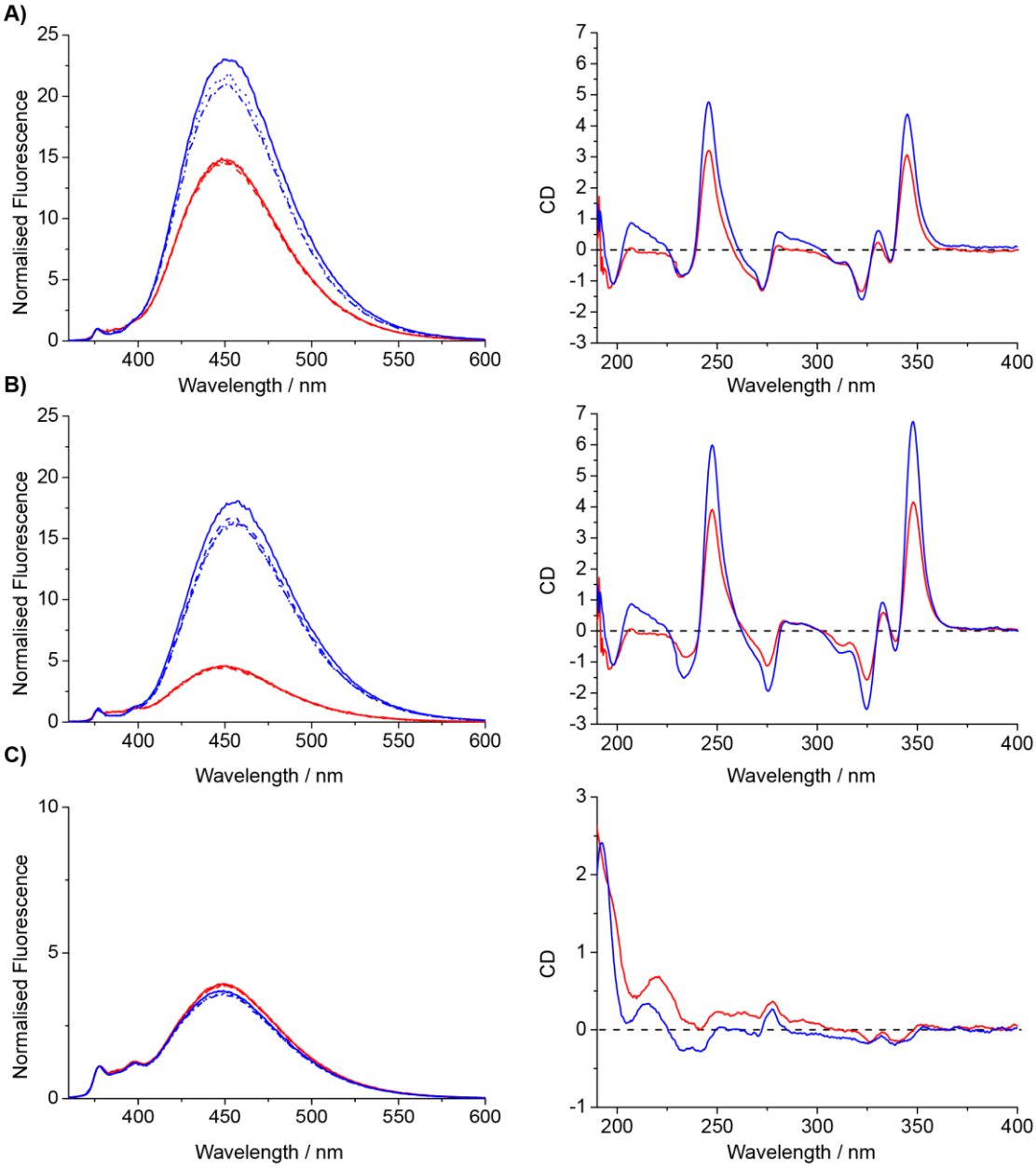

Figure 45 - Fluorescence spectra and circular dichroism of compounds **121** (red) and **122** (blue) in MeOH (**A**) MeCN (**B**) and DCM (**C**). Fluorescence measured at 10 µM (——) 5 µM (— — —) 2.5 µM (— ▪ —) and 1.25 µM (▪▪▪) concentrations and normalised to 377 nm.

In comparison to the earlier probe structures, differing fluorescence results for the *S*,*S*-BisPyrEt **120** structure when attached to the Cbz-L-Phe controlled *M*-helix **121** or the Cbz-D-Phe *P*-helix **122** were greatly improved (Figure 45). Normalising the fluorescence of individual spectra to their monomer peaks (377 nm) allows for a simplified read-out. With normalised spectra, a successful probe structure will give a minimal difference in fluorescence signals over the concentration range and a large difference between the excimer fluorescence for the *M*-helix and the *P*-helix. Any helix with expected *M* screw-sense preference is coloured red, and any helix with expected *P* screw-sense preference is blue. This colour coding is maintained throughout.

5.14 Solvent Dependence of the *S*,*S*-BisPyrEt Amine Probe

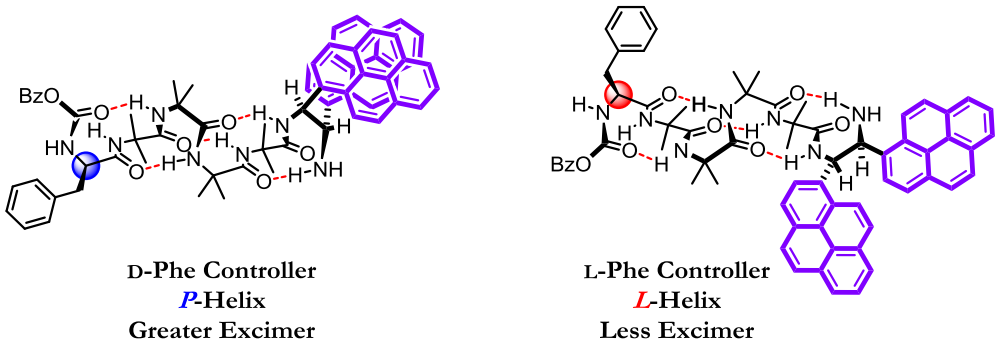

Figure 46 - Proposed conformations of the *S*,*S* BisPyrEt-NH2 probe in M and P helices

Looking at the performance of the probe in MeOH (Figure 45 A)and MeCN (Figure 45 B) a large difference between the *M*- and *P*- helix is observable indicating a highly successful probe structure. The change in E/M ratio across the concentration range is slight for the *M*-helix and negligible for the *P*-helix. Both are insignificant when compared to the much larger E/M difference in E/M for the opposing screw-sense preferences.

Curiously, there is negligible difference between the normalised *M* and the *P* fluorescence ratios in DCM (figure 45C). The reasons for this solvent dependant behaviour may be related to the localised solvent interactions with the pyrene groups in the probe. In polar solvents, the pyrene groups are forced to stack together forming a sandwich. (Figure 47) Changing screw-sense preference in the helix changes the conformation of the probe and the proximity of the pyrenes in the sandwich leading to and observable difference in E/M ratio. In DCM the solubility of the pyrene groups is higher and stacking less prevalent, resulting in an orientation that is less responsive to changes in screw-sense preference.

The lower E/M ratios observed in DCM (Figure 45C) support this, indicating the pyrenes are not stacking as heavily as in the other solvents.

A further reason for the difference in E/M ratio across the solvent range is related to competing control. In the polar solvents, the control delivered by the phenylalanine residue clearly out-weighs C-terminal control delivered by the chiral *S*,*S*-BisPyrEt **120** structure. In DCM perhaps the balance of control between the two chiral influences is changed, and the screw-sense preference of the helix is no longer effectively controlled by the phenylalanine residue.

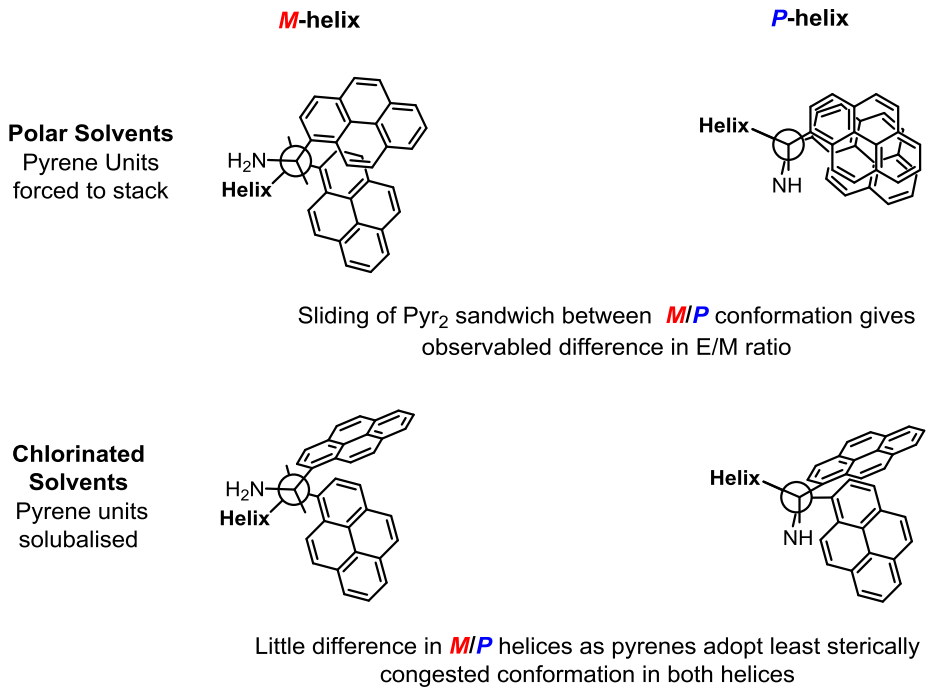

Figure 47 Possible reasons for lack of probe response in DCM.

5.15 Membrane Behaviour of 3rd Geneneration *S,S*-BisPyrEt-NH_2 Probe

Given the highly promising results for the *S,S*-BisPyrEt **120** structure in solution, investigation of their fluorescence behaviour in membrane environments was of high interest. Compounds **121** and **122** were added to EYPC lipid films and extruded through a polycarbonate membrane to produce two separate solutions of 1mM 800 nm EYPC vesicles loaded with 1 mol% of either **121** or **122** at 10 μM concentrations. These were purified by gel permeation column (PD-10) to remove any solution-based materials before measuring the fluorescence.

Pleasingly, a small difference was detected between the *M*- and the *P*- helix within the membrane environment of these vesicles. Curiously, the ratios were inverted, suggesting a new probe conformation in the membrane. These results were the first observable measurements of signal relay through controlled helical peptides in a membrane environment. Having developed a successful fluorescence probe for solution and membrane environments, the next stage of the project investigated the fine-tuning of the probe response. A series of synthetic modifications of the probes core structure provided a wealth of understanding on the factors governing the probes function.

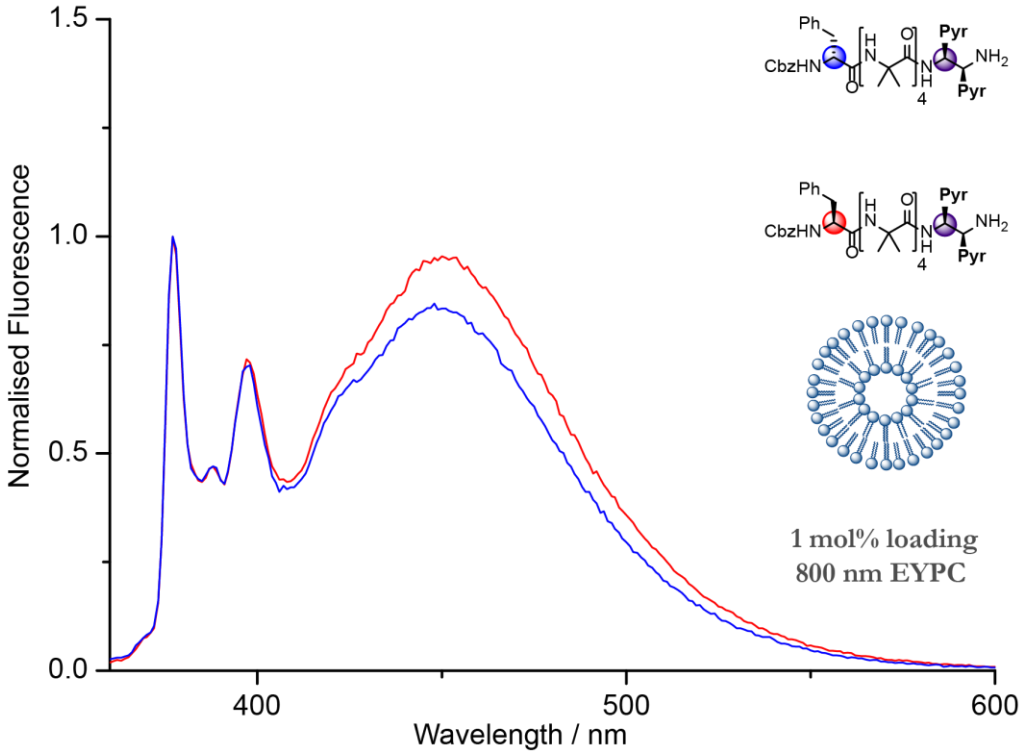

Figure 48 - Fluorescence spectra of compounds **121** and **122** (10 μM) in 800 nm EYPC vesicles.

5.16 Optimising the Probe Structure: Spacers

Considering the *S*,*S*-BisPyrEt **120** structure as a hinge with two pyrene groups attached, it was thought that increasing the distance between the pyrene groups and the hinge point may improve the fluorescent response to differing screw-sense preferences.

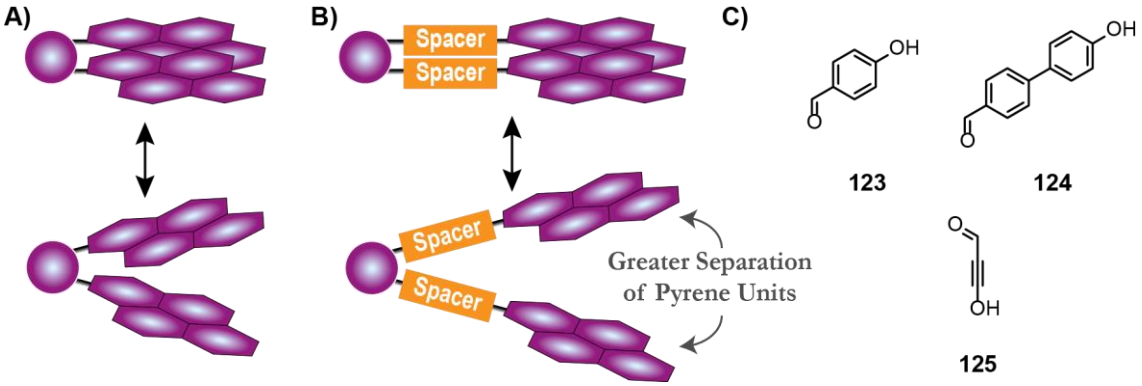

Figure 49A) A probe without a spacer and reduced pyrene movement around the hinge **B)** A probe structures with spacers allowing for a larger change in probe separation with and identical hinge motion. **C)** Possible spacer fragments

A variety of linkers were proposed that were compatible with the previously described cyclisation method including phenols **123**, and **124** and alkyne **125** structures. Of these the phenol structure **123** was chosen first. 4-(pyren-1-ylmethoxy)benzaldehyde **126** † was reacted with (1R,2R)-1,2-Bis(2-hydroxyphenyl)ethylenediamine **114** following the method outlined by Jik Chin and co-workers. Cleavage of the rearranged diimine in THF gave the desired compound (1S,2S)-1,2-bis(4-(pyren-1-ylmethoxy)phenyl)ethane-1,2-diamine dihydrochloride "S,S-BisPhenPyrEt" **126** in a satisfactory 60% yield. This was coupled to **63** and **64** to give **128** and **129** in good yields.

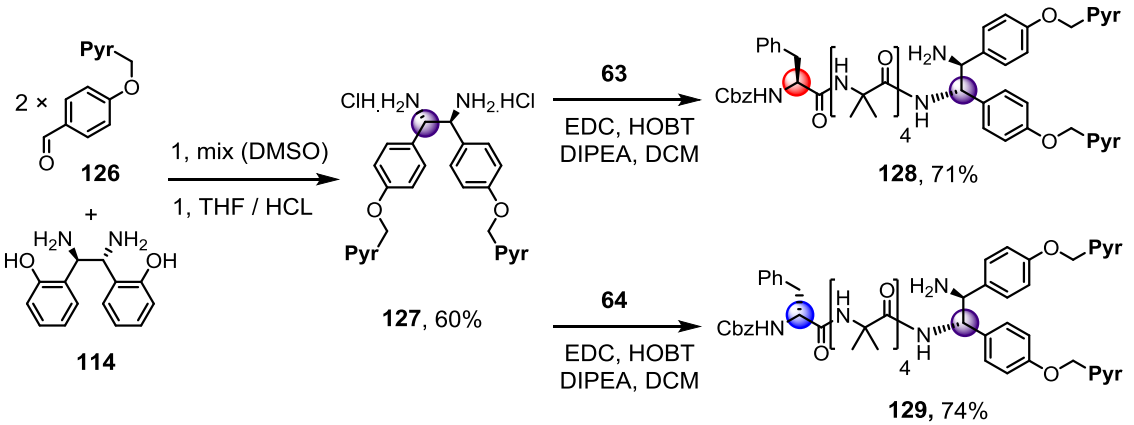

Scheme 25 - Synthesis of elongated diamine probe **126** and attachment to Phe controlled Aib helices.

† Supplied by Dr. S. Pike

The elongated probe structure **127** was found to be less effective at conveying the difference between *M* and *P* helicity when compared to **120**. Large concentration dependence in all solvents indicate the probe is prone to aggregation and a poor structure for a screw-sense preference probe (Figure 50). The freedom of rotation around the ether linkage was found to reduce the difference in achievable inter-pyrene distances for the *M* and the *P* helices. As this would remain the same for all of the other proposed linker structures and a successful probe structure was already in hand no further work was performed on elongated probe structures.

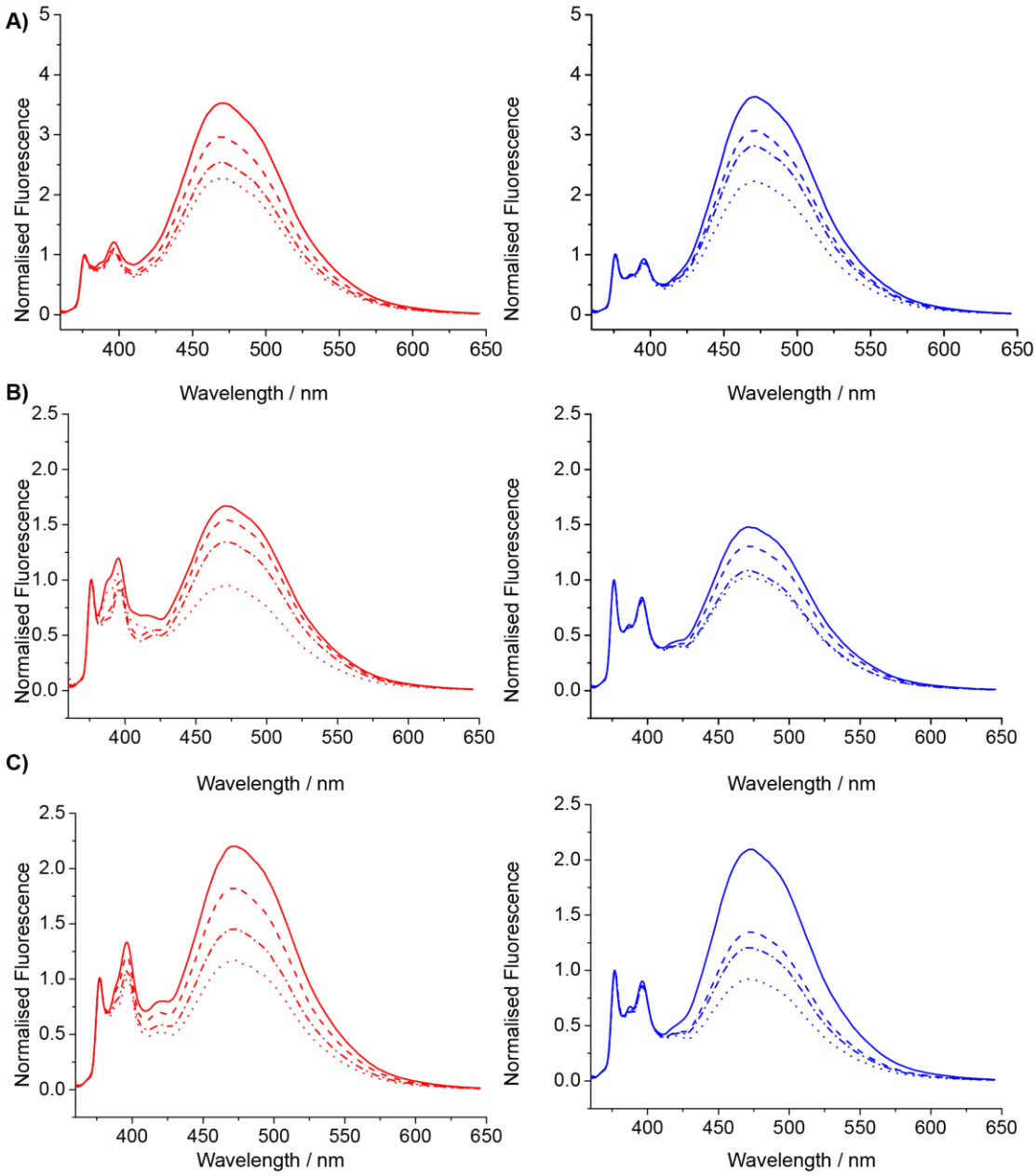

Figure 50 - Fluorescence spectra of compounds **128** (red) and **129** (blue) in MeOH (A) MeCN (B) and DCM (C). Fluorescence measured at 10 µM (——) 5 µM (— — —) 2.5 µM (— ▪ —) and 1.25 µM (▪▪▪) concentrations and normalised to 377 nm.

5.17 Optimising The Probe Structure: α-Methylvaline Control

The degree of control delivered through the Aib_4 helix to the *S*,*S*-BisPyrEt **120** probe was modified to confirm the probe was functioning properly. If the chiral signal is relayed through the helix to the probe, changing the control on the helix should result in a change in the observed E/M ratio. Work within the group had also suggested that the control delivered by phenylalanine residue was greatly reduced in chlorinated solvents. This provides a possible reason for the poor results observed for **121** and **122** in DCM**.** Maximal control of the Aib helix is achievable with two α-Methylvaline residues (αMv) at the N-terminus.[48] To remove any unforeseen problems with concentration dependant control the phenylalanine residue was replaced with a quaternary αMv residues. Helices with two αMv residues at the N-terminus were also synthesised to determine the probes maximum response to *M* and P helicity and allow quantification of the probes response to helical excess.

Cbz-L-αMv-OH **130** was converted to Cbz-L-αMv-F **131** and reacted with H-Aib_4OtBu **98** over 7 days to give 37 % of Cbz-L-αMv-Aib_4OtBu **132.** This was divided into two portions, the first was de-protected at the N-terminus **133** and coupled with additional Cbz-L-αMv-F **131** over a further 7 days to give Cbz-L-αMv_2-Aib_4O^tBu **134** in quantitative yield. This strategy was performed in tandem for the Cbz-D-αMv-OH species **135** to give **136**, **137**, **137** and **139**.

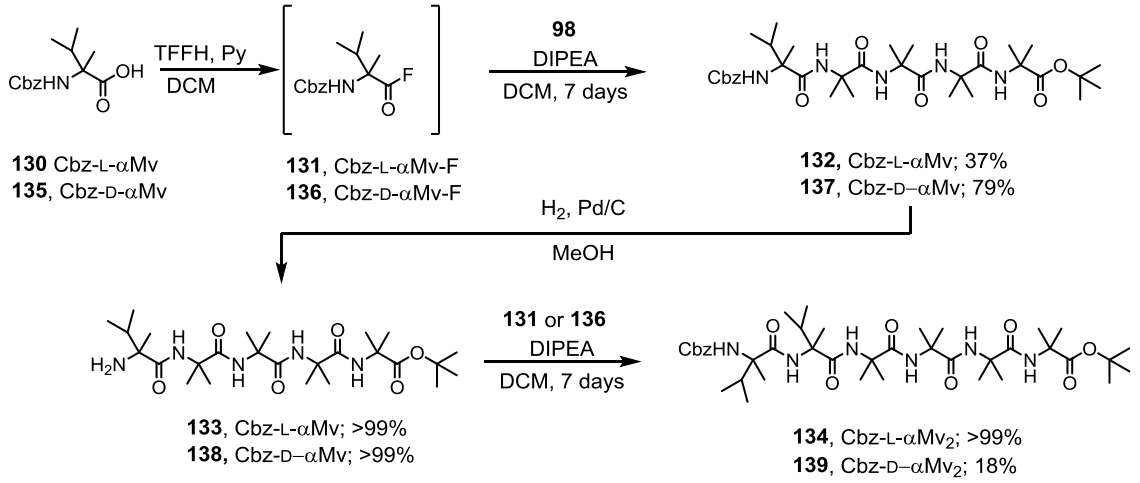

Scheme 26 - Synthesis of α-methylvaline controlled helices.

The four helices were deprotected using TFA to give Cbz-L-αMv-Aib$_4$OH **140** Cbz-D-αMv-Aib$_4$-OH **141** in good to excellent yields. Additional purification was required for Cbz-L-αMv$_2$-Aib$_4$-OH **142** and Cbz-D-αMv$_2$-Aib$_4$-OH **143** lowering their overall yields.

Overall this gave four key compounds: two helical scaffolds; *P*-**140** vs *M* -**141** with a helical excess of 68:32[48] and two, *P*-**142** vs *M*-**143** with a higher helical excess of 95:5[48] ready for attachment to the *S*,*S*-BisPyrEt probe.

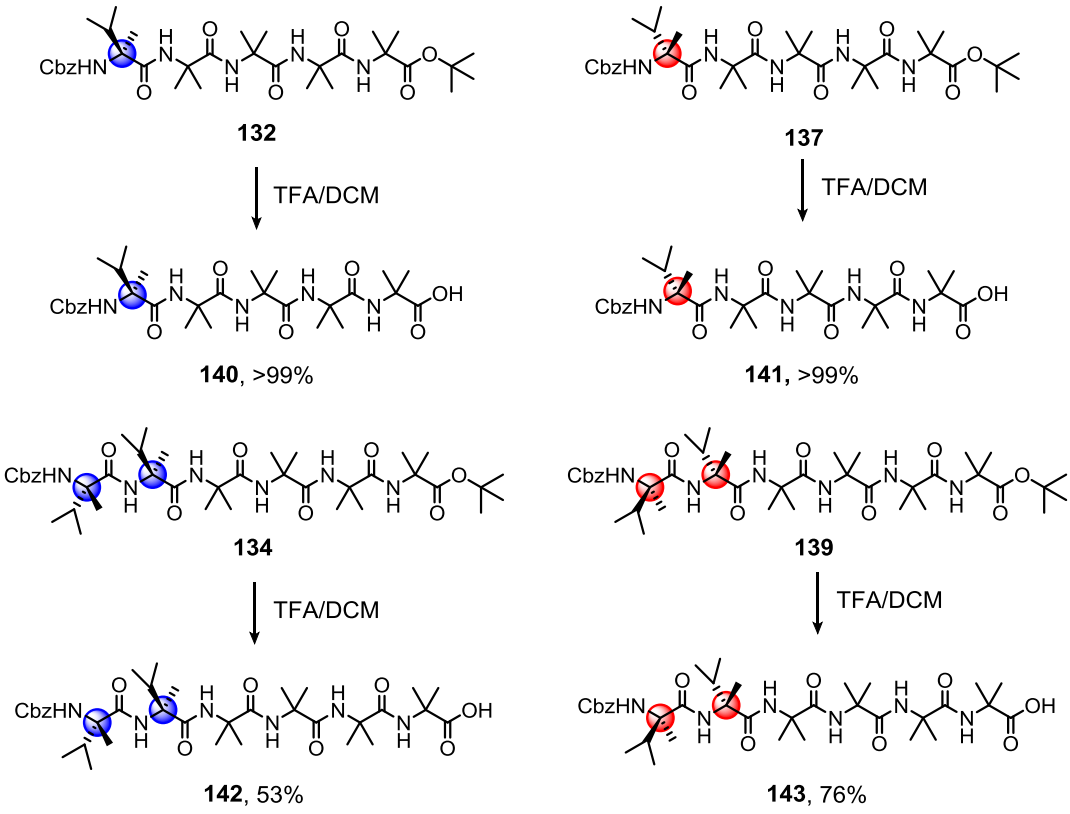

Scheme 27 - Synthesis of α-methylvaline controlled helices.

5.18 Coupling the *S,S*-BisPyrEt Probe to αMv Controlled Helices

Coupling of the *S*,*S*-BisPyrEt probe **120** proceeded smoothly to the Cbz-D-αMv **144** and Cbz-L-αMv **145** controlled structures**.** As the controlling residues were quaternary, the induced screw-sense control was inverted with Cbz-D-αMv inducing an *M* screw-sense and Cbz-L-αMv inducing a *P* screw-sense (Section 1.10).

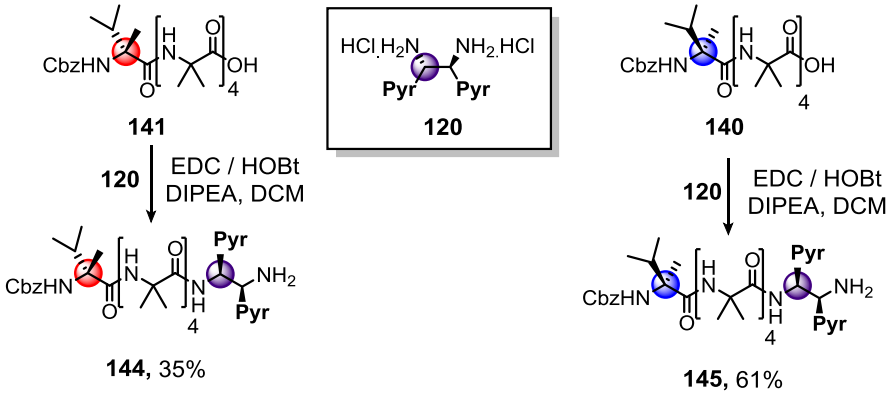

Scheme 28 - Coupling *S*,*S*-BisPyrEt probe to αMv helices.

5.19 Fluoresence of *S,S*-BisPyrEt-NH Probe in αMv Controlled Helices

As the controlling strengths of the phenylalanine residue and the αMv residue are roughly equivalent, the fluorescence response of the probe when attached to the new αMv controllers (Figure 51) was expected to mirror that of the earlier phenylalanine controlled compounds (Figure 45, p 69). Strangely, the response was worse for the αMv controlled compounds, with no observable difference seen for *M* and *P* screw-sense preference in DCM and THF. A reasonable difference was observed in MeOH.

This variable probe behaviour across a range of solvents is likely due to the inter-play between the control delivered to the helix from the N-terminus, which is desired, and the control delivered to the helix by the probe, which is not. In polar solvents the earlier phenylalanine controller overpowered the control from the probe, producing a satisfactory fluorescence response. In DCM the lack of response can be explained as a change in the power balance between the probe and controller: the phenylalanine control is reduced, the probe dominates the helix, no detectable difference in E/M ratio is observed. For the αMv controllers, the fluorescence results suggest the N-terminal control placed on the helix is lower than that

delivered by the Phe residue, and the probe dictates the conformation of the helix. These findings suggested that modification of the probe structure further; to reduce control placed on the helix from the C-terminus was a high priority.

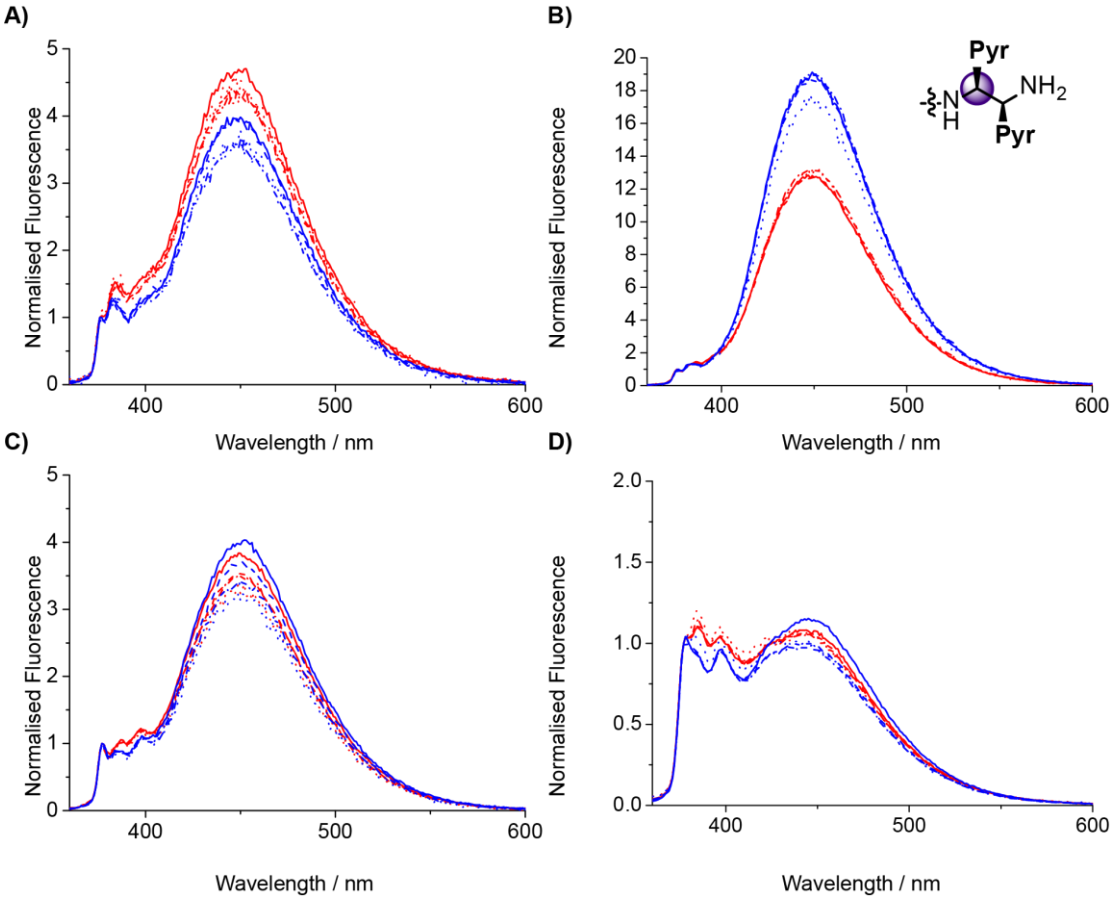

Figure 51 - Fluorescence spectra of compounds **144** (red) and **145** (blue) in MeCN (**A**) MeOH (**B**) DCM (**C**).and THF (**D**). Fluorescence measured at 10 µM (——) 5 µM (— — —) 2.5 µM (— ▪ —) and 1.25 µM (▪▪▪) concentrations and normalised to 377 nm.

5.20 Optimising the Probe Structure: Protecting the Amine

It was thought that the bonding interaction of the NH_2 of the diamine probe **120** had a large effect on its ability to respond to changing helicity, protecting this NH had the potential to modify this bonding interaction and improve probe response. Considering the probes future use in the development of switchable systems, a secondary issue with the NH_2 fragment required consideration. The presence of the NH_2 provided a potential C-terminal binding site at the probe (Figure 52A). Systems designed to relay information from a chiral binding interaction at the N-terminus required the removal of this potential binding site

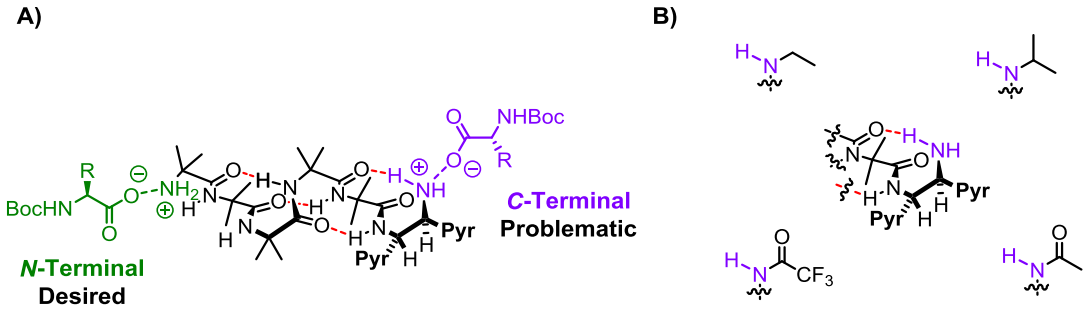

Figure 52A) Problematic direct binding site in *S*,*S*-BisPyrEt-NH_2 Probe structure. **B**) Possible amine modifications to remove binding site

Compounds **144** and **145** were dissolved in anhydrous DCM and stirred with Ac_2O for 3 hours. Purification by column chromatography gave **146** and **147** in 19% and 66% yields.

.

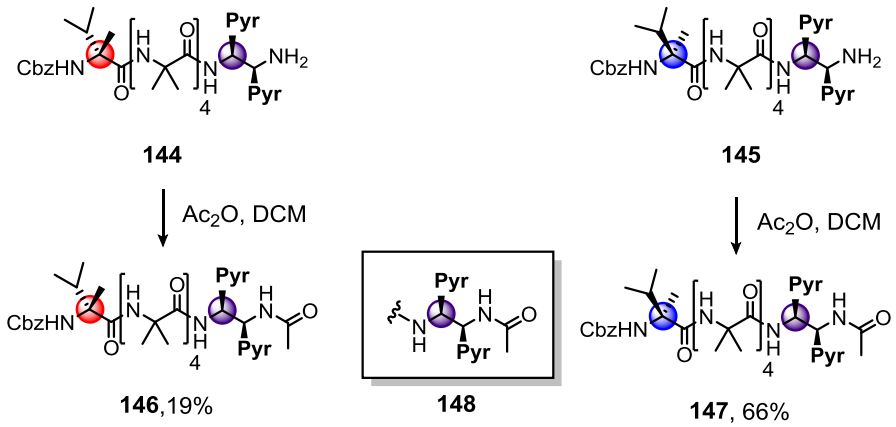

Scheme 29 - Acetylation of *S*,*S*-BisPyrEt-NH_2 probe on αMv helices.

5.21 Fluorescence of the Acetamide Probe

To our delight the acetylated probe structure "*S*,*S*-BisPyrEt-NHAc" **148** gave an excellent response to opposing screw-sense preference in all solvents tested (Figure 53). Dividing the E/M ratio of the *P*- helix by E/M ratio of the *M*- helix gives a third ratio which is a measure of the quality of the probes response. Values ≈1 indicate no observable difference between *M* and *P* screw-sense preference. >>1 indicate improving probe response to opposing helical environments. Values <1 indicate that response of the probe has inverted with respect to the two screw-sense preferences. The values for this third ratio, plotted against concentration for individual solvents are shown in Figure 54. The amine probe **120** performs poorly, with very little difference across all four solvents. The results for the acetamide probe **148** clearly highlight its superiority. In polar solvents the E/M ratio for the P screw-sense preference was ~3× that of the *M*. In DCM, where previous probe structure **120** had shown no response the difference the E/M ratio for the *P* helix was found to be 6.4 times that of the *M*.

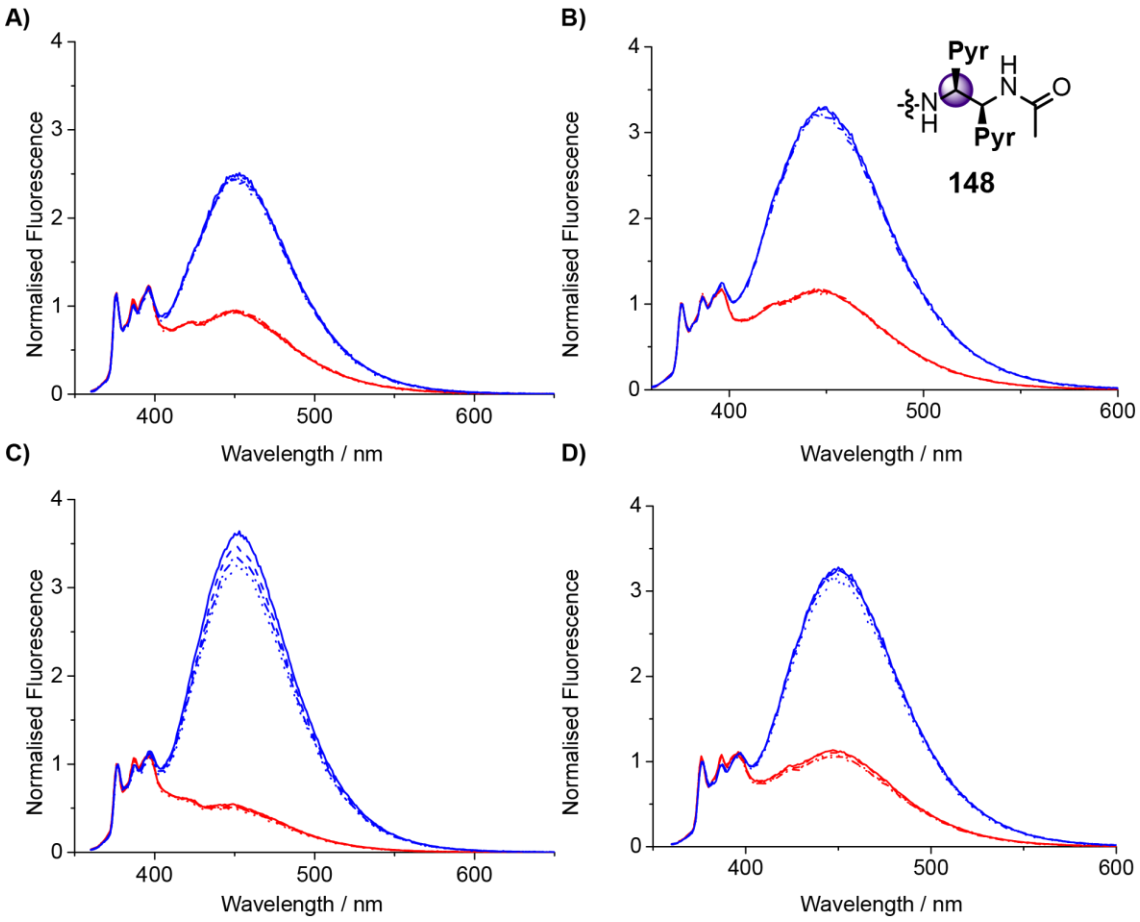

Figure 53 - Fluorescence spectra of compounds **146** (red) and **147** (blue) in MeCN (**A**) MeOH (**B**) DCM (**C**) and THF (**D**). Fluorescence measured at 10 µM (——) 5 µM (— — —) 2.5 µM (— ▪ —) and 1.25 µM (▪▪▪) concentrations and normalised to 377 nm.

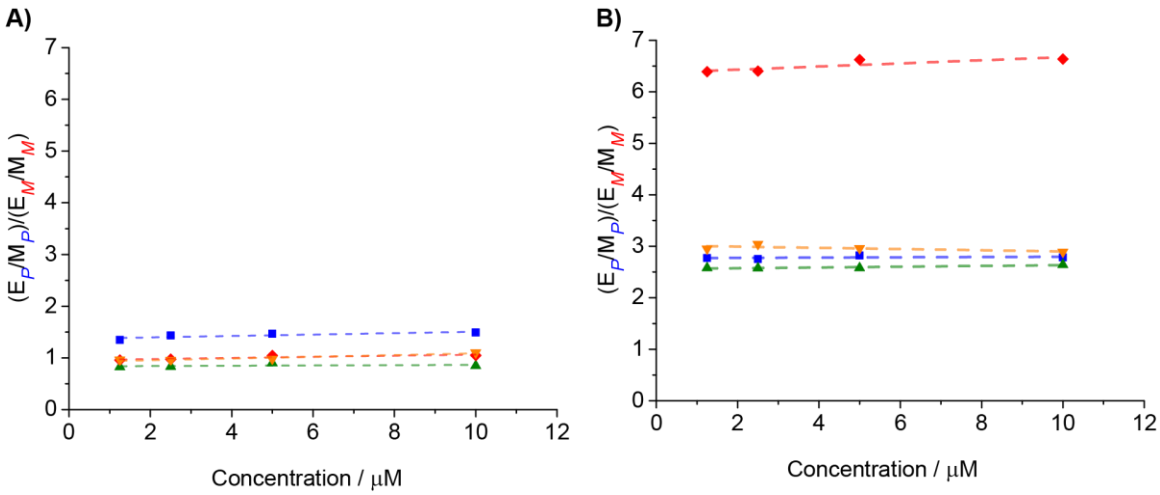

Figure 54 - Comparison of amine **A**) and acetamide **B**) fluorescence response in DCM (◆) MeOH (■) MeCN (▲) and THF (▼). DCM and THF response for amine identical.

To investigate the membrane behaviour of both probe structures, the four αMv controlled helices **144**, **145**, **146**, and **147**, were loaded into to 800 nm EYPC vesicles (Figure 55) Both structures gave a good response in the membrane, with the amine probe structure giving a marginally better response. Despite this, the improved and consistent response of the acetamide probe in solution as well as the removal of the free amine made it the better of the two probe structures.

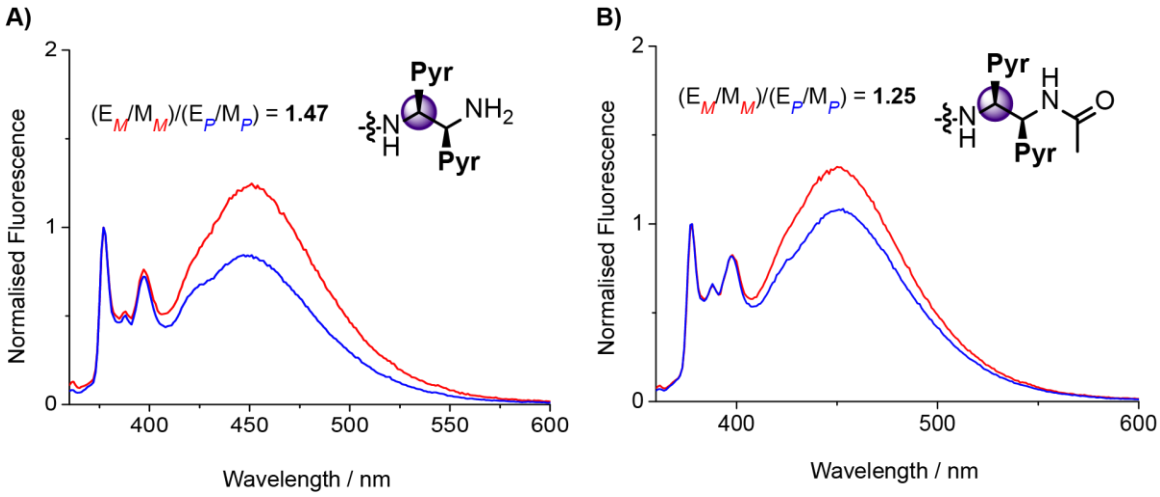

Figure 55 - Comparison of amine **120** (10 μM) (**A**) and acetamide **148** (10 μM) (**B**). Fluorescence response as 1mol% loading in 800 nm EYPC vesicles.

5.22 Quantifying Probe Control

To determine the degree of control placed on the helix by the amine **120** and acetamide **148** probe structures, they were attached to Cbz-Gly-Aib$_4$-OH **149**. Chiral influence relayed through the helix from either probe structure at the C-terminus could be quantified using the ^{1}H NMR signals of the glycine residue at the N-terminus. The results could be compared against a library of known C-terminal controllers.[124]

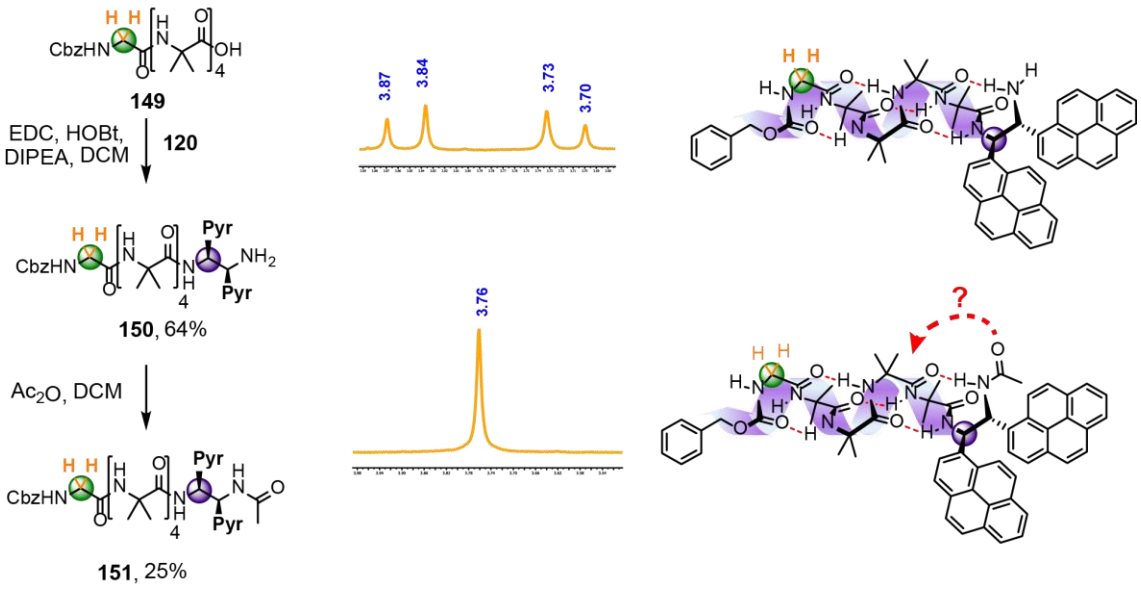

Scheme 30 - The different controlling strengths of the probe structures. NMR in MeOD.

Attachment of **120** to Gly-Aib$_4$-OH **149** gave Gly-Aib$_4$-*S*,*S*-BisPyrEt-NH$_2$ **150** in a 64% yield. A portion of this was acetylated to give Gly-Aib$_4$-*S*,*S*-BisPyrEt-NHAc **151.** Analysis of the glycine proton signals in deuterated methanol allowed for the control placed on the helix by **120** and **148** to be determined. A large splitting of 130 ppb was observed for the free amine **120** indicating a high level of control is placed on the Aib helix by the amine probe. Interestingly, the acetamide **148** which gave the better response in controlled helices **146** and **147** gave no observable splitting, indicating that this structure places very little control on the Aib$_4$ fragment. This suggests that the lower the probes ability to control, the better its ability to respond to control from the N-terminus.

As expected, the normalised excimer fluorescence of **151** is between that of the *M*-**146** and *P*-**147** helices, giving an E/M value of 2.48 for a non-controlled Aib helix in MeOH (Figure 56A) During this stage of the project fluorescence microscope images of compounds **146** and **147** were obtained in EYPC GUVs. The uniform fluorescence of **147**, which was observed for both **146** and **147**, indicates the helices are equally dispersed throughout the vesicle structure (Figure 56B)

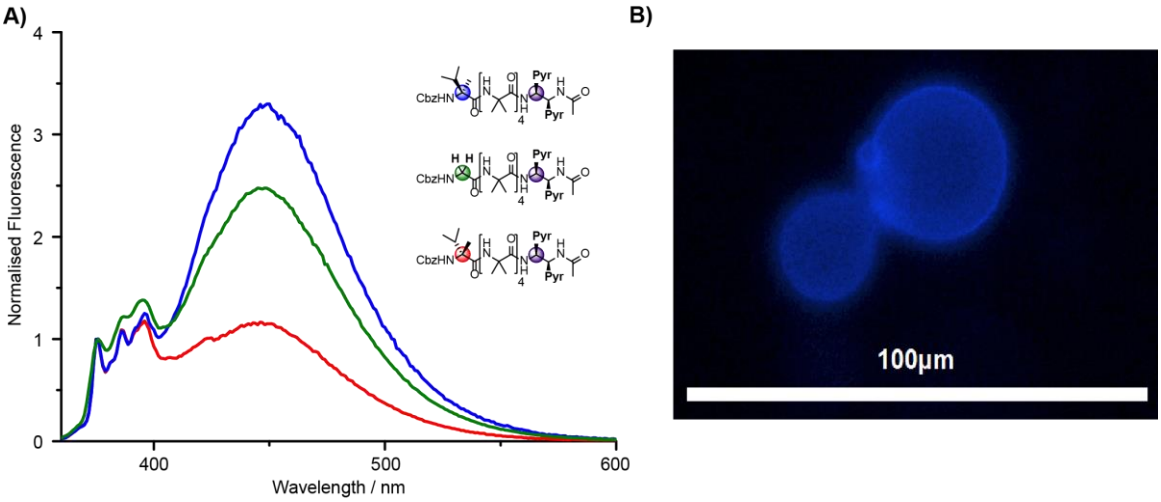

Figure 56A) The fluorescence spectra for **146**, **147**, and **151** (10µM, MeOH) normalised to 377 nm. **B)** Fluorescence microscope of **147** as a 1 mol% loading in EYPC GUVs.

5.23 Alternative Synthetic Routes to Helical Probe Structures

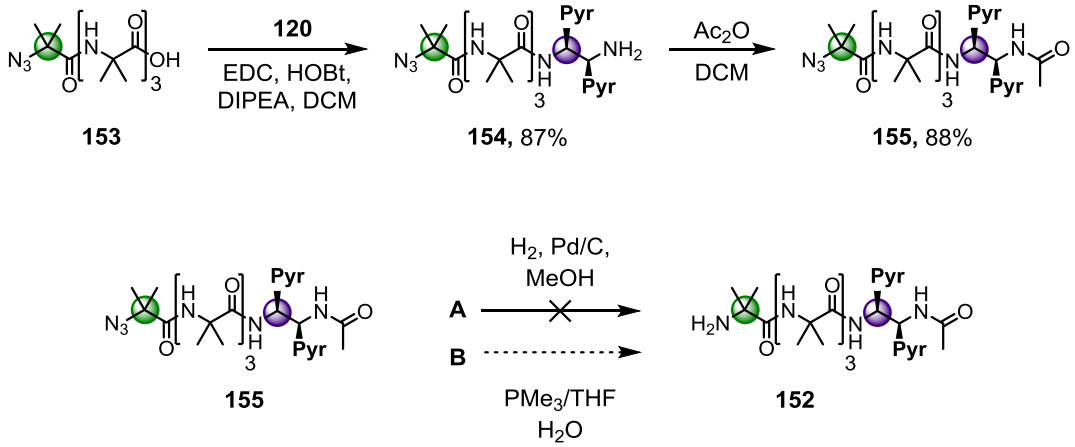

Scheme 31 - Attachment of *S*,*S*-BisPyrEt Probe to N_3Aib_4OH and failed attempts at azide reduction.

As the large-scale production of H-Aib_4-*S*,*S*-BisPyrEt-NHAc **152** would have improved the synthetic route to desired target compounds, attachment of **120** to N_3Aib_4-OH **153** to give **154** and acetylation of the free amine to **155** was attempted successfully. Reduction over Pd/C was attempted despite the expectation of probe cleavage but was found to be unsuccessful. Attempts to reduce **155** under Staudinger

conditions to **152** appeared successful but removal of the trimethylphosphine oxide impurity proved to be unsatisfactory. If further work on this synthetic route is desirable in the future, solid supported phosphine may offer a solution. Overall this method was abandoned in favour of late stage coupling of **120** to a desired helical acid.

5.24 Coupling the *S,S*-BisPyrEt Probe to αMv$_2$ Controlled Helices

To measure the acetamide probe's **148** maximum responses to *M* or *P* helicity **120** was attached to **141** and **142** and acetylated directly to give 56% of a *P*- **156** and 49% of an *M*- **157** helical structure. The controlling fragment Cbz-(aMe)$_2$Val is known to induce complete N-terminal control of Aib helices,[48,61] allowing for the maximal response of the probe at the C-terminus to *M* and *P* screw-sense preference.

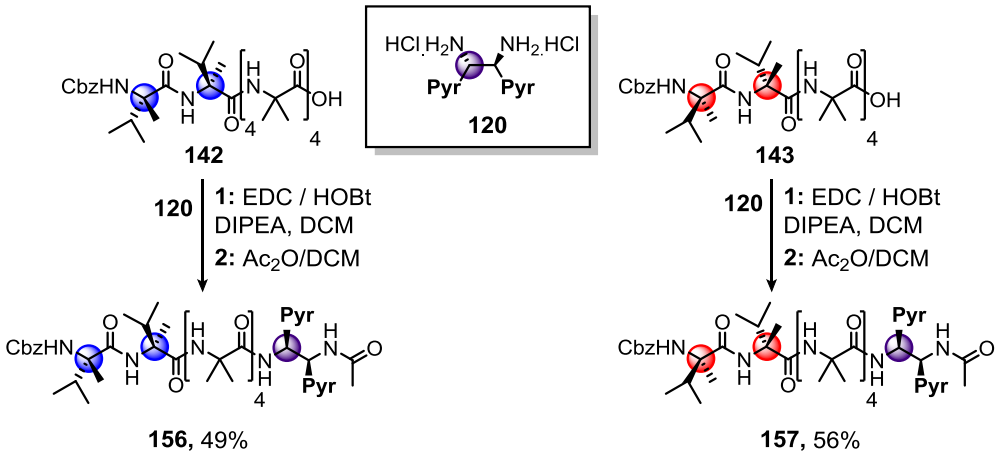

Scheme 32 - Attachment of *S,S*-BisPyrEt Probe to αMv$_2$ helices.

5.25 Fluoresence of *S,S*-BisPyrEt-NHAc probe in αMv$_2$ Helices

Figure 53 shows the normalised spectra for the αMv$_2$ compounds **156** and **157** overlaid on the spectra for **146**, **147**, and **151** showing the maximum response range for the acetamide probe. Increasing *P* helicity is observable as an increasing E/M ratio for the *S*,*S*, acetamide probe **148**. Increasing *M* helicity results in a decrease in E/M ratio that is non-linear.

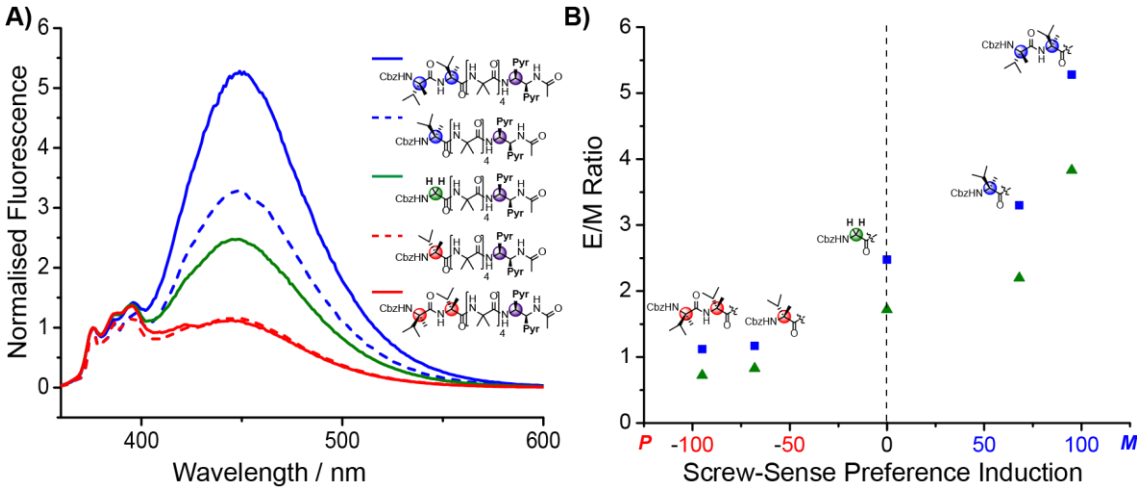

Figure 57 - Normalised spectra for S,S-BisPyrEt-NHAc probe structure **148** attached to helices of varying screw-sense preference. All 10μM MeOH. **B)** Plot of observed E/M values against the literature reported screw-sense induction values[48] for amino acid residues in MeOH (■) and MeCN(▲).

This observation can be explained by considering the structure of the probe. Increasing *P* screw-sense leads to increasing separation of the two pyrene groups and a reduced excimer fluorescence. The control delivered by single Cbz-D-(αMe)Val residue of **146** already reaches the maximum separation of the pyrenes, switching the probe excimer off. The additional control delivered by Cbz-D-(αMe)Val$_2$ residues of **157** may separate the pyrene probes further, but the excimer is already reduced to its minimum value.

5.26 X-ray Crystal Structure of Cbz-D-αMv$_2$-Aib$_4$-*S,S*-BisPyrEt-NHAc

Explanation for the low observable control and the high functionality of the acetamide probe **148** can be found in the crystal structure for **157**. The expected *M*-helix has both α-helical and 3_{10} character with the acetamide probe adopting a bifurcated NH bond between the carbonyl of the third Aib residue and amide NHs of the probe. This unusual conformation is probably the reason for the reduced control placed on the helix by the acetamide. The large separation of the pyrene groups agrees with the observation of low excimer for compound **157**.

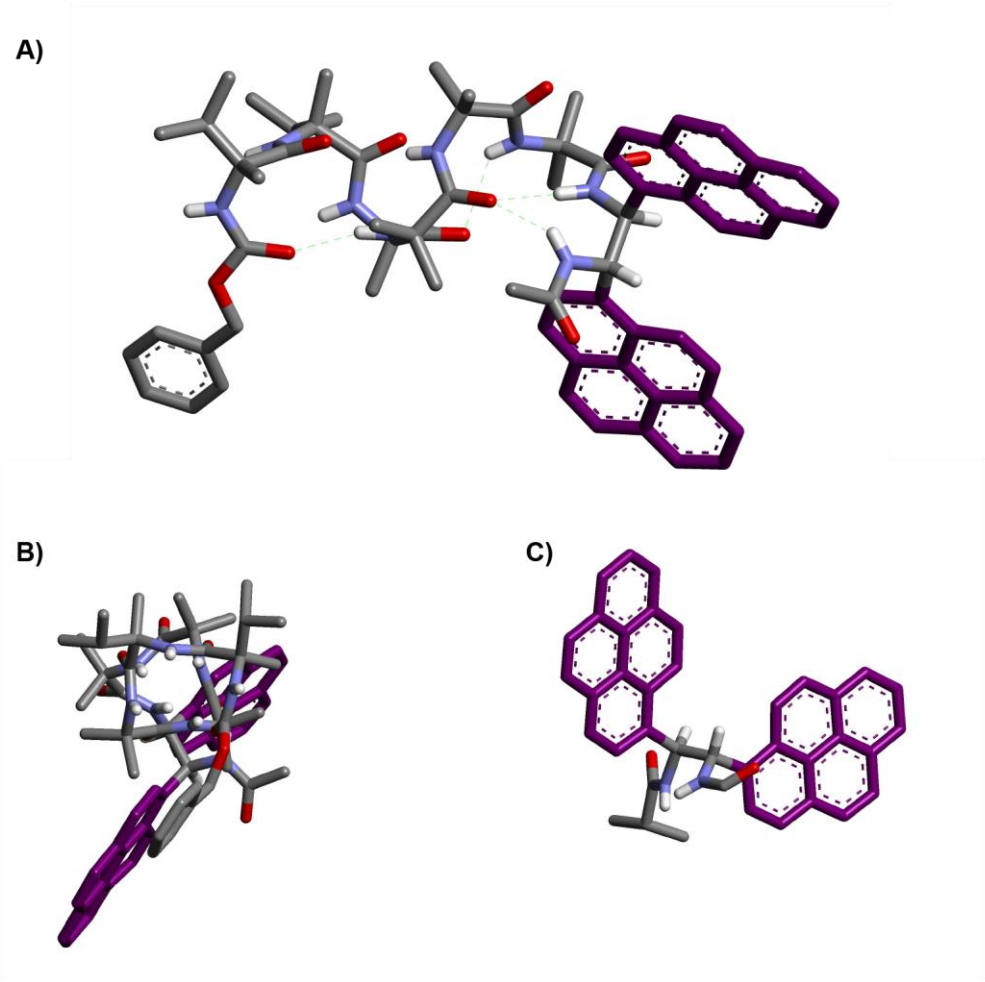

Figure 58 - X-Ray crystal structure for **157 A**) Showing side on *M* helical structure with mixed 3_{10} / α character and bifurcated NH bond between the carbonyl of Aib$_3$ and amide NHs of the probe. **B**) End on N-C through helix. **C**) Isolated structure of probe highlighting large separation of pyrene groups.

6.0 Pyrene excimer probes for biological analytes

6.1 Background

Having developed a successful probe structure for Aib helical screw-sense preference further potential uses for the *S*,*S*-BisPyrEt probe structure **120** were also investigated. Within the literature there are a number of examples of fluorescent molecules designed to bind and detect analytes in solution with a fluorescent response.[126] Examples of fluorescent probes operating in living systems are also reported.[127]

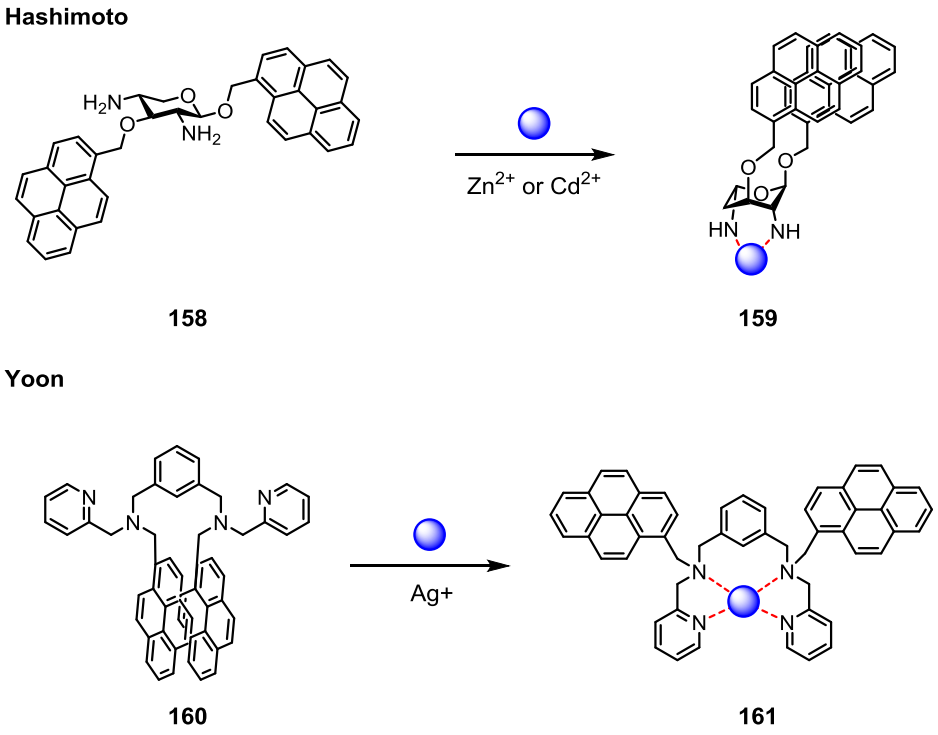

Scheme 33 – Examples of conformationally responsive excimer probes.

Among these, work by the groups of Hashimoto[128] and Yoon[129] highlight the potential for the use of **120** as a core structure in a conformationally responsive fluorescent probe, producing a changing E/M response on binding an analyte in solution. In the presence of Zn^{2+}or Cd^{2+} ions the amine groups in **158** bind to the metal centre inducing a ring-flip in the probe structure **159**, leading to increased excimer. For the second structure **160** the aromatic pyrene groups π-stack in aqueous buffer solution leading to high excimer fluorescence. In the presence of Ag^{2+} the pyridine arms of the probe chelate the Ag^{2+} ions, pulling the pyrenes apart **161**, reducing excimer fluorescence.

Synthetic modification of the *S*,*S* diamine structure had the potential to create a series of new fluorescent structures capable of detecting analytes in solution.

A successful structure equipped with a selective binding site would, on binding an analyte, change conformation and the proximity of the pyrene groups. As with the Aib helices the conformational change induced by binding could be detected by a change of E/M ratio.

Binding sites incorporating additional amine **162** groups have the potential to bind metal ions in solution **163**. It was thought that ions of different radii would lead to different conformations of the probe backbone resulting in different E/M fluorescence for each ion.

A secondary type of binding site incorporating boronic ester fragments **164** is also an interesting synthetic target as a potential fluorescent sugar binder **165**. The different stereochemical structures of common sugars have the potential to bind in different ways with **164** allowing for the detection of individual sugars by differing E/M ratios. Potentially, the binding of certain saccharide structures would have been more favourable than others allowing for their selective detection in a solution. Once developed in solution, the fluorescent nature of the probes would allow their translation into more complex biological environments.

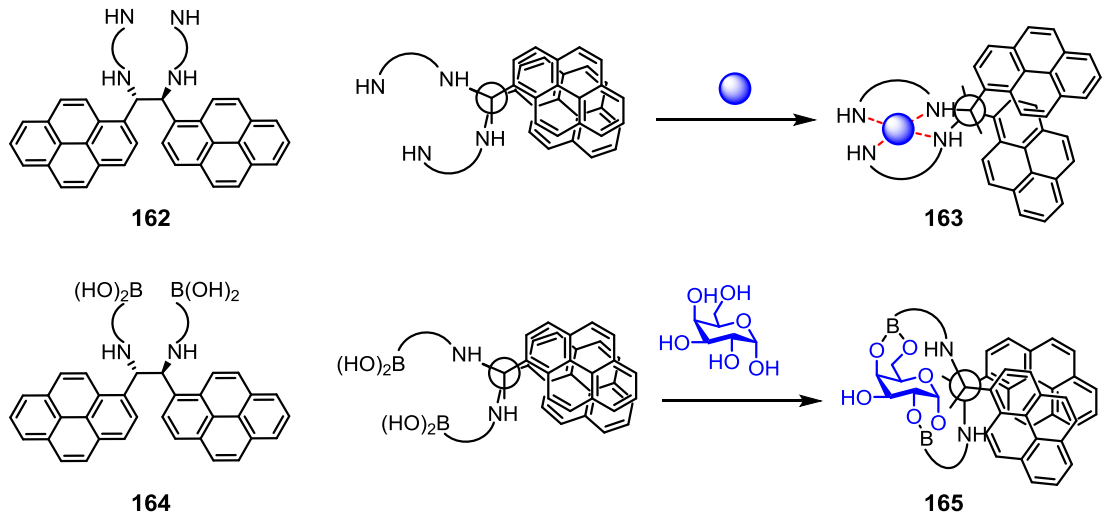

Scheme 34 - Potential binding structures incorporating the *S*,*S*-BisPyrEt structure.

6.2 Synthetic Attempts at a Metal Binding Excimer Probe

Unfortunately attempts to form a useful metal binding structure through the formation of a diimine **166** with picolinaldeyde **167** (Table 1) were unsuccessful. The instability of the diimine and the polarity of the picolinic groups severely hampered attempts to purify the mixture by column chromatography. It was thought that the reverse [3,3] sigmatropic rearrangement **166→168** destroys the backbone of the *S*,*S*-BisPyrEt structure resulting in a mixture of products. While attempts to synthesise a structure diimine structure **166** may appear ill-concieved given the potential for [3,3]-sigmatropic inversion Li *et al.* report the synthesis of the analogous **169**.[130]

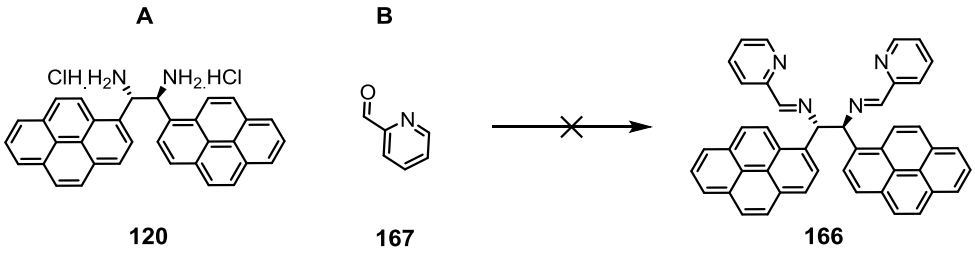

Scheme 35 - Failed synthesis of *S*,*S*-BisPyrEt pyridyl diimine.

Entry	A	B	Additives	Solvent	Temp	Time	Observations
1	1	2.1	DIPEA (2)	MeOH (2 mL)	RT	o/n	Failed
2	1	2.1	DIPEA (2)	DCM (2 mL)	RT	o/n	Failed
3	1	14	$NaHCO_3$ (3.6)	DCM(2 mL) H_2O (2 mL)	RT	o/n	Failed
4	1	1.9	$NaHCO_3$ 5	DCM (2 mL) H_2O (2 mL)			Failed. Attempt to reduce *in situ* also failed. Monomeric pyrene fragment isolated
5	1	1	K_2CO_3 1.5 eq	Tol (2 mL)	60 °C	6 h	Failed

Table 1 - Conditions for failed synthesis of *S*,*S*-BisPyrEt pyridyl diimine.

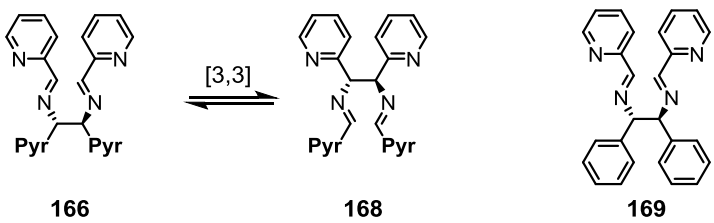

Scheme 36 - Likely reason for reaction failure

An attempt to form a similar metal binder structure using 2-aminobenzaldehyde **170** to form diimine **171** was equally unsuccessful (Table 2; 1). To avoid synthesis of a diimine intermediate, synthesis of the diamide **172** using picolinic acid **173** was also attempted (Table 2; 2). Unfortunately this produced an intractable solid. Attempts to acetylate **120** (Table 3; 3) to form **174** also gave an intractable solid. As good solubility was a key design feature of any potential probe structure, particularly for further applications in biological systems, the syntheses of further amide structures were abandoned.

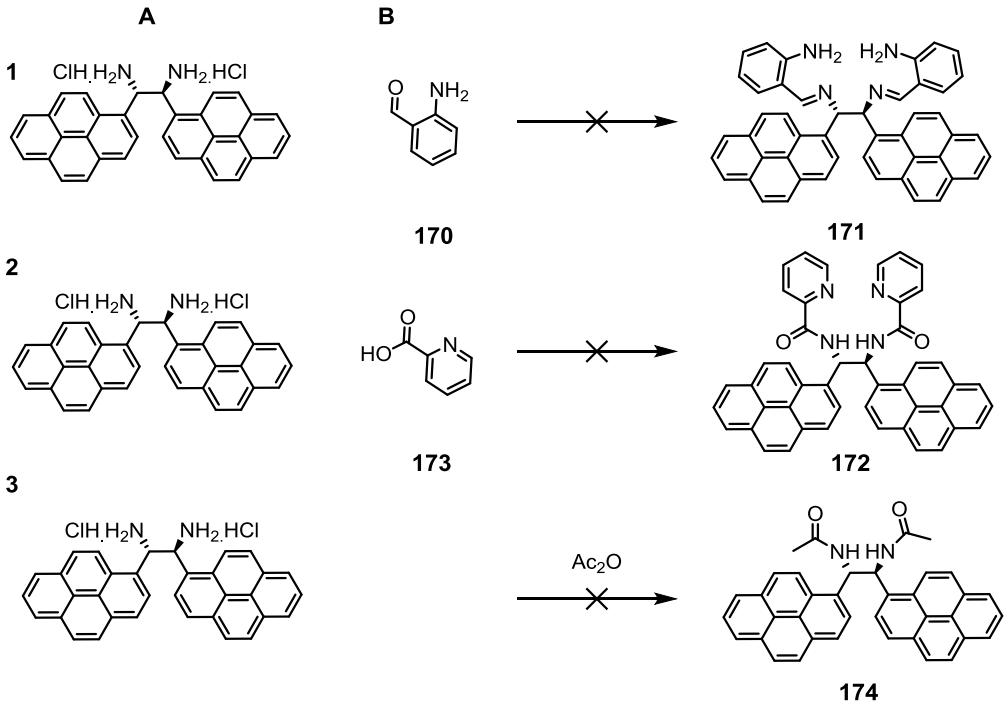

Scheme 37 - Failed modifications of *S*,*S*-BisPyrEt probe **120**.

Entry	A	B	Additives	Solvent	Temp	Time	Observations
1	1	2.4	N/A	EtOH (2 mL)	−20 °C →RT	o/n	Failed, possible polymerisation
2	1	2.1	EDC (2.1) HOBT (2.2) DIPEA (5)	DCM (5 mL)	0 °C →RT	2 days	Poor solubility, including DMSO *Unsuitable for sensor.*
3	1	/	Ac_2O (2 mL) K_2CO_3 (1.1)	DCM (2 mL)	RT	o/n	Poor solubility profile. *Unsuitable for sensor.*

Table 2 - Failed modifications of *S*,*S*-BisPyrEt probe.

Attempts to synthesise a similar structure **175** through alkylation with **176** were also unsuccessful. It was hoped that the steric bulk of the first alkylation would prevent alkylation of the newly formed secondary amine. Unfortunately, the major product in an impure mixture had the correct mass of the desired product but unsymmetrical NMR signals, suggesting it was the result of double alkylation to a single nitrogen of the probe structure.

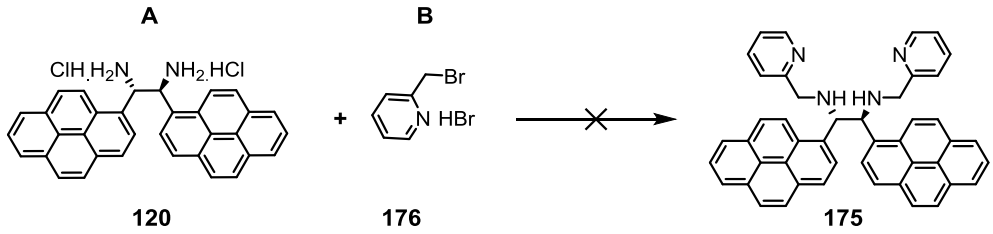

Scheme 38 - Failed alkylation of *S*,*S*-BisPyrEt probe.

Entry	A	B	Additives	Solvent	Temp	Time	Observation
1	1	2	Et_3N	(2 mL) DCM	RT	o/n	Failed
2	1	2	Et_3N	(2 mL) DMF	RT	o/n	Failed
3	1	2	K_2CO_3 (4.5 eq)	(2ml) DMF	RT	o/n	Colour change to rosy red. Failed, m/z 734 (3×) alkylation
4	1	3	K_2CO_3 (4.5 eq)	(2ml) DMF	RT	5 days	Colour change to rosy red. Failed, m/z 734 (3×) + 825 (4×) alkylation products

Table 3 - Conditions for failed alkylation of *S*,*S*-BisPyrEt probe.

6.3 Synthetic Attempts at a Sugar Binding Excimer Probe

Attempts to develop an analogous sugar binding fluorescence probe were carried out in tandem with the unsuccessful development of the metal binder. Attempts to make a diimine structure **177** with 2-formylphenylboronic acid **178** were equally unsuccessful.

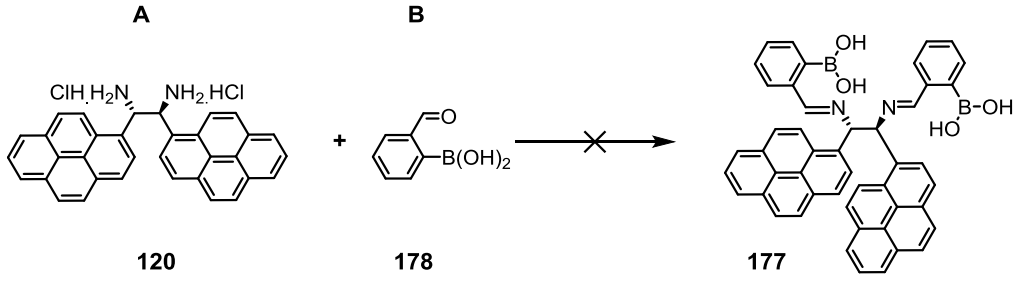

Scheme 39 - Failed *S*,*S*-BisPyrEt diamine sugar binder.

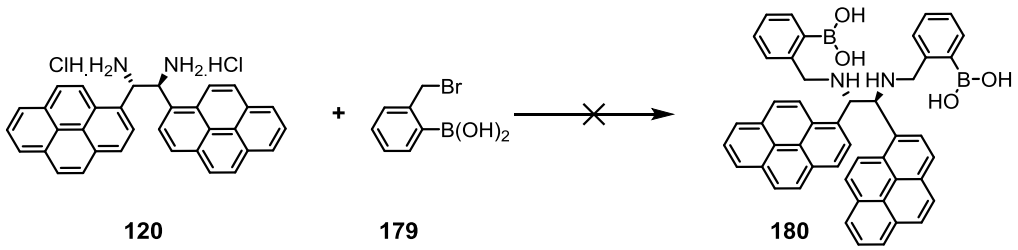

120 179 180

Scheme 40 - Failed alkylation of *S*,*S*-BisPyrEt probe

Attempts to alkylate **120** with 2-bromomethyl phenylboronic acid **179** towards the synthesis of **180** had the additional problem of protodeboronation of the unprotected boronic acid. Protection of the boronic acid with a bulky protecting group had the potential to prevent loss of boron and provide enough steric bulk on the alkylating unit to prevent the secondary amine alkylation observed in the attempts to synthesise the metal binding structure.

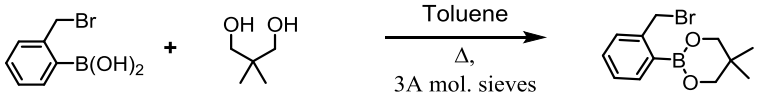

179 181 182

Scheme 41 - Protection of 2-bromomethyl phenylboronic acid.

2-bromomethyl phenylboronic acid **179** was protected with neopentylglycol **181** as the neopentylglycol boronic ester **182** following the method of Spencer *et al.*[131] Unfortunately using this protected structure in the synthesis of **183** was no more successful than the other fragments.

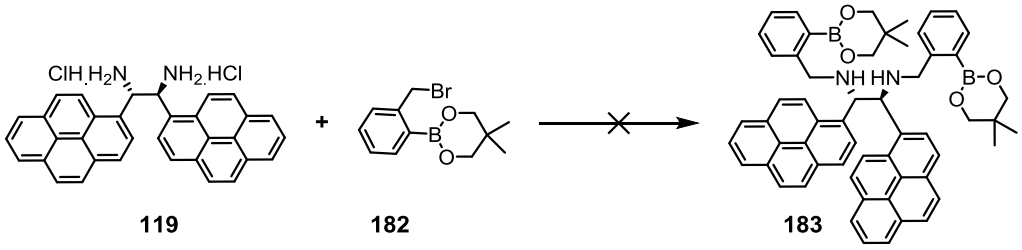

119 182 183

Scheme 42 - Failed alkylation of *S*,*S*-BisPyrEt probe with protected boronate.

7.0 The Development of a Biomimetic GPCR

7.1 Background: Metal Binding Sites for Biomimetic Receptors

BQPA (*N*,*N*-bis(2-quinolyl)methyl-*N*-(2-pyridyl)methylamine) metal complexes, developed by Karlin[132] and later Anslyn and Canary[133] have been used to determine the chirality of bound amino acids in solution. BQPA ligands form five-coordinate, square pyramidal geometries on complexation to metals ions such as Zn^{II} and Cu^{II}.[134] In the absence of chiral influence, these complexes exist as a dynamic equilibrium between *M* and *P* propellers (Figure 59A). Addition of a chiral carboxylate ion displaces the solvent molecule occupying the vacant coordination site and induces a preference for a particular propeller (Figure 59B).[133] The chirality of the bound acid could then be determined through CD analysis of the metal complex.

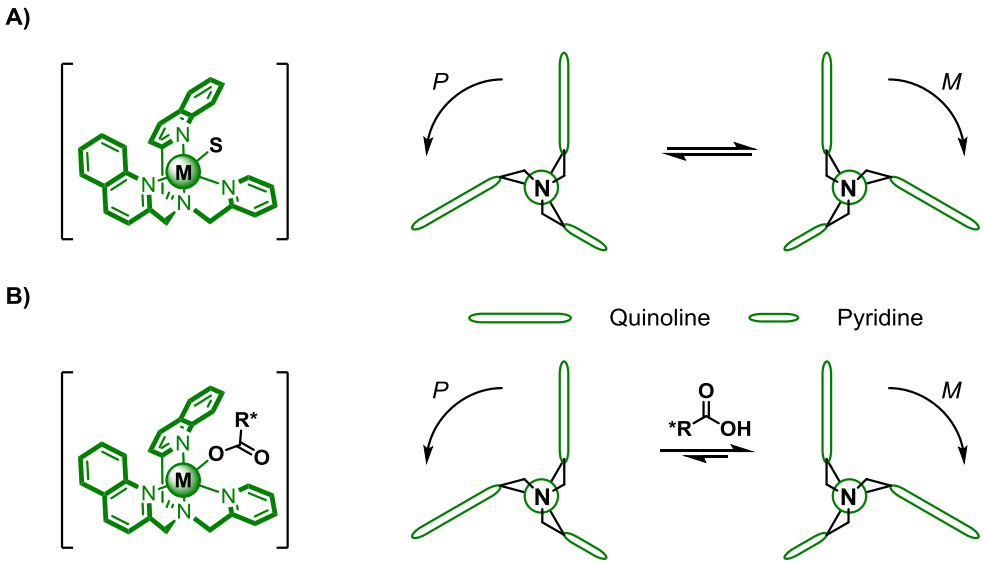

Figure 59A) BQPA metal complexes exist in equilibrium between M and P propellers. **B)** Binding of chiral carboxylate biases equilibrium (M=Zn^{II} or Cu^{II}, S=solvent, R* = chiral group).

During the successful development of the fluorescence probe structure, a separate N-terminal binding site structure was developed by Dr. Bryden Le Bailly within the Clayden group. Introduction of a carboxylic acid at the 3-position of the pyridine ring in the BQPA ligand **184** provided a handle for attachment to the N-terminus of Aib-based helices. Attachment to Aib_4GlyNH_2 **185** gave the helical ligand **186**. Choosing a Zn^{II} for its NMR compatibility Le Bailly [†] formed Zn^{II} complex **187**. CD analysis of the BQPA binding site and NMR analysis of the glycinamide probe showed that the BQPA metal complex was an effective receptor mimic, binding a

range of carboxylate agonists in NMR solvents and relaying their chiral information through the helix to the remote NMR probe.

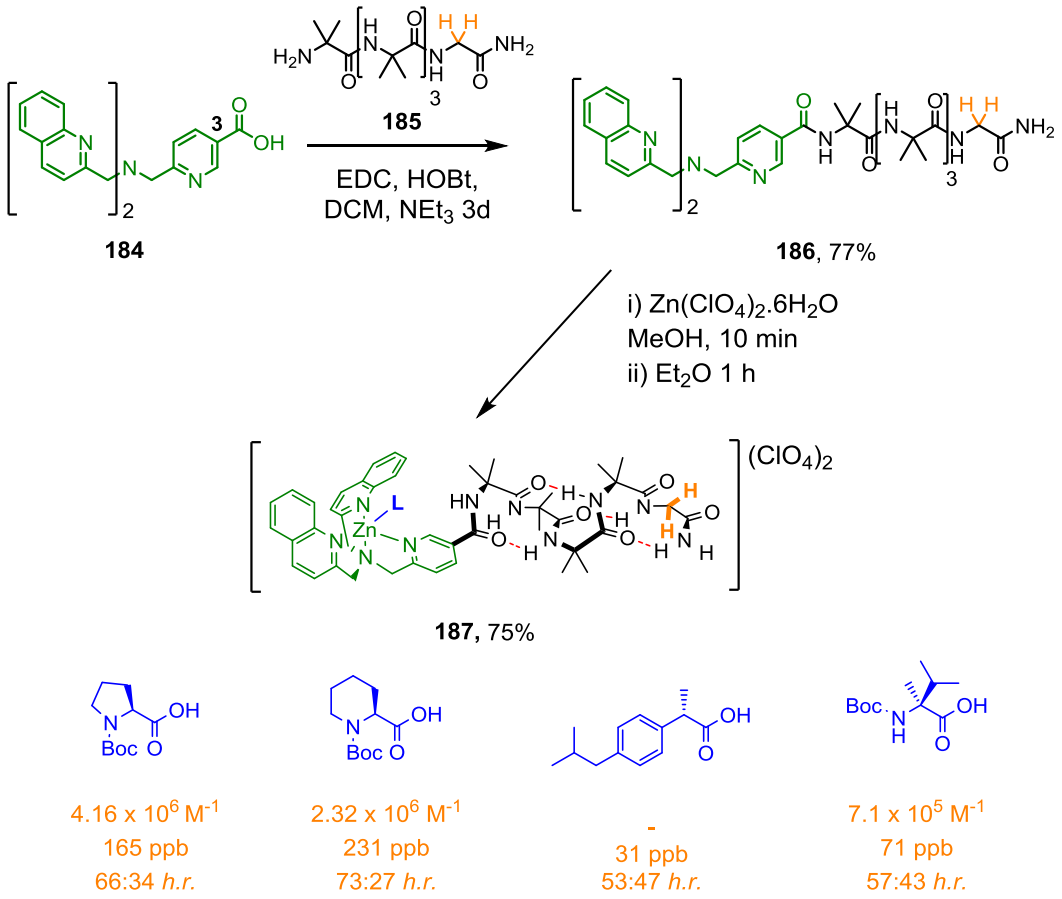

Scheme 43 - The BQPA binding site developed for Aib helices‡

‡ B. A. F. Le Bailly, PhD Thesis, University of Manchester, 2015

7.2 Aims: Membrane Based GPCR mimics.

With a fully-functioning fluorescence probe and binding site (developed within the group), both the components were incorporated into a potential synthetic GPCR mimic. The aim was to attach both the BQPA binding site to the N-terminus and the *S*,*S*-BisPyrEt-NHAc probe to the C-terminus of an Aib-based helical peptide. The compound would then be embedded in the membrane of lipid vesicles and the effect of carboxylate addition to the surrounding solution investigated (Figure 60). Upon addition, a chiral carboxylate was expected to bind at the N-terminal metal centre. The stereochemical information of carboxylate binding would be relayed through the membrane, through screw-sense control of the peptidic helix. Detection and quantification of the helical screw-sense preference could be achieved using the pyrene probe at the C-terminus. Use of amino acids with differing binding strengths would allow reversible switching between *M* and *P* screw-sense preferences.

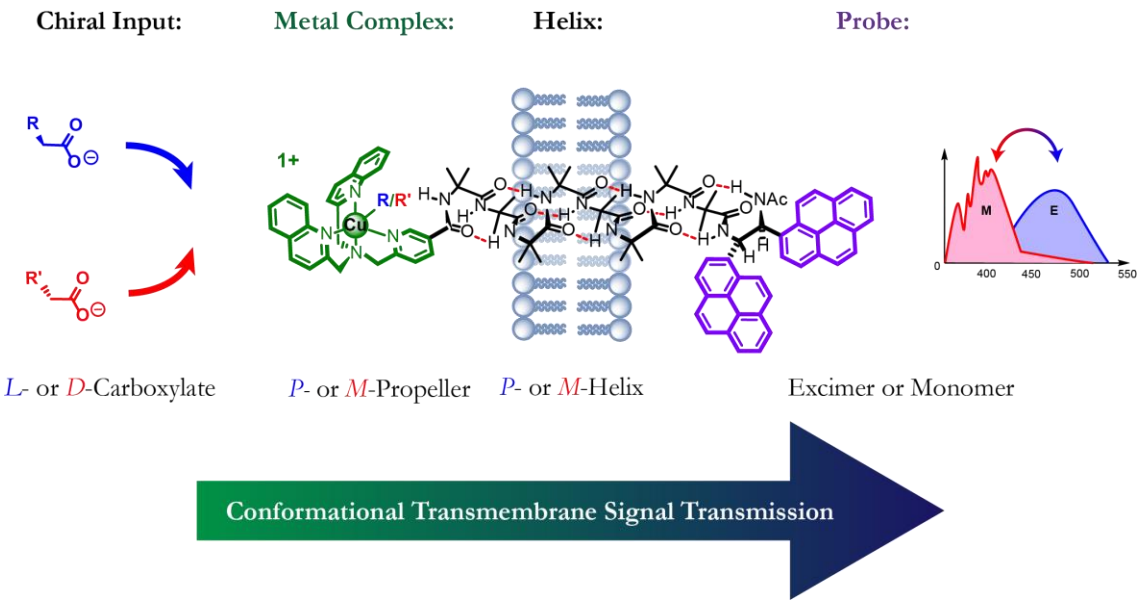

Figure 60 - Proposed Design of a biomimetic GPCR.

7.3 Synthesis of BQPA-3-CO-Aib$_4$-*S*,*S*-BisPyrEt-NHAc

Synthetic idiosyncrasies of both the BQPA and *S*,*S*-BisPyrEt-NAc fragment meant the synthesis of the desired BQPA-3-CO-Aib$_4$-*S*,*S*-BisPyrEt-NAc **188** structure was not completely straightforward (Scheme 44). Attaching the BQPA fragment to the Aib$_4$ helix required a free amine at the N-terminus. The poor success of reducing N$_3$Aib$_4$-*S*,*S*-BisPyrEt-NAc **155** (Section 5.23) meant the *S*,*S*-BisPyrEt **120** would have to be attached after BQPA coupling. Typically the C-terminus of the Aib$_4$O^{t}Bu helix **189** is de-protected using TFA giving a C-terminal acid to couple *S*,*S*-BisPyrEt **120**. Exposure of the BQPA fragment to TFA leads to undesired protonation of the basic nitrogen positions.

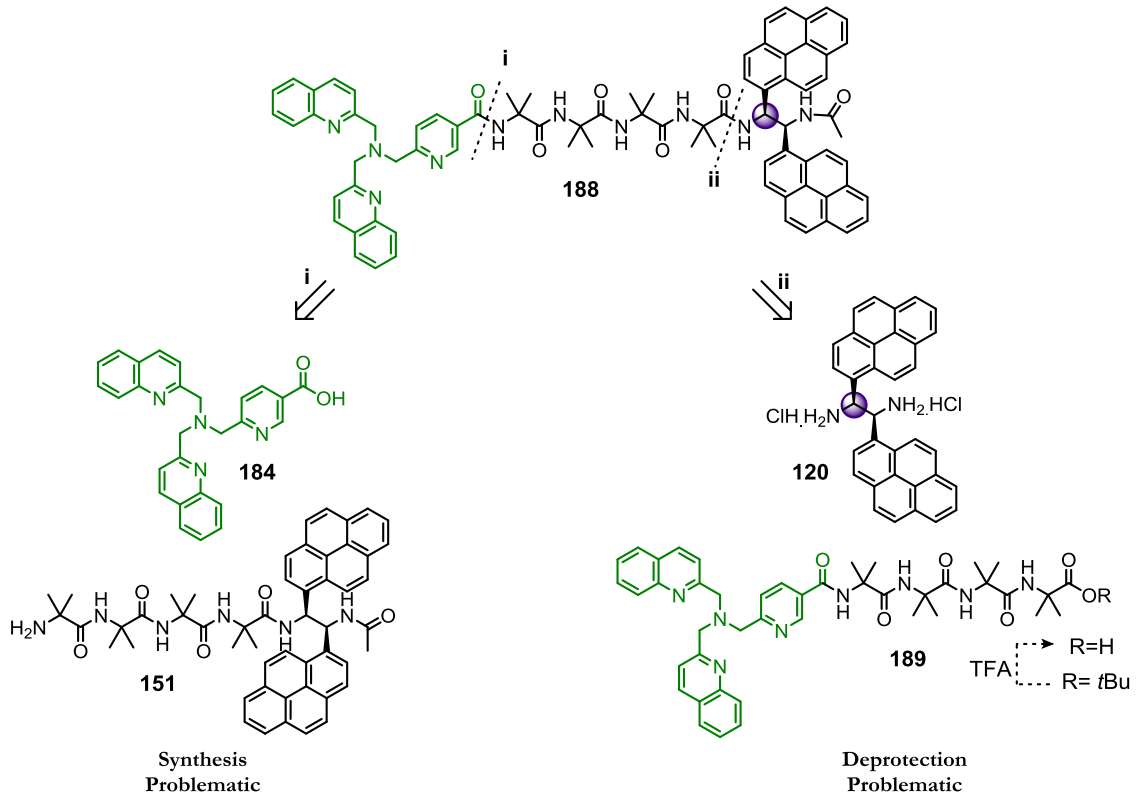

Scheme 44 - Synthetic challenges in the synthesis of BQPA-3-CO-Aib$_4$-*S*,*S*-BisPyrEt-NAc.

Strategically, (Scheme 45) it was decided to use a methyl ester at the C-terminus. The BQPA-3-COOH **184** would be attached first to H-Aib$_4$-OMe **190** to give **191.** Cleavage of the methyl ester could be performed without TFA giving BQPA-3-CO-Aib$_4$-OH **192** ready for coupling to *S*,*S*-BisPyrEt dihydrochloride **120.** Following this procedure **192**[§] was reacted with **120.** Due to the high polarity of the BQPA fragment and previous observations of probe instability when left as the free amine the crude mixture was acetylated in a 1-pot procedure giving BQPA-3-CO-Aib$_4$-*S*,*S*-BisPyrEt-NAc **188** in 56% yield

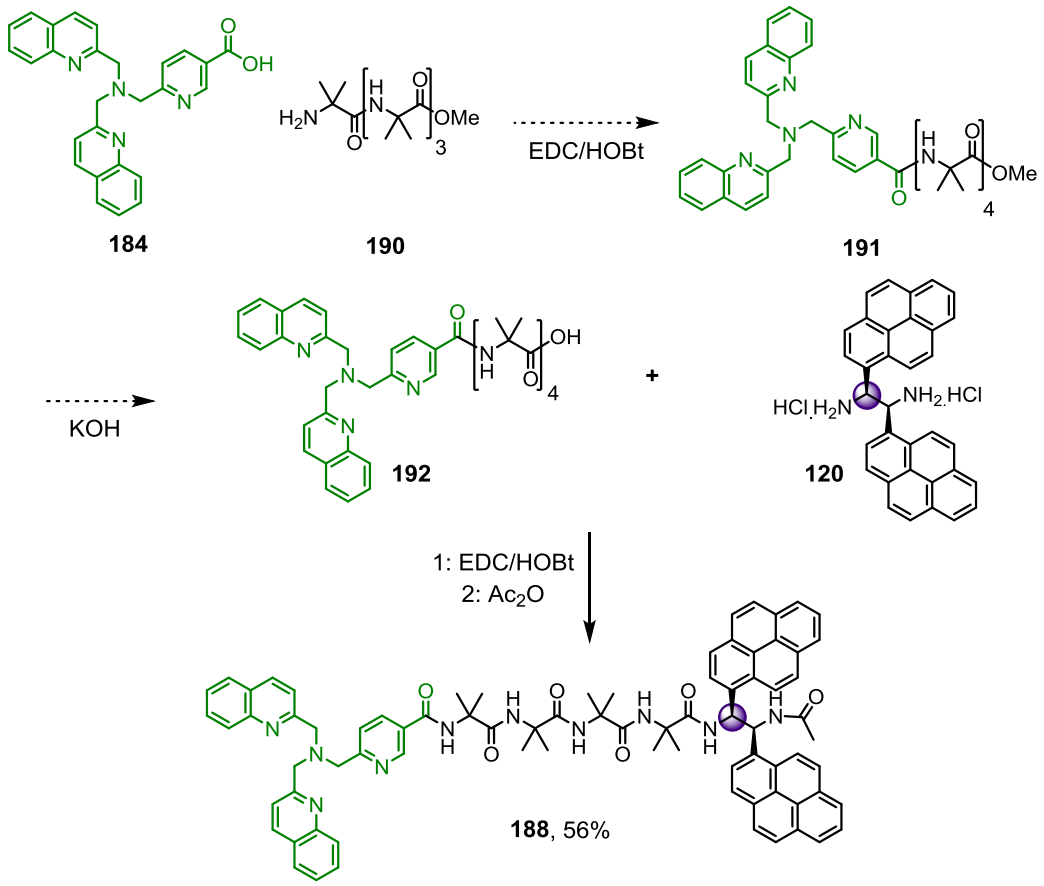

Scheme 45 – synthesis of BQPA-3-CO-Aib$_4$-*S*,*S*-BisPyrEt-NAc.

§ Supplied by Dr. B. Le Bailly

7.4 Synthesis & Solution Behaviour of 1st Generation GPCR Mimic

Formation of a Zn^{II} complex with **188** and its subsequent precipitation gave the metal complex **193** in 70 % yield, the first viable receptor mimic.

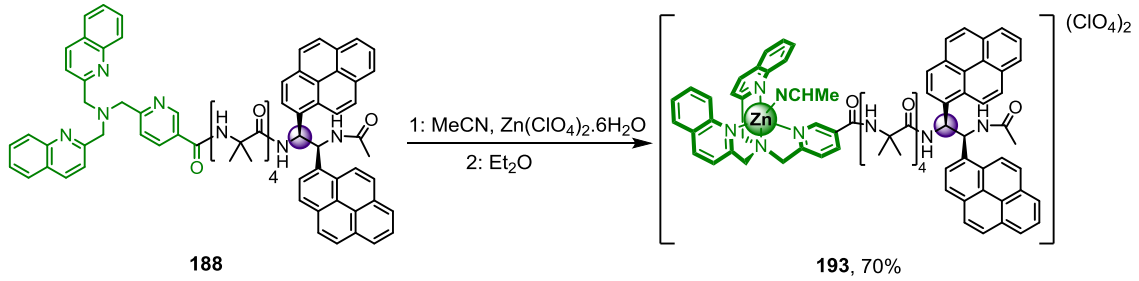

Scheme **46** - synthesis of the first receptor mimic.

Dilution studies, identical to those used for earlier compounds (Section 5.13) in the project were performed in a range of organic solvents (Figure 61A). The E/M ratio observed in MeCN was 1.80±0.03. In MeOH it was found to be 2.51±0.01. The metal complex **193** was found to aggregate slightly more in DCM with an E/M ratio of 1.38±0.03. These results indicate that the sensitivity of the pyrene probe to intermolecular aggregation is low at these concentrations, confirming the pyrene probe can be used in conjunction with metal complex binding sites.

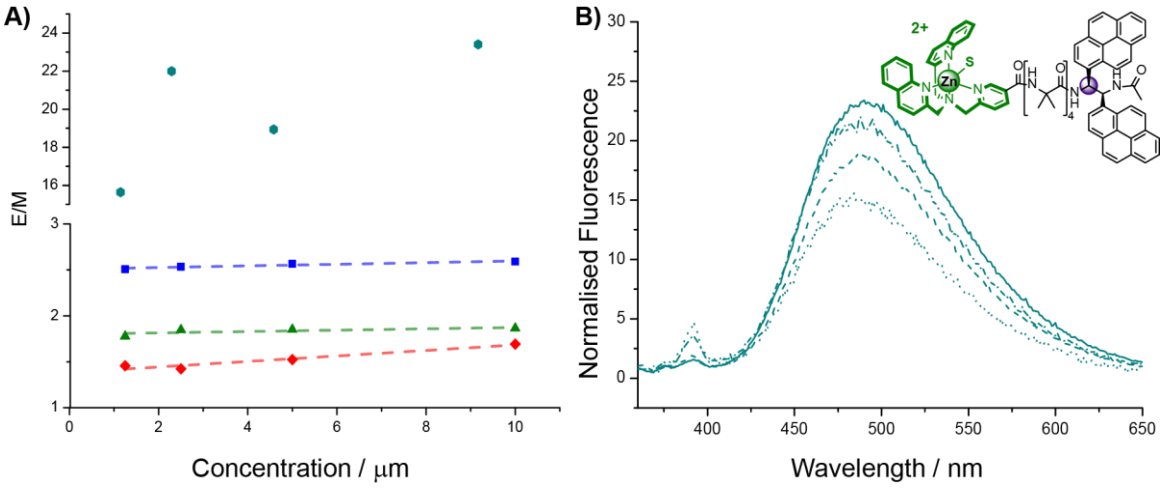

Figure 61A) The observed excimer/monomer ratios of metal complex **193** at varying concentration in DCM ◆, MeOH ■, MeCN▲ and MOPS Buffer solution (20 mM + 100 mM NaCl)●. **B)** Fluorescence spectra of metal complex **193** in MOPS Buffer solution at 10 (———), 5 (— — —), 2.5 (— · —), and 1.25 (▪▪▪) μM concentrations.

The fluorescence of **193** was also investigated in the MOPS buffer solution used previously to prepare vesicles (Sections 5.15 & 5.21). The high levels of excimer fluorescence and strong concentration dependence of the E/M ratio of **193** was

thought to arise from the intermolecular interaction of aggregating pyrene groups. This heavy aggregation may be considered problematic; however the hydrophobic forces that cause aggregation of the pyrene groups in **193** are desirable in driving their incorporation into the hydrophobic region a membrane. It was hoped that the hydrophobic pyrene groups would penetrate the bilayer, leaving the charged binding site exposed on the outer surface of the vesicle, primed to accept carboxylate agonists.

Having confirmed the fluorescence of the probe reflected the intramolecular properties of the peptidic helix, the effect of carboxylate addition to receptor mimic **193** was investigated in both MeOH and MeCN (Figure 62A). It has been shown by B. Le Bailly using the C-terminal NMR probe that Boc-Pro induces the greatest control of screw-sense preference on interaction with the metal complex binding site.[**]

The fluorescent response of **193** on titration with optically pure Boc-Pro was measured in both MeOH and MeCN (Figure 62A). Increasing concentrations of Boc-Pro (up to a 1:1 ratio with **193**) led to changes in the E/M ratio. As expected, opposite enantiomers of Boc-Pro gave opposite fluorescence reponses. The earlier fluorescence results observed for the *S*,*S*-BisPyrEt-NAc probe **148** when attached to helices of known screw-sense preference provided useful key information on the probes behaviour (Section 5.25). Helices with a *P* preference gave increased E/M ratios whereas those with an *M* preference gave reduced E/M ratios. Based on these results, the fluorescent response of **193** to Boc-L-Pro and Boc-D-Pro addition indicates that Boc-L-Pro binding induces a *P* screw-sense preference and Boc-D-Pro induces an *M* screw-sense preference.

** B. A. F. Le Bailly, PhD Thesis, University of Manchester, 2015

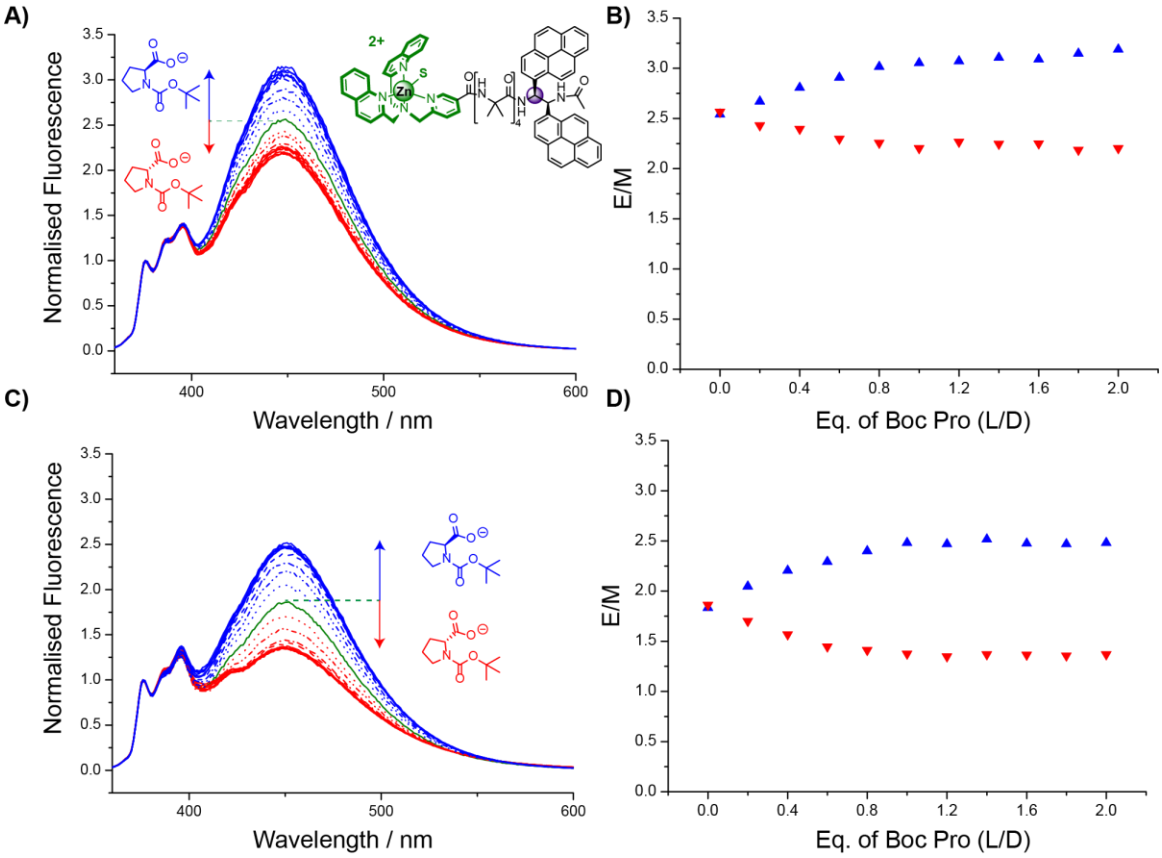

Figure 62A) Fluorescence spectra of **193** (10 μM) in MeOH (—) on titration with Boc-L-Pro [0-20 μM] (—) and lutidine [0-24 μM] or Boc-D-Pro [0-20 μM] (—) and lutidine [0-24 μM] **B**) Titration curve of **193** (10 μM) in MeOH with increasing concentrations of with Boc-L-Pro [0-20 μM] (▲) and lutidine [0-24 μM] or Boc-D-Pro [0-20 μM] (▼)and lutidine [0-24 μM]. **C**) Fluorescence spectra of **193** (10 μM) in MeCN, other conditions identical to **A**. **D**) Titration curve of **193** in MeCN other conditions identical to **B.**

Above a 1:1 ratio with **193**, a plateau in the E/M response is observed for both L and D Boc-Pro. As the metal complex is known to bind carboxylates in a 1:1 ratio, these plateaus are good evidence of binding site control of screw-sense preference. Once the binding site is fully saturated, no further screw-sense control is placed on the helix. The fluorescence plateaus also highlight that the probe is functioning effectively and not interacting directly with the carboxylate in solution.

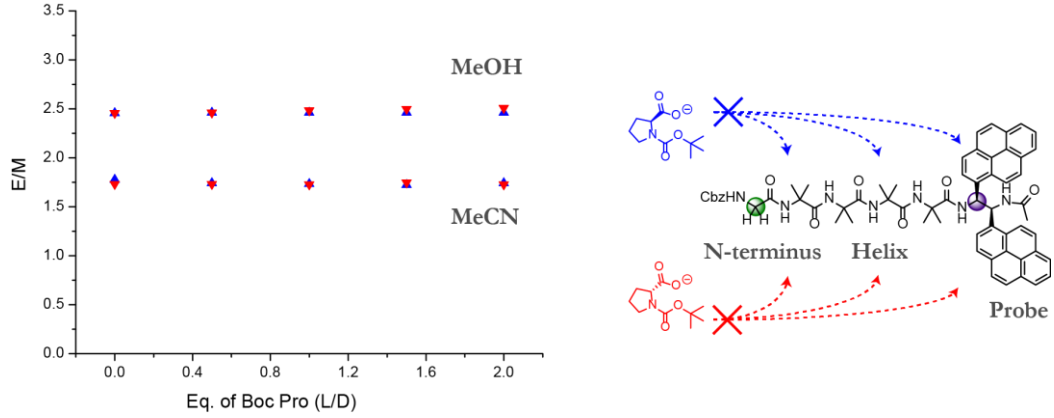

Figure 63A) Titration curves of **151** (10 μM) in MeOH and MeCN with increasing concentrations of with Boc-L-Pro [0-20 μM] (▲) or Boc-D-Pro [0-20 μM] (▼). Both with lutidine [0-24 μM].

The titration curve of the structurally similar Gly-Aib$_4$-*S*,*S*-BisPyrEt-NAc **151** (Figure 63A) which lacks the N-terminal binding-site, provides a useful control experiment for the switchable system. Addition of Boc-Pro under identical conditions used for **193** led to no change in the observed E/M ratio. This provides further evidence that the carboxylate is not interacting directly with the probe structure, or the peptide itself.

Considering the results of titration experiments for **151** and **193** together it is clear that the receptor mimic is functioning effectively in solution, with Boc-Pro, the synthetic agonist, binding at the metal complex, the synthetic receptor. With the fluorescence probe allowing detection of signal relay through the achiral helix from this binding interaction, the next step was to investigate the behaviour of these systems in the membrane environments of synthetic vesicles.

7.5 Membrane Behaviour of 1st Generation GPCR mimic

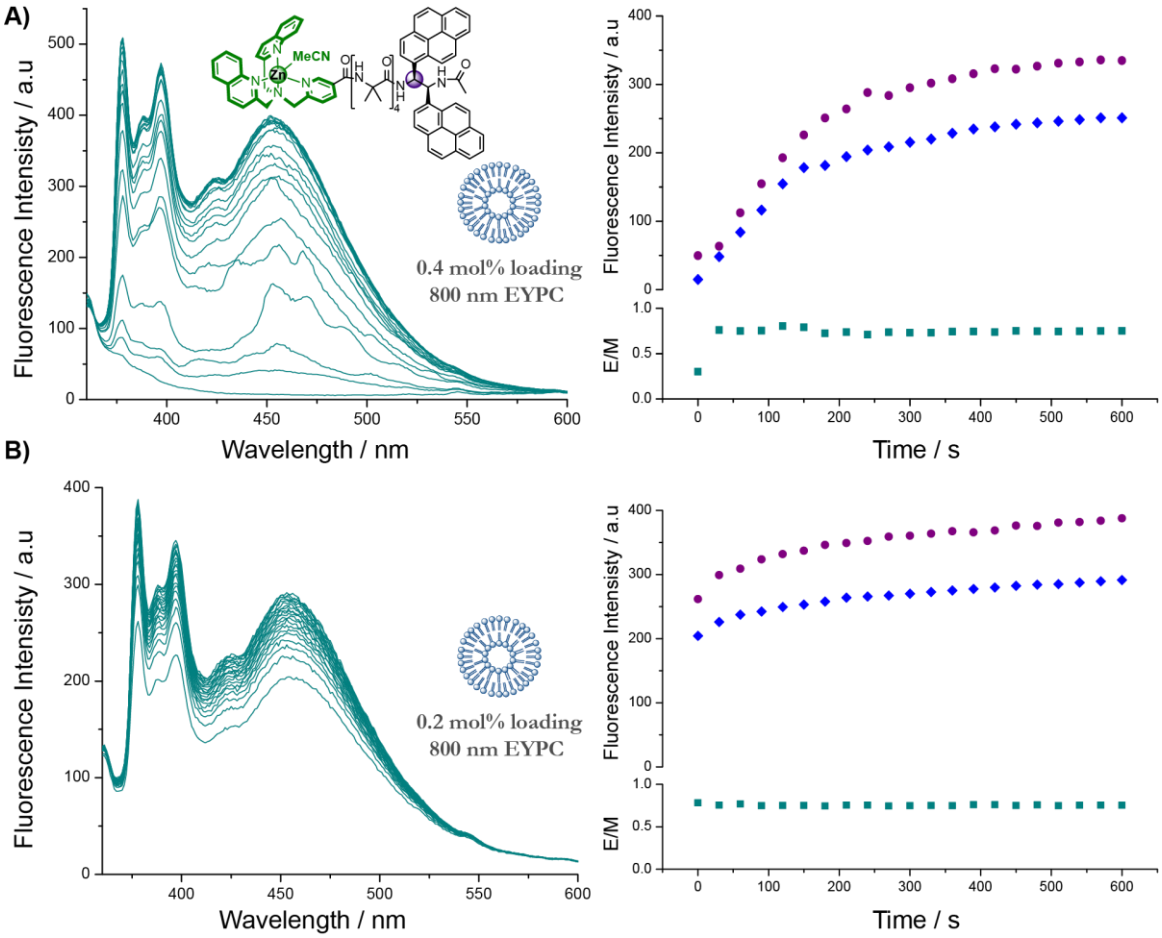

Figure 64 - Timed fluorescence spectra of **193** (10 μM) (—) added to 5 mM (**A**) and 2.5 mM (**B**) solutions of 800 nm EYPC vesicles in MOPS buffer solution (20mM + 100 mM NaCl). Time plots (RHS) show the measured values for maximum for Monomer [378 nm] (●), Excimer [450 nm] (◆) and the ratio of Excimer to Monomer fluorescence (■) over time.

Having developed an effective mimic of a GPCR receptor in solution the key phase in the project was to develop its functionality in membrane environments. Egg-yolk phosphatidylcholine (EYPC) a mixture of saturated lipids extracted from hen's eggs was initially chosen to construct the synthetic vesicles as it was most structurally similar to naturally occuring membranes. Lipid films were prepared by evaporating chlorinated stock solutions and rehydrating with a MOPS buffer solution. These lipid suspensions were extruded through a polycarbonate membrane following the method of Szoka *et al.*[85] To give suspensions of 800 nm EYPC vesicles. Keeping the concentration of **193** at 10 μM throughout the experiments, the concentration of vesicles was varied to provide information of the effect of loading concentration in the vesicle. Compound **193** (10 μM) was added to stirred solutions of vesicles at concentrations of 5 mM and 2.5 mM inside the fluorimeter allowing flourescence to be measured over time (Figure 64).

The injection data indicated that **193** is entering the membrane of EYPC vesicles, appearing to reach a stable state over an hour of mixing. Comparing the fluorescence spectra of **193** when added to vesicles (Figure 64) to the fluorescence spectra observed in buffer solution (Figure 65A), it is clear that the complex is interacting with the membrane of the vesicles rather than aggregating in solution as the E/M ratio of 0.75 observed after 1 h is 30 times smaller than that observed at the same concentration in buffer solution alone (E/M = 23.4).

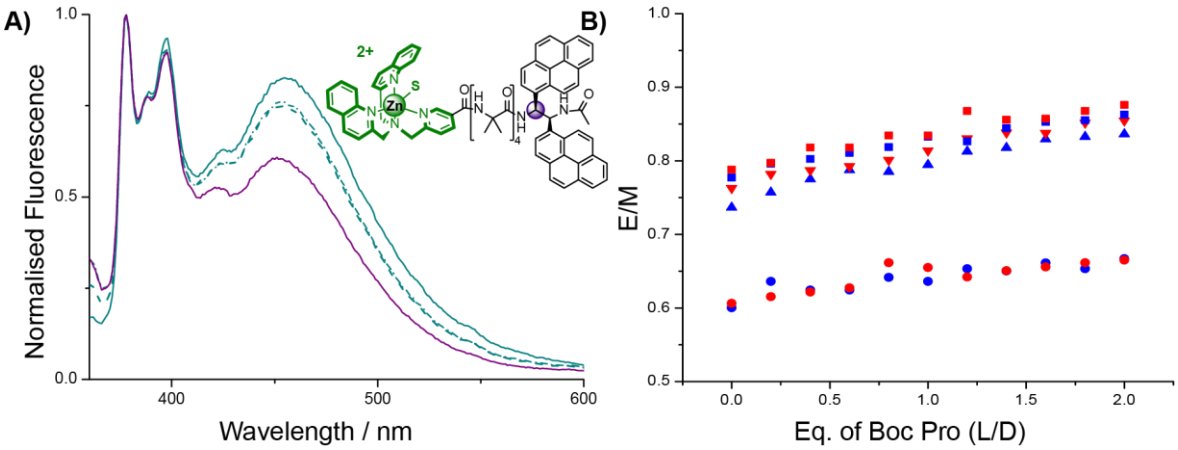

Figure 65A) Fluorescence spectra of **193** 1h after addition to 1mM (——), 2.5 mM (— — —), 5 mM (— ▪ —) solutions 800 nm EYPC vesicles and (——) 5 mM of 800 nm 2:8 cholesterol:EYPC vesicles. **B)** Titration curves for **193** with increasing concentrations of (0-20 μM) Boc-L-Pro or Boc-D-Pro and lutidine (0-24 μM) in 5mM preparations of 800 nm vesicles: EYPC with 20 mM MOPS 100mM NaCl buffer (▲/▼). EYPC with salt-free 20 mM MOPS buffer.(■/■), 2:8 cholesterol:EYPC with salt-free 20 mM MOPS buffer (●/●).

If as the data suggests, the compound has entered the membrane environment, its concentration relative to itself will be much higher than that in solution, as its motion is confined to the far smaller volume of vesicle membranes. Bearing this in mind, the effect of loading concentration on the observed fluorescence ratios was measured by addition of **193** to vesicle suspensions of 1, 2.5 and 5 mM to give three 10 μM solutions with membrane loadings of 1, 0.4 and 0.2 mol% respectively. The effect of varying lipid constituency on the baseline E/M ratio was also measured with addition of **193** to a 5 mM suspension of vesicles comprised of 2:8 Cholesterol:EYPC (Figure 65A). The findings in EYPC indicate that the E/M ratio is stable at loadings of 0.4 mol% (5 mM vesicles) and 0.2 mol% (2.5 mM vesicles). Increasing the loading to 1% leads to increased relative excimer, likely due to intermolecular excimer formation due to membrane confinement.

Having prepared the vesicle suspensions, aliquots of Boc-Pro were then added, attempting to induce analogous switching behaviour observed in solution. (Figure 65B). Unfortunately, addition of both L and D Boc-Pro lead to an increase in the E/M ratio, suggesting a separate process was affecting the fluorescence signal. It was thought that the lutidine present in the titrations of either enantiomer might be partitioning in the membrane and changing is local environment leading to the rise in E/M ratio.

7.6 Searching for the Binding Site

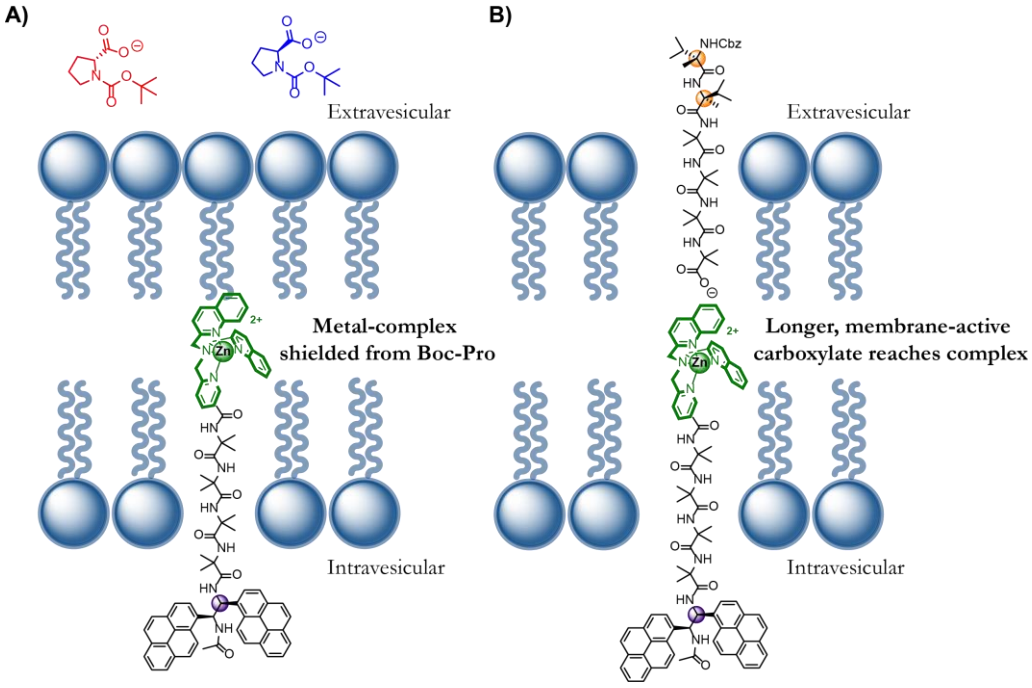

Figure 66A) Proposed problem and solution with the first generation GPCR mimic **A**) Burial of binding site within lipid bilayer prevents binding of carboxylate in vesicle structure. **B**) Longer, membrane active carboxylate reaches binding site.

One of the possible issues with the early GPCR mimic is that the Zn binding site might be buried within the membrane environment of the vesicles, an illustrative example is depicted in Figure 66A although a variety of possible membrane orientations may prevent access to the binding site. If the binding site is submerged within the bilayer, the longer carboxylate Cbz-L-(αMe)Val_2-Aib_4OH **142** was more likely to partition in the membrane and be of sufficient length to reach the binding site (Figure 66B). The controlling effect of **142** was investigated in MeOH using identical conditions used for Boc-Pro addition (Figure 66A&B)

The results in solution (Figure 67A&B) indicate that Cbz-(αMe)Val_2-Aib4OH **142**, a known P-helix,[48] binds and induces *M* screw-sense preference in the receptor structure. Inai and co-workers observed similar behaviour for a right handed *P* helix composed of chiral amino acids inducing left-handed helicity in a configurationally achiral helix to which it was attached.[135] Unfortunately the results in the membrane were unsatisfactory: changes in the E/M value were observed but were noisy and followed no obvious relationship to the concentration of carboxylate present.

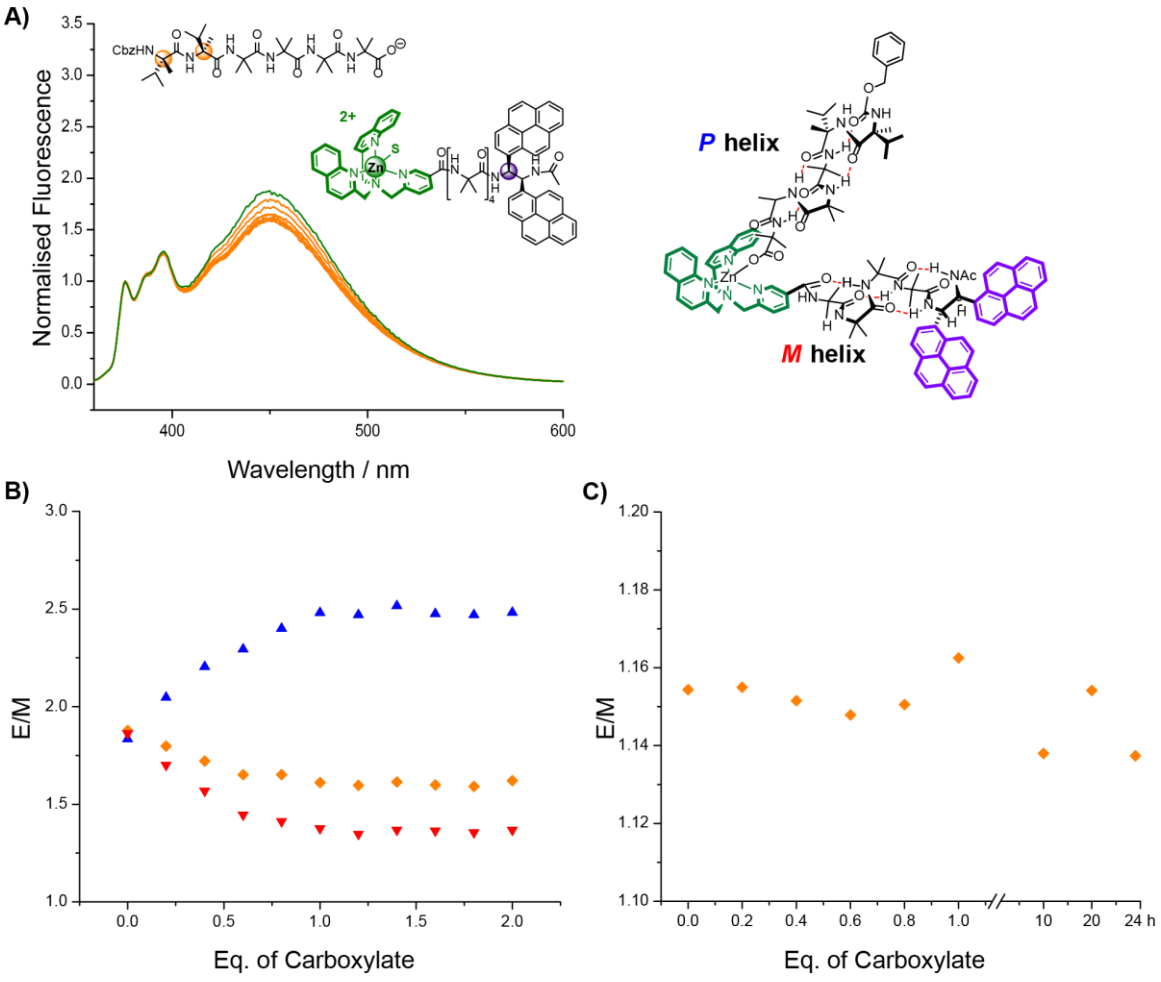

Figure 67A) Fluorescence spectra of **193** (10 μM) in MeOH (—) on titration with Cbz-(αMe)Val_2-Aib_4OH [0-20 μM] (—) and lutidine [0-24 μM].**B)** Titration curve of **193** (10 μM) in MeOH with increasing concentrations of with Boc-L-Pro [0-20 μM] (▲), Boc-D-Pro [0-20 μM] (▼) or Cbz-(αMe)Val_2-Aib_4OH [0-20 μM] (◆) all with lutidine [0-24 μM]. **C)** Titration curve of **193** in 2.5mM solution of 800 nm DOPC vesicles [1h wait time, 20 MOPS, no salt] with Cbz-(αMe)Val_2-Aib_4OH [0-10 μM] (◆) and lutidine [0-12 μM]. The effect of leaving the vesicles on completion of titration over 24 h period is also plotted.

7.7 Development of 2nd Generation GPCR mimic

The failure of the Zn^{II} binding site of **193** was identified as a possible reason for no observable signal transfer in membrane environments. In organic solvents, the Zn^{II} BQPA complex adopts a 5-coordinate geometry with a solvent molecule transiently occupying the 5th position. Binding of a carboxylate displaces the solvent molecule and indices as screw-sense preference in the complex which in-turn controls the screw-sense preference of the helix. In aqueous environments there is the potential for the Zn^{II} complex to adopt a 6-coordinate geometry that induces no control on the helix. In their work with BQPA structures Anslyn and co-workers use a Cu complex in the centre which can only adopt the controlling 5-coordinate geometry. As copper is paramagnetic its use in the NMR systems was impractical. While copper ions are known fluorescence quenchers, it was thought that the separation of binding site and probe by the helix would prevent quenching.

To save the synthetically expensive pyrene ligand **188** the comparative binding strength of the Cu^{II} and Zn^{II} BQPA sites was assessed using the metal complexes of BQPA-3-CO-Aib_4-Gly-NH_2 **194**. Zn^{II} BQPA-3-CO-Aib_4-Gly-NH_2 **195** Was supplied by Dr B. Le Bailly. Cu^{II} BQPA-3-CO-Aib_4-Gly-NH_2 **196** was synthesised in 80% yield from **194**

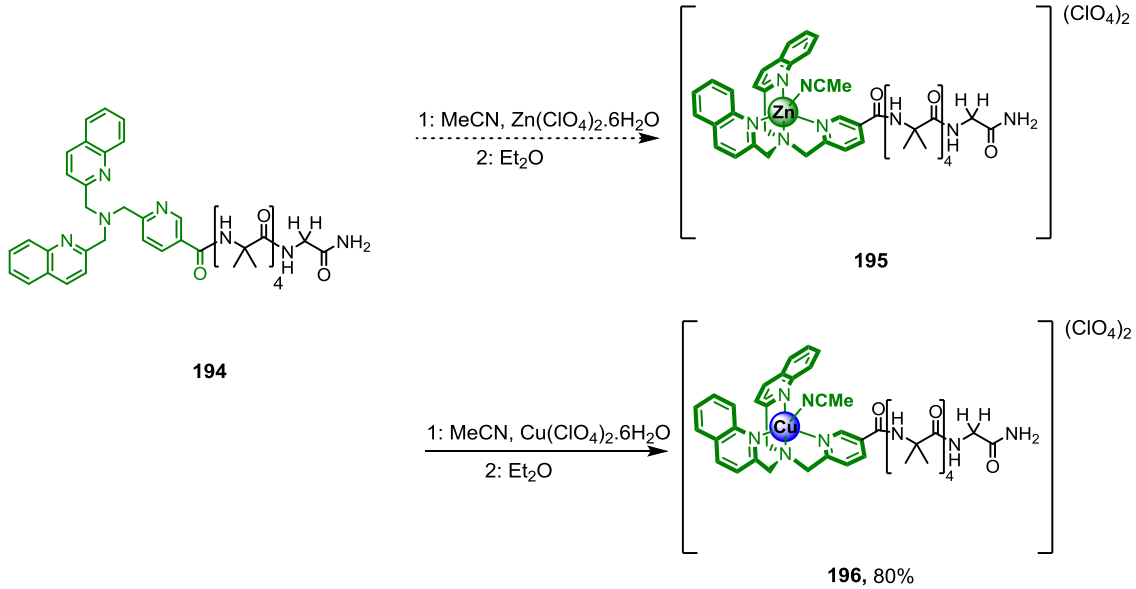

Scheme 47 - Synthesis of Cu^{II} BQPA-3-CO-Aib_4-Gly-NH_2

The concentration of the compounds had to be increased compared to the fluorescence compounds to observe a CD signal. Both compounds were added to 5 mM solutions of 800 nm EYPC vesicles to make 0.1 mM concentration solutions of the metal complexes as 1 mol% loading in the vesicles. Addition of increasing amounts of Boc-L-Pro allowed for the analysis of binding strength using the CD response of the BQPA structure. The binding constant of Zn^{II} BQPA-3-CO-Aib_4-Gly-NH_2 in EYPC was found to be (50±30) M^{-1} (> 20,000 × weaker than in MeCN) As hoped, the binding constant of Cu^{II} BQPA-3-CO-Aib_4-Gly-NH_2 was found to be measurably stronger than that of the Zn binding site. (900±300)M^{-1}. These results clearly indicate that the adoption of a Cu binding site in the GPCR mimic is likely to greatly improve its function in membrane environments.

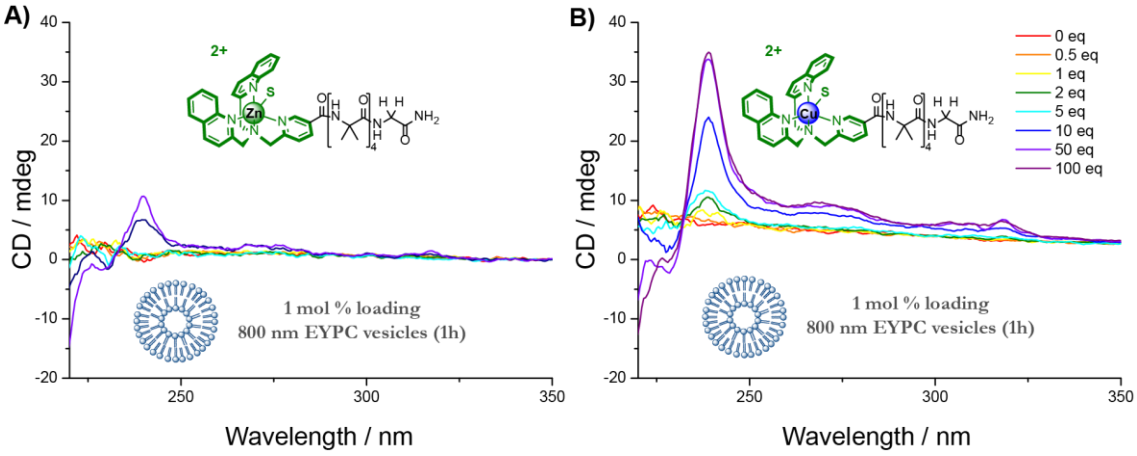

Figure 68 - comparative CD of **195** and **196** CD response to changing equivalents of Boc-L-Pro-Na when embedded in EYPC vesicles.

7.8 Synthesis of 2nd generation GPCR mimic

With the binding site analysis indicating the unsatisfactory binding strength of the Zn^{II} site, the development of a second generation GPCR mimic replaced the Zn^{II} with a Cu^{II} centre. Following identical methodology for the synthesis of **193** the second generation GPCR mimic was synthesised from **188** and $Cu^{II}(ClO_4)_2.H_2O$ isolating the metal complex **197** in 80% yield.

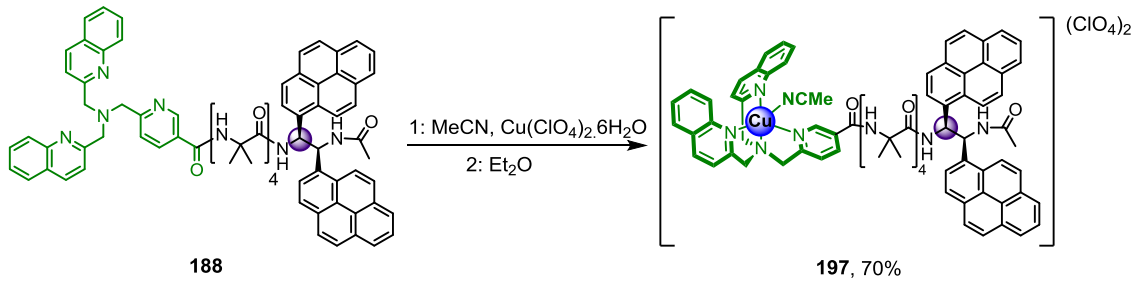

Scheme 48 - The synthesis of Cu^{II}BQPA-3-CO-Aib$_4$-Gly-*S*,*S*,-PyrEt-NHAc

The solution fluorescence of **197** was measured over the usual 1.25-10 μM range to confirm the pyrene probe was compatible with the new Cu^{II} metal centre (Figure 69A). The E/M ratios observed were similar to those observed for the Zn^{II} complex. The E/M ratio in MeCN was 1.53±0.02 (cf. Zn 1.80) In MeOH the E/M was 2.55±0.02 (cf. Zn 2.52).

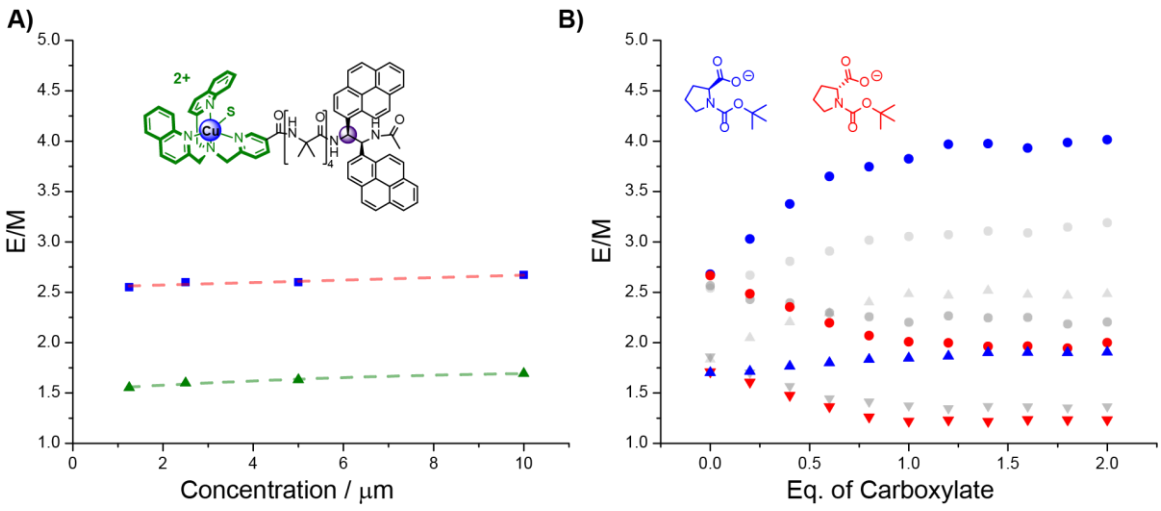

Figure 69A) The observed Excimer/Monomer ratios (E/M) of metal complex **197** at varying concentration in MeOH ■ and MeCN ▲ **B)** Titration curve of **197** (10 μM) in MeOH (●/●) and MeCN (▲/▼) with increasing concentrations of Boc-L-Pro [0-20 μM] (●/▲), Boc-D-Pro [0-20 μM] (●/▼). Results for **193** (Fig58) shown in grey for comparison.

Analysis of the switching behaviour of the Cu^{II} analogue produced some interesting results (Figure 69B). The magnitude of the switch for the Cu^{II} complex in MeOH was 2.01, 2.05 times larger than the Zn^{II} complex (1.12). In MeCN the size of the switch was 0.68, 1.65 times smaller than that of the Zn^{II}complex (1.12). As discussed earlier (Section 5.14) clearly the chirality of the probe and the solubility of the pyrene groups in an individual solvent affects the readings. A carboxylate that binds and induces *P* helicity is expected to induce greater excimer fluorescence. In real terms this means the forcing together of the two pyrene fragments which, due to the chirality of the probe, is not energetically equal for both screw-sense preferences. A solvent that favours π-stacking of the pyrene groups will lower the energy required to force them together. This in turn will result in carboxylates that induce *P*-helicity having artificially high binding constants. In the development of the BQPA ligand system, the binding constant for Boc-L-Pro and Zn^{II} BQPA-3-CO-Aib_4-Gly-NH_2 **195** was found to be $>10^6$ M^{-1} in MeCN.[††] As **195** is achiral both Boc-L-Pro and Boc-D-Pro can be expected to bind with equal strength. Comparing this result with the results for Zn^{II}BQPA-3-CO-Aib_4-*S*,*S*-BisPyrEt-NAc **193** is interesting. The values were found to be $(2\pm1)\times10^6$ M^{-1} for Boc-L-Pro, which induces higher excimer, pushing the pyrenes together. In D the value was double that of the L at $(4\pm2)\times10^6$ M^{-1}. This suggests that the forcing together of the pyrene groups is less favourable in MeCN. A further measurement that supports this is the observed E/M ratios for the Zn^{II} complex in various solvents (Figure 61A). The value for MeCN is lower than that for MeOH, implying that the pyrene groups prefer to stack less in MeCN.

These considerations become more important in membrane environments where the aggregation and stacking of pyrene groups is likely to be heavily affected by the macroscopic environments of different bilayer compositions. Comparison of the E/M ratios observed in membranes at various compositions, prior to any switching behaviour could provide a measure of the local freedom of movement of the pyrenes, or lack thereof.

[††] B. A. F. Le Bailly, PhD Thesis, University of Manchester, 2015

7.9 Membrane Behaviour of the 2nd Generation GPCR Mimic

Once the solution behaviour of the Cu^{II} complex **197** was confirmed, its fluorescence properties in the membrane were investigated. The complex was added to 2.5 mM solutions of a variety of 800 nm vesicles (Figure 70). Like the Zn^{II} complex **193**, the fluorescence signals appeared to stabilise over an hour of stirred addition. A far lower level of excimer was observed for all lipid vesicles investigated.

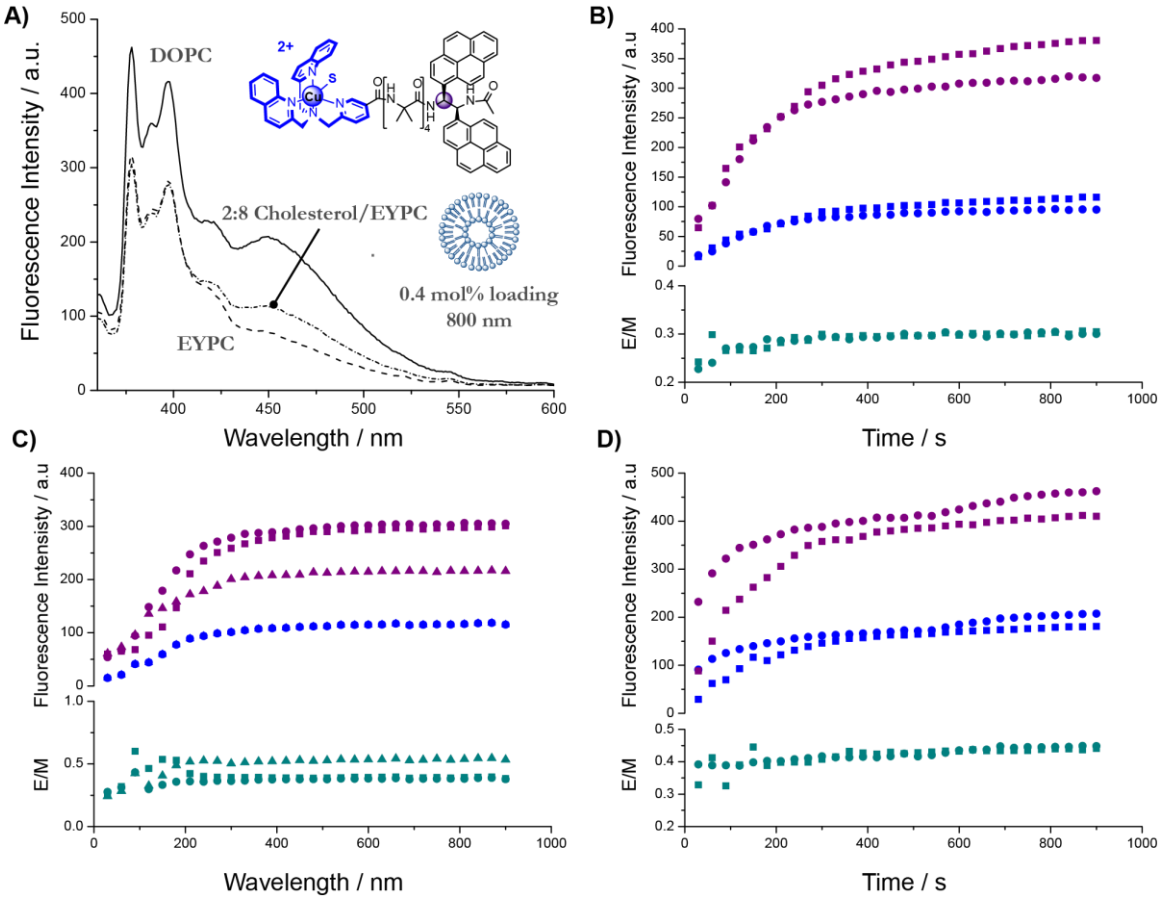

Figure 70 - Observed fluorescence spectra for **197** after 1 h stirring, loading and composition indicated pictorially.(**A**).Timed fluorescence spectra of **197** (10 μM) added to 2.5 mM solution of 2:8 cholesterol/EYPC (**B**), EYPC (**C**) and DOPC (**D**) 800 nm vesicles. Each symbol indicates separate experiment. Colour designates maximum value measured for Monomer [378 nm] (■), Excimer [450 nm] (■) and the ratio of Excimer to Monomer fluorescence (■) over time.

7.10 Membrane Switching of the 2nd Generation GPCR mimic

During the earlier investigations with the Zn^{II} complex (Section 7.5, Figure 64) it was noted that addition of both enantiomers of the optically pure Boc-Pro lead to a rise in the E/M ratio in the membrane environment. It was thought this was due to the presence of lutidine, used to ensure the carboxylic acids existed as a carboxylate in solution. To avoid the use of lutidine, Boc-Pro and subsequent amino acids used were converted to their sodium salts prior to use. Another issue highlighted in the earlier vesicle work is the high concentration of NaCl (100mM) in the buffer solution 10000× higher than the concentration of the complex (10μM). Further work is required to confirm if chloride binding was affecting the switch but the NaCl was removed as a precaution.

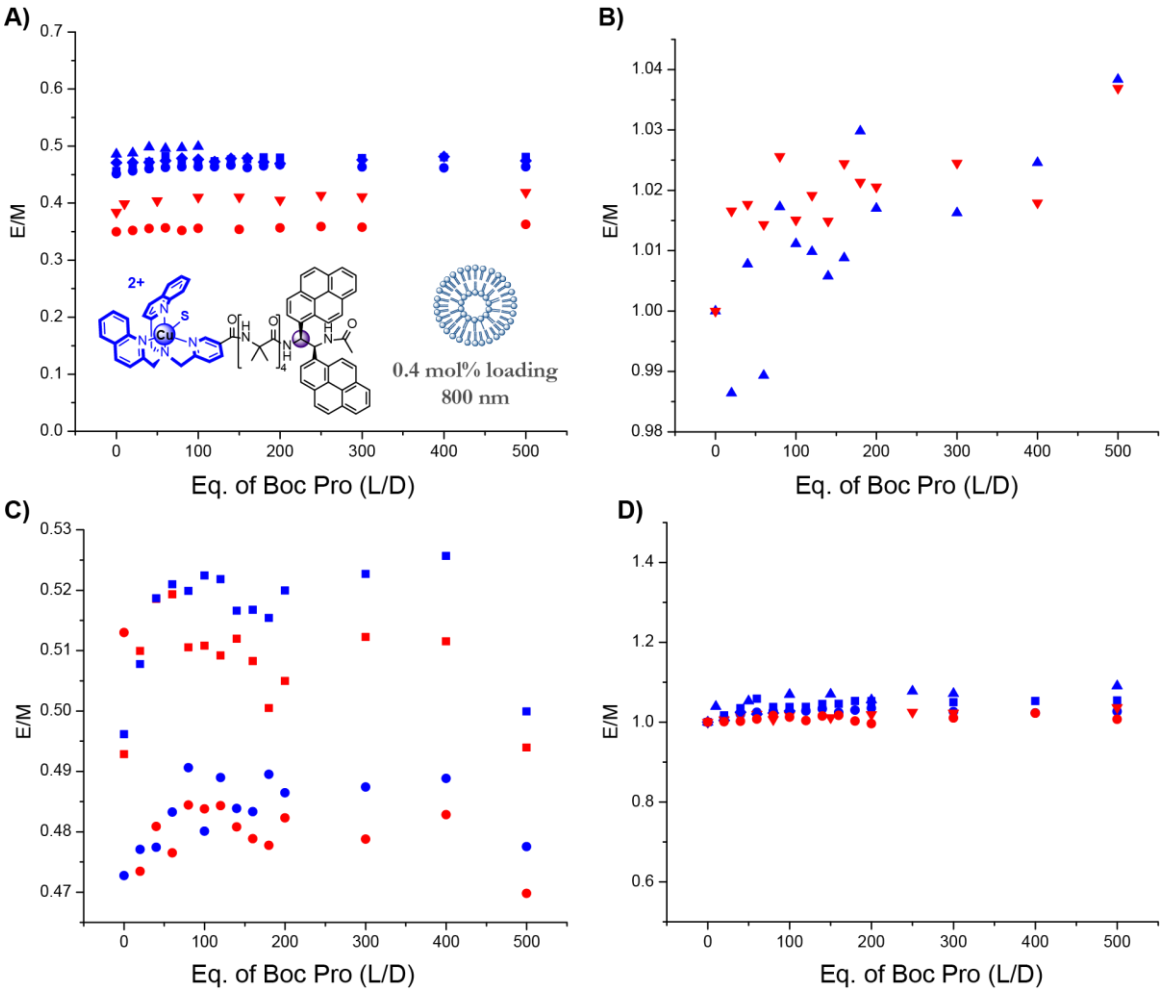

Figure **71** - Titration curves for **197** with increasing concentrations (0-5000 μM) of Boc-L-Pro-Na or Boc-D-Pro-Na in 5mM preparations of 800 nm vesicles comprised of EYPC (**A**) 2:8 cholesterol:EYPC (**B**) or DOPC (**C**). Each symbol indicates separate experiment. Figure **71D**) shows the values measured in (**A**) with the starting values for E/M all normalised to 1.

Unfortunately, none of the attempts to induce switching behaviour in **197** were successful in a variety of membrane environments (Figure 71) The start values obtained for addition of the complex to the vesicle suspensions were less uniform than those obtained for the Zn^{II} complex **193**. In cases where changes were observed, no meaningful signal could be separated from the noise. The difference in starting values obtained is particularly clear in EYPC vesicles (Figure 71A). Due to this it appears that Boc-L-ProNa and Boc-D-ProNa are giving different E/M values in the membrane. Unfortunately however, normalising the start points of this data to 1 (Figure 71D) highlights that the apparent switch behaviour is related to the starting E/M of the experiment, not the addition of Boc-Pro. Pleasingly however there is no change in the E/M ratio for this failed switch, highlighting that the removal of lutidine has removed the erroneous signal changes observed for the Zn^{II} complex

7.11 Membrane Fluidity and the 2nd Generation GPCR Mimic

Restriction of conformational freedom due to the membrane layer was also considered as a possible reason for switch failure in **193** and **197.** Once embedded in the membrane it is possible that the pyrene groups are locked in position due to their bulky nature, preventing a switch. A second possibility which has previously discussed for the Zn^{II} complex **193** (Section 7.6) is that once loaded into the membrane, the binding site of the GPCR mimic is no longer exposed to the extravesicular medium.

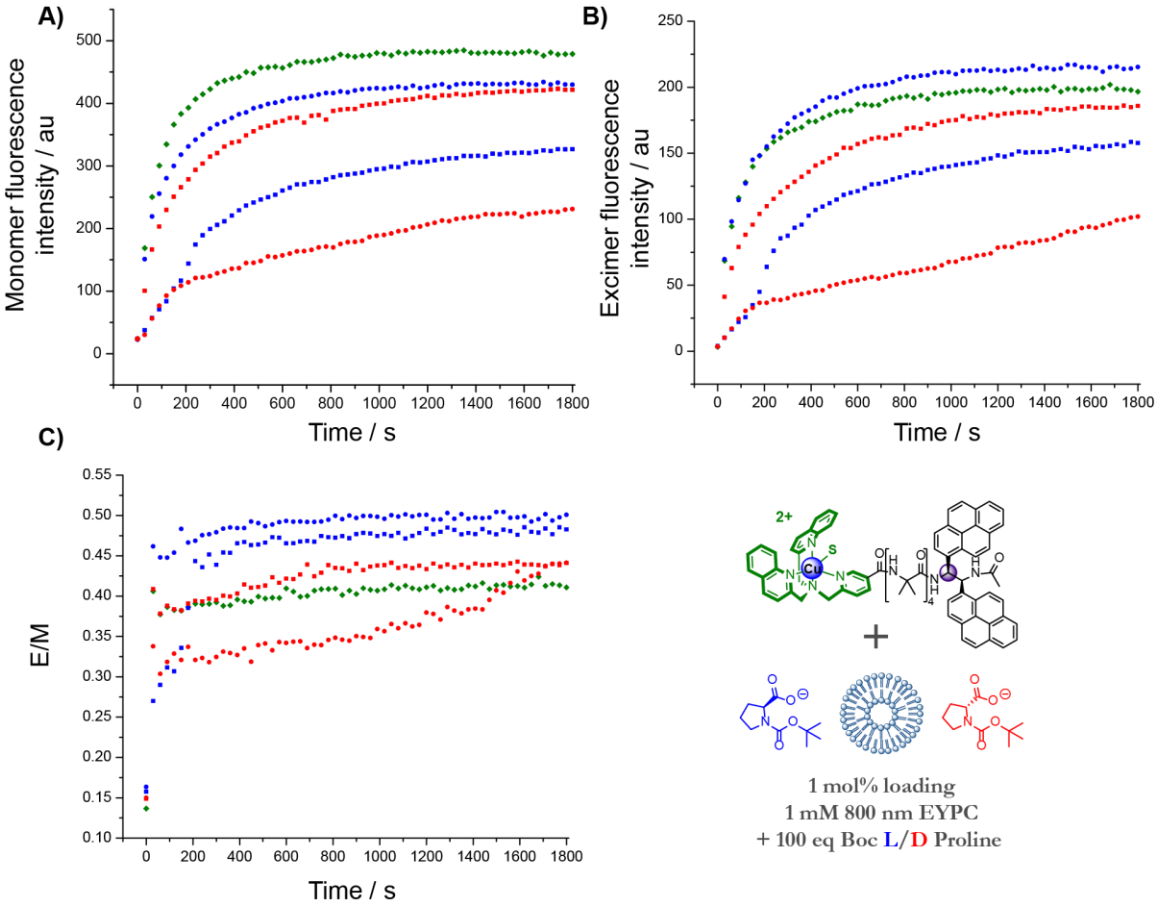

Figure **72 -** Timed fluorescence curves for **197** (10 μM) added to 1 mM solutions of 800 nm EYPC vesicles on its own (●) or with 100 eq Boc-L-Pro-Na (●) or Boc-D-Pro-Na (●) added solution prior to addition. Maximum values measured are for Monomer [378 nm] (**A**), Excimer [450 nm] (**B**) and the ratio of Excimer to Monomer fluorescence ratio (**C**).

Suspensions of vesicles were prepared with 100 equivalents of Boc-Pro-Na added to the surrounding solution prior to addition of the Cu^{II} complex **197** (Figure 72). It was hoped that as the complex was injected into the suspension it would bind Boc-Pro-Na prior to entering the membrane. Any observable difference in timed fluorescence spectra for the L and D solutions would indicate that signal relay occurs in a transient state as **197** enters. Unfortunately, nothing meaningful could be gathered from the data.

7.12 Intriguing Differences in the Membrane Fluorescence of Zn^{II} and Cu^{II} species.

On comparison of the Zn^{II} and Cu^{II} it is of note that the excimer fluorescence of the Cu^{II} is heavily quenched in the membrane environment (Figure 73A). This is of particular interest considering the strength of excimer emission for both species match reasonably well in solution. If quenching in the Cu^{II} species was apparent in both solvent and membrane it would suggest that Cu^{II} was directly quenching the pyrene probe intra-molecularly, over the length of the helix. As the excimer is only quenched in the membrane this suggests that an intermolecular quench is arising, where the head group of one Cu^{II} quenches the pyrene fluorescence of another molecule.

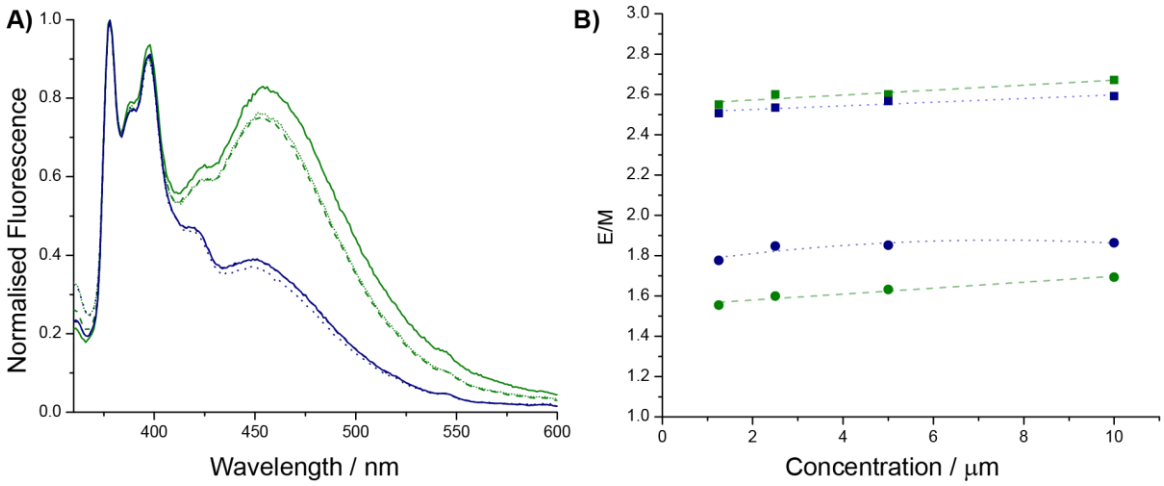

Figure 73A) Fluorescence of **193** and **197** after 1h addition to 1 μM [1mol% loading] (——) 2.5 μM [0.4mol% loading]. (— — —) and 5 μM [0.2mol% loading] (▪▪▪) concentrations of 800 nm EYPC vesicle suspensions. Spectra normalised to 378 nm. B) Comparison of solution fluorescence for **193** and **197** and in MeOH (■) and MeCN (●).

As the metal-complex head group is charged at one end, it is likely that the head groups remain at the surface of the vesicle. Considering this reduces the modes of interaction with the membrane to two key dynamic processes: trans-membrane and on the surface of the vesicle (Figure 74).

Two possible quenching interactions related to these modes are described in Figure 74. In the trans-membrane mode a quench arising from the motion of the helices as they enter and exit the membrane alternately (Quench A). If the helices are arrayed on the surface of the vesicle a head-to-tail arrangement of the helices brings the pyrene of one molecule in close proximity to Cu^{II} head group of another (Quench B).

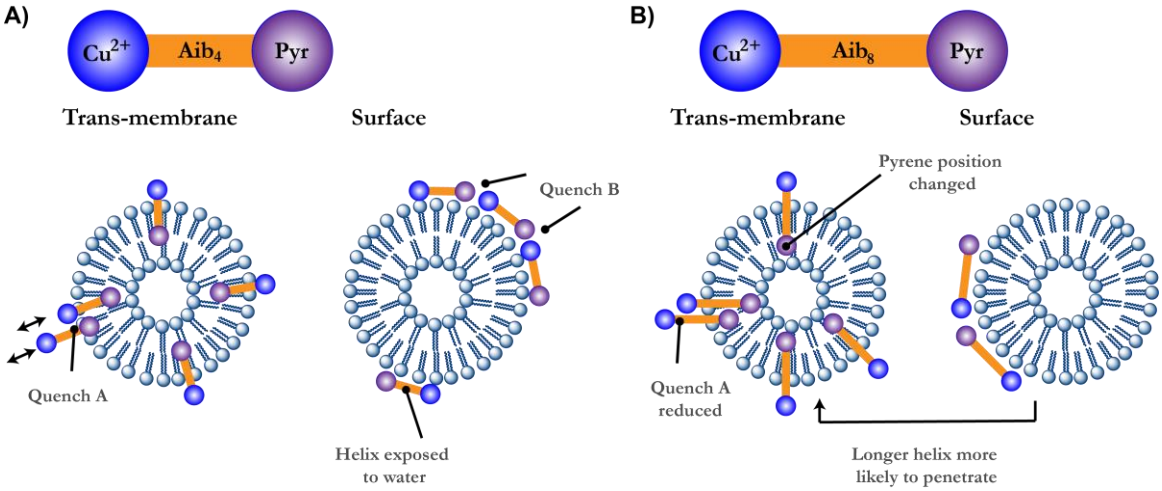

Figure 74A) likely causes of Cu^{II} quench, **B)** Advantages of longer helix.

Considering these two systems, a structure with a longer helical fragment offers advantages. The extra length of the helix may drive the system towards the trans-membrane mode. This offers a series of advantages. In the trans-membrane mode Quench B is removed. A longer helix is less susceptible to quench A. If the switch is occurring in the second generation GPCR mimic it is possible that it is unobservable due to the quenching of the excimer fluorescence. Reduction of quenching interactions would solve this problem, allowing for the observation of a switch.

A further issue that may be affecting the switch of the systems in membrane environments is the exposure of the helix to water. Work within the group[54] highlighted that signal relay through Aib helices is effectively switched off in aqueous environments. If the helix is arrayed on the surface of the vesicle, exposure to water could be preventing signal relay. Earlier work in this report (Sections 5.15 & 5.21) has shown signal relay and detection by fluorescence probe in membrane environments is achievable when a controlling residue is attached to the helix. The CD study of the copper and zinc binding sites (Section 7.7) show that copper is an effective carboxylate binder in membrane environments. Considering this, is it likely that the issue is related to the interplay of the binding site and the helix at the membrane-water interface. A longer helix is expected to solve a variety of these issues.

7.13 Development of a 3rd Generation GPCR Mimic.

Evaluating the results of the earlier GPCR mimics it was clear that a longer helix may provide a functioning switch in a membrane environment. Towards this N_3Aib_5OH **198** was converted to the azlactone and coupled to H-Aib_3-OMe **88** to give N_3Aib_8OtBu **199** in 97% yield. The Boc protecting group was converted to a methyl ester protecting group, in line with the synthetic strategy developed for the synthesis of BQPA-3-CO-Aib_4-*S*,*S*-PyrEt-NHAc species **188.** After isolating the ester **200** in 83% yield continual attempts to reduce to the amine **201** were unsuccessful due to the formation of an inseparable impurity formed during the reduction. Surprisingly the reduction, which is typically left over night, was complete within 30-60 mins and the impurity appeared to form at a slower rate. Initial attempts to solve the reduction issue had investigated the quality of available Pd/C using synthetically cheaper $N_3AibOtBu$ during which no impurity formation was observed in an overnight reduction. Multiple attempts to reduce **200** overnight, including using $Pd/BaSO_4$ had over-looked reduction in reaction time and a large amount of **200** was lost. It would appear that the issues are substrate specific and it is advisable with longer analogues to monitor the reactions closely to avoid similar issues in the future. Eventually **200** was reduced using the shorter reaction time to give **201**, ready for coupling to BQPA-3-COOH **184**.

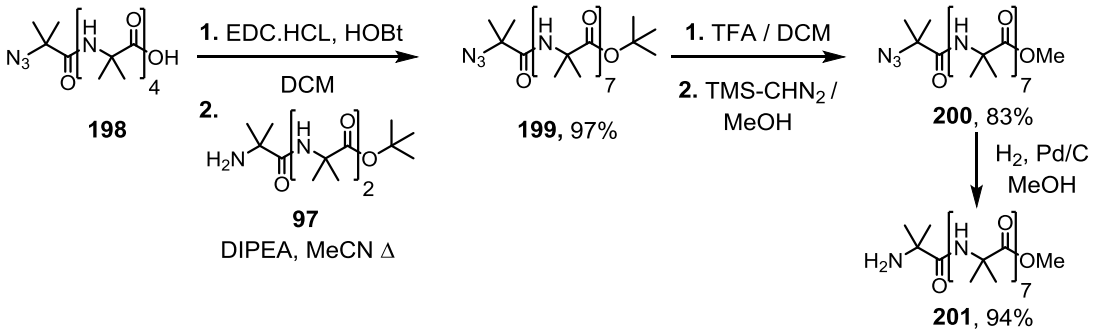

Scheme 49 – Synthesis of H-Aib_8OMe.

The coupling proceeded smoothly giving BQPA-3-CO-Aib$_8$-OMe **202** in a reasonable 60% yield. De-protection of the methyl ester with KOH was satisfactory, giving BQPA-3-CO-Aib$_8$-OH **203** in 72% yield. Coupling of BQPA-3-CO-Aib$_8$-OH and *S*,*S*-BisPyrEt dihydrochloride **120** followed by direct acetylation gave the desired BQPA-3-CO-Aib$_8$-*S*,*S*-BisPyrEt-NHAc species **204** in 68% yield. This was used directly in the formation of the metal complex. Degradation of small samples left in NMR tubes was observed for compounds **202**, **203** and **204** Due to earlier issues with pyrene compounds the majority of the samples were stored at −5°C in the dark when not in use.

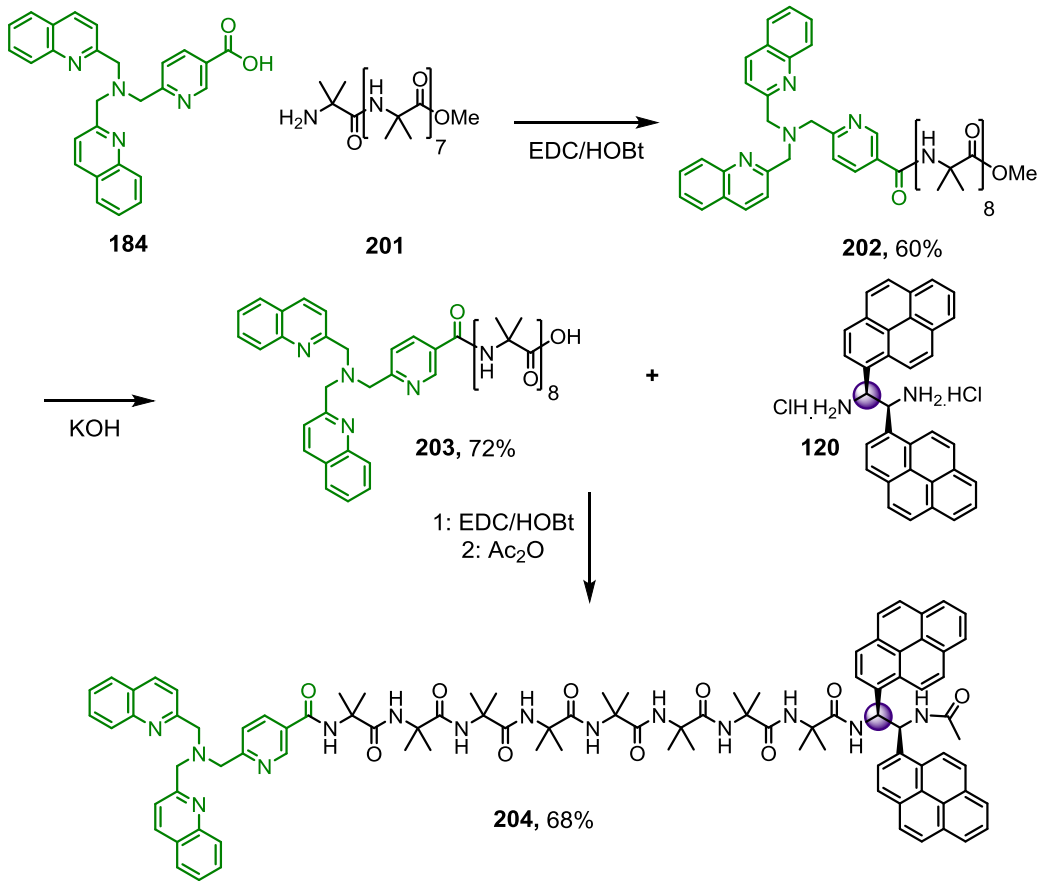

Scheme 50 – Synthesis of BQPA-3-CO-Aib$_8$-*S*,*S*-BisPyrEt-NHAc.

7.14 Synthesis and Solution Behaviour of the 3rd Generation GPCR Mimic

Following identical methodology for the synthesis of the earlier generations of GPCR mimics, the longer third generation GPCR mimic was synthesised from **204** and Cu(II)$(ClO_4)_2$ providing the metal complex **205** in 68% yield.

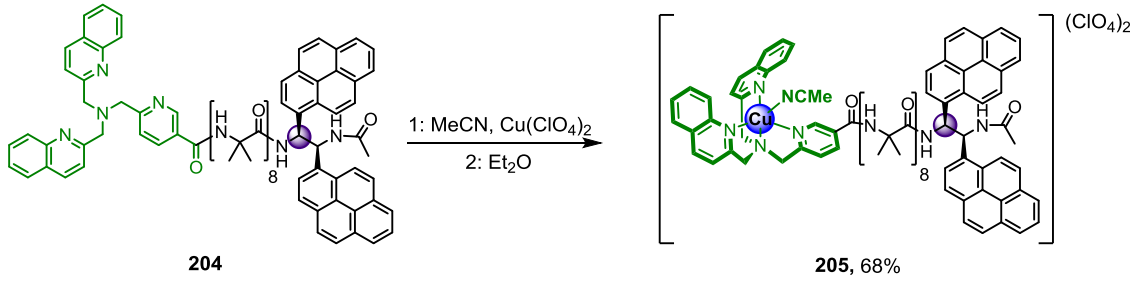

Scheme 51 - The synthesis of Cu^{II}BQPA-3-CO-Aib_8-Gly-*S*,*S*,-PyrEt-NHAc.

Prior to membrane investigation the solution fluorescence of **205** was measured over the usual 1.25-10 μM range in MeCN. Comparing against the the E/M ratio of the shorter copper complex **197**, the E/M ratio in MeCN was 1.574±0.008 (cf. $Cu^{II}Aib_4$ complex 1.53) As expected the switching behaviour closely matched that of **197**. The magnitude of the switch for the $Cu^{II}Aib_8$ complex **205** in MeCN was 0.36 (53% of the magnitude observed for the analogous Cu(II)Aib_4 structure.

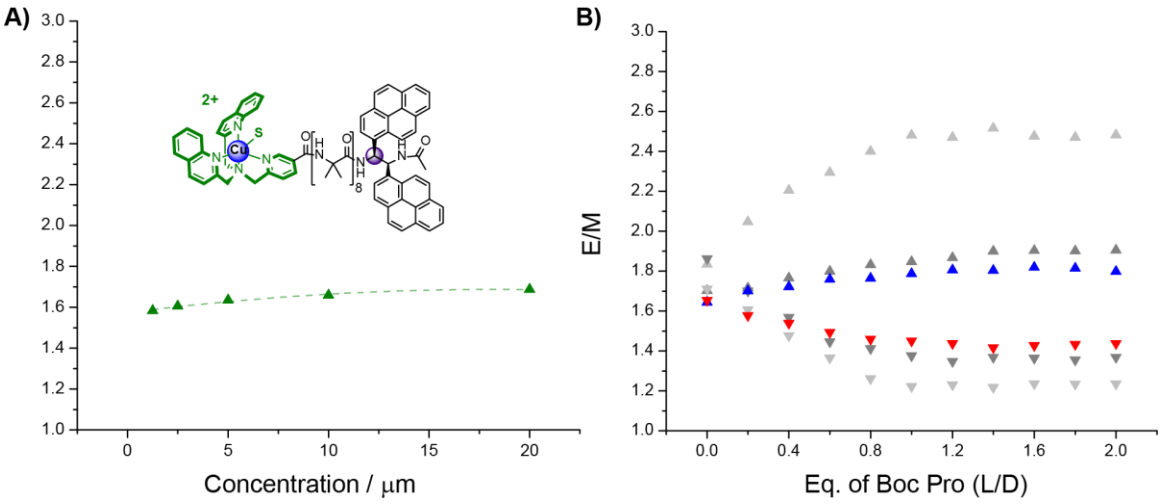

Figure 75A) The observed excimer/monomer ratios (E/M) of metal complex **205** at varying concentration in MeCN ▲ **B)** Titration curve of **205** (10 μM) in MeCN with increasing concentrations of with Boc-L-Pro [0-20 μM] (▲), Boc-D-Pro [0-20 μM] (▼).Results for **193** (Fig58B, light grey) and **197** (Fig65B, grey) are added for comparison.

7.15 Membrane behaviour of the 3rd Generation GPCR mimic

Following the earlier protocol **205** was added to 800 nm DOPC vesicles and left to stir for 1h (Figure 76A). Over a longer period of time the E/M ratio changes, presumably as the compound migrates across the leaflets of the vesicle membrane. After 1h, addition of Boc-Pro-Na was found to bind the copper center, relaying the signal through the Aib_8 helix to the probe. The first successful example of biomimetic conformational signal relay in a membrane environment.

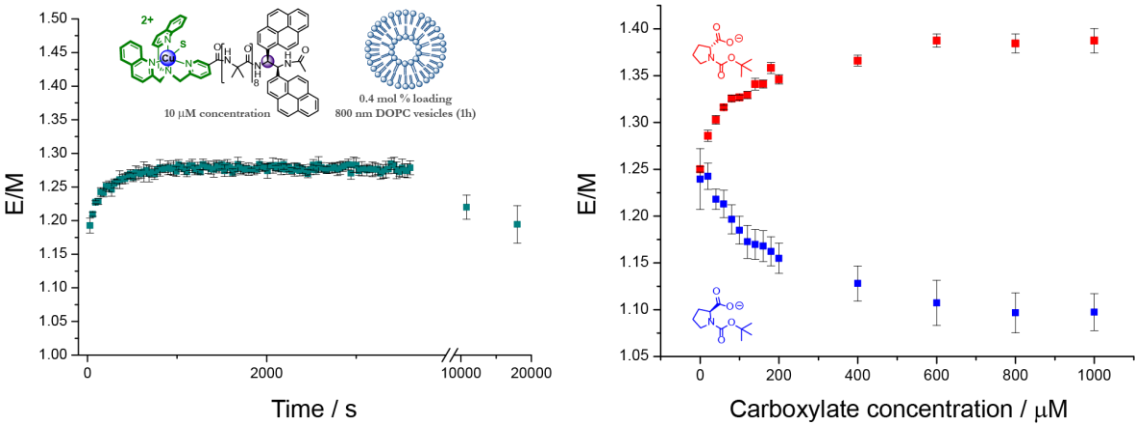

Figure 76A) Timed fluorescence curves for **205** (10 μM) added to 2.5 mM solutions of 800 nm DOPC vesicles in 20 mM MOPS buffer solution. **B**) Titration curve of **205** (10 μM) added to 2.5 mM solution of 800 nm DOPC vesicles [0.2 mol% loading] after 1h with increasing concentrations of Boc-L-Pro [0-1000 μM] or (■) , Boc-D-Pro [0-1000 μM] (■).

Interestingly, the direction of E/M change is inverted in the membrane environment compared to solution. Increasing Boc-L-Pro-Na leading to a reduction in E/M ratio in the membrane and an increase in solution and vice versa for Boc-D-Pro-Na The reason for this behaviour is currently unclear, but the inverted response in membrane environments was also observed for this pyrene reporter when attached to helices controlled by covalently linked amino acid residues (Section 5.21, Figure 55). Clearly the results indicate the probe is highly responsive, both to the control delivered through the helix and the local environment in which it is placed. Returning to this earlier work and using controlled helices of varying length in a variety of lipid mixtures may provide a better explanation of this observed signal inversion.

To confirm the change in E/M ratio on addition of Boc-Pro-Na was related to an interaction with **205** embedded in the membrane and not with **205** in solution, it was decided to confirm that the receptor **205** had no significant fluorescence outside of the membrane environment. A 1 mL solution of **205** (20μM) in 20 mM MOPS buffer solution was prepared and placed in the fluorimeter. No fluorescence signals were observed. Addition of a 1 mL solution of 800 nm DOPC vesicles (5mM) was added to this solution to give a 10 μM solution of **205** and 2.5 mM concentration of DOPC vesicles. This reverse addition resulted in near identical fluorescence growth curves over an hour of monitoring (Figure 77B).

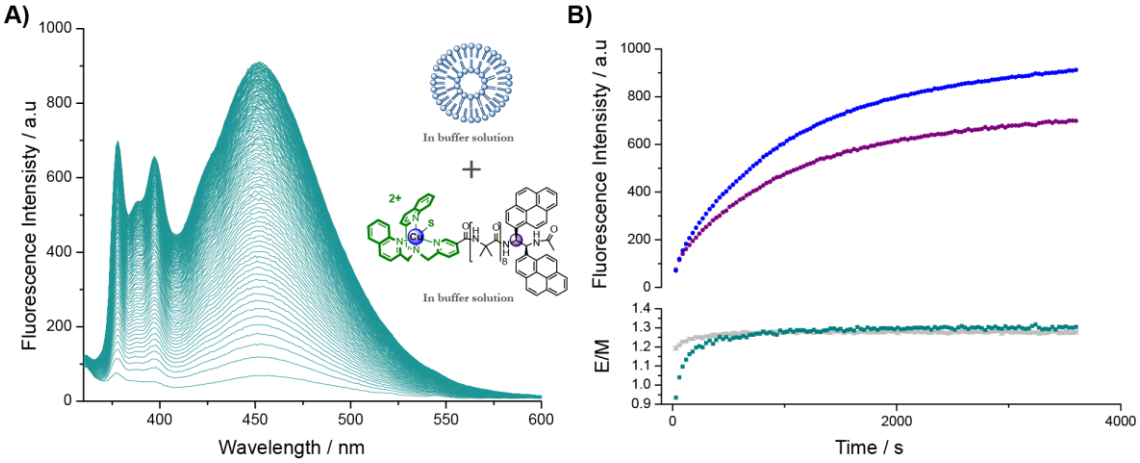

Figure 77 - Timed fluorescence curves for reverse addition of 800 nm DOPC vesicles to a solution of **205** (10 μM) in 20 mM MOPS buffer solution.

Fluorescence images of **205** after two hours of stirring with DOPC vesicles further support the theory that the observed switching behaviour is occurring within the membrane environment. The fluorescence of the pyrene illuminates the small vesicular structures against a dark background.

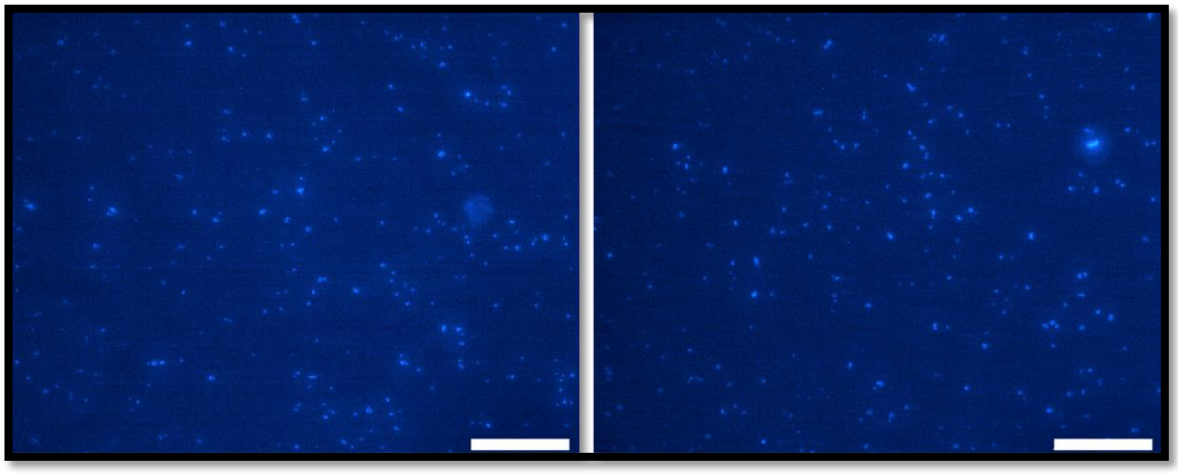

Figure 78 - Fluorescence images of **205** as a 0.2 mol% loading in 800 nm DOPC vesicles after 2h of stirring. Scale bar corresponds to 100μm.

7.16 Towards a Synthetic δ-Opioid Receptor

Having observed a successful binding interaction and signal relay in the membrane environment of 800 nm DOPC vesicles using Boc-Pro-Na as a preliminary agonist a variety of other biologically relevant agonists were investigated using the same protocol. (Figure 79). The results highlight the effectiveness of **205** as a synthetic GPCR receptor. Of particular note is Leu-enkephalin, the endogenous agonist for both the μ- and δ-opiod receptor. Interestingly, binding of Boc-Leu-Na resulted in induction of opposite screw-sense control, suggesting a more complex interaction for the Leu-Enkephalin agonist. Compared to the Boc protected L-proline the free amino acid induces minimal control at the binding site. Clearly the carbamate carbonyl present in the protected amino acid agonists is critical to inducing high screw-sense control through the binding interaction.

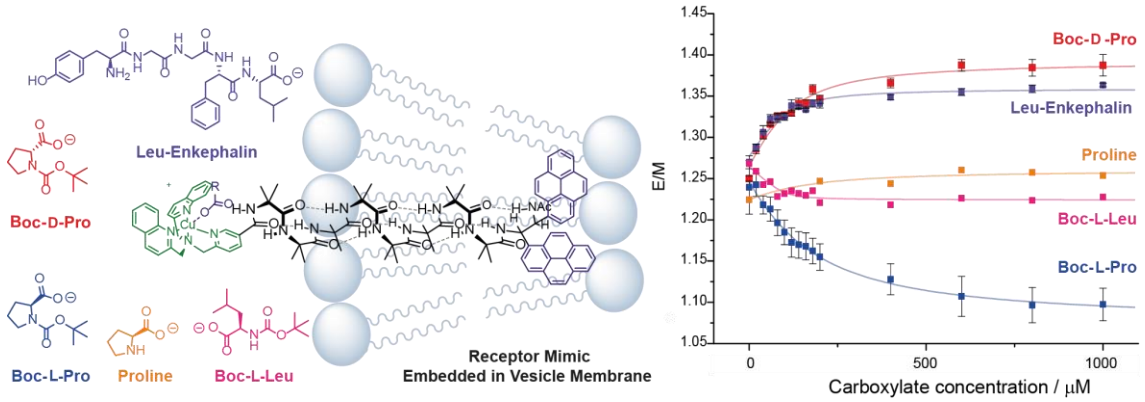

Figure 79 - A variety of agonists induce a binding response in the synthetic GPCR mimic **205**.

7.17 Binary Signal Transmission in Membrane Environments

Having developed the biomimetic GPCR system with a variety of agonists, the final aim of the project was to induce switching behaviour from an *M* to a *P* screw-sense preference. **205** (10μM) was added to 2.5 mM solution of DOPC vesicles and left to stir for 1h giving a vesicular solution with 0.4 mol% loading of **205**. Addition of Leu-enkephalin to the extravesicular medium lead to an increase in E/M ratio. Comparing this to earlier results and the observed signal inversion for the pyrene probe in the membrane suggests the binding interaction induces an *M* screw-sense preference in the helix. Subsequent addition of Boc-L-Pro-Na to the solution leads to a reduction in E/M value. Selective binding of two different agonists has allowed reversible control of the helical screw-sense preference. Through this process a chiral signal is relayed though an achiral helix, 8 residues long, to a fluorescent probe and detected in a membrane environment.

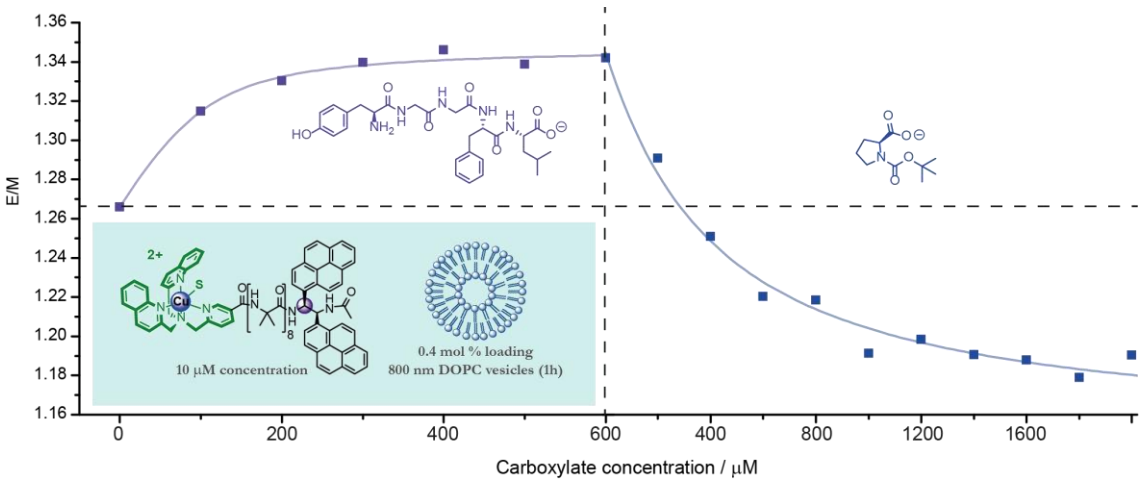

Figure **80** - Switchable behaviour of 3rd generation GPCR mimic in 800 nm DOPC vesicles.

7.18 Understanding the Switch

Throughout the investigation a variety of vesicles, with varying lipid compositions were investigated (Figure 81). Thus far, switching behavior has only been observed in DOPC vesicles and vesicles comprised of the structurally similar DPoPC. Time curves for the addition of **205** to varying lipid compositions indicate that while the E/M ratios for **205** stabilise over one hour in DOPC and 1,2-dipalmitoleoyl-sn-glycero-3-phosphocholine at ~1.27, the observed E/M ratios for saturated lipids are all ≤ 0.9 and, in the case of EYPC have not stabilised over the hour.

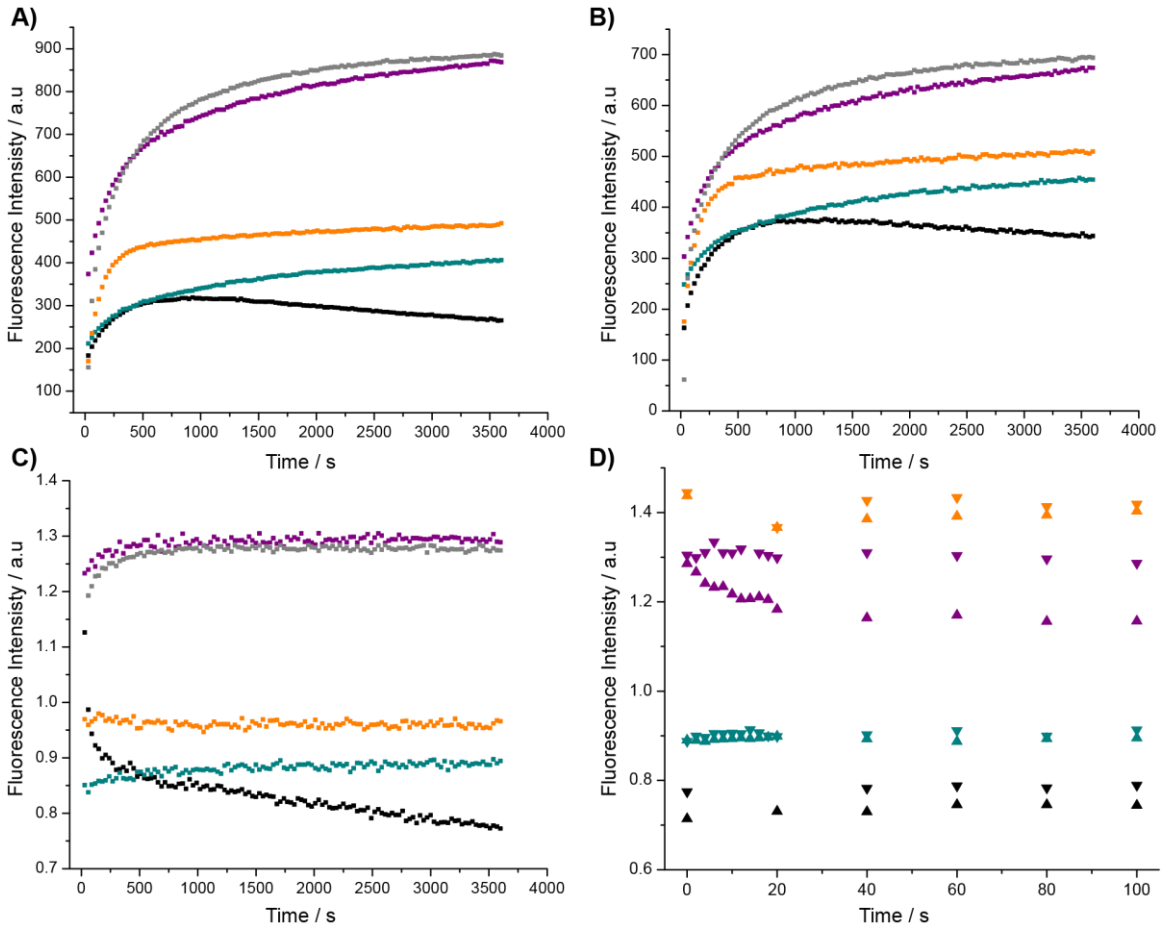

Figure 81 - Timed fluorescence curves, for addition of **205** (10μM) to 1,2-dipalmitoleoyl-sn-glycero-3-phosphocholine [DPoPC] (■), 1,2-dioleoyl-sn-glycero-3-phosphocholine [DOPC] (■) 1,2-dimyristoyl-sn-glycero-3-phosphocholine [DMPC] (■), 1-palmitoyl-2-oleoyl-sn-glycero-3-phosphocholine [POPC] (■) and L-α-lysophosphatidylcholine [EYPC] (■) Maximum values measured are for Monomer [378 nm] (**A**), Excimer [450 nm] (**B**) and the ratio of Excimer to Monomer fluorescence ratio (**C**). The observed response to increasing concentrations of Boc-L-Pro-Na [0-1000 μM] (▲) or Boc-D-Pro-Na [0-1000 μM] (▼) for each lipid type is reported in identical colour (**D**).

Vesicles formed of 1,2-dimyristoyl-sn-glycero-3-phosphocholine (DMPC) have a phase transition temperature T_m of 24 °C. Throughout the study, other lipids studied possessed lower transition temperatures giving vesicles with a liquid crystalline phase (Lα) at room temperature. Using DMPC and varying the temperature in the fluorimeter allows for the investigation of helix function in both the liquid crystalline Lα and solid-ordered Lβ phases (Figure 82). Solutions of 2.5 mM 800 nm vesicles were prepared and left to stir with **205** (10 μM) for 1h. 100 equivalents of Boc-L-Pro and Boc-D-Pro were added to separate solutions. Varying the temperature from 10-40 °C causes the vesicle to change phase behavior from Lβ to Lα. Interestingly, the switch shows no-difference between the Boc-L/D-Pro solutions in the Lβ phase. Warming the solution above 24 °C changes the bilayer phase of the vesicles to Lα and a measurable difference is observed between the solutions. This provides further evidence that the helix is embedded in the membrane, as it is responding to the phase changes around it.

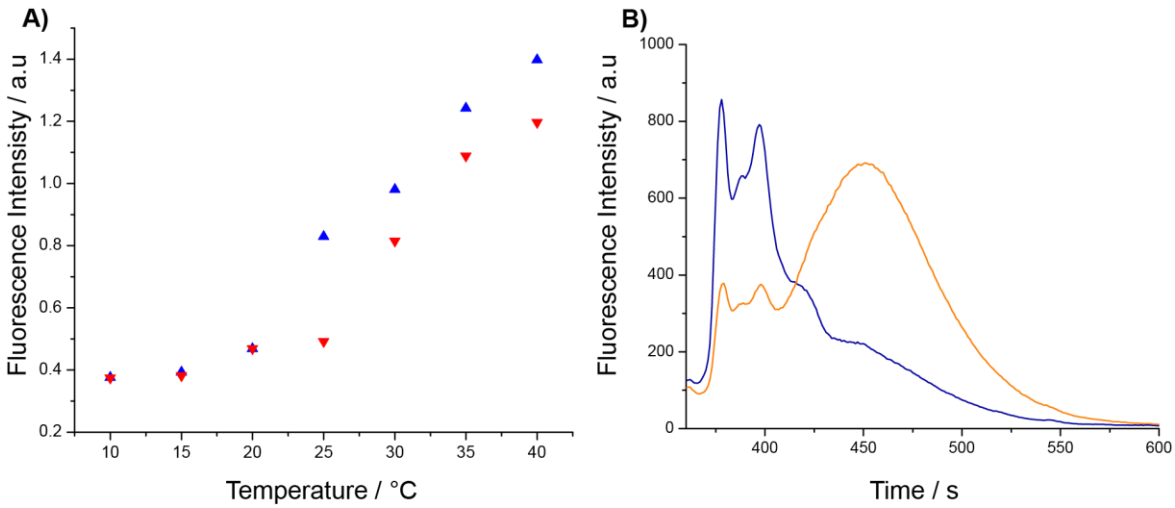

Figure 82A) E/M Fluorescence ratios **205** (10 μM) after 1 h addition to DMPC vesicles (2.5 mM) with 1000 μM concentration of either Boc-L-Pro-Na (▲) **or** Boc-D-Pro-Na (▼) in solution. **B)** Fluorescence spectra of Boc-L-Pro-Na suspension at 10 °C (——) and 40 °C (——).

During our investigations a final control experiment produced some surprising results (Figure 83). If after 1h of mixing **205** with vesicles the solution is passed through a PD-10 de-salting column, which removes solution impurities, a large amount of **205** is removed from solution. The resulting vesicle solution has a reduced starting E/M and displays minimal switching behavior.

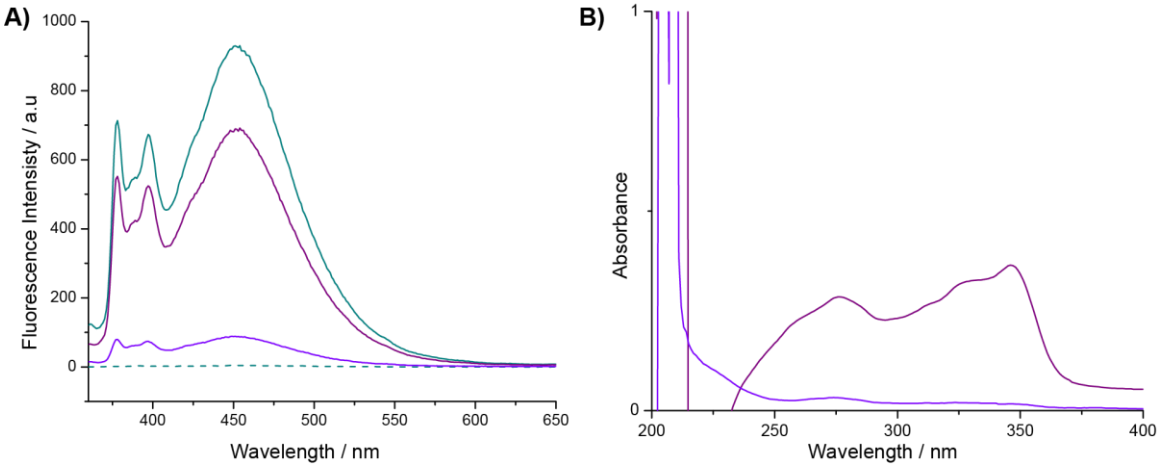

Figure 83A) Fluorescence spectra of **205** (14 μM) after 1h of stirring with 3.5 mM DOPC vesicles (——), after dilution with MOPS buffer to 10 μM (2.5 mM DOPC) (——) and after purification by PD-10 de-salting column (——). **B)** UV absorbance spectra of diluted (——) and PD-10 (——) suspensions.

Purification by PD-10 column had been used throughout the earlier investigations (Sections 5.15 & 5.21) so it was clear that the probe was working and the Aib helix could relay signals in other membrane types (EYPC). Further checks on the solution behavior of **205** in buffer solution were performed confirming the switch observed is occurring within the membrane or a membrane associated state (Figure 80A) 10μM solutions of **205** and **205** with 100 equivalents of Boc-Pro-Na were sonicated with a probe sonicator to ensure they were fully dissolved. Pleasingly the fluorescence signal from either solution is negligible while UV absorption confirms **205** is in solution. This control removes the possibility that the observed fluorescence signal and switching behavior is occurring in solution through some form of peptide micellar structure.

Further controls looked at the addition method of **205** to the vesicles**.** Sonication of a suspension of 2.5 mM DOPC and 10μM **205** in 20 mM MOPS buffer solution until the solution is clear forms smaller SUVs. When this solution is passed through the de-salting column **205** is retained in the vesicles with 98% incorporation. If the original method is left for to stir for 24 hours, 87% of **205** is retained by the vesicle. Most pleasingly, both new methods display similar switching behavior, with reduced magnitude after column purification (Figure 84B,C,D).

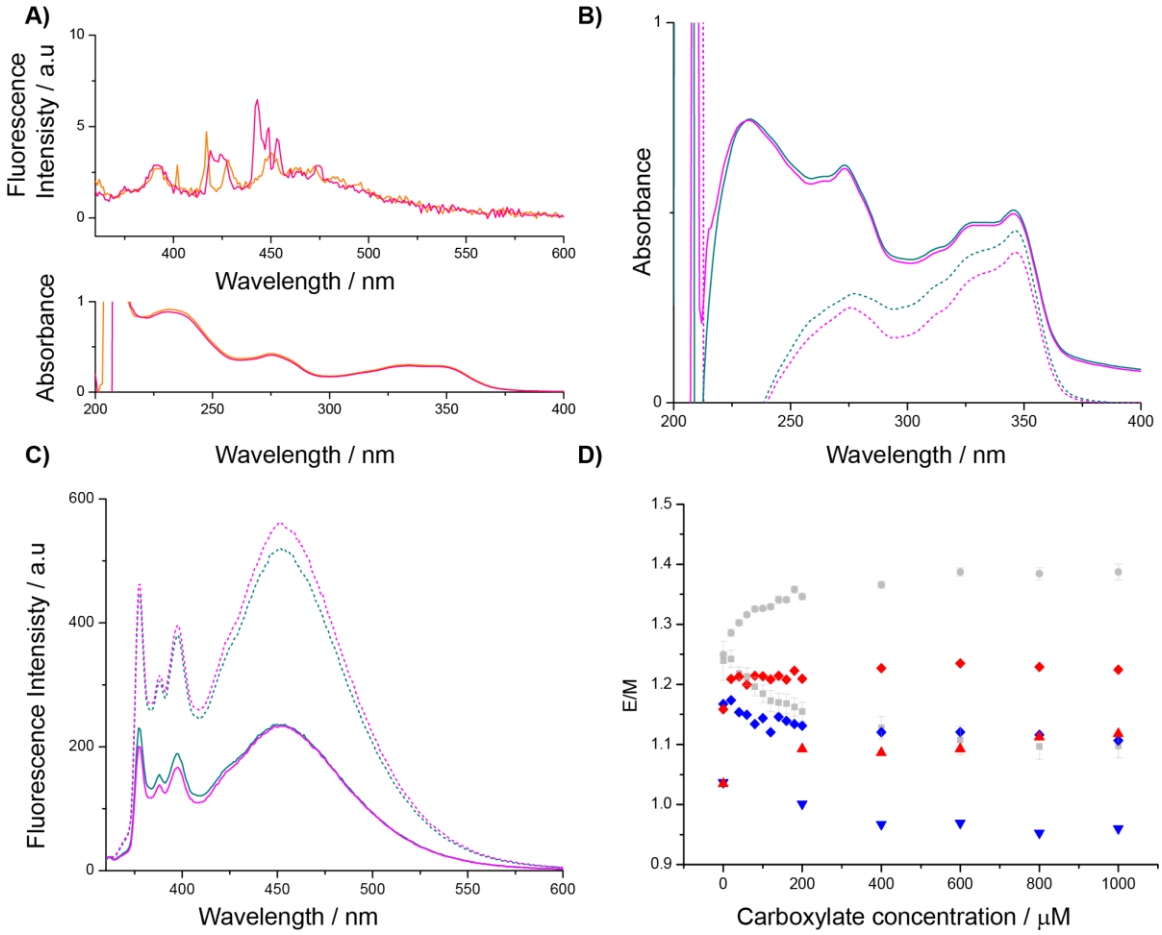

Figure **84A**) Fluorescence spectra and UV absorbance of **205** in MOPS buffer [20 mM] (—) and with additional Boc-L-Pro Na [1000 μM] (—). **B)** UV spectra of **205** in SUVs diluted (—) PD-10 (—); UV spectra of **205** in 24 h LUVs diluted (---), PD-10 (---) **C**) Fluorescence spectra of **205** in SUVs diluted (---), PD-10 (---); Fluorescence spectra of **205** in 24 h LUVs diluted (—), PD-10 (—) **D**) Response of 24 h LUVS(▲/▼) and SUVs (■/■) both PD-10, to increasing concentrations of Boc-L-Pro-Na [0-1000 μM] (▲/■) or Boc-D-Pro-Na [0-1000 μM] (▼/■). **205** is 10 μM throughout. All vesicles are 2.5 mM suspensions of DOPC purified by PD-10 column [PD-10] or diluted to the same degree with MOPS buffer solution [diluted]. 24 h LUVs are 800 nm vesicles left to stir with **205** for 24 h prior to use. SUVs formed by the sonication of **205** and DOPC suspension until clear.

Perhaps, as the fluorescence data from the earlier switch points towards it occurring in a membrane environment, it is only loosely associated with the membrane after one hour and the switch is occurring at the surface of the membrane. Purification by column at this stage washes away the weakly associated peptide resulting in low incorporation and poor switching behaviour. Leaving for a longer 24 hours or forcibly inserting the peptide into the vesicle structure through sonication causes the peptide to embed deeper within the membrane, perhaps in a trans-membrane alignment. At greater membrane depths, the motion of the helix and the probe is likely to be reduced, a possible explanation for the observed reduction in switch magnitude.

8.0 Project 2 Introduction

8.1 Photo-Responsive Controller Design

Photo-responsive receptors are of key importance across all biological domains. They are at the heart of the vision process, with transmembrane signaling mediated by the rhodopsin family of GPCRs. They are also of importance in bacterial processes such as phototaxis,[136] the movement of cells towards or away from a light source and in the plant kingdom, with many critical processes mediated by response to light.

Integral to many of these receptors is the incorporation of a photochromic molecule into their active site. Action of a particular wavelength of light on these highly specific molecules induces a structural change within them which in turn leads to a conformational change in the receptor protein, triggering subsequent signaling pathways and biological processes.

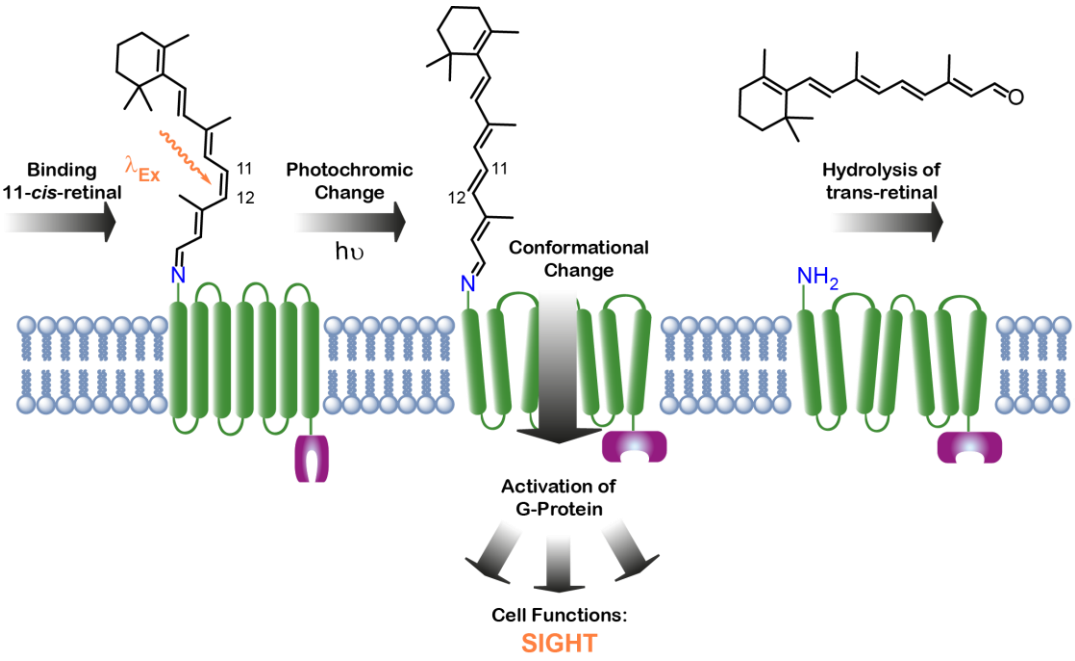

Figure 85 – The photochromic function of retinal in the rhodopsin GPCR.

The photoisomerisation of the biomolecule retinal (Figure 85), forms an integral part to the function of the GPCR Rhodopsin,[23] which is responsible for the vision process in higher organisms. The interaction of a photon isomerises 11-cis-retinal into the all trans conformation. This photoisomerisation in turn leads to a series of conformational changes in the helical transmembrane domain, leading to activation of G-proteins and the subsequent downstream signal transmission and amplification by effector proteins. The trans retinal is then hydrolysed leaving the active site free to bind another cis-retinal.[137]

A similar system can be found in photoreceptors in plants. Photoisomerisation of phytochromobilin in the phytochrome receptor and the subsequent signal transduction by the receptor are critical in many stages of plant development including germination and growth towards sunlight.[138]

8.2 Molecular Switches and Photochromism

Photochromic molecules (Scheme 52) are readily isomerised between two or more thermodynamically stable structures when light of the correct wavelength is applied to them. Controlled reversal of this isomerisation is facilitated by application of a second specific wavelength of light or heat making them highly suitable for their use in molecular switching devices.[139]

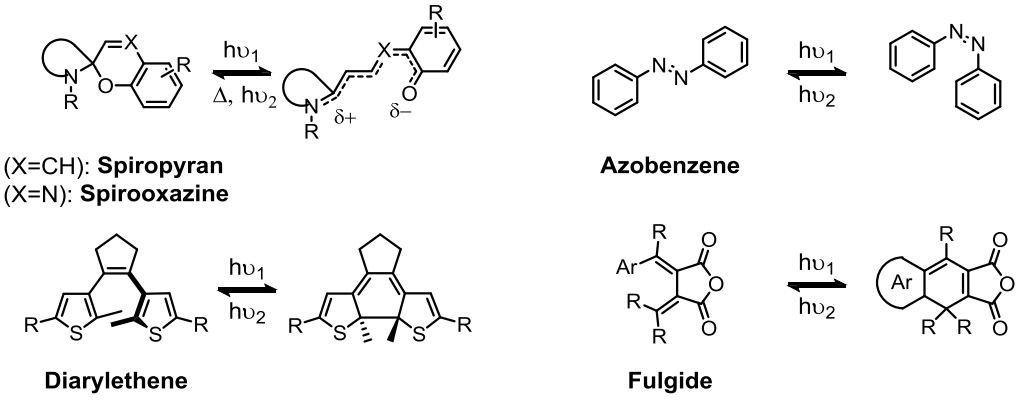

Scheme 52 – Photochromic molecules.

The photochromic fulgide[140] diarylethene[141] spiropyran, spirooxazine[142] and azobenzene[143] species have been the subject of intense research in a variety fields including the development of molecular switches and machines,[144–146] data signalling and processing,[147] bio machinery[148] and the control of biological function[149,150] and photoresponsive materials.[139]

The modification of protein function by attachment of photochromic molecules has been of particular interest in the development of biomachines and materials[148] where the attachment of a photochromic stucture to a protein allows for light induced control of its function. Typically a photoswitch will be attached to a position on the protein that disrupts its function, for example blocking its active site. Photoisomerisation of the switch will remove this disruption, reactivating the inherent protein function. Examples can be found of photoswitches regulating binding of substrates[151] and the reversible control of peptide conformation.[152]

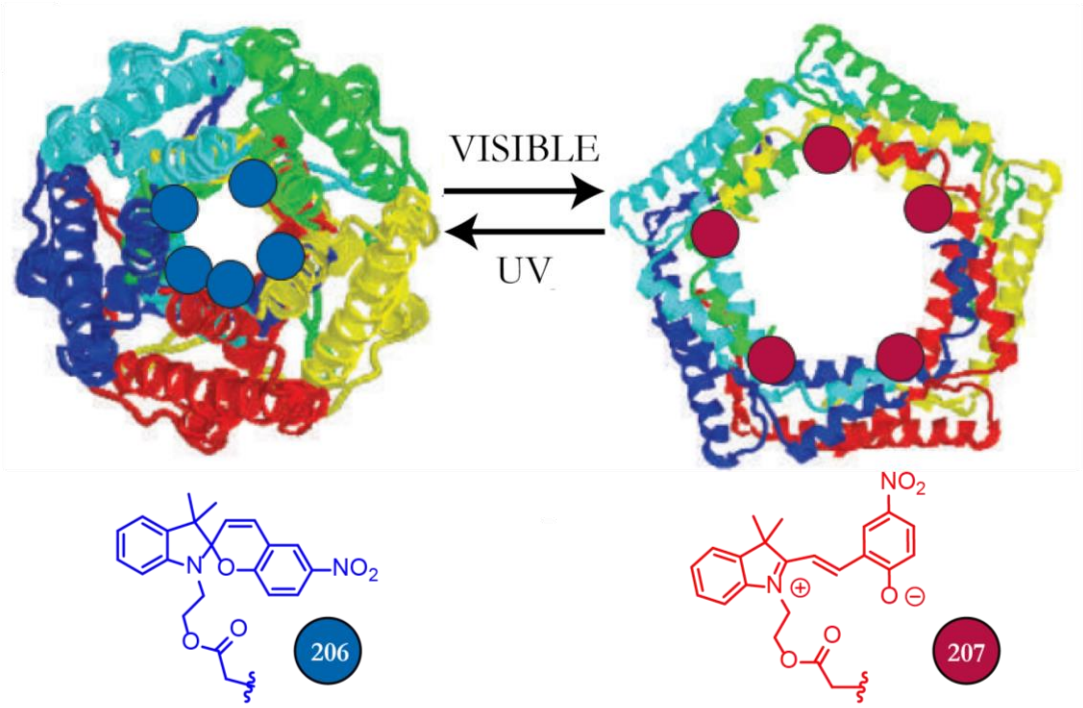

Figure 86 – Photochromic control of channel protein. Feringa and coworkers 2005[137,153]

The modification of a channel protein derived from *Escherichia coli* with spyropyran units by Feringa *et al.* allowed the light mediated opening and closing of 3 nm sized pore.[137,153] The change from the spiro form **206** to the charged merocyanine structure **207** causing the pore to open. Photoisomerisation between the open **208** and closed forms **209** of bis(pyridinium) diarylethene pictured allow for the reversible paralysis of *Caenorhabditis elegans* nematodes.[154]

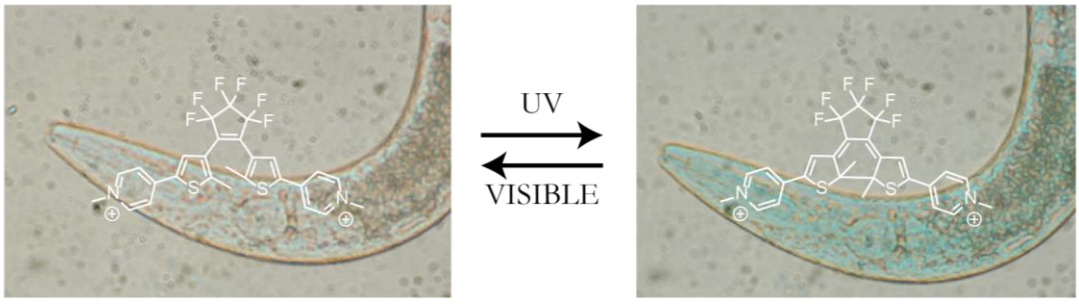

208-Open
Not reduced *in vivo*
metabolic pathway unaffected

209-Closed
Easily reduced *in vivo*
Metabolic pathway disrupted
Paralysis

Figure 87 – Reversable paralysis of *Caenorhabditis elegans* nematodes. Branda and coworkers 2009[154]

8.3 Synthesis of Spirooxazines

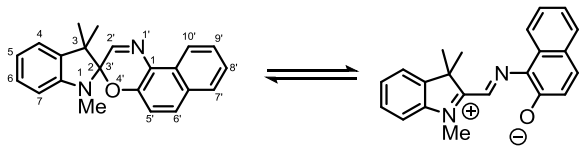

210 **211**

Scheme 53 - Photochromic forms of spirooxazines.

Spirooxazines are a class of photochromic molecules that undergo a light induced transition between a closed spirooxazine (SPO) structure **210** and an open zwitterionic merocyanine (MCN) form **211**. Notably, the change in hybridisation of the central carbon *C-2* from chiral sp^3 to the achiral sp^2 offers an intriguing possibility in the development of a photochromic chiral controller where the chirality is directly controlled by the action of light.

The review by Lokshin *et al.*[155] traces the developments in synthesis of SPOs over the last decade, highlighting the state of the art in SPO structural possibilities and their subsequent effects on photophysical properties.

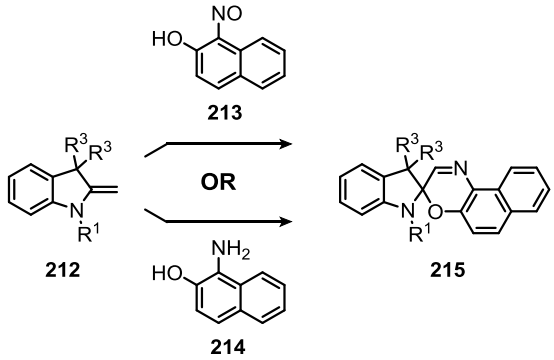

213 **212** **OR** **215** **214**

Scheme 54 - Synthetic routes to spirooxazines.

Their review indicates that there are two prominent synthetic methods developed for SPO synthesis. Both involve the coupling of an alkylidene fragment, which are generally an indolenene structure, **212** with an aromatic oxazine fragment (**213** or **214**) to form the spirooxazine **215**. The main difference between the two synthetic methods arises in the coupling of the oxazine fragment.

The earlier method, termed the *nitroso* method utilises α-hydroxynitroso compounds **213** to introduce this oxazine fragment. This method is successful and can be performed in a wide range of solvents but suffers from low yields (30-50%) due mainly to the low reactivity of the nitroso group, instability of SPO and nitroso groups to the reaction conditions and the challenges arising in separating starting materials

and products on column.

The second method, developed later, particularly by Minkin *et al.*[156,157] makes use of amino naphthols **214** and a mild oxidant, finding the best results in DMSO with sodium bicarbonate. This method offers many advantages over the *nitroso* method including higher yields, relative ease in purification and the use of milder reactions conditions. The commercial availability of a variety of amino naphthols, allowing facile late stage modification of the SPO structure **215** is a further advantage.

8.4 Synthesis of Alkylidine Fragment

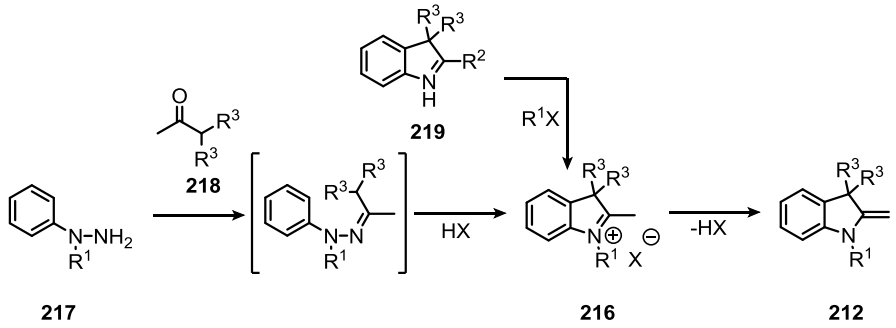

Scheme 55 – Synthesis of alkylidene fragment

Generally, the indolene structures **212** used in the synthesis of SPOs are generated *in situ* from their indole salts **216**. The synthesis of indole salts **216** is well known and a variety of complex substitution and annelation patterns in the indol fragment can be achieved through the Fischer indole synthesis (**217** + **218**) if control of substitution at R^1 or R^3 is desired. Equally, R^1 substitution is achievable via direct alkylation of the indole nitrogen with commercially available indoles such as 2,3,3 trimethylindolenine **219** (R^2=R^3=Me).

8.5 Synthesis of Azobenzenes

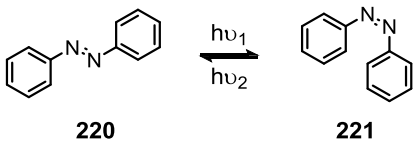

Scheme 56 - Photochromic states of azobenzene molecules.

Azobenzene (AZ) molecules are a class of highly studied photochromic switches that interconvert between two states, the *trans* **220** and the *cis* **221** isomers, under the action of light. These photochromic properties of AZ molecules, first discovered by Hartley *et al.* in 1937[158] have led to their use in a variety of applications.

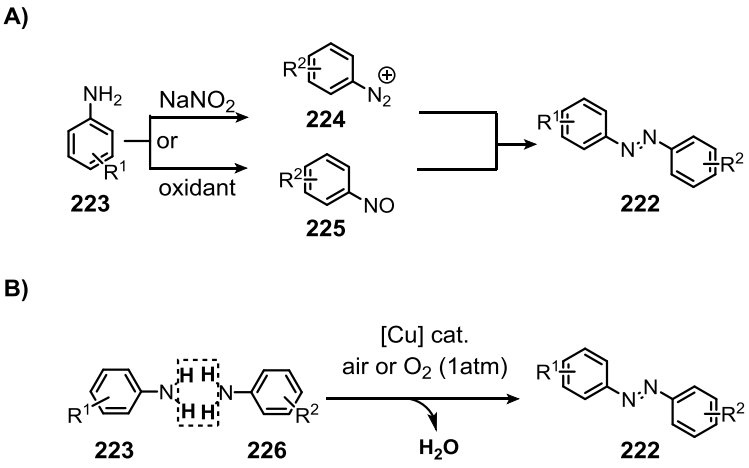

Scheme 57 - Methods for unsymmetrical azobenzene synthesis.

The synthesis of unsymmetrical AZ compounds **222** is synthetically challenging and is typically approached *via* in a two-step process coupling aniline **223** with either a diazonium **224** or nitroso benzene **225** fragment (Scheme 57A).

Recent work by Jiao and Zhang[159] (Scheme 57B) has shown it is possible to form unsymmetrical AZ compounds directly from commercially available anilines (**223** + **226**) using a copper catalyst and molecular oxygen.

With optimised conditions a variety of asymmetric AZ compounds were synthesised. Rates of homo coupling were higher for electron donating substituents so an excess (5 equivelants) of the aniline with an electron withdrawing substituent was used to maximise the cross coupling yield. Side products from Ullmann type reactions were not observed.

8.6 Photoresponsive Helical Polypeptides

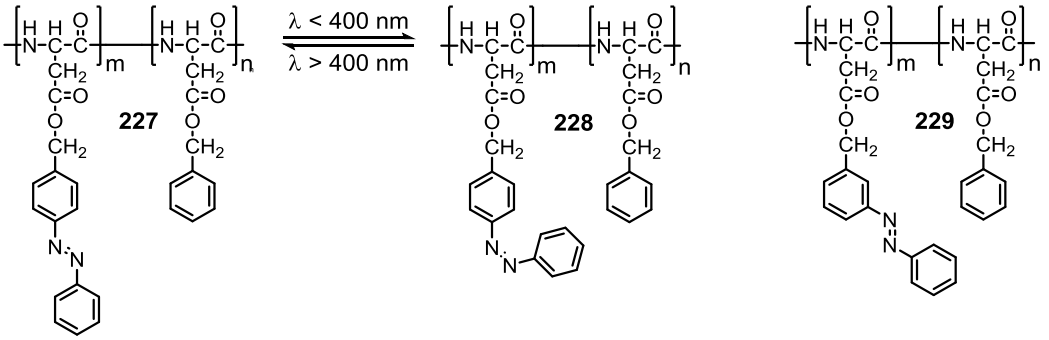

Scheme 53 - Photoresponsive helical polypeptides.

A variety of photochromic polymeric structures are present in the literature and are the subject of review[160–162] Of these, photoresponsive azobenzene (AZ) containing helical polypeptides which undergo an inversion of screw sense preference when irradiated with a particular wavelength of light **227↔228** are the most relevant.

Of the published articles featuring photoresponsive AZ polypeptides, the majority are comprised of varying amounts of AZ side groups connected to the peptide backbone via either an amide or ester linkage in the para position. In the case of examples exhibiting photo-mediated helical inversion, all examples appear to be highly solvent dependant. In most cases the photo-peptides are based on parent peptide structures that already exhibit solvent dependant helical inversion properties.

For the AZ containing compounds studied those substituted with the *meta* linked azobenzene units **229** required far lower levels of incorporated AZ material (~10 %) to exhibit the same photo-mediated behaviour. It could therefore be assumed that the degree of control on these helical systems per AZ unit is greater for these *meta* structures. This suggests *meta* may be a more suitable target for a singularly controlled Aib helix.

The use of spirooxazine (SPO) units instead of AZ units has also been studied resulting in light induced helix-random coil transitions and in some cases reversible aggregation of peptides (due to the zwitterionic attraction of the open form merocyanine structures)[161]

9.0 Project 2 Aims

The aim of this project is to develop a photochromic structure for use with Aib-based peptidic structures that changes the screw-sense control placed on the foldamer helix in response to light. Its development would be advantageous in the further development of a biomimetic rhodopsin system and other signal relay devices in living systems where light can provide a highly tunable biorthogonal input.

As the signal transmission through Aib helices is dependent on the *chirality* of the controller, a light responsive controller must undergo a structural change that induces a change in chiral influence on the helical system (Figure 88A). The photo control of a helical system could be achieved by either a direct (Figure 88B) or indirect (Figure 88C) system of control.

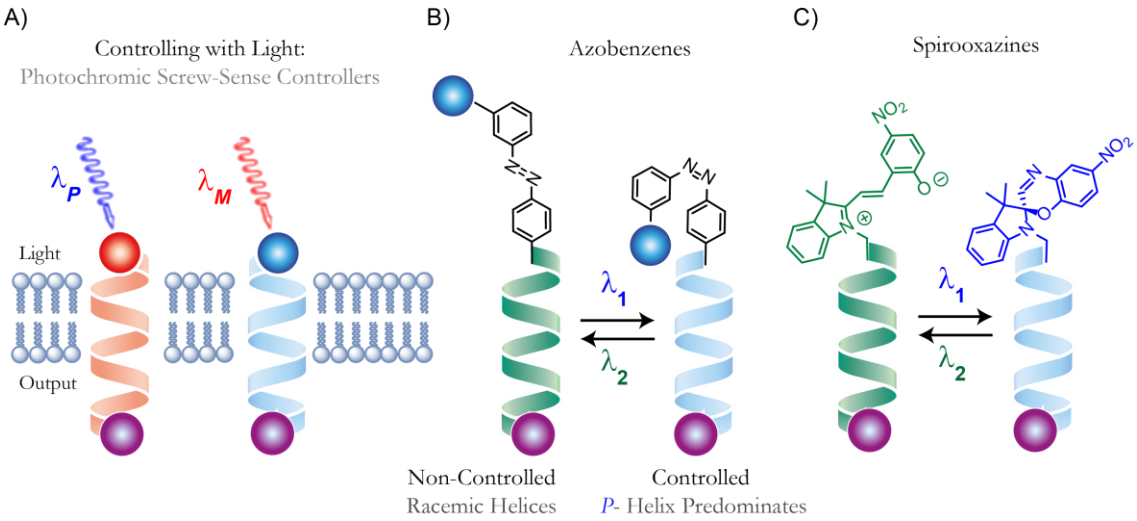

Figure 88 – Potential photochromic structures for screw-sense controllers.

In a direct system the chirality of the controller inverts under the action of a particular wavelength of light, leading to the inversion of helical preference. This could be achieved with a spirooxazine species through the photoisomerisation from sp^2 to sp^3 of spirocarbon centre the achiral open merocyanine would be expected to have no control over the helical system. Use of the correct wavelength of light λ_1 would cause the structure to close forming the sp^3 spiro centre. The chiral nature of the sp^3 centre could then induce control in the helical system, albeit racemic. The change from non-control to racemic control and the reversibility of the system could be probed using a suitable NMR reporter, with an observed diasterotopicity arising in the controlled system. Once the interaction between the racemic spirooxazine controller and the helix has been optimised, synthesis of similar, chiral spirooxazines could be investigated to create a photochromic controller capable of reversibly inverting the

screw-sense preference of Aib helices.

In an indirect system a structure that can impart a chiral influence on the helix is held at a distance by a photochromic linker, preventing the relay of chirality to the helix. Photoisomerization by light, for example of a cis/trans azobenzene system would then bring this chiral influence into contact with the helix, leading to a signal transmission.

10.0 Photochromic Screw-Sense Controller Development

Focussing on control delivered to the N-terminus of the Aib helix and the SPO and the AZ classes of photochromic strcutures a variety of structures are planned.

As mentioned above, An N-terminally attached SPO fragment could be designed that controls the helix as a racemate in the closed form **230** with the control switched off in the open form. **231**. Attachment of an SPO structure in to one of the methyls in an Aib residue **232**, may provide a straightforward way to induce a switch from *M* to *P* helicity with the SPO fragment. Another interesting strategy, although synthetically more complex, would be to embed a chiral centre within the structure of the SPO that biases the chirality of the SPO centre as it opens and closes **233**. This would in turn be expected to induce a screw-sense preference in the helix.

AZ structures could also be attached to the N-terminus as a photochromic protecting group **234**. As the bonding interaction between the carbonyl of the protecting group and NH of second Aib residue in the helix contributes greatly to the stabilisation of a controlling turn structure,[48] photo-modulation of a proximal AZ fragment is likely to have a pronounced effect on screw-sense preference.

Synthesis of α-methyl AZ Amino acid and its attachment to the N-terminus **235** may also produce an effective photochromic controller.

Depending on the stage of the project, a suitable spectroscopic reporter located at the C-terminus (Figure 89), will provide information the strength **12** and later, the direction of screw-sense induction **15**.

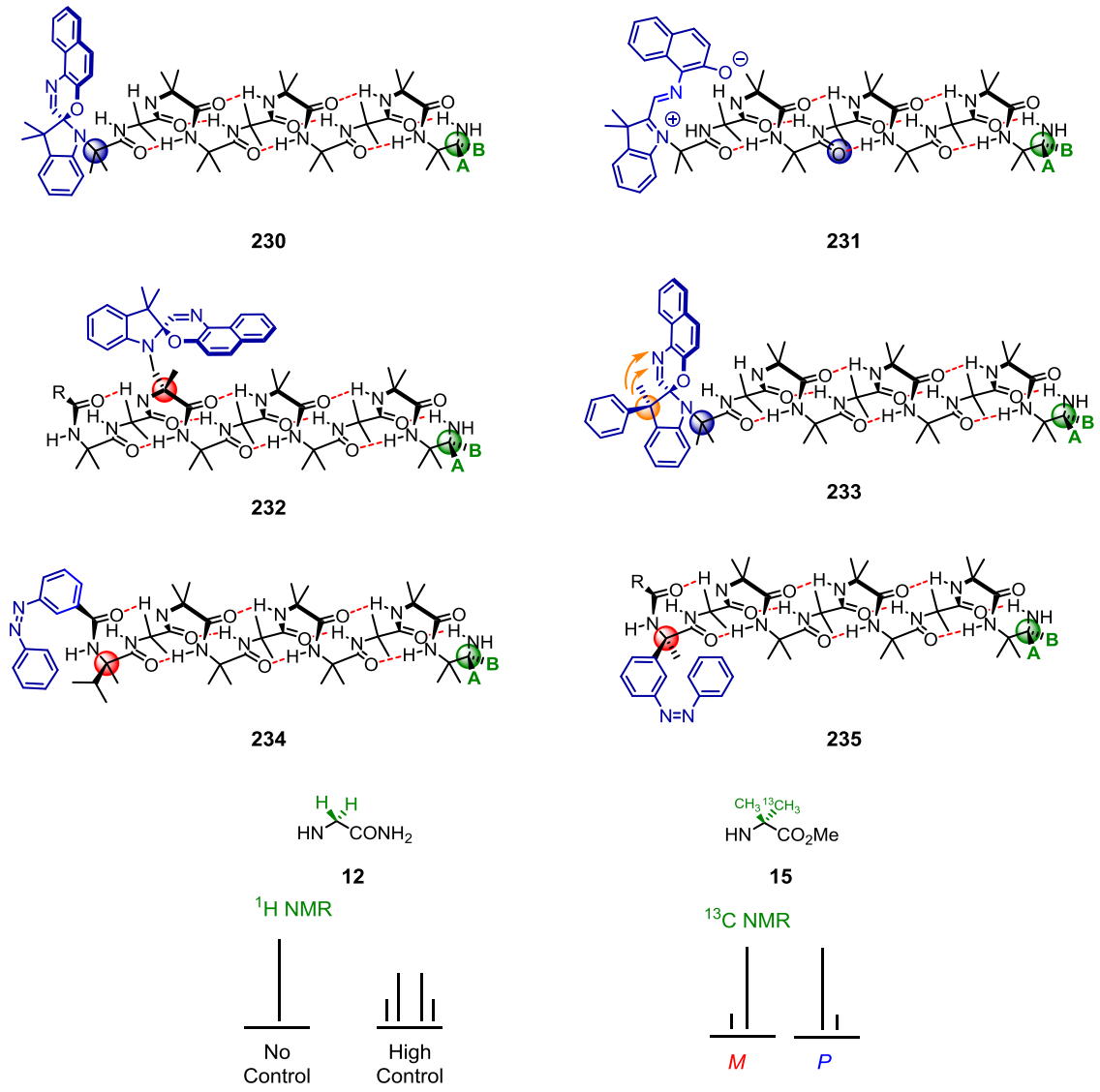

Figure 89 - Target stuctures for photochromic controllers.

10.1 Spirooxazine Controller Development

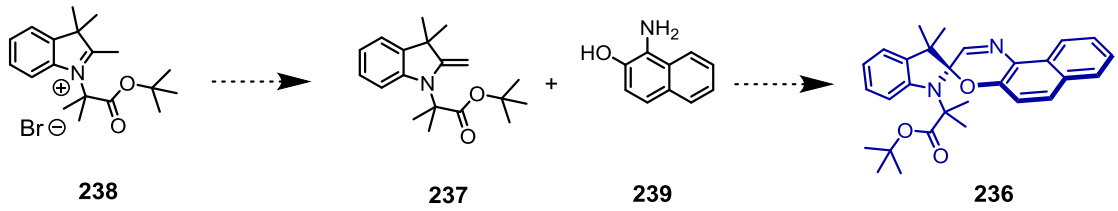

Scheme 54 - Photoresponsive helical polypeptides.

The SPO controlled structure **236** was chosen as a primary synthetic target due to its close structural match with the peptidic back bone of the Aib foldamer. The aim was to synthesise **236** following the second key method for SPO synthesis, reacting

the alkilidene fragment **237**, formed *in situ* from the indole salt **238** with commerically available amino napthols **239**

Attempts made to synthesise **238** through the alkylation of 2-methylidene-1,3,3-trimethylindoline **219** using tert-butyl 2-bromoisobutyrate **89** directly were unsuccessful; the steric congestion at the α-centre due to the geminal methyl groups was too great, preventing alkylation *via* the S_N2 pathway.

Alkylation of 2,3,3, trimethylindolenine **219** with tert-butyl 2-bromoacetate **240** to form the the less sterically hindered salt **241** also attempted but unsuccessful.

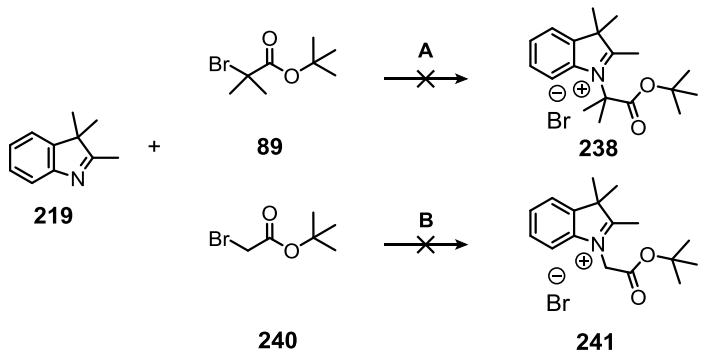

Scheme 55 - Attempts to synthesise indole salts.

To increase the reactivity of the alkylating agent tert-butyl 2-bromoacetate **240** was first converted to tert-butyl 2-Iodoacetate **242** in 75% yield following the method of Ladame *et al.*[163]

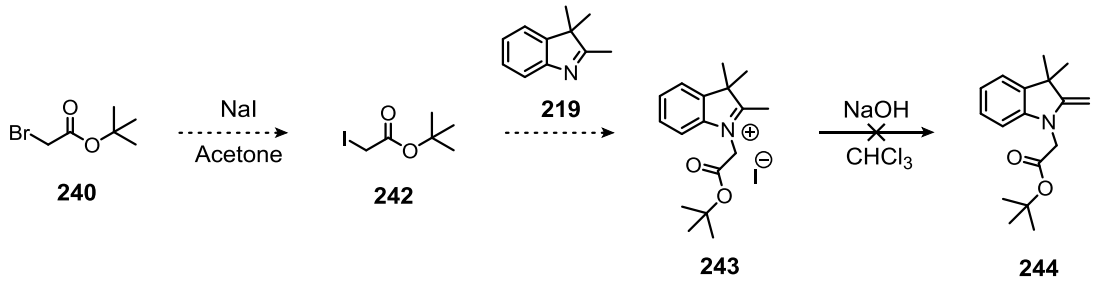

Scheme 56 - Further attempts to synthesise indole salts.

A modification of a further procedure by Ladame and co-workers was used to perform the alkylation, which appeared to proceed smoothly to the salt **243**. However, continuation of the method involved conversion to the indolene **244** at which stage purification by column chromatography lead to the loss of compound which appeared to be unstable. Further work in the development of photochromic controllers was postponed in preference of other research projects.

11.0 Conclusions

11.1 Project 1 : Screw-Sense Responsive Fluorescence Probe

After many synthetic attempts, a successful fluorescence probe for detecting the screw-sense preference of helical Aib foldamers was developed. The structure succeeded where earlier generations of probe structures did not for two key reasons:

A closer proximity of the two pyrene units within the probe structure led to substantially greater excimer fluorescence when attached to the Aib-based helix.

Synthetic modifications to the eventual probe structure reduced the control it placed on the Aib foldamer allowing it to respond to changes in screw-sense prefence rather than directing them.

Using this probe at the C-terminus of Aib helices it was possible to detect the relay of conformational signals from a remote N-terminal controller through changes in the ratios of excimer to monomer fluorescence emission.

Having optimised and developed the probe in solution, it was found to be a highly successful screw-sense probe in membrane enviroments, providing a wealth of information about both the screw-sense preference of the peptide to which it was attached and the membrane environment in which it was located.

Like the earlier NMR probes developed within the Clayden group have allowed a large variety of research projects to develop in solution, it is expected that this fluorescent probe will allow the development of new research projects focussed around the membrane environment, a few potential projects are suggested in the future work.

The success of the pyrene probe was exemplified through the development of a series of biomimetic structures aiming to replicate the behaviour of a GPCR in a membrane environment. Of these the longer compound **205** was found to function in the membrane environment of DOPC vesicles. The N-terminal binding site, developed separately within the Clayden group, bound carboxylate structures inducing a screw-sense preference in the achiral foldamer. Signal relay was achievable (Figure 90) with the biomimetic structure binding Leu-Enkephalin and adopting an *M* screw-sense preference. Addition of a second agonist, Boc-L-Pro displaces the Enkephalin at the synthetic binding site inducing a switch to *P* screw-

sense preference. This relay of binary information (M/P) through the achiral helix could be detected at the distal terminus using the fluorescent probe.

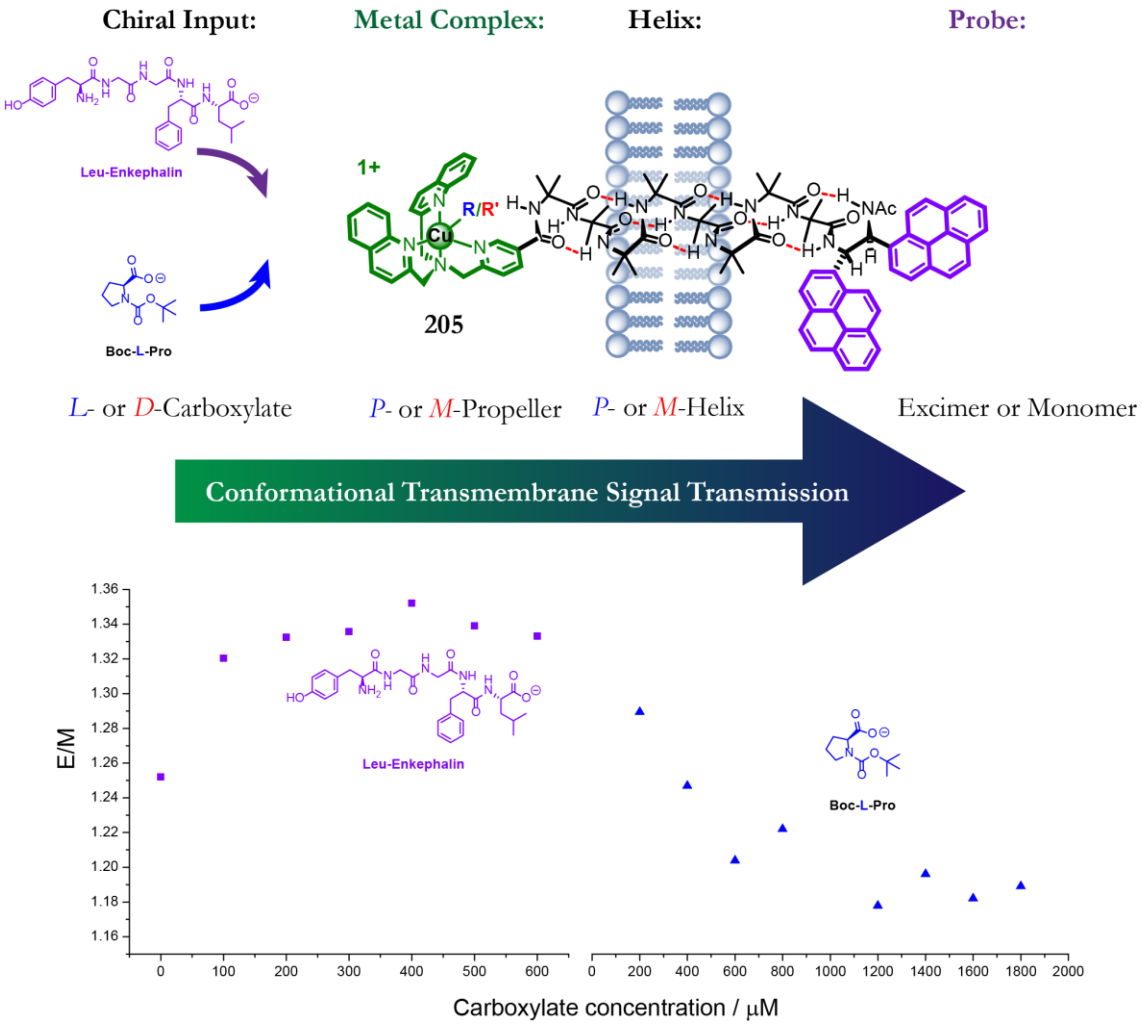

Figure 90- Chiral information, delivered through agonist binding at synthetic receptor site is relayed through achiral helix in membrane environment where it is detected by the pyrene probe.

11.2 Project 2: Photochromic Screw-Sense Controllers

The success of project 1 led to greater focus placed on its further development. Due to this, less time was available for the development of a photochromic screw-sense controllers. Early attempts were made to synthesise structures based on spirooxazine and azobenzene structures. While these were found to be unsuccessful there is great potential for the development of further structures and the advantages of a photochromic controller for use in membrane enviroments are clear. The development of a non-reversible light-controlled switch is discussed in the future work.

12.0 Future work

12.1 Fluorescent Probes in Living Systems

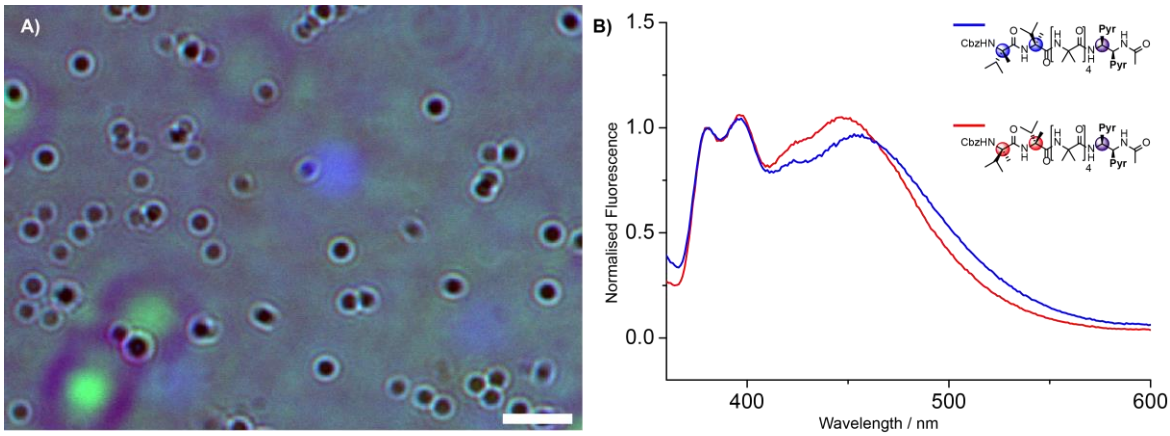

Figure 91A) Bright field image of Living Hi5 cells loaded with compound **156** scale bar 10 μM. **B**) Comparative fluorescence spectra of **156** and **157** in the cell matrix of Hi5 cells.

Preliminary work in collaboration with Dr. Edward A McKenzie at the University of Manchester has highlighted the potential for the development of signal transmission systems in living biological systems (Figure 91). Methanolic solutions of compounds **145** and **157** were fed to Hi5 insect cells and incubated for 72 hrs. The cells were rinsed with buffer solution to remove any compound that was not incorporated within the cell. Healthy cell samples were found to contain both compounds with different observable E/M ratios and an additional difference in the maximal position for the *M* and the *P* helices in living cells.

Further work in this area could lead to some highly interesting research projects. Introducing a photocleavable protecting group to the N-terminus of a controlled Aib helix **245** could allow a compound that is compatible with living systems and can be both controlled and probed using light. The level of control delivered from a single chiral amino acid residue attached to the N-terminus of an Aib helical foldamer is greatly enhanced by the presence of the protecting group carbonyl.[48]

Photocleavage of a suitable protecting group[164,165] would remove this carbonyl switching off control to the helix **246**. Once these systems have been developed using the fluorescent probe its replacement with more complex outputs such as reactive and catalytic sites could lead to structures that interact with and control the living systems in which they are placed.

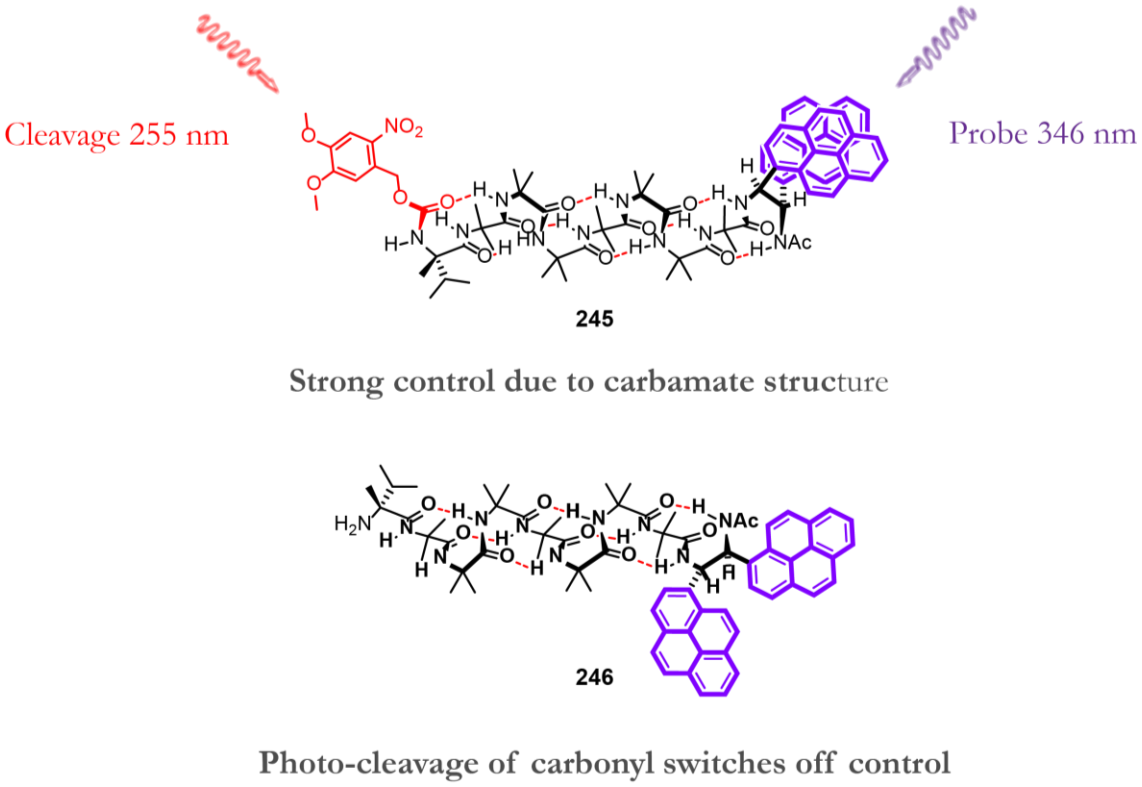

Figure 92 - Light controlled and detected signal transmission for use in living systems.

12.2 A Colour Changing Fluorescent Probe

The pyrene probe has proven to be highly effective in both membrane and solution but unfortunately only the excimer fluorescence is in the visible wavelength. A colour changing probe would allow the visualisation of the 3D structure of vesicles or living organisms, opening up new possibilities for research using microscopy techniques.

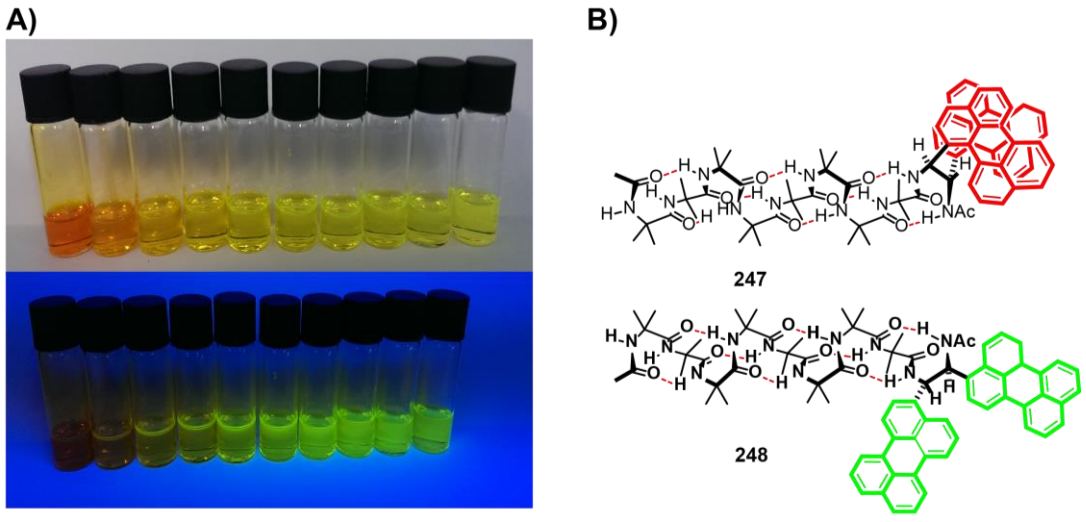

Figure 93A) Serial dilution of perylene aldehyde showing colour change due to intermolecular interactions. **B)** Proposed analogue probe structure providing colour changing read-out of screw-sense preference.

Replacement of the pyrene fragments with a chromophore that is coloured and forms an excimer or self-quenches leading to a change in colour, for example perylene (Figure 93A) could allow for the creation of a probe structure that is red **247** in one screw-sense preference and green in the other **248**. Unfortunately, various attempts to synthesise the perylene analogue have thus far been thwarted by the solubility of the perylene units. However, the dilution of perylene illustrates the point: a suitable colour changing fragment could be found with the simple screening of commercially available coloured aldehydes. If, on serial dilution a significant colour change is observed the aldehyde would have high potential in the synthesis of a colour analogue. Those aldehydes that change colour could then be used in the synthesis of a colour changing probe analogue.

Visualisation of organisms could provide detailed information about the aggregation and uptake of helical structures. If for example, molecules aggregate in specific regions of a bacterium, an inter-molecular quenching would result in red regions were the structures were collecting

The inter-molecular interaction of the probe (apparent at higher concentration ratios of probe to cell) could provide information on the cellular aggregation properties of Aib oligomers. Areas were the structures were concentrated, for example the cell wall or the nucleus, would appear red against the dilute green of the probe.

13.0 Experimental Section

13.1 General Methods and Materials

All non-aqueous reactions were carried out in oven-dried glassware under an atmosphere of nitrogen using standard anhydrous techniques. All reagents were obtained from commercially available sources and used without further purification, or where indicated prepared internally. Air- and moisture- sensitive liquids and solutions were transferred *via* syringe or stainless steel cannula. Reactions performed at 0 °C were done so using an ice bath. Anhydrous dichloromethane (DCM) and tetrahydrofuran (THF) were obtained by distillation from calcium hydride, and sodium wire with a benzophenone indicator, respectively. Other anhydrous reaction solvents were obtained using Innovative Technologies Puresolve P5-mp-5 solvent purification system. All products were dried on a rotary evaporator followed by connection to a high vacuum system to remove any residual solvent. Flash chromatography was performed on silica gel (Merck 60H, 40-60 nm, 230 – 300 mesh). Analytical thin layer chromatography (TLC) was performed on Macherey Nagel alugram SIL G/UV254 and were visualised using both UV lamp (254 nm), and ninhydridrin or phosphomolybdic acid dips depending on the compound properties.

Instrumentation

All ^{1}H and ^{13}C nuclear magnetic resonance (NMR) spectra were obtained using Bruker Ultrashield 300, 400, 500 or 600 MHz spectrometers. Chemical shifts are quoted in parts per million (ppm) and coupling constants (*J*) are quoted in Hz. ^{1}H-NMR were referenced to the residual deuterated solvent peak ($CDCl_3$ 7.27; CD_3OD 3.31; D_2O 4.79; $(CD_3)_2SO$ 2.50 ppm) and ^{13}C-NMR were referenced to the carbon resonance of the solvent ($CDCl_3$ 77.0; CD_3OD 49.05; $(CD_3)_2SO$ 39.52 ppm) Multiplicities are denoted as s (singlet), d (doublet), t (triplet), q (quartet), spt (septet) and m (multiplet) or denoted as br. (broad), or some combination of these, where appropriate. Where ^{1}H NMR spectra were run in CD_3OD, D_2O exchangeable protons (NH, OH) are reported only where observed. Assignments were made using 2D ^{1}H-COSY and HMQC experiments The anisochronicity, in parts per billion (ppb), of AB systems arising from the germinal ^{1}H nuclei of the $GlyNH_2$ diastereotopic NMR probe was given by $\upsilon_0\Delta\delta = [(f_1 - f_3)^2 - J_{AB}^2]^{1/2} = [(f_2 - f_4)^2 - J_{AB}^2]^{1/2} = [(f_1 - f_4)\ (f_2 - f_3)]^{1/2}$ where $f_{1,2,3,4}$ are the observed resonant frequencies in order of the four lines comprising the AB multiplet, J_{AB} is the coupling constant and υ_0 is the spectrometer frequency. In molecules containing multiple spin systems of the form ABX, the separate

systems, identified by COSY, are denoted with prime (') and double prime (") i.e A of ABX or B' of ABX'.

Melting points (mp) were determined on a GallenKamp apparatus and are uncorrected. Optical rotaton ($[\alpha]_D^{25}$) were obtained on a JASCO J-815 spectropolarimeter at 25°C using a cell with pathlength of 0.25 dm. solvent and concentration are stated with individual readings. Infra-red spectra (IR) were recorded on a ATi Perkin Elmer Spectrum RX1 FT-IR. Only absorption maxima (ν_{max}) of interest are reported and quoted in wavenumbers (cm^{-1}). Low and high resolution mass spectra were recorded by staff at the University of Manchester. Electrospray (ES) spectra were recorded on a Waters Platform II. High resolution mass spectra (HRMS) were recorded on a Thermo Finnigan MAT95XPand are accurate to ±0.001 Da

Clayden Group Supplied Chemicals

4-(pyren-1-ylmethoxy)benzaldehyde **126** was supplied by Dr. S. Pike**.** Cbz-L-αMv-Aib_4-OH **140** was supplied by Dr. Liam Byrne. BQPA-3-CO-Aib_4-$GlyNH_2$ **194**, BQPA-3-CO-Aib_4-OH **192** and BQPA-3-CO-OH **184** were supplied by Dr. Bryden Le Bailly. N_3Aib_5OH **198** was supplied by Dr. Vincent Demier.

13.2 General Methods

General procedure 1: Sequential deprotection and coupling of Boc-pyrene probe structures

Deprotection: The Boc protected bis pyrene fragment (0.039 mmol, 1.0 eq) was suspended in anhydrous DCM (25 mL) and cooled to at 0 °C. TFA (1 mL) was added dropwise with stirring and the solution was left to stir for 2 h, warming to RT. The reaction completion was confirmed by TLC and the solvent was concentrated under reduced pressure. Repeat azeotroping with Et_2O removed residual TFA. The crude salt was placed under high vacuum for an hour. The deprotected salt was dissolved in 1 mL of a suitable mixture of DCM/DMF and used directly in the coupling procedure.

Coupling: A suspension of Cbz-Phe-Aib_4OH (0.039 mmol, 1.0 eq.) and HOBt (1.1 eq.) in anhydrous DCM 0.5 mL was cooled to 0 °C. To this was added EDC (1.0 eq.). Once the suspension had fully dissolved, the solution of de-protected amine was added to the reaction and left to stir for three days. After checking reaction completion by TLC the solvent was concentrated under reduced pressure. The residue was dissolved in EtOAc (25 mL). The solution was then washed sequentially

with $KHSO_4$ (3×5 mL), $NaHCO_3$ (3×5 mL), brine (5 mL) and dried ($MgSO_4$). Removal of the solvent under reduced pressure gave the crude product. This was purified by column chromatography.

General procedure 2: Coupling of diamine hydrochloride salts

A round bottom flask was charged with X-Aib_n-OH Fragment (1 eq.), HOBt (1.2 eq.), and the diamine diydrochloride salt (1.1 eq) and EDC.HCl (1.1 eq) and 5 mL of DCM forming a suspension. The suspension was placed under a nitrogen atmosphere. Addition of DIPEA (3.7 eq) lead to dissolution of the solid. After leaving to stir for 2 days the solvent was concentrated under reduced pressure leaving a residue. This was re-dissolved in EtOAc (25 mL) and washed sequentially with $NaHCO_3$ (3×5 mL), brine (5 mL) and dried ($MgSO_4$). Removal of the solvent under reduced pressure gave the crude product. Further purification methods are specified in the individual compound entry.

General procedure 3: Acid fluoride coupling of alphamethyl valine

2.0 equiv of Cbz-αMv-OH was dissolved in of anhydrous DCM (5 mL/mmol). To this was added 3.0 eq. Tetramethylfluoroformamidinium Hexafluorophosphate. 2.0 eq. of pyridine was added to the suspension which was left to stir for 3.5 h. DCM (30 mL/mmol) was added to the solution, which was washed with ice-cold water (3×20 mL/mmol), and dried ($MgSO_4$) and filtered. The solvent was removed and the residue dried under high vacuum for 1h. Once dry, the residue was dissolved in (1 mL/mmol) anhydrous DCM and added to a separately prepared solution of amine (1 eq) and DIPEA (1 eq) in DCM (1 mL/mmol). The reaction was left to stir under and atmosphere of nitrogen for 7 days. The solvent was subsequently removed under vacuum, and the residue dissolved in 30 mL EtOAc. The organic layer was washed with $NaHCO_3$ (Sat. aq. 2 × 10 mL/mmol), $KHSO_4$ (5% aq., 2 × 10 mL/mmol), dried ($MgSO_4$), filtered and removed under reduced pressure to give a crude solid. Further required purification methods are specified in the individual compound entry.

General Procedure 4: Sequential coupling and acetylation of diamine hydrochloride salts.

A round bottom flask was charged with X-Aib$_n$-OH Fragment (1 eq.), HOBt (1.3 eq.), and the diamine diydrochloride salt (1.1 eq) and EDC.HCl (1.1 eq) and 5 mL of DCM forming a suspension. The suspension was placed under a nitrogen atmosphere. Addition of NEt_3 (5 eq) lead to dissolution of the solid. After leaving to stir for 2 daysm, 15 mL of additional DCM was added to the reaction mixture. This washed with distilled water (4×3 mL) and dried over Na_2SO_4. The solvent was concentrated under reduced pressure at RT to leave a crude residue. The residue was re-dissolved in 2 mL of anhydrous DCM and placed under a nitrogen atmosphere. Ac_2O (1.5 eq) was added to the solution which was left to stir over night. The solvent was concentrated under reduced pressure. Further required purification methods are specified in the individual compound entry.

13.3 Synthetic Details

L-Pyrenylalanine 41[110]

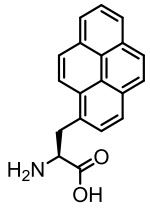

N-acetyl-DL-pyrenylalanine **47** (5.46g, 16.5 mmol) was dissolved in 1M NaOH (50 mL). Slow addition of 1M HCl lowered the pH of the solution to 8 without the precipitation of **47**. A separate acylase solution was prepared as follows: 1.29 g of Acylase 1 (Sigma Aldrich *Aspergillus melleus*) was dissolved in distilled 50 mL of distilled H_2O. Insoluble particles were removed from the solution and care was taken not to disturb the solution, preventing lathering or foam formation. The solution was activated with the addition of 40 mg $CoCl_2$ dissolved in 1 mL of distilled water. The activated acylase solution was then added to the basic solution which was left to stir at 40°C in the dark for 2 days. The precipitate was collected by filtration, washed with H_2O and MeOH. Drying under reduced pressure gave the title compound **41** 1.84 g, (30%) of as a brown solid. Due to solubility issues the free amino acid was protected and characterised as the Boc protected species **82** in line literature methods.[110,112]

N-Benzoyl-DL-pyrenylalanine 42[110]

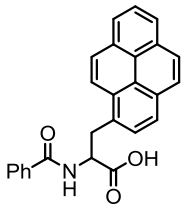

N-Benzoyl-DL-1-pyrenylalanine ethyl ester **75** (3.6 g, 8.5 mmol) was dissolved in 200 mL of EtOH. NaOH (2M, 20 mL) was added and the mixture was heated to 60 °C until the starting material was consumed (TLC monitoring). Neutralisation of the solution (HCl) yielded the title compound (3.3 g, >99%) as a white solid. **mp** 248-251 °C; (lit[110] 255-258 °C); **IR** (ATR, cm^{-1}): 3303, 2924, 2469, 1715, 1608; **^{1}H NMR** (400 MHz, $(CD_3)_2SO$) δ_H 8.91 (d, J = 8.3, 1 H, NH), 8.48 (d, J = 9.3, 1 H, PyrH), 8.34 - 8.24 (m, 3H, PyrH), 8.20 (d, J = 7.8, 1 H, PyrH), 8.17 - 8.02 (m, 4 H), 7.82 - 7.70 (m, 2H, Bz *ortho*), 7.53 - 7.46 (m, 1H, Bz *para*), 7.45 - 7.37 (m, 2 H, Bz, *meta*), 4.90 (ddd, J = 10.5, 8.2, 4.3, 1H, $^{\alpha}$CH), 4.05 (dd, J = 13.9, 4.2, 1 H, $^{\beta}CH_AH_B$), 3.76 (dd, J = 13.9, 10.5, 1H, $^{\beta}CH_AH_B$) **^{13}C NMR** (100 MHz, $(CD_3)_2SO$) δ_C 173.2 (CO), 166.3 (CO), 133.8 (Bz *ipso*), 132.5 (PyrC), 131.4 (Bz *para*), 130.8,

130.3, 129.7, 128.5 (4×PyrC), 128.4 (PyrCH), 128.2 (2×C, Bz *meta*), 127.6, 127.4 (2×PyrCH), 127.3 (2×C, Bz *ortho)*, 126.8, 126.2, 125.2, 125.0, 124.6 (5×PyrC), 124.2, 124.0 (PyrCH), 123.0 (PyrC), 54.2 ($^{\alpha}$C), 34.0 ($^{\beta}$C).

N-acetyl-DL-pyrenylanine **47**[166]

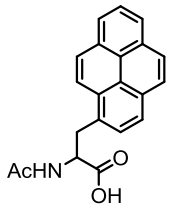

Diethyl (1-pyrenylmethyl) acetimidomalonate **78** (5 g, 11.6 mmol) was suspended in a 1:1 mixture of EtOH and 1,4-dioxane. Aqueous NaOH 1M (50 mL) was added with stirring and the mixture was heated to 90 °C. After 2 h and full consumption of **71** (loss confirmed by TLC R_f = 0.25 in 1% MeOH/DCM) the temperature was lowered to 60 °C. Aqueous HCl (60 mL; 1M) was added portion-wise with the evolution of gas (CO_2). The reaction was left at 60°C until bubbling ceased. After confirming an acidic reaction pH the reaction solution was poured into rapidly stirring water (500 mL) leading to precipitation. The precipitate was isolated and dried under reduced pressure to give the title compound **47** 3.1 g, (81%) as an off white solid **mp** 230-233 °C; **IR** (ATR, cm^{-1}) 3313, 1719, 1603, 1534, 1275; **^{1}H NMR** (400 MHz, CD_3OD) δ_H 13.85 - 13.47 (m, 1H, COOH), 9.27 (d, *J* = 8.5, 1H, NH), 9.21 (d, *J* = 9.3, 1H , PyrH), 9.13 - 9.00 (m, 4H, PyrH), 8.96 - 8.93 (m, 2H, PyrH), 8.87 (t, *J* = 7.7, 1H, PyrH), 8.80 (d, *J* = 7.8, 1H, PyrH), 5.49 (ddd, X of ABX *J* = 9.5, 8.5, 5.3, 1H, $^{\alpha}$CH-Pya), 4.69 (dd, A of ABX *J* = 14.0, 5.3, 1H, $^{\beta}C\mathit{H}_A H_B$), 4.35 (dd, B of ABX, *J* = 14.0, 9.5, 1H, $^{\beta}CH_A\mathit{H}_B$) **^{13}C NMR** (100 MHz, CD_3OD) δ_C 182.8 (CO), 179.0 (CO), 141.8, 140.5, 140.0, 139.5, 138.2, 138.1, 137.2, 137.1, 136.5, 135.9, 134.8, 134.7, 134.3, 133.8, 133.7, 132.7 (16×PyrC), 63.3 ($^{\alpha}$CH), 44.3 ($^{\beta}CH_2$), 32.0 (NC(O)$\mathit{C}H_3$); **MS** (ES^-, MeOH) 330 (100%, $[M-H]^-$); Data is consistent with literature.[166]

Cbz-L-Phe-Aib$_4$-OH 63[167]

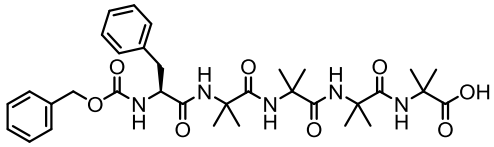

Cbz-L-Phe-Aib$_4$-O*t*Bu **101** was dissolved in 5 mL anhydrous DCM. To this was added 0.3 mL of trifluoroacetic acid with stirring. The reaction was left for to stir for 2h. After reaction completion (TLC) the solvent was concentrated under reduced pressure. Residual trifluoroacetic acid was removed by azeotroping with Et_2O. Further trituration of the resultant residue and drying under reduced pressure gave the desired compound (78 mg, 94%) as a white solid. $\mathbf{[\alpha]_D^{25}} = -10.4$ (c = 1, MeOH); **^{1}H NMR** (400 MHz, CD_3OD) δ_H 8.30 (s, 1H, NH), 7.64 (s, 1H, NH), 7.51 (s, 2 H, NH), 7.20 - 7.37 (m, 10H, ArH), 5.10 (d, *J* = 12.8, 1H, A of AB, OH_AH$_B$C-Ph), 5.05 (d, *J* = 12.8, 1H, B of AB, OH$_A$$H_B$C-Ph), 4.21 (apparent t, *J* = 8.0, 1H, X of ABX $^{\alpha}$CH-Phe), 3.03 (dd, *J* = 13.6, 8.0, 1H, A of ABX, PhCH_AH$_B$CH$_X$), 2.95 (dd, *J* = 13.6, 8.0, 1H, B of ABX, PhCH$_A$$H_BCH_X$), 1.49 (s, 6H, 2×CH$_3$), 1.47 (s, 3H, CH$_3$), 1.42 (s, 3H, CH$_3$), 1.38 (s, 3H, CH$_3$), 1.34 (s, 3H, CH$_3$), 1.28 (s, 3H, CH$_3$), 1.24 (s, 3H, CH$_3$) **^{13}C NMR** (100 MHz, D_3OD) δ_C 178.4 (CO), 176.9 (2×CO), 176.6 (CO), 174.4 (CO), 158.7 (CO), 138.3 (C), 138.2 (C), 130.7 (2C), 129.7 (2C), 129.7 (2C), 129.2, 128.7 (2C), 128.0 (10×ArCH) 67.8 (CH$_2$-Cbz), 58.3 (C) 57.9 (C), 57.7 (C), 57.1 (C), 38.3 ($^{\beta}$CH$_2$), 26.9 (CH$_3$), 26.7 (CH$_3$), 26.4 (CH$_3$), 25.9 (CH$_3$), 24.9 (CH$_3$), 24.6 (CH$_3$), 24.3 (CH$_3$), 24.1 (CH$_3$). Data is consistent with literature.[167]

Cbz-D-Phe-Aib$_4$-OH 64[167]

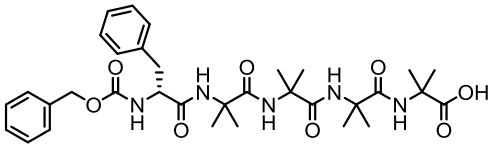

Cbz-D-Phe-Aib$_4$-O*t*Bu **102** was dissolved in 5 mL anhydrous DCM. To this was added 0.3 mL of trifluoroacetic acid with stirring. The reaction was left for to stir for 2h. After reaction completion was confirmed by TLC, the solvent was removed under reduced pressure. Residual trifluoroacetic acid was removed by azeotroping with Et_2O. Further trituration of the resultant residue and drying under reduced pressure gave the desired compound (58 mg, 68%) as a white solid. $\mathbf{[\alpha]_D^{25}}$ = 11.3 (c = 1, MeOH); **^{1}H NMR** (400 MHz, CD_3OD) δ_H 8.20 (s, 1H, NH), 7.54 (s, 1H, NH), 7.41 (s, 1H, NH), 7.10 - 7.27 (m, 10H, ArH), 5.00 (d, *J* = 12.8, 1H, A of AB, OH_AH$_B$C-Ph), 4.95 (d, *J* = 12.8, 1H, B of AB, OH$_A$$H_B$C-Ph), 4.11 (apparent t, *J* = 8.0, 1H, X of ABX, $^{\alpha}$CH-Phe), 2.92 (dd, *J* = 13.6, 8.0, 1H, A of ABX, $^{\beta}$CH_AH$_B$-Phe), 2.85 (dd, *J* = 13.6, 8.0, 1H, B of ABX, $^{\beta}$CH$_A$$H_B$-Phe), 1.38 - 1.41 (m, 6H, 2×CH$_3$), 1.37 (s, 3H, CH$_3$), 1.32 (s, 3H, CH$_3$), 1.28 (s, 3H, CH$_3$), 1.23 (s, 3H, CH$_3$), 1.18 (s, 3H, CH$_3$), 1.15 (s, 3H, CH$_3$) **^{13}C NMR** (100 MHz, D_3OD) δ_C 178.4 (CO), 176.9 (2×CO), 176.6 (CO), 174.4 (CO), 158.7 (CO), 138.3 (C), 138.2 (C), 130.7 (CH), 129.7 (CH), 129.7 (CH), 129.2 (CH), 128.7 (CH), 128.0 (CH), 67.8 CH$_2$-Cbz), 58.3 (C), 57.9 (C), 57.7 (C), 57.1 (C), 38.3 ($^{\beta}$CH**)**, 26.9 (CH$_3$), 26.7 (CH$_3$), 26.4 (CH$_3$), 25.9 (CH$_3$), 24.9 (CH$_3$), 24.6 (CH$_3$), 24.3 (CH$_3$), 24.1 (CH$_3$), Data is consistent with literature.[167]

Boc-L-Pya-L-Pya-OMe 67

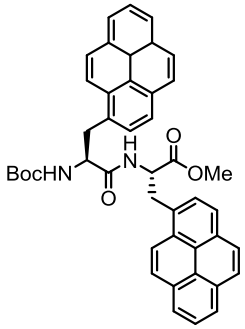

Boc-L-Pya **82** (149 mg, 0.38 mmol, 1 eq.) was dissolved in 2 mL dry DCM. 68.8 mg (1.3 eq) HOBt was added and the suspension was cooled to 0 °C. 67 µl (1 eq) of EDC was added to the suspension which was left to stir for 30 mins at 0 °C until the solid dissolved into solution. At this point L-Pya-OMe **83** (130 mg, 1 eq) was added followed by 0.25 mL DIPEA (2.5 eq). The reaction was left to stir for 12 h. The reaction solvent was removed under reduced pressure to give a crude residue. This was purified by column chromatography, eluting with a solvent gradient of 1-2.5% Acetone in chloroform to give the title compound as an off-white solid (150 mg, 57%) **Rf** 0.45 (5% acetone/chloroform) **mp** 212-214 °C; $\mathbf{[\alpha]_D^{25}}$ = -85.2 (c = 1.0; DMSO); **IR** (ATR, cm^{-1}) 3313, 1737, 1659 **^{1}H NMR** (500 MHz, $(CD_3)_2SO$) δ_H 8.57 (d, *J* = 7.6, 1H, NH), 8.39 (d, *J* = 9.1, 1H, PyrH), 8.34 - 8.24 (m, 6H, PyrH), 8.21 (d, *J* = 7.9, 1H, PyrH), 8.18 - 8.03 (m, 8H, PyrH), 7.97 (d, *J* = 7.9, 1H, PyrH), 7.81 (d, *J* = 7.9, 1H, PyrH), 6.98 (d, *J* = 8.8, 1H, NH), 4.81 (dd, X of ABX, *J* = 14.5, 7.9, 1H, $^{\alpha}$CH), 4.43 (td, X' of ABX', *J* = 9.0, 5.0, 1H, $^{\alpha}$C'H), 3.88 (dd, A of ABX, *J* = 14.0, 6.1, 1H, Pyr-$^{\beta}$CH_AH$_B$), 3.72 (dd, B of ABX, *J* = 14.0, 8.5, 1H, Pyr-$^{\beta}$CH$_A$$H_B$), 3.58 (dd, A' of ABX', *J* = 14.0, 5.0, 1H, Pyr-$^{\beta}$C'H_AH$_B$), 3.53 (s, 3H, OCH_3), 3.40 (dd, B' of ABX' *J* = 14.0, 9.5, 1H, Pyr-$^{\beta}$C'H$_A$$H_B$) 1.16 (s, 7H, Boc) 0.75 (s, 2H, Boc); **^{13}C NMR** (125 MHz, $(CD_3)_2SO$) δ_C 171.7 (CO), 171.4 (CO), 154.9 (CO-Boc), 132.1, 131.4, 130.8, 130.8, 130.3, 129.9, 129.6, 128.6, 128.6, 128.4, 127.7, 127.4, 127.3, 127.2, 126.9, 126.7, 126.2, 126.1, 125.2, 125.1, 125.0, 124.8, 124.7, 124.5, 124.2, 124.1, 124.0, 124.0, 123.3, 123.0 (30×PyrC) 78.1, 55.8 (C'$_{\alpha}$), 51.9 ($^{\alpha}$C), 35.2 ($^{\beta}$C), 34.4 ($^{\beta}$C), 27.9 (C$(CH_3)_3$) 2×PyrC could not be located.; **MS** (ES^+) 697 (100%; $[M+Na]^+$); **HRMS** (ES^+ TOF) Calcd for $C_{44}H_{38}N_20_5+H^+$ = 675.2853, found 675.2853.

Boc-L-Pya-D-Pya-OMe 68

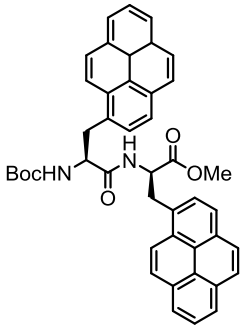

Boc-L-Pya **82** (156 mg, 0.39 mmol, 1 eq.) was dissolved in 2 mL dry DCM. 71.6 mg (1.3 eq) HOBt was added and the suspension was cooled to 0 °C. 71 μl (1 eq) of EDC was added to the suspension which was left to stir for 30 mins at 0 °C until the solid dissolved into solution. At this point D-Pya-OMe **84** (151 mg, 1.1 eq) was added followed by 0.27 mL DIPEA (2.5 eq). The reaction was left to stir for 12 h. The reaction solvent was removed under reduced pressure to give a crude residue. This was purified by column chromatography, eluting with a solvent gradient of 1-2.5% Acetone in chloroform to give the title compound as an off-white solid (137 mg, 50%) **mp** 214 °C; $\mathbf{[\alpha]_D^{25}}$ = +146.4 (c = 1.0; DMSO); **IR** (ATR, cm^{-1}) 3305 (NH) 1737 (C(O)OMe), 1685, 1655(C(O)NC); **^{1}H NMR** (500 MHz, $(CD_3)_2SO$) δ_H 8.83 (d, *J* = 7.9, 1H, NH), 8.39 - 8.22 (m, 7H, PyrH), 8.19 - 7.96 (m, 10H, PyrH), 7.76 (d, *J* = 7.9, 1H, PyrH), 6.84 (d, *J* = 9.1, 1H, NH), 4.82 (td, X of ABX, *J* = 8.5, 5.4, 1H, $^{\alpha}$CH), 4.48 (td, X of ABX' *J* = 9.0, 4.5, 1H, $^{\alpha}$C'H), 3.87 (dd, A of ABX *J* = 14.0, 5.7, 1H, Pyr-$^{\beta}$CH_AH$_B$), 3.65 (s, 3H, OMe), 3.59 (dd, B of ABX *J* = 14.0, 9.0, 1H, Pyr-$^{\beta}$CH$_A$$H_B$), 3.45 (dd, A' of ABX' *J* = 14.0, 4.5, 1H, Pyr-$^{\beta}$C'H$_A$H$_B$), 3.11 (dd, B' of ABX' *J* = 14.0, 9.8, 1H, Pyr-$^{\beta}$C'H_AH$_B$), 1.14 (s, 7H, Boc), 0.78 (br. s., 2H, Boc) **^{13}C NMR** (125 MHz, $(CD_3)_2SO$) δ_C 171.8 (CO), 171.4 (CO), 154.9 (CO-Boc), 132.0, 131.4, 130.8, 130.8, 130.3, 130.3, 129.9, 129.5, 128.7, 128.6, 128.5, 128.4, 127.7, 127.4, 127.3, 127.1, 126.9, 126.7, 126.2, 126.0, 125.2, 125.1, 124.9, 124.8, 124.6, 124.4, 124.2, 124.0, 124.0, 124.0, 123.5, 122.9 (32×PyrC), 79.2, 77.9, 55.1 (C'$_{\alpha}$), 53.5 ($^{\alpha}$C) 52.1 (OCH_3), 35.2 ($^{\beta}$C'), 34.5 ($^{\beta}$C), 27.9 ($C(CH_3)_3$); **MS** (ES^+) 697 (100%; $[M+Na]^+$) **HRMS** (ES^+ TOF) Calcd for $C_{44}H_{38}N_20_5$ + Na^+ = 697.2673, found 697.2679.

2-Phenyl-4-(1-pyrenylmethy1ene)-5-oxazolone 73[110]

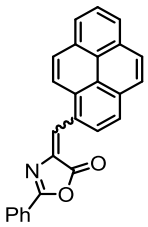

Finely powdered sodium acetate (28.2 g, 340 mmol) was added to Ac_2O (150 mL) and heated to 110°C. To this a finely powdered mixture of *N*-benzoyl glycine (7.1 g, 39 mmol) and 1-pyrenecarboxaldehyde (7.99 g, 34 mmol) was added with vigorous stirring by powder funnel against a pressure of nitrogen. The mixture was left to heat with stirring overnight with one of the septa vented with a needle. The reaction was allowed to cool and diluted with EtOH (400 mL). The reaction mixture was then poured into 2 litres of distilled water with vigorous stirring yielding a red precipitate. This precipitate was collected and dried under vacuum giving the title compound **73** (9.96 g, 75%) as a crude red solid. This solid was found to be poorly soluble in a range of solvents preventing further purification or analysis. Following the method outlined by Egusa *et al.*[110] it was used in the next reaction without further purification.

Ethyl-3-(l-pyreny)-2-benzamidopropenoate 74[110]

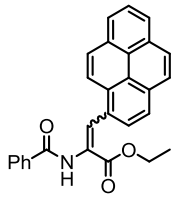

Crude 2-Phenyl-4-(1-pyrenylmethy-1-ene)-5-oxazolone **73** (9.2 g, 24 mmol) was suspended in 1:3 mixture of anhydrous Tol and EtOH. To this was added 10.8 mL (1.2 eq) of a 21% wt solution of NaOEt in ethanol. The mixture was heated to reflux and left to stir until the solid fully dissolved (1 h). After the solid had completely dissolved the solution was allowed to cool to room temperature and neutralised with glacial acetic acid yielding a crude precipitate. Recrystallisation of this precipitate in EtOH gave the title compound as yellow needles (5.61g, 56%). **mp** 193-194 °C (lit[110] 189-190 °C) **IR** (ATR, cm^{-1}) 3251, 1715, 1650, 1637; **^{1}H NMR** (400 MHz, $CDCl_3$) δ_H 8.31 (d, J = 9.1, 1H, PyrH), 8.24 - 8.20 (m, 3H, 2×PyrH + $^{\beta}$CH), 8.20 - 8.01 (m, 6H, PyrH) 7.81 (s, 1H, NH), 7.76 - 7.70 (m, 2H, *o*-Bz), 7.52 - 7.45 (m, 1H, *p*-Bz), 7.41 - 7.35 (m, 2H, *m*-Bz) 4.47 (q, J = 7.1, 2H, OCH_2), 1.46 (t, J

= 7.2, 3H, CH_3); **^{13}C NMR** (100 MHz, $CDCl_3$) δ_C 165.5 (CO), 165.2 (CO), 133.6 (*i*-Bz), 132.0 (*p*-Bz), 131.8, 131.2, 130.8, 129.2 (4×PyrC) 128.6 (*m*-Bz), 128.4 (PyrC), 128.4, 128.2 (2×PyrCH), 127.5 ($^{\beta}$C), 127.3 (*o*-Bz), 127.3 (PyrCH), 126.9 (PyrC), 126.2, 125.8, 125.8, 125.7 (4×PyrCH), 124.9 (PyrC), 124.7 (PyrCH), 124.6 (PyrC), 123.6 (PyrCH), 62.1 (OCH_2), 14.3 (CH_3) **MS** (ES^+) 420 (100%, $[M+H]^+$); **HRMS** (ESI^+ ORBITRAP) calcd for $C_{28}H_{21}NO_3$ 420.1594 found 420.1593.

N-Benzoyl-DL-1-pyrenylalanine ethyl ester 75[110]

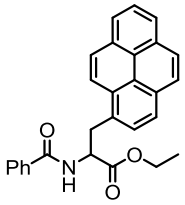

Ethyl 3-(l-pyrenyl)-2-benzamidopropenoate **74** (4.75 g, 11.3 mmol) was dissolved with sonication in a 1:1 mixture of EtOH and EtOAc (500 mL). To this was added Pd/C (10% wt). The mixture was placed under an atmosphere of hydrogen. When TLC analysis indicated the reaction was complete the reaction was filtered through a Celite® plug. The filtrate was evaporated to give a crude product. This was further recrystalised (DCM:Pet40-60), collected and dried under vacuum to give the title compound **67** (3.71 g, 78%) as a white solid **mp** 167-171 °C (lit[110] 168-170 °C); **IR** (ATR, cm^{-1}) 3320, 2978, 1749, 1654; **^{1}H NMR** (400 MHz, $CDCl_3$) δ_H 8.42 (d, *J* = 9.3, 1H, PyrH), 8.19 (t, *J* = 7.3, 2H, PyrH), 8.12 (d, *J* = 7.8, 1H, PyrH), 8.11 (d, *J* = 9.6, 1H, PyrH), 8.06 (d, *J* = 3.3, 2H, PyrH), 8.05 - 7.99 (m, 1H, PyrH), 7.84 (d, *J* = 7.8, 1H, PyrH), 7.69 (d, *J* = 7.1, 1H, *o*-Bz), 7.48 (t, *J* = 7.1, 1H, *p*-Bz), 7.38 (t, *J* = 7.3, 2H, *m*-Bz), 6.72 (d, *J* = 7.3, 1H, NH), 5.34 (td, *J* = 7.1, 5.7, 1H, $^{\alpha}$CH), 4.19 - 4.04 (m, 2H, OCH_2CH_3), 4.05 (dd, A of AB, *J*=14.0, 5.7, 1 H, $^{\beta}CH_AH_B$), 3.97 (dd, B of AB *J* = 14.0, 7.1, 1H, $^{\beta}CH_AH_B$), 1.11 (t, *J* = 7.2, 3H, CH_3); **^{13}C NMR** (100 MHz, $CDCl_3$) δ_C 171.8 (C(O)OEt), 167.0 (NHC(O)Ph), 133.8 (*i*-Bz), 131.7 (*p*-Bz), 131.3, 130.8, 130.1, 129.8 (4×PyrC), 128.5 (*m*-Bz), 128.2, 127.9, 127.4, 127.3, (4×PyrC) 127.0 (*o*-Bz), 126.0, 125.2, 125.0, 124.8, 124.7, 123.2, (6×PyrC) 61.7 (OCH_2), 54.2 ($^{\alpha}$CH), 35.6 ($^{\beta}CH_2$), 13.9 (CH_3), 2×PyrC could not be located); **MS** (ES^-) 420 (100%, $[M-H]^-$).

1-Bromomethylpyrene 77[168]

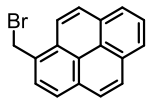

A solution of 1-pyrenemethanol (5.07 g, 21.5 mmol) and pyridine (0.86 mL, 10.7 mmol) in dry DCM was cooled to 0°C. A cloudiness of the first solution was observed with cooling. A separate solution of phosphorous tribromide (1 mL, 10.7 mmol) in anhydrous DCM (16 mL) was added, dropwise at 0°C, to the first solution. The reaction mixture was left at 0°C for 3 h then allowed to warm to room temperature over 16 h. TLC analysis (1:1 EtOAc/40-60 petrol ether, R_f prod = 0.9) indicated reaction completion. DCM (80 mL) and H_2O (60 mL) were added to the reaction mixture and the organic layer was separated and washed sequentially with H_2O (80 mL) sat. $NaHCO_3$ (80 mL) and brine (80 mL). The organic layer was then dried ($MgSO_4$) and removed under reduced pressure to give the title compound (5.3 g, 83%). as a yellow solid. **^{1}H NMR** (300 MHz, $CDCl_3$) δ_H 8.37 (d, J = 8.9, 1H, PyrH), 8.27-8.19 (m, J = 14.5, 5.3, 3H, PyrH), 8.12-7.98 (m, 5H, PyrH), 5.25 (s, 2H, CH_2Br). All other spectroscopic data consistent with that previously reported in the literature.[168] [300] 2012-05-05-jpc-36

Diethyl (1-pyrenylmethyl)acetimidomalonate 79[166]

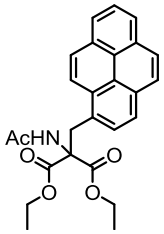

A 40 mL solution of sodium ethoxide (1% w/v sodium metal) was prepared under a nitrogen atmosphere. Diethyl acetimidomalonate **78** (3.49 g, 16.0 mmol) was dissolved in the prepared ethoxide solution. A separate solution of 1-bromomethylpyrene **77** (4.75 g, 16.1 mmol) in dry DCM (50 mL) was prepared and added dropwise with stirring to the first solution. The reaction was left to stir until its completion (4 h). The solvent was concentrated under reduced pressure leaving a residue. This was re-dissolved in a mixture of $KHSO_4$ (40 mL; 5% aq.) and EtOAc (100 mL). The organic layer was removed and the aqueous layer extracted with further EtOAc (2 x 50 mL). The organic layers were combined, washed with brine (50 mL), dried ($MgSO_4$) and removed under reduced pressure to give the 7.34 g of a crude mixture. This was purified by silica gel column chromatography (1% MeOH/DCM) to give the title compound **71** (5.3 g, 77%) as a white solid. **mp** 173-

175 °C; **IR** (ATR, cm^{-1}) 3347, 3038, 2982, 1736, 1661, 1518, 1280, 1248, 1211, 191, 1157, 1101, 1054, 1016; **^{1}H NMR** (400 MHz, $CDCl_3$) δ_H 8.23 (d, *J* = 9.3, 1H, PyrH), 8.13 (d, *J* = 7.7, 4.2, 2H, PyrH), 7.98 - 8.10 (m, 5H, PyrH), 7.69 (d, *J* = 8.1, 1H, PyrH), 6.39 (s, 1H, NH), 4.42 (s, 2H, CH_2-Pyr), 4.38 - 4.23 (m, 4H, C*H*$_2$CH$_3$), 1.94 (s, 3H, NC(O)CH_3), 1.36 (t, *J* = 7.2, 6H, 2×CH_3); **^{13}C NMR** (100 MHz, $CDCl_3$) δ_C 169.7 (CO), 167.6 (CO), 131.2, 130.6, 130.52, 130.46, 129.3 (5×ArC), 128.2, 127.3 (2C), 127.1, 125.9, 125.1, 124.83 (7×ArCH), 124.80, 124.6 (2×ArC), 124.5, 123.3 (2×ArCH), 67.6 ($^{\alpha}$C), 62.7, (4×CH_2), 34.6 (CH_2-Pyr), 23.0 (NC(O)*C*H$_3$), 14.0 (4×CH_3). **MS** (ES^+, DCM) 432 (100%, $[M+H]^+$); **HRMS** (ESI^+ ORBITRAP) calcd for $C_{26}H_{26}NO_5$ 432.1805 found 432.1802.

N-acetyl-D-pyrenylalanine 80

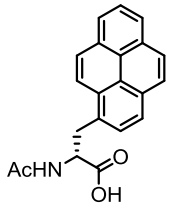

N-acetyl-D-pyrenylalanine was collected from the supernatant of the enzymatic reaction used to synthesise **41**. The supernatant was acidified to pH 3 with 1M HCl and extracted with DCM (3×30 mL). The organic layers were combined, dried ($MgSO_4$) and removed under reduced pressure to give a crude residue. This was purified by silica gel column chromatography (1% AcOH, 5% MeOH/DCM) to give the title compound **80** 1.82g (33%) as an off-white solid. **mp** 186-188 °C **$[\alpha]_D^{25}$** = +72.0 (C=0.3, MeOH) **IR** (ATR, cm^{-1}) 3299, 3039, 1742, 1637, 1537, 1434, 1371, 1203, 1181, **^{1}H NMR** (400 MHz, $(CD_3)_2SO$) δ_H 8.46 - 8.36 (m, 2 H, PyrH), 8.32 - 8.26 (m, 2H, PyrH), 8.25 - 8.18 (m, 1H, PyrH), 8.14 (s, 2H, PyrH), 8.07 (t, *J* = 7.6, 1H, PyrH), 7.98 (d, *J* = 7.8, 1H, PyrH), 4.68 (td, *J* = 8.8, 5.2, 1H, $^{\alpha}$CH), 3.87 (dd, A of AB, *J* = 13.9, 5.0, 1H, $^{\beta}$C*H*$_A$H$_B$), 3.54 (dd, B of AB, *J* = 13.9, 9.3, 1H, $^{\beta}$CH$_A$*H*$_B$), 1.74 (s, 3H, NC(O)CH_3) **^{13}C NMR** (100 MHz, $(CD_3)_2SO$) δ*C* 173.2 (*C*(O)OCH$_3$), 169.3 (N*C*(O)CH$_3$), 132.1, 130.8, 130.3, 129.8, 128.6, 128.4, 127.5, 127.4, 126.9, 126.2, 125.2, 125.0, 124.7, 124.2, 124.1, 123.1 (16×PyrC), 53.7 ($^{\alpha}$CH), 34.6 ($^{\beta}CH_2$), 22.3 (NC(O)*C*H$_3$) **MS** (ES^-, MeOH) 330, (100%, $[M-H]^-$).

D-pyrenylalanine hydrochloride 81

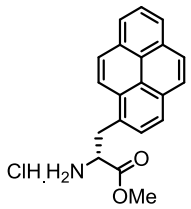

N-acetyl-D-pyrenylalanine **80** (150 mg, 0.45 mmol) was suspended in a mixture of 15 mL glacial acetic acid and 3.8 mL of conc. HCl. The suspension was heated to reflux overnight by which point the solid had fully dissolved. The solution was allowed to cool and the precipitate was collected by filtration and dried under vacuum to give the title compound **73** 146 mg (95%) as and off white solid. **mp** did not melt below 250 °C $\mathbf{[\alpha]_D^{25}}$ = 49.2 (c = 1.0, DMSO) **IR** (ATR, cm^{-1}) 2986, 2923, 1736, 1508, 1486, 1236, 1215; **^{1}H NMR** (400 MHz, $(CD_3)_2SO$) δ_H 8.71 (br. s., 2H, NH_2), 8.47 (d, *J* = 9.3, 1H, PyrH), 8.37 - 8.24 (m, 4H, PyrH), 8.22 - 8.15 (m, 2H, PyrH), 8.09 (t, *J* = 7.6, 1H, PyrH), 8.00 (d, *J* = 8.1, 1H, PyrH), 4.23 (t, X of ABX, *J* = 7.1, 1H, $^{\alpha}$CH), 3.97 (dd, A of ABX, *J* = 14.0, 6.6, 1H, $^{\beta}C\mathit{H}_A H_B$), 3.82 (dd, B of ABX, *J* = 14.0, 8.2, 1H, $^{\beta}CH_A\mathit{H}_B$) **^{13}C NMR** (100 MHz, $(CD_3)_2SO$) δ*C* 165.9 (CO), 126.2, 125.8, 125.7, 124.8, 124.3 (5×PyrC), 124.2, 123.3, 122.8, 122.7, 121.8, 120.8, 120.7, 120.4 (8×PyrCH), 119.6, 119.4 (2×PyrC), 118.5 (PyrCH), 48.9 ($^{\alpha}$CH), 29.1 ($^{\beta}CH_2$) **MS** (ES^-, DMSO) 330 (100%, $[M-H]^-$) **Elemental Analysis** Expected (%) = C, 70.69; H, 5.34; Cl, 10.43; N, 4.12; Found (%) = C, 68.68; H, 4.82; Cl, 10.68; N, 4.33.

N-Boc-L-pyrenylalanine 82

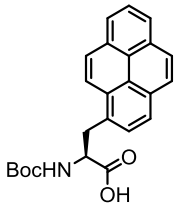

N-Boc L-pyrenylalanine was prepared according to the procedure outlined by Mihara *et al.*[112] L-pyrenylalanine **41** (329 mg, 1.10 mmol) was suspended in a mixture of 1,4-dioxane : H_2O (5 mL; 1:1). To this was added Et_3N (0.24 mL, 1.72 mmol, 1.5 eq) and Boc_2O (294 mg, 1.35 mmol, 1.2 eq). The suspension fully dissolved over the course of the reaction (14 h) to give a brown solution. The solution was acidified to pH 3 with the addition an aqueous citric acid solution (1.5 mL; 1M) causing the precipitation of a white solid. EtOAc was added to the suspension to dissolve the solid. The organic layer was separated and the aqueous layer was extracted with additional EtOAc (3 × 30 mL). The organic layers were combined, dried ($MgSO_4$) and evaporated to give a crude solid (452 mg). This was purified by silica gel column chromatography (AcOH:MeOH:DCM; 2:5:93) gave the title compound **74** 303 mg (70%) as a brown solid. **mp** (decomposes) 210 °C; $\mathbf{[\alpha]_D^{25}}$ **=** -82.6 (c = 0.3; MeOH) Lit[112]= -73.3 (c=0.3 MeOH) **IR** (ATR, cm^{-1}) 3036, 1656, 1587, 1404, 1350; **^{1}H NMR** (400 MHz, CD_3OD) δ_H 8.28 (d, *J* = 9.1, 1H , PyrH), 8.11 - 7.97 (m, 4H, PyrH), 7.94 - 7.90 (m, 2H, PyrH), 7.90 - 7.84 (m, 1H, PyrH), 7.80 (d, *J* = 7.8, 1H, PyrH), 7.16 - 6.96 (m, 1H, NH), 4.51 (dd, *J* = 9.5, 4.9, 1H, $^{\alpha}$CH), 3.87 (dd, A of AB, *J* = 14.1, 5.0, 1H, $^{\beta}C\mathit{H}_A H_B$), 3.46 (dd, B of AB, *J* = 14.1, 9.1, 1H, $^{\beta}CH_A\mathit{H}_B$), 1.15 (s, 9H, $OC(CH_3)_3$); **^{13}C NMR** (100 MHz, CD_3OD) δ_C 157.9 (CO), 133.0, 132.9, 132.4, 129.6, 128.8, 128.6, 128.1, 127.1, 126.3, 126.3, 126.2, 126.1, 125.8, 124.3 (14×PyrC) 80.6 ($OC(CH_3)_3$), 56.6 ($^{\alpha}CH_2$) 36.6 ($^{\beta}CH_2$), 28.7 ($OC(CH_3)_3$), 2×PyrC Could not be located; **MS** (ES^-, MeOH) 388 (100%, $[M-H]^-$); **HRMS** (ESI^- TOF) calcd for $C_{29}H_{22}NO_4$ 388.1554 found 388.1550. data are consistent with the literature.[166]

L-Pyrenylalanine methyl ester 83[110]

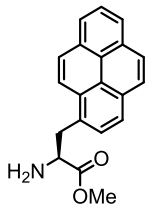

L-pyrenylalanine **41** (75 mg, 0.26 mmol) was suspended in dry MeOH (2 mL) and cooled to 0 °C. $SOCl_2$ (0.5 mL) was added with stirring. The solution was then heated to reflux. After 14 h the solution was cooled to RT and the solvent removed under reduced pressure. Residual $SOCl_2$ was removed by azeotroping with Et_2O to leave a crude residue. This was purified by silica gel column chromatography (5% MeOH/DCM with 0.1% NH_2 (aq.)) to give the title compound **75** (57.4 mg, 72%) as a yellow solid **mp** 76-78 °C (Lit[110] 79.5-80.5 °C) $\mathbf{[\alpha]_D^{25} =}$ -23.0 (c = 0.3, MeOH) **IR** (ATR, cm^{-1}) 3376, 3029, 2948, 1732, 1173; **^{1}H NMR** (500 MHz, CD_3OD) δ_H 8.18 - 8.12 (m, 1H, PyrH), 8.09 - 8.03 (m, 2H, PyrH), 8.01 - 7.95 (m, 2H, PyrH), 7.94 - 7.85 (m, 3H, PyrH), 7.76 - 7.68 (m, 1H, PyrH), 3.85 (t, *J* = 6.9, 1H, $^{\alpha}$CH), 3.61 (dq, *J* = 6.8, 6.8, 6.6, 1H, $^{\beta}$CH_AH$_B$), 3.50 (s, 3H, OCH_3), 3.46 (dd, *J* = 13.1, 7.4, 1H, $^{\beta}$CH$_A$$H_B$) **^{13}C NMR** (125 MHz, CD_3OD) δ_C 176.5 (CO), 132.8, 132.6, 132.2, 131.9, 130.4 (5×C, PyrC), 129.4, 128.8, 128.5, 128.1, 127.1, 126.3 (6×PyrCH), 126.2 (PyrC), 126.1 (PyrCH), 126.0 (PyrC), 125.8 124.0 (2×PyrCH), 57.1 ($^{\alpha}$C), 52.5 (OCH_3), 39.6 ($^{\beta}CH_2$) **MS** (ES^-, MeOH) 288 (100%, $[M-H]^-$).

D-pyrenylalanine methyl ester 84[110]

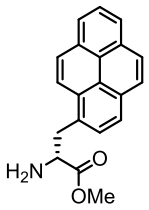

D-pyrenylalanine hydrochloride **81** (138 mg, 0.42 mmol) was suspended in dry MeOH (3 mL) and cooled to 0 °C. $SOCl_2$ (0.5 mL) was added with stirring. The solution was then heated to reflux. After 14 h the solution was cooled to RT and the solvent removed under reduced pressure. Residual $SOCl_2$ was removed by azeotroping with Et_2O to leave a crude residue. This was purified by silica gel column chromatography (5% MeOH/DCM with 0.1% NH_2 (aq.)) to give the title compound **76** 68.7 mg (53%) as a yellow solid **mp** 75-77 °C (Lit[110] 79.5-80.5 °C) **$[\alpha]_D^{25}$ =** 20.1 (c = 0.3, MeOH) **IR** (ATR, cm^{-1}) 3376, 3039, 2948, 1732, 1173; **^{1}H NMR** (400 MHz, CD_3OD) δ_H 8.25 (d, *J* = 9.3, 1H, PyrH), 8.17 – 8.11 (m, 2H, PyrH), 8.08 (d, *J* = 7.4, 1H, PyrH), 8.06 (d, *J* = 5.9, 1H, PyrH), 7.99 (s, 2H, PyrH), 7.95 (d, *J* = 7.7, 1H, PyrH), 7.80 (d, *J* = 7.8, 1H, PyrH), 3.90 (t, X of ABX, *J* = 7.0, 1H, $^{\alpha}$CH), 3.69 (dd, A of ABX, *J* = 14.0, 7.0, 1H, $^{\beta}CH_AH_B$) 3.54 (*J* = 14.0, 7.0, 1H, $^{\beta}CH_AH_B$), 3.53 (s, 3H, OCH_3). **^{13}C NMR** (100 MHz, CD_3OD) δ_C 176.4 (CO), 132.7, 132.5, 132.1, 131.9, 130.3 (5×PyrC), 129.3, 128.7, 128.4, 128.1, 127.1, 126.2 (6×PyrCH) 126.1 (PyrC), 126.0 (PyrCH), 125.9 (PyrC), 125.8, 124.0 (2×PyrCH), 57.0 ($^{\alpha}$CH) 52.4 (OCH_3), 39.5 ($^{\beta}CH_2$). **MS** (ES^-, MeOH) 288 (100%, $[M-H]^-$).

Boc-L-Pya-NH-CH_2-Pyr 86

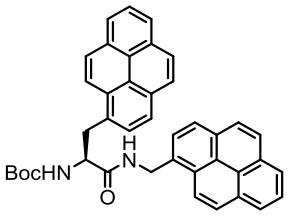

Boc-L-Pya **82** (50 mg, 0.39 mmol, 1 eq.) was dissolved in 1 mL dry DCM. 22.9 mg (1.3 eq) HOBt was added and the suspension was cooled to 0 °C. 33.5 µL (1 eq) of EDC was added to the suspension which was left to stir for 30 mins at 0 °C until the solid dissolved into solution. At this point 1-pyrenemethylamine hydrochloride **77** (51.1 mg, 1.5 eq) was added followed by 102 µL DIPEA (2.5 eq). The reaction was left to stir for 12 h. The reaction solvent was removed under reduced pressure to give a residue. This was washed sequentially with $KHSO_4$ (3×20 mL) $NaHCO_3$ (3×20 mL) and brine (20 mL). The organic layer was then dried ($MgSO_4$) and removed under reduced pressure do give a crude residue. This was triturated with MeCN and dried under reduced pressure to give the desired product (72.9 mg, 97%) **mp** 210-212 °C; $\mathbf{[\alpha]_D^{25}}$ = +13.2 (C=1 in DMSO); **IR** (ATR, cm^{-1}) 3275, 3039, 2967, 2929, 1683, 1644, 1522, 1290, 1167, 841; **^{1}H NMR** (500 MHz, $(CD_3)_2SO$) δ_H 8.73 (t, *J* = 5.5, 1H, N*H*CH_2Pyr), 8.47 (d, *J* = 9.1, 1H, PyrH), 8.02 - 8.32 (m, 15H, PyrH), 7.97 (d, *J* = 7.9, 1H,), 7.84 (d, *J* = 7.9, 1H), 7.23 (d, *J* = 8.5, 1H, NH-Boc), 5.02 (d, *J* = 5.7, 2H, NHC*H_2*Pyr), 4.55 (td, X of ABX *J* = 9.0, 6.3, 1H, $^{\alpha}$CH-Pya), 3.81 (dd, A of ABX, *J* = 13.6, 5.7, 1H, $^{\beta}$C*H_A*H_B-Pya), 3.55 (dd, B of ABX, *J* = 14.0, 9.0, 1H, $^{\beta}$CH_A*H_B*-Pya), 1.21 (s, 7H, Boc), 0.82 (br. s., 2H, Boc); **^{13}C NMR** (100 MHz, $(CD_3)_2SO$) δ_C 171.9 (CO), 155.7 (CO), 132.9, 132.7, 131.27, 131.23, 130.8, 130.7, 130.5, 130.1, 129.2 (9×PyrC), 129.1 (PyrCH), 128.4 (PyrC), 127.91, 127.86, 127.82, 127.77, 127.4, 127.2, 126.8, 126.7, 126.6, 125.7, 125.6, 125.5, 125.3, 125.07, 124.99 (15×PyrCH), 124.6, 124.5, 124.4, 124.3 (4×PyrC), 124.0, 123.6 (2×PyrCH), 78.6 (*C*$(CH_3)_3$), 56.7 ($^{\alpha}$CH), 41.0 (NHC*H_2*-Pyr) 35.8 ($^{\beta}$$CH_2$-Pya), 28.5 (3C, C(*C*$H_3)_3$); **MS** ($ES^+$) 625 (5%; $[M+Na]^+$) **HRMS** (ES^+ TOF) Calcd for $C_{41}H_{34}N_2O_3+H^+$ = 603.2642, found 603.2628.

N_3-Aib-OH 89[169]

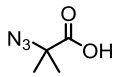

Sodium azide (6.65 g, 100.8 mmol) was dissolved in anhydrous DMF. To this stirred solution 2-bromo-2-methylpropionic acid **79** (15 g, 89.9 mmol) was added and the solution was left to stir at RT for 72 h. The mixture was diluted with 30 mL of water, acidified to pH 1 with HCl (50 mL; 1M aq.) and subsequently extracted with *tert*-butyl methyl ether (3×50 mL). The organic layers were combined, washed with HCl (1M, 4×20 mL) and dried ($MgSO_4$). Removal of the solvent under reduced pressure gave the compound as a yellow oil (8.55 g, 74%) **^{1}H NMR** (400 MHz, $CDCl_3$) δ_H = 1.54 (s, 6H) **^{13}C NMR** (100 MHz, $CDCl_3$) δ_C 178.9 (CO) 62.8 ($^{\alpha}$C), 24.3 Data agrees with that reported in the literature.[169]

N_3-Aib-O*t*Bu 90[170]

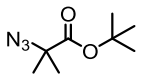

Sodium azide (6.65 g, 100.8 mmol) was dissolved in anhydrous DMF. To this stirred solution *tert*-butyl 2-bromo-2-methylpropionate **88** (15 g, 67.2 mmol) was added and the solution was left to stir at RT for 72 h. The mixture was diluted with water (30 mL), acidified to pH 1 with addition of HCl (50 mL; 1M aq.) and subsequently extracted with *tert*-butyl methyl ether (3 × 50 mL). The organic layers were combined, washed with additional HCl (4 × 20 mL) and dried ($MgSO_4$). Removal of the solvent under reduced pressure gave the compound as a yellow oil (8.98 g, 73%) **^{1}H NMR** (400 MHz, $CDCl_3$) δ_H 1.38 (9H, 3×CH_3) 1.30 (6H, 2×CH_3). **^{13}C NMR** (100 MHz, $CDCl_3$) δ_C 171.8 (CO), 82.5 ($^{\alpha}$C), 63.4 ($^{\alpha}$C) 27.9 (CH_3) 24.4 (CH_3). Data agrees with that reported in the literature.[170]

H-Aib-O*t*Bu 91[167]

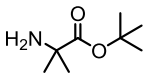

AzibOtBu **90** (8.98 g, 48.4) mmol was dissolved in MeOH 40 mL under an atmosphere of nitrogen. 898 mg of Pd/C (10% wt) was added carefully and the reaction was stirred under an atmosphere of hydrogen for 3 days until the reaction was complete (TLC monitoring). Filtration through a pad of Celite® and removal of the solvent under reduced pressure gave the compound as a clear oil (5.17 g, 68%) **^{1}H NMR** (400 MHz, CDCl3) δ_H 1.47 (s, 1H), 1.32 (s, 1H). Data agrees with that reported in the literature.[167]

AzibCl 92[51]

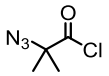

N_3-Aib-OH **89** (10.24 g, 79.3 mmol) was dissolved in dry DCM (15 mL). Thionyl chloride (11.6 mL, 2 eq, 162 mmol) was added drop-wise and the resulting solution stirred for 3 h. The mixture was concentrated and subsequently distilled under reduced pressure to give the desired compound as clear oil (9.04 g, 77%). This was used immediately.

N_3-Aib_2-O*t*Bu 93[167]

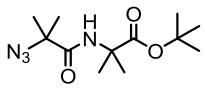

H-AibO*t*Bu **91** (9.58 g, 60.2 mmol 1 eq) was dissolved in dry DCM (120 mL) and cooled to 0°C. To this was added Et_3N (12.8 mL, 90.25 mmol, 1.5 eq,) followed by drop-wise addition of a solution of freshly distilled AzibCl (8.36g, 56.7 mmol, 0.94 eq) in dry DCM (19 mL). The reaction was left to warm to RT overnight with stirring (24 h). The reaction mixture was concentrated to dryness under reduced pressure, re-dissolved in EtOAc (60 mL) and subsequently washed with $KHSO_4$ (2 × 20 mL; 5% aq.) and $NaHCO_3$ (2 × 20 mL: Sat. aq.). The organic layer was dried ($MgSO_4$) and removed under reduced pressure to give the title compound (10.5 g, 68%) as a pale yellow oil. **^{1}H NMR** (400 MHz, $CDCl_3$) δ_H 7.10 (br. s., 1H, NH), 1.52 (s, 6H, 2×CH_3), 1.51 (s, 6H, 2×CH_3), 1.45 (s, 9H, 3×CH_3, O*t*Bu) **^{13}C NMR** (100 MHz, $CDCl_3$) δ_C 173.4 (CO), 171.1 (CO), 81.6 (*C*(CH_3)$_3$), 64.2 ($^{\alpha}$C), 56.7 (N_3C), 27.8 (CH_3), 24.3 (CH_3). Data agrees with that reported in the literature.[167]

N-Aib$_2$-O*t*Bu 94[167]

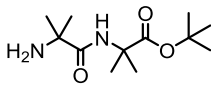

N_3Aib$_2$O*t*Bu **93** (10.5 g, 38.9 mmol) was dissolved in 70 mL MeOH and placed under a nitrogen atmosphere. Pd/C (1.05 g, 10% w/w.) was added to the solution with stirring as a slurry in DCM (2 mL). The reaction mixture was then placed under and atmosphere of H_2 and left stirring at RT for 48 h, monitoring the course of the reaction with TLC. The mixture was then filtered through celite, with subsequent removal of the solvent under reduced pressure giving 9.4g (77%) of the title compound as a colourless oil.**^{1}H NMR** (CD_3OD,400 MHz) δ_H 1.44 (s, 9H, CO_2*t*Bu), 1.43 (s, 6H, 2×CH_3), 1.30 (s, 6H, 2×CH_3) **^{13}C NMR** (100 MHz, D_3OD) δ_C = 179.1 (CO), 175.1 (CO), 82.0 (*C*(CH_3)$_3$), 57.2 ($N_3{}^{\alpha}$C), 55.4 ($^{\alpha}$C) , 28.3, 28.1, 25.0. Data agrees with that reported in the literature.[167]

N$_3$-Aib$_3$-O*t*Bu 95[167]

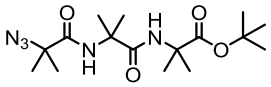

H_2N-Aib$_2$O*t*Bu **94** (8.5 g, 34.8 mmol 1 eq) was dissolved in dry DCM (120 mL) and cooled to 0°C. To this was added Et_3N (12.8 mL, 52.3 mmol, 1.5 eq,) followed by drop-wise addition of a solution of freshly distilled AzibCl (5.7 g, 39.0 mmol, 1.12 eq) in dry DCM (10 mL). The reaction was left to warm to RT overnight with stirring (24 h). The reaction mixture was concentrated to dryness under reduced pressure, re-dissolved in EtOAc (60 mL) and subsequently washed with $KHSO_4$ (2 × 20 mL; 5% aq.) and $NaHCO_3$ (2 × 20 mL: Sat. aq.). The organic layer was dried ($MgSO_4$) and removed under reduced pressure to give a crude residue, This was purified by column chromatography (1-5% MeOH/DCM) to give the title compound (8.9 g, 72%) as white solid **^{1}H NMR** ($CDCl_3$,400 MHz) δ_H = 7.22 (s, 1H, NH), 6.99 (s, 1H , NH), 1.56 (s, 6H, 2×CH_3), 1.54 (s, 6H, 2×CH_3), 1.52 (s, 6H, 2×CH_3), 1.46 (s, 9H, OC(CH_3)$_3$) **^{13}C NMR** ($CDCl_3$,100 MHz) δ_C 174.1 (CO), 173.0 (CO), 171.8 (CO), 81.8 (*C*(CH_3)$_3$), 64.3 ($^{\alpha}$C), 57.1 ($N_3{}^{\alpha}$C), 56.9 ($^{\alpha}$C), 27.8, 24.8, 24.4, 24.0 Data agrees with that reported in the literature.[167]

H-Aib$_3$-O*t*Bu 96[167]

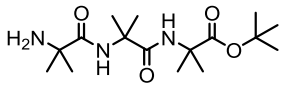

N_3Aib$_3$O*t*Bu **95** (2.05 g, 5.8 mmol) was dissolved in 30 mL EtOH and placed under a nitrogen atmosphere. 156 mg Pd/C (10% wt.) was added to the solution with stirring as a slurry in EtOH (3 mL). The reaction mixture was then placed under an atmosphere of H_2 and left stirring at RT for 12 h. The mixture was then filtered through a pad of Celite®, with subsequent removal of the solvent under reduced pressure giving 1.86g (98%) of the title compound as a white solid. **^{1}H NMR** ($CDCl_3$,400 MHz) δ_H , 2×AibCH$_3$= 8.09 (s, 1H, NH), 7.39 (s, 1H, NH), 1.47 (s, 6H, 2×CH$_3$), 1.44 (s, 6H, 2×CH$_3$), 1.38 (s, 9H, O*t*Bu), 1.30 (s, 6H, 2×CH$_3$) **^{13}C NMR** (100 MHz, $CDCl_3$) δ_C 177.4 (CO), 174.0 (CO), 173.4 (CO), 81.2, 56.9, 56.6, 55.0, 28.7, 27.8, 25.1, 24.2; Data agrees with that reported in the literature.[167]

N$_3$-Aib$_4$-O*t*Bu 97[167]

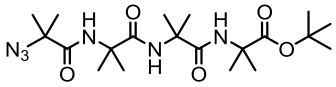

NH_2Aib$_3$O*t*Bu **96** (1.59 g, 4.8 mmol) was dissolved in 10 mL of anhydrous DCM and cooled to 0 °C. To this was added a solution of freshly prepared AzibCl (1.06 g 1.5 eq) in anhydrous DCM (4 mL). The reaction was allowed to warm to RT and left to stir for 12 h. The reaction mixture was concentrated to dryness under reduced pressure and dissolved in EtOAc (60 mL) and subsequently washed with $KHSO_4$ (2 × 20 mL; 5% aq.) and $NaHCO_3$ (2 × 20 mL). The organic layer was dried ($MgSO_4$) and removed under reduced pressure to give the crude compound as a brown syrup. This was purified by column chromatography (1-5% MeOH/DCM) and subsequent trituration (Et_2O) to give the title compound as a white solid. (1.71 g, 80%) **^{1}H NMR** (500 MHz, $CDCl_3$) δ_H 7.00 (s, 1H, NH), 6.96 (s, 1H, NH), 6.50 (s, 1H, NH), 1.52 (s, 6H, 2×CH$_3$), 1.51 (s, 6H, 2×CH$_3$), 1.50 (s, 6H, 2×CH$_3$), 1.47 (s, 6H, 2×CH$_3$), 1.43 (s, 9H, 3×CH$_3$, O*t*Bu). **^{13}C NMR** (125 MHz, $CDCl_3$) δ_C 173.9 (CO), 173.1 (CO), 172.5 (CO), 172.4 (CO), 81.0 ($^{\alpha}$C), 64.3 ($^{\alpha}$C), 57.2 ($^{\alpha}$C), 57.0 ($^{\alpha}$C), 56.7 ($^{\alpha}$C), 27.7 (CH$_3$), 25.3 (CH$_3$) 25.1 (CH$_3$), 24.5 (CH$_3$), 24.4 (CH$_3$). Data agrees with that reported in the literature.[167]

H-Aib$_4$-O*t*Bu 98

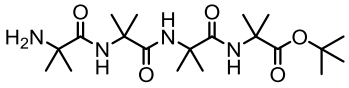

N_3Aib_4OtBu **97** 1.46g (3.31 mmol) was dissolved in 23 mL of EtOH and placed under an atmosphere of nitrogen. 110 mg Pd/C (10% wt) was added with stirring under N_2. The atmosphere was replaced with hydrogen and left to stir for 3 days. The solution was filtered through a plug of Celite® and removed under reduced pressure to give 1.37g (3.31 mmol, >99%) of the product as a white solid. **^{1}H NMR** ($CDCl_3$, 500MHz) δ_H 8.14 (s, 1H, NH), 7.26 (s, 1H, NH), 6.67 (s, 1H, NH), 1.50 (s, 6H, 2×CH_3), 1.48 (6, 6H, 2×CH_3), 1.47 (s, 6H, 2×CH_3), 1.43 (s, 9H, 3×CH_3), 1.40 (s, 6H, 2×CH_3) **^{13}C NMR** (125 MHz, $CDCl_3$) δ_C 177.14 (CO) 174.0 (CO), 173.1 (CO), 172.9 (CO), 80.6 ($^{\alpha}$C), 56.7 (2C, 2×$^{\alpha}$C), 56.4 ($^{\alpha}$C), 55.2 ($^{\alpha}$C), 28.3 (CH_3), 27.8 (CH_3), 25.4 (CH_3), 25.1 (CH_3), 24.5 (CH_3). Data agrees with literature.[167]

Cbz-L-Phe-Aib$_4$-O*t*Bu 101[167]

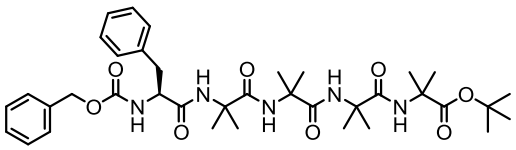

Cbz-L-Phe-OH (75 mg, 0.25 mmol, 1 eq.) was dissolved in 4 mL dry DCM. HOBt 22.9 mg (1.3 eq) was added and the suspension was cooled to 0 °C. 33.5 µL (1 eq) of EDC was added to the suspension which was left to stir for 30 mins at 0 °C until the solid dissolved into solution. At this point H-Aib$_4$-O*t*Bu **98** (125 mg, 1.2 eq) was added followed by 54 µL DIPEA (1.2 eq). The reaction was left to stir for 24 h. The reaction solvent was removed under reduced pressure to give a crude residue, This was re-dissolved in EtOAc (50 mL) and washed sequentially with $KHSO_4$ (3 × 20 mL) $NaHCO_3$ (3 × 20 mL) and sat. brine (20 mL). The organic layer was then dried ($MgSO_4$) and removed under reduced pressure to give a crude residue. This was purified by silica gel chromatography (5% MeOH/DCM) to give the title compound **101** (90 mg, 87%) as a white solid. **^{1}H NMR** (400 MHz, $CDCl_3$) δ_H 7.39- 7.17 (m, 14H, 10×ArH + 4×NH), 7.09 (s, 1H, NH), 6.61 (s, 1H, NH), 6.11 (d, *J* = 5.0, 1H, NH-Phe), 5.08 (s, 2H, CH_2-Ph), 4.08 (dt, *J* = 8.5, 5.5, 1H, X of ABX, $^{\alpha}$CH-Phe), 3.19 (dd, *J* = 14.0, 5.5, 1H, A of ABX, PhCH_AH$_B$CH$_X$), 3.02 (dd, *J* = 14.0, 8.5, 1H, B of ABX, PhCH$_A$$H_BCH_X$), 1.47 (s, 3H, CH_3), 1.47 (s, 3H, CH_3), 1.46 (s, 3H, CH_3), 1.45 (s, 3H, CH_3), 1.41 (s, 9H, CO_2*t*Bu), 1.39 (s, CH_3), 1.37 (s, 3H, CH_3), 1.35 (s, 3H, CH_3), 1.32 (s, 3H, CH_3) **^{13}C NMR** (100 MHz, $CDCl_3$) δ_C 174.1, 174.0, 173.8, 173.5, 171.4, 156.7 (6×CO), 136.4, 136.0 (2×ArC), 129.2, 128.7, 128.5 (2C), 128.3, 127.9 (2C), 127.0 (ArCH), 79.8 (C), 67.1 (CH_2-Cbz), 60.2 ($^{\alpha}$CH) 57.4 (C), 56.8 (C) 56.7 (C) 56.5 (C) 55.9 (C) 36.1 (CH_2-Phe), 27.8 (3×CH_3, *t*Bu), 26.0 (CH_3), 25.6 (CH_3), 25.4 (CH_3), 24.9 (CH_3), 24.8 (CH_3), 24.5 (CH_3), 24.4 (CH_3), 24.1 (CH_3). Data agrees with the literature.[167]

Cbz-D-Phe-Aib$_4$-O*t*Bu 102[167]

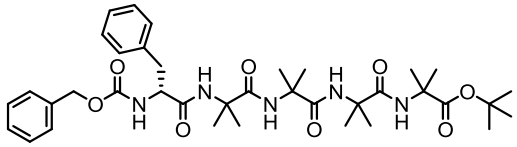

Cbz-D-Phe-OH (75 mg, 0.25 mmol, 1 eq.) was dissolved in 4 mL dry DCM. 22.9 mg (1.3 eq) HOBt was added and the suspension was cooled to 0 °C. 33.5 µL (1 eq) of EDC was added to the suspension which was left to stir for 30 mins at 0 °C until the solid dissolved into solution. At this point H-Aib$_4$-O*t*Bu **98** (125 mg, 1.2 eq) was added followed by 54 µL DIPEA (1.2 eq). On conformation of a basic reaction pH the reaction was left to stir for 24 h. The reaction solvent was removed under reduced pressure to give a crude residue. This was re-dissolved in EtOAc and washed sequentially with $KHSO_4$ (3 × 20 mL) $NaHCO_3$ (3 × 20 mL) and brine (20 mL). The organic layer was then dried ($MgSO_4$) and removed under reduced pressure to give a crude residue. This was purified by column chromatography (5% MeOH / DCM) to give the title compound **102** as a white solid (93 mg, 89%) **^{1}H NMR** (400 MHz, $CDCl_3$) δ_H 7.39-7.16 (m, 14H, 10×ArH + 4×NH), 7.07 (s, 1H, NH), 6.54 (s, 1H, NH), 6.03 (d, J = 5.0, 1H, NH-Phe), 5.09 (s, 2H, CH_2-Ph), 4.08 (dt, J = 8.5, 5.5, 1H, X of ABX, $^{\alpha}$CH-Phe), 3.18 (dd, J = 14.0, 5.5, 1H, A of ABX, PhCH_AH$_B$CH$_X$), 3.02 (dd, J = 14.0, 8.5, 1H, B of ABX, PhCH$_A$$H_BCH_X$), 1.48 (s, 3H, CH_3), 1.47 (s, 3 H, CH_3), 1.46 (s, 3H, CH_3), 1.45 (s, 3H, CH_3), 1.42 (s, 9H, OCH)$_3$)$_3$) 1.40 (s, 3H, CH_3), 1.38 (s, 3H, CH_3), 1.35 (s, 3H, CH_3), 1.32 (s, 3H, CH_3) **^{13}C NMR** (100 MHz, $CDCl_3$) δ_C 174.1, 174.0, 173.7, 173.4, 171.4, 156.7 (6×CO), 136.4, 136.0 (2×ArC), 129.2, 128.8, 128.6 (2C), 128.4, 128.0 (2C), 127.1, 79.8 (C), 67.2 (CH_2-Cbz), 57.4 ($^{\alpha}$CH), 56.8 (C), 56.7 (C), 56.5 (C), 56.0 (C), 36.2 (CH_2-Phe), 27.8 (CH_3), 25.9 (CH_3), 25.5 (CH_3), 25.4 (CH_3), 24.9 (CH_3), 24.8 (CH_3), 24.5 (CH_3), 24.2 (CH_3). Data agrees with literature.[167]

Cbz-L-Phe-Aib$_4$-L-Pya-L-PyaOMe 103

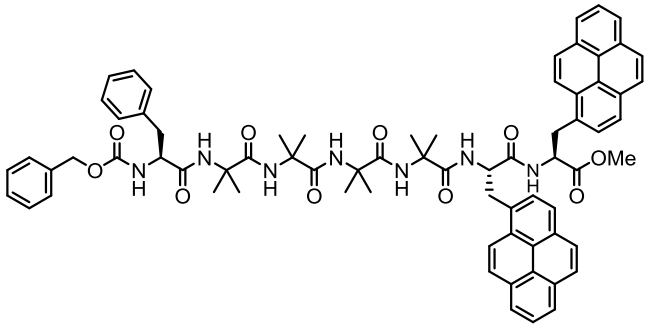

Cbz-L-PheAib$_4$OH **63** (25.0 mg, 0.039 mmol 1 eq.) was coupled to Boc-L-Pya-L-Pya **67** (1.2 eq.) using General procedure 1: Deprotected **67** was added to the activated acid in 0.5 mL of anhydrous DCM. The resulting residue was purified using column chromatography (1-5% IPA/DCM) to give the title compound (34.5 mg, 75%) as a white solid **mp** 122-126 °C; $[\alpha]_D$ = -17.1 (c = 1.0, $CHCl_3$), **IR** (ATR, cm^{-1}) 3296, 2921, 2852, 1655, 1530, 1455, 1260, 1022; **^{1}H NMR** (500 MHz, $CDCl_3$) δ_H 8.51 (d, *J* = 9.1, 1H , PyrH), 8.47 - 8.40 (m, 2H, PyrH + NH), 8.26 - 7.93 (m, 16H, PyrH), 7.63 (br. s., 2H, 2×NH), 7.34 - 7.23 (m, 8H, ArH), 7.19 - 7.14 (m, 2H, ArH), 7.08 (s, 1H, NH), 6.62 (s, 1H, NH), 5.64 (d, *J* = 2.8, 1H, NH), 5.15 (apparent t, *J* = 7.5, 1H, $^{\alpha}$CH), 5.08 (d, *J* = 12.3, 1H, PhCH_AH_BO), 4.99 - 4.91 (m, 2H $^{\alpha}$CH' + PhCH_AH_BO), 4.36 (dd, *J* = 15.1, 2.8, 1H, Ar-$^{\beta}$C'H_AH_B), 4.18 - 4.08 (m, 2H, Ar-$^{\beta}$CH_AH_B+ $^{\alpha}$CH"), 3.99 (dd, *J* = 13.9, 6.9, 1H, Ar-$^{\beta}$CH_AH_B), 3.69 (t, *J* = 12.6, 1H, Ar-$^{\beta}$C'H_AH_B), 3.45 (s, 3H, OCH_3), 3.11 (dd, *J* = 14.3, 5.2, 1H, Ar-$^{\beta}$C"H_AH_B), 2.89 (dd, *J* = 14.3, 8.7, 1H, Ar-$^{\beta}$C"H_AH_B), 1.65 (s, 3H, CH_3), 1.57 (s, 3H, CH_3), 1.53 (s, 3H, CH_3), 1.34 (s, 6H, 2×CH_3), 1.30 (s, 3H, CH_3), 1.23 (s, 3H, CH_3), 1.05 (s, 3H, CH_3) **^{13}C NMR** (125 MHz, $CDCl_3$) δ_C 175.8, 175.4, 175.3, 173.8, 172.5, 172.2, 171.7 (7×CO), 157.1 (CO, Cbz), 136.0, 135.6, 133.1, 131.7, 131.5, 131.0, 130.6, 130.1, 129.4 (9×ArC), 129.2 (2C), 129.1 (2C), 128.71 (2C) (6×ArCH), 128.65, 128.60 (2×ArC), 128.2 (2C), 127.9, 127.8, 127.9, 127.6, 127.5, 127.1, 126.7, 125.9, 125.8 (11×ArCH), 125.2 (ArC), 125.1 (2C), 125.01 (3×ArCH), 124.95 (ArC), 124.8, 124.3, 123.6, 123.5 (4×ArCH), 67.6 (CH_2-Cbz), 58.0 ($^{\alpha}$CH) 57.2, 57.0, 56.7, 56.6 (4×$^{\alpha}$C), 55.2 ($^{\alpha}$CH) 54.7 ($^{\alpha}$CH), 52.1 (OCH_3), 36.8 ($^{\beta}CH_2$), 35.9 ($^{\beta}CH_2$), 34.7 ($^{\beta}CH_2$), 26.94, 26.90, 26.8, 26.4, 26.3, 23.31, 23.27, 23.2 (8×CH_3) 3×ArC could not be located. **MS** ES^+ 1218 (15%, $[M+Na]^+$):

Cbz-D-Phe-Aib$_4$-L-Pya-L-PyaOMe 104

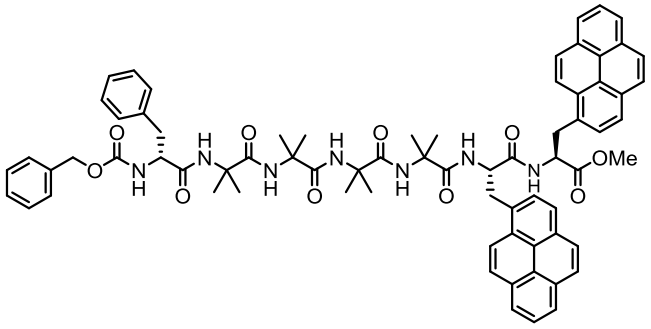

Cbz-D-PheAib$_4$OH **64** (25.0 mg, 0.039 mmol 1 eq.) was coupled to Boc-L-Pya-D-Pya **67** (1.2 eq.) using General procedure 1: Deprotected **67** was added to the activated acid in 0.5 mL of anhydrous DCM. The resulting residue was purified using column chromatography (1-5% IPA/DCM) to give the title compound (40.0 mg, 88%) as a white solid **mp** 148-153 °C **$[\alpha]_D$** = +53.2 C=1 in $CHCl_3$; **IR** (ATR, cm^{-1}) 3293, 2924, 2853, 1655, 1530; **^{1}H NMR** (400 MHz, $CDCl_3$) δ_H = 8.47 (d, *J* = 9.3, 1H, PyrH), 8.41 - 8.28 (m, 2H, PyrH + NH), 7.87 - 8.22 (m, 16H, PyrH), 7.87 - 7.78 (m, 2H, 2×NH), 7.59 (s, 1H, NH), 7.54 (s, 1H, NH), 7.31 - 7.22 (m, 8H, ArH), 7.13 - 7.00 (m, 3H, 2×ArH + NH), 6.53 (s, 1H, NH), 5.51 (d, *J* = 5.0, 1H, NH), 5.14 - 5.11 (m, *J* = 7.6, 1H $^{\alpha}$CH), 5.04 (d, *J* = 13.0, 1H, A of AB, PhCH_AH$_B$O), 4.96 (d, *J* = 13.0, 1H, B of AB, PhCH$_A$$H_B$O), 4.84 (t, *J* = 7.7, 1H, $^{\alpha}$C'H), 4.22 (dd, *J* = 14.5, 3.2, 1H, Ar-$^{\beta}$C'H_AH$_B$), 4.10 (dd, *J* = 13.9, 7.8, 1H, Ar-$^{\beta}$CH_AH$_B$) 3.98 - 3.91 (m, 1H, $^{\alpha}$C"H) 3.93 (dd, *J* = 13.9, 6.3, 1H, Ar-$^{\beta}$CH$_A$$H_B$), 3.62 (dd, *J* = 14.5, 11.1, 1H, Ar-$^{\beta}$C'H$_A$$H_B$)3.48 (s, 3H, OCH$_3$), 3.04 (dd, *J* = 14.0, 6.6, 1H, Ar-$^{\beta}$C"H_AH$_B$), 2.89 (dd, *J* = 14.0, 8.7, 1H, Ar-$^{\beta}$C"H$_A$$H_B$) 1.58 (s, 3H, CH$_3$), 1.53 (s, 3H, CH$_3$), 1.51 (s, 3H, CH$_3$), 1.29 (s, 3H, CH$_3$), 1.28 (s, 3H, CH$_3$), 1.15 (s, 3H, CH$_3$), 1.05 (s, 3H, CH$_3$) 0.95 (s, 3H, CH$_3$); **^{13}C NMR** (125 MHz, $CDCl_3$) δ_C 175.52, 175.16, 173.47, 172.40, 172.15, 171.29, 165.59 (7×CO), 156.69 (CO, Cbz), 135.8, 135.7, 134.3, 133.3, 131.9, 131.5, 131.4, 131.1, 130.6, 130.2(10×ArC), 129.9 (ArCH), 129.5 (ArC) 129.3, 129, 128.9, 128.8, 128.7, 128.2, 127.9, 127.71, 127.65, 127.5, 127.0, 126.6, 125.9, 125.7 (14×ArCH), 125.2, 125.03, 124.98 (3×ArC), 124.8, 124.7, 124.3 (3×ArCH), 123.9 (ArC), 123.7 (3×ArCH), 67.7 (CH$_2$-Cbz), 63.2 ($^{\alpha}$CH), 57.8, 57.2, 57.0, 56.9, 55.2 ($^{\alpha}$CH) 54.6 ($^{\alpha}$CH) 52.1 (OCH$_3$), 36.7 ($^{\beta}$CH$_2$), 36.0 ($^{\beta}$CH$_2$), 34.7, 32.1, 29.5, 26.9, 24.0, 23.9, 23.3, 22.9 (8×CH$_3$), 6×ArCH Could not be located; **MS** ES$^+$ 1218 (15%, [M+Na]$^+$).

Cbz-L-Phe-Aib$_4$-L-Pya-D-PyaOMe 105

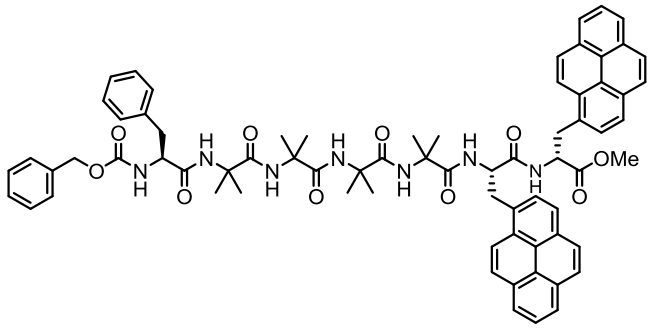

Cbz-L-PheAib$_4$OH **63** (25.0 mg, 0.039 mmol 1 eq.) was coupled to Boc-L-Pya-D-Pya **68** (1.2 eq.) using General procedure 1: Deprotected **68** was added to the activated acid in 1 mL of 1:1 anhydrous DCM/DMF. The resulting residue was purified using column chromatography (1-5% IPA/DCM) to give the title compound (18.7 mg, 41%) as a white solid **mp** 217-219 °C $[\alpha]_D$ = +12.8 (C=1: $CHCl_3$) **IR** 3275, 2919, 2850, 1645, 1534, 1455 **^{1}H NMR** (500 MHz, $CDCl_3$) δ_H 8.47-8.38 (m, 3H, 2 × PyrH + NH), 8.19 - 7.93 (m, 17H, 16 × PyrH + NH) 7.71 (br. s., 1H , NH), 7.47 (br. s., 1H , NH), 7.27 - 7.35 (m, 8H, ArH), 7.17-7.13 (m, 2H, ArH), 7.15 (br. s., 1H , NH), 7.03 (br. s., 1H , NH), 6.33 (br. s., 1H , NH), 5.31 (br. s., 1H, NH), 5.11 (d, J = 11.3, 1H, PhCH_AH$_B$O), 4.92 - 5.02 (m, 2H, PhCH$_A$$H_B$O + $^{\alpha}$CH), 4.89 (m, 1H, $^{\alpha}$C'H), 4.41 (d, J = 14.5, 1H, Ar-$^{\beta}$C'H_AH$_B$), 4.20 - 4.11 (m, 1H, $^{\alpha}$C"H), 4.12 (dd, J = 14.2, 6.6, 1H, Ar-$^{\beta}$CH$_A$H$_B$), 3.99 (dd, J = 14.2, 7.9, 1H, Ar-$^{\beta}$CH$_A$$H_B$), 3.69 (dd, J = 13.7, 12.5, 1H, Ar-$^{\beta}$C'H$_A$$H_B$), 3.58 (s, 3H, OCH_3), 3.12 (dd, J = 13.7, 3.0, 1H, Ar-$^{\beta}$C"H$_A$$H_B$), 2.89 (dd, J = 13.9, 8.2, 1H, Ar-$^{\beta}$C"H$_A$$H_B$), 1.55 (br. s., 3H, CH_3) 1.53 (s, 3H, CH_3), 1.49 (s, 3H, CH_3), 1.35 (br. s., 3H, CH_3), 1.26 (br. s., 3H, CH_3), 1.20 (br. s., 6H, 2×CH_3), 1.09 (s, 3H, CH_3) **^{13}C NMR** (100 MHz, $CDCl_3$) δ_C 176.0, 175.8, 175.0, 173.5, 173.0, 172.6, 171.5 (7×CO), 157.0 (CO, Cbz), 135.7, 135.1, 132.5, 131.3, 131.3, 131.2, 130.9, 130.8, 130.4, 130.1 (10×ArC), 129.0, 129.0, 128.7, 128.6 (4×ArCH), 128.6 (ArC), 128.1 (ArCH), 127.7, 127.6, 127.6, 127.5, 127.3, 126.8, 126.6, 125.7, 125.6 (9×PyrCH), 125.0 (ArC), 124.9, 124.9, 124.8, 124.7, 124.1 (5×ArCH), 123.4 (PyrCH), 123.1 (PyrCH) 67.7 ($PhCH_2O$), 57.7 ($^{\alpha}$C"), 57.0, 56.8, 56.7, 56.5 (4×C$^{\alpha}$, Aib), 55.2 ($^{\alpha}$C), 55.0 ($^{\alpha}$C'), 52.2 (OCH_3), 36.7 ($^{\beta}$C"), 34.6 ($^{\beta}$C'), 34.5 ($^{\beta}$C) 33.4, 31.9, 29.6, 29.6, 29.4, 29.4, 23.3, 22.7 (8×CH_3), 10ArC + 7ArCH could not be located; **MS** (ES$^+$, $CHCl_3$) 1219 (20%, $[M+Na]^+$).

Cbz-D-Phe-Aib$_4$-L-Pya-D-PyaOMe 106

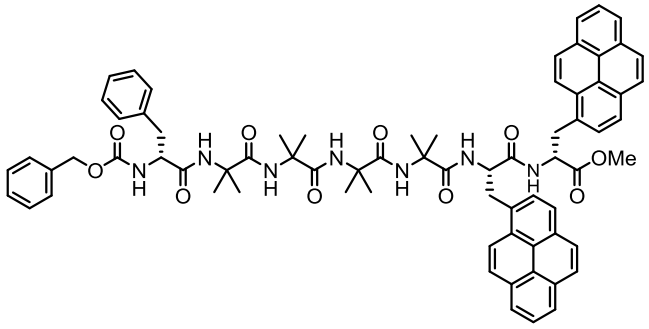

Cbz-D-PheAib$_4$OH **64** (25.0 mg, 0.039 mmol 1 eq.) was coupled to Boc-L-Pya-D-Pya **68** (1.2 eq.) using General procedure 1: Deprotected **68** was added to the activated acid in 1 mL of 1:1 anhydrous DCM/DMF. The resulting residue was purified using column chromatography (1-5% IPA/DCM) to give the title compound (25.5 mg, 56%) as a white solid **mp** 226-228 °C; $\mathbf{[\alpha]_D^{25}}$ = +28.0 (C=1; $CHCl_3$); **IR** 3293, 2923, 2852, 1652, 1532; **^{1}H NMR** (500 MHz, $CDCl_3$) δ_H 8.49 (d, *J* = 9.1, 1H, PyrH), 8.44 (d, *J* = 9.1, 1H, PyrH), 8.39 (d, *J* = 7.3, 1H, NH), 7.91 - 8.19 (m, 18H, 16×PyrH + 2×NH), 7.68 (s, 1H, NH), 7.52 (s, 1H, NH), 7.36 - 7.21 (m, 8H, ArH), 7.09 - 7.03 (m, *J* = 7.9, 2H, ArH), 6.28 (s, 1H, NH), 5.42 (d, *J* = 4.7, 1H, NH), 5.06 (d, *J* = 12.3, 1H, PhCH_AH_BO), 4.98 (dd, *J* = 15.0, 7.6, 1H, $^{\alpha}$CH), 4.97 (d, *J* = 12.3, 1H, PhCH$_A$$H_B$O) 4.87 (ddd, *J* = 11.0, 8.2, 2.5, 1H, $^{\alpha}$C'H), 4.44 (dd, *J* = 14.8, 1.9, 1H, Ar-$^{\beta}$C'H_AH_B), 4.14 (dd, *J* = 14.0, 7.4, 1H, Ar-$^{\beta}$CH_AH_B), 3.99 (dd, *J* = 14.0, 8.0, 1H, Ar-$^{\beta}$CH$_A$$H_B$), 3.89 (dd, *J* = 12.3, 7.3, 1H, $^{\alpha}$C"H), 3.66 (dd, *J* = 15.1, 11.7, 1H, Ar-$^{\beta}$C'H$_A$$H_B$), 3.56 (s, 3H, OCH_3), 3.03 (dd, *J* = 13.6, 6.9, 1H, Ar-$^{\beta}$C"H_AH_B), 2.90 (dd, *J* = 13.7, 8.4, 1H, Ar-$^{\beta}$C"H$_A$$H_B$), 1.60 (s, 3H, CH_3), 1.59 (s, 3H, CH_3), 1.53 (s, 3 H, CH_3), 1.31 (s, 3 H, CH_3), 1.25 (s, 6H, 2×CH_3), 1.24 (s, 3H, CH_3), 1.16 (s, 3H, CH_3) **^{13}C NMR** (125 MHz, $CDCl_3$) δ_C 175.8, 175.1, 174.9, 173.6, 172.8, 172.5, 171.2 (7×CO), 156.4 (CO, Cbz), 135.9, 135.7, 133.1, 131.7, 131.3, 131.2, 131.0, 130.9, 130.4, 130.0 (10×ArC), 129.1, 129.0, 128.9, 128.6, 128.5, 127.9 (6×ArCH), 127.7 (ArC), 127.6, 127.6, 127.5, 127.4, 127.3, 126.7, 126.5, 125.6, 125.6 (9×ArCH), 125.0 (ArC), 124.9 (ArC), 124.8, 124.8, 124.8, 124.6, 124.1, 123.6, 123.3 (7×ArCH), 67.4 ($PhCH_2O$), 57.5 (C□"), 57.0, 56.8, 56.7 (3×$^{\alpha}$C), 55.1 ($^{\beta}$C), 55.0 ($^{\alpha}$C'), 51.9 (OCH_3), 36.4 ($^{\beta}$C"), 34.8 (2C, $^{\beta}$C + $^{\beta}$C'), 27.1, 26.8, 26.7, 23.3 (2C), 23.3, 22.8, 22.8 (8×CH_3), 9ArC + 6ArCH could not be located; **MS** ES$^+$ (100%, $[M+Na]^+$) 1218.

Cbz-L-Phe-Aib$_4$-L-Pya-NH-CH$_2$-Pyr 107

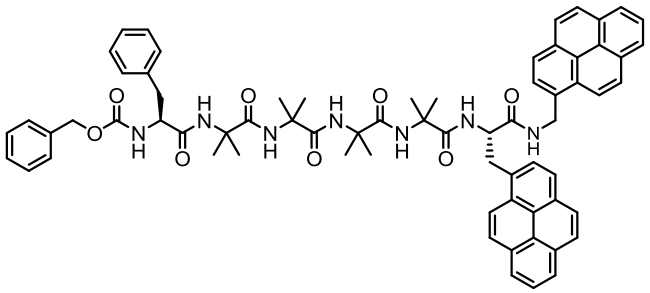

Cbz-L-PheAib$_4$OH **63** (25.0 mg, 0.039 mmol 1 eq.) was coupled to Boc-L-Pya-NH-Pyr **86** (1.2 eq.) using General procedure 1: Deprotected **86** was added to the activated acid in 1 mL of 1:1 anhydrous DCM/DMF. Purification with flash chromatography (1-5% IPA:DCM) gave the title compound (32.9 mg, 75%) as an off white solid **mp** 144-147 °C; **[α]$_D$** = +6.4 (C=1; $CHCl_3$); **IR** (ATR, cm^{-1}) 3287, 3040, 2921, 2850, 1651, 1527, 1455, 1234, 1171; **^{1}H NMR** (500 MHz, $CDCl_3$) δ_H = 8.63 (d, *J* = 9.5, 1H, PyrH), 8.51 (d, *J* = 9.1, 1H, PyrH), 8.39 (t, *J* = 5.8, 1H , NH, N*H*CH$_2$Pyr), 8.24 - 8.11 (m, 7H, PyrH), 8.10 - 7.95 (m, 7H, PyrH), 7.84 (s, 1H, NH), 7.82 (s, 1H, NH), 7.50 (s, 1H, NH), 7.39 - 7.27 (m, 8H, ArH), 7.16 - 7.12 (m, 2H, ArH), 6.95 (s, 1H, NH), 6.17 (s, 1H, NH), 5.49 (dd, *J* = 15.1, 6.6, 1H, A of ABX, NHC*H*$_A$H$_B$Pyr), 5.20 (dd, *J* = 15.1, 5.4, 1H, B of ABX, NHCH$_A$*H*$_B$Pyr), 5.16 (d, *J* = 3.5, 1H, NH), 5.13 (d, *J* = 12.3, 1H, PhC*H*$_A$H$_B$O), 5.08 (ddd, *J* = 11.3, 8.8, 2.5, 1H, $^{\alpha}$CH), 4.96 (d, *J* = 12.3, 1H, PhCH$_A$*H*$_B$O), 4.63 (dd, *J* = 14.8, 2.5, 1H, Ar-$^{\beta}$C*H*$_A$H$_B$), 4.10 (ddd, *J* = 8.3, 5.3, 3.2, 1H, $^{\alpha}$C'H), 3.66 (dd, *J* = 14.8, 11.7, 1H, Ar-$^{\beta}$CH$_A$*H*$_B$), 3.10 (dd, *J* = 14.3, 5.5, 1H, Ar-$^{\beta}$C'*H*$_A$H$_B$), 2.88 (dd, *J* = 14.2, 8.5, 1H, Ar-$^{\beta}$C'H$_A$*H*$_B$), 1.43 (s, 3H, CH_3), 1.36 (s, 3H, CH_3), 1.30 (s, 3H, CH_3), 1.27 (s, 6H, CH_3), 1.19 (s, 3H, CH_3), 1.11 (s, 3H, CH_3), 0.96 (s, 3H, AibCH$_3$); **^{13}C NMR** (125 MHz, CDCl3) δ_C 175.6, 175.3, 174.7, 173.3, 172.5, 171.2 (6×CO), 157.1 (CO, Cbz), 135.7, 135.1, 133.5, 132.8, 131.5, 131.4, 131.2, 131.1, 130.7, 130.2, 129.4, 129.23, 129.1, 129.0, 128.9, 128.4, 128.0, 127.9, 127.8, 127.7, 127.5, 127.5, 126.8, 126.7, 126.7, 125.8, 125.7, 125.2, 125.1, 125.03, 124.96, 124.8, 124.7, 124.2, 123.9, 123.8 (36×ArC/ArCH), 68.05 (PhCH$_2$O), 57.75, 57.11 ($^{\alpha}$CH), 56.81, 56.75, 55.34 ($^{\alpha}$C'H), 41.70 (NHCH$_2$Py), 36.98 ($^{\beta}$C'H$_2$), 35.39 ($^{\beta}$CH$_2$), 27.12, 26.96, 26.63, 23.49, 23.19, 23.08, 22.84, 22.63 (8×CH_3), 4 × ArC/ARCH could not be located. **MS** (ES$^+$) 1146 (100%, [M+Na]$^+$).

Cbz-D-Phe-Aib$_4$-L-Pya-NH-Pyr 108

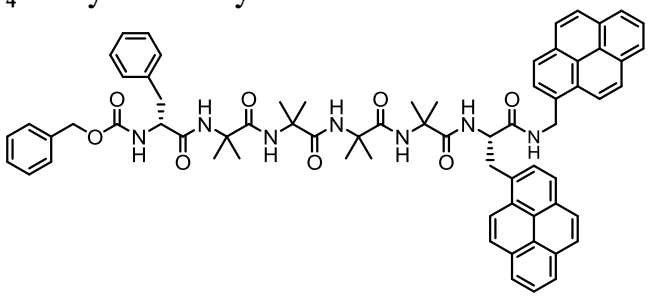

Cbz-L-PheAib$_4$OH **64** (25.0 mg, 0.039 mmol 1 eq.) was coupled to Boc-L-Pya-NH-Pyr **86** (1.2 eq.) using General procedure 1: Deprotected **86** was added to the activated acid in 1 mL of 1:1 anhydrous DCM/DMF. Purification with flash chromatography (1-5% IPA:DCM) gave the title compound (23.3 mg, 53%) as an off white solid. **mp** 110-112 °C; $[\alpha]_D$ = +11.6 (c = 1.0, $CHCl_3$); **IR** (ATR, cm^{-1}) 3295, 2924, 2852, 1656, 1527, 1455, 1208, 1164; **^{1}H NMR** (500 MHz, $CDCl_3$) δ_H 8.57 (d, *J* = 9.5, 1H , PyrH), 8.49 - 8.44 (m, 2H, NH + PyrH), 8.21 - 8.10 (m, 7 H, PyrH), 8.09 - 7.93 (m, 9H, PyrH), 7.91 (s, 1H, NH), 7.89 (s, 1H, NH), 7.57 (s, 1H, NH), 7.44 (s, 1H, NH), 7.23 - 7.27 (m, 3H, ArH), 7.23 - 7.16 (m, 5H, ArH), 7.08 (s, 1H, NH), 7.02 – 6.98 (m, 2H, ArH), 6.61 (s, 1H, NH), 5.52 (d, *J* = 4.7, 1H), 5.47 (dd, *J* = 15.0, 6.6, 1H, NHCH_AH$_B$Pyr), 5.13 (dd, *J* = 15.0, 5.2, 1H, NHCH$_A$$H_B$Pyr), 5.03 – 4.97 (m, 1H, $^{\alpha}$CH), 4.99 (d, *J* = 12.3, 1H, A of AB PhCH_AH$_B$O), 4.89 (d, *J* = 12.3, 1H, B of AB PhCH$_A$$H_B$O), 4.54 (dd, *J* = 14.5, 2.5, 1H, Ar-$^{\beta}$CH_AH$_B$), 3.89 (dd, *J* = 12.6, 7.3, 1H, $^{\alpha}$C'H), 3.65 (dd, *J* = 14.5, 11.5, 1H, Ar-$^{\beta}$CH$_A$$H_B$), 2.96 (dd, *J* = 13.6, 6.6, 1H, Ar-$^{\beta}$C'H_AH$_B$), 2.81 (dd, *J* = 13.7, 8.4, 1H, Ar-$^{\beta}$C'H$_A$$H_B$), 1.43 (s, 3H, CH_3), 1.31 (s, 3H, CH_3), 1.26 (s, 3H, CH_3) 1.21 (s, 3H, CH_3), 1.20 (s, 3H, CH_3), 1.14 (s, 3H, CH_3), 1.08 (br. s, 3H, CH_3), 0.97 (s, 3H, CH_3) **^{13}C NMR** (125 MHz, $CDCl_3$) δ_C 175.7, 175.5, 175.1, 173.8, 172.5, 171.4, 156.3 (7×CO), 136.0, 135.8, 132.9, 132.4, 131.3, 131.2, 130.88, 130.87, 130.5, 130.1, 129.1, 129.0, 128.72, 128.66, 128.61 (3C), 128.4, 127.9, 127.8, 127.6, 127.5, 127.4, 127.1, 126.7, 126.6, 126.5, 125.7, 125.0, 124.88 (2C), 124.86 (2C), 124.81, 124.78, 124.71, 124.2, 123.5, 123.5 (39×ArC/CH), 67.1 (Ph*C*H$_2$O), 57.2 ($^{\alpha}$C'H), 56.9, 56.6, 56.6, 56.5 (4×$^{\alpha}$C), 55.7 ($^{\alpha}$CH), 41.5 (NHCH$_2$Pyr), 36.4 (CH_2), 35.3 (CH_2), 27.0, 26.7, 26.6, 26.4, 23.3, 22.8, 22.7, 22.6 (8×CH_3). 5×ArC/CH Could not be located; **MS** (ES^-, MeOH): 1236.6 (100%, $[M+TFA-H]^-$).

Boc-L-Pya-OCH_2-Pyr 111

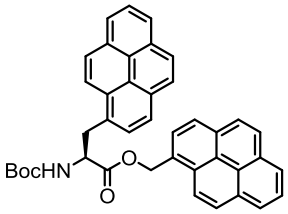

Boc-L-Pya **82** (100 mg, 0.39 mmol, 1 eq.) was dissolved in 2 mL dry DCM. HOBt 46 mg (1.3 eq) was added and the suspension was cooled to 0 °C. 45 μL (1 eq) of EDC was added to the suspension which was left to stir for 30 mins at 0 °C until the solid dissolved into solution. At this point 1-pyrenemethanol **76** (51.1 mg, 1.5 eq) was added followed by 102 μL of DIPEA (2.5 eq). The reaction was left to stir for 12 h. The reaction solvent was removed under reduced pressure to give a residue which was re-dissolved in EtOAc (50 mL) and washed sequentially with $KHSO_4$ (3 × 20 mL; 5% Aq.) $NaHCO_3$ (3×20 mL; Sat.) and brine (20 mL). The organic layer was then dried ($MgSO_4$) and removed under reduced pressure do give a crude residue. This was purified by column chromatography (DCM) gave the title compound **111** (126 mg, 81%) as a white solid **mp** 111-114 °C $\mathbf{[\alpha]_D}$ -18.0 (c = 1, $CHCl_3$) **IR** 3342, 3040, 2922, 2852, 1688, 1524, 1164; **^{1}H NMR** (400 MHz, $CDCl_3$) δ_H 8.37 - 8.12 (m, 3H, PyrH), 8.09 - 7.49 (m, 15H, PyrH), 5.72 (d, *J* = 12.3, 1H, OCH_AH_BPyr), 5.64 (d, *J* = 12.3, 1H, OCH_AH_B-Pyr), 5.23 (d, *J* = 8.0, 1H, NH-Pya), 4.96 (dd, *J* = 13.8, 7.0, 1H, $^{\alpha}$CH-Pya), 3.81 (dd, *J* = 14.8, 6.0, 1H, $^{\beta}CH_A$-Pya), 3.73 (dd, *J* = 14.6, 7.3, 1H, $^{\beta}CH_B$-Pya); **^{13}C NMR** (125 MHz, $CDCl_3$) δ_C 172.23 (CO), 155.21 (CO), 131.81, 131.28, 131.24, 130.77, 130.63, 130.44, 130.00, 129.52 (8×ArC), 128.01, 127.95, 127.82, 127.39, 127.21, 126.94, 126.09, 125.88, 125.58, 125.54 125.14, 124.92 (12×ArCH), 124.73 124.70 (2×ArC), 124.60 (ArCH), 124.55 (ArC), 124.37, 123.12, 122.53, (3×ArCH), 80.17 ($C(CH_3)_3$), 65.55 (OCH_2Pyr), 55.30 ($^{\alpha}$C-Pya), 36.49 ($^{\beta}CH_2$-Pya), 22.84 ($C(CH_3)_3$) 3×ArC + 2×ArCH could not be located; **MS** (ES^+) 626 (100%, $[M+Na]^+$); **HRMS** (ESI^+ TOF) calcd for $C_{41}H_{33}NO_4Na$ ($[M+Na]^+$) 626.2307 found 626.2310.

(1*S*,2*S*)-1,2-(1-pyrene)ethylenediamine dihydrochloride 120

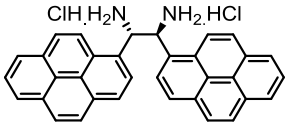

(1*S*,2*S*)-1,2-Bis(1-pyrene)ethylenediamine dihydrochloride was synthesised following a modification of Method B reported by Chin and Co-workers[125] 1-pyrenecarboxaldehyde (720 mg, 3.1 mmol, 2.1 eq) **71** was added to a solution of (1*R*,2*R*)-1,2-Bis(2-hydroxyphenyl)ethylenediamine **114** (364 mg, 1.49 mmol, 1 eq) in 6 mL of DMSO. After stirring for 24 h the mixture was poured into 100 mL of rapidly stirred distilled water, leading to the precipitation of a yellow solid. The resulting yellow solid was collected, washed with distilled water and left to air dry on the sinter. The resultant yellow powder was redissolved in 25 mL of THF. Conc. HCl (0.3 mL) was added dropwise to this stirred solution. This was left for 3 h, leading to the formation of an air-sensitive white precipitate. At times when a precipitate did not form after 3 hours, the solvent was concentrated under reduced pressure. The residue was subsequently triturated in 5 mL of THF. The solid was collected, washed with additional THF and dried under reduced pressure to give 675 mg (85%) of the title compound as a yellow solid. **mp** decomposes > 220 °C; $\mathbf{[\alpha]_D^{24}}$ = +972.0 (c = 1.0, DMSO); **IR** (ATR, cm^{-1}) 2848, 1587, 1504, 1238, 845, 629; **^{1}H NMR** (500 MHz, $(CD_3)_2SO$) δ_H 9.60 (br. s., 6H, NH_3Cl), 8.76 (d, *J* = 8.8, 2H, PyrH), 8.65 (d, *J* = 7.6, 2H, PyrH), 8.38 (d, *J* = 9.1, 2H, PyrH), 8.31 (d, *J* = 7.3, 2H, PyrH), 8.19 (d, *J* = 7.6, 2H, PyrH), 8.04 (t, *J* = 7.6, 2H, PyrH), 7.98 (d, *J* = 8.8, 2H, PyrH), 7.95 (d, *J* = 8.2, 2H, PyrH), 7.80 (d, *J* = 8.8, 2H, PyrH), 6.88 (br. s., 2H, CH); **^{13}C NMR** (125 MHz, $(CD_3)_2SO$): δ_C 130.6 (PyrC), 130.5 (PyrC), 129.8 (PyrC), 128.5 (PyrC), 128.4 (PyrCH), 128.0 (PyrCH), 127.9 (PyrC), 126.9 (PyrCH), 126.6 (PyrCH), 125.9 (PyrCH), 125.6 (PyrCH), 125.3 (PyrCH), 124.6 (PyrCH), 123.23 (PyrC) 123.2 (PyrC), 122.6 (PyrCH), 52.5 (CHN); **MS** (ES^+, DMSO) 461 (70%, $[M-(HCl)_2+H]^+$) **HRMS** (ES^+, DMSO) *m/z* calcd. for $C_{34}H_{25}N_2$ $[M-(HCl)_2+H]^+$ = 461.2018, found 461.2038.

Cbz-L-Phe-Aib$_4$-*S*,*S*-BisPyrEt-NH$_2$ 121

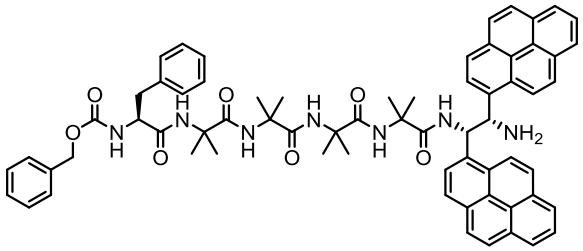

Cbz-L-Phe-Aib$_4$-OH **63** (43.7 mg 0.068 mmol, 1 eq) was coupled to (1*S*,2*S*)-1,2-Bis(1-pyrene)ethylenediamine dihydrochloride **120** (40.0 mg 1.1 eq) using General procedure 2. The resulting residue was purified by crystallisation (DCM/Et_2O) to give 37.3 mg (50%) of the title compound as an off-white solid. **mp** 182-185 ºC; **[α]$_D^{24}$** = +234.3 (c = 1.0, $CHCl_3$); **IR** (ATR, cm^{-1}) 3305, 3040, 2962, 2928, 1652,1526; **1H NMR** (500 MHz, $CDCl_3$) δ_H 8.60 (m, 2H, PyrH), 8.50 (d, *J* = 7.3, 1H, PyrH), 8.40 (d, *J* = 8.8, 1H, C(O)N*H*CH-Pyr), 8.27 (d, *J* = 5.4, 1H, PyrH), 8.07 - 7.95 (m, 5H, PyrH), 7.90 - 7.81 (m, 7H, PyrH), 7.81 - 7.75 (m, 2H, PyrH), 7.71 (m, 1H, NH), 7.66 (s, 1H, NH), 7.38 - 7.29 (m, 5H, ArH+ NH), 7.26 - 7.14 (m, 6H, ArH), 6.94 - 6.79 (m, 2H, NH + C(O)NHC*H*-Pyr), 6.30 (br. s., 1H, NH, Phe), 6.00 (d, *J* = 8.5, 1H, NH_2CH-Pyr), 5.19 (d, *J* = 12.5, A of AB, 1H, PhCH_AH_BO) 5.03 (d, *J* = 12.5, 1H, B of AB, 1H, PhCH_AH_BO Cbz), 4.23 - 4.15 (m, X of ABX, 1H $^{\alpha}$CH-Phe), 3.13 (dd, A of ABX, *J* = 14.2, 5.4, 1H , $^{\beta}$CH-Phe), 2.96 (dd, B of ABX, *J* = 14.2, 8.8, 1H, $^{\beta}$CH-Phe), 1.73 (s, 3H, CH_3), 1.68 (s, 3H, CH_3), 1.60 (s, 3H, CH_3), 1.52 (s, 3H, CH_3), 1.43 (s, 3H, CH_3), 1.35 (s, 3H, CH_3) 1.31 (s, 3H, CH_3), 1.09 (s, 3H, CH_3) **^{13}C NMR** (125 MHz, $CDCl_3$): δ_C 175.5 (CO), 175.2 (CO), 175.0 (CO), 173.8 (CO), 171.9 (CO), 157.1 (CO, Cbz), 136.4, 136.2, 135.8, 135.2, 132.4, 131.1, 131.0 (7×ArC), 130.9 (ArCH), 130.6, 130.5, 130.0, 129.9 (4×ArC), 129.0 (2×ArCH), 128.8 (2×ArCH), 128.6 (2×ArCH), 128.52 128.47 (2×ArC), 128.4, 127.9 (2C), 127.3, 127.2, 127.1, 127.1, 126.6, 126.6, 125.6, 125.41, 125.36 (12×ArCH), 124.9 (ArC), 124.7 (ArCH), 124.7 (ArC), 124.6, 124.5 (2×ArCH), 124.5 (ArC), 124.4, 123.2, 122.9, 122.9 (4×ArCH), 77.6, 77.2, 67.3 (CH_2-Cbz), 57.7 ($^{\alpha}$C-Phe), 57.2 ($^{\alpha}$C, Aib), 57.0 ($^{\alpha}$C, Aib), 56.8 ($^{\alpha}$C, Aib), 56.5 ($^{\alpha}$C, Aib), 38.7, 36.4 ($^{\beta}$C-Phe), 26.9, 26.6, 26.3, 25.9, 23.7, 23.5, 23.8, 23.0 (8×CH_3, Aib) 2×ArCH could not be located; **MS** (ES^+) 1082 (100%, $[M+H]^+$); **HRMS** (ESI^+ ORBITRAP) calcd for $C_{67}H_{68}N_7O_7$ 1082.5175 found 1082.5162.

CBz-D-Phe-Aib$_4$-*S,S*-BisPyrEt-NH$_2$ 122

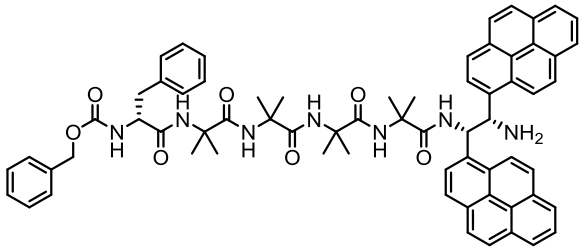

Cbz-D-Phe-Aib$_4$-OH **64** (43.7 mg 0.068 mmol, 1 eq) was coupled to (1*S*,2*S*)-1,2-Bis(1-pyrene)ethylenediamine dihydrochloride **120** (40.0 mg 1.1 eq) using General procedure 2. The resulting residue was purified by crystallisation (DCM/Et_2O) to give 40.6 mg (55%) of the title compound as an off-white solid. **mp** 173-176 ºC; **[α]$_D^{24}$** = +333.8 (c = 1.1, $CHCl_3$) **IR** (ATR, cm^{-1}) 3295, 3038, 2981,2963, 1651, 1528; **^{1}H NMR** (500 MHz, $CDCl_3$) δ_H 8.58 (d, *J* = 9.5, 1H, PyrH), 8.50 (d, *J* = 6.5, 1H, PyrH), 8.46 - 8.35 (m, 2H, PyrH), 8.31 (d, *J* = 8.6, 1H, C(O)N*H*CH-Pyr), 8.07 (br. s., 1H, NH) 8.02 (d, *J* = 7.5, 1H, PyrH) 7.98 (d, *J* = 7.4, 1H, PyrH) 7.96 – 7.84 (m, 1H, PyrH) 7.84 – 7.76 (m, 7H, PyrH) 7.76 – 7.69 (m, 4H, PyrH) 7.69 - 7.63 (m, 3H, 2×ArH + NH), 7.62 (s, 1H, NH) 7.52 - 7.45 (m, 2H, ArH), 7.45 - 7.38 (m, 1H, ArH), 7.20 (d, *J* = 7.5, 2 H, ArH, Phe), 7.03 (t, *J* = 7.4, 2 H, ArH, Phe), 6.93 - 6.84 (m, 2H, ArH, Phe + C(O)NHC*H*-Pyr), 6.15 (d, *J* = 8.3, 1H, NH_2C*H*Pyr), 5.56 (d, *J* = 13.0, 1H, A of AB, PhCH_AH_BO), 5.39 (d, *J* = 13.1 Hz, 1H, B of AB, PhCH$_A$$H_B$O), 4.35 - 4.28 (m, 1H, $^{\alpha}$CH-Phe), 3.35 (d, *J* = 10.0, 1H, $^{\beta}$CH-Phe), 3.13 (t, *J* = 12.2, 1H $^{\beta}$CH-Phe), 1.79 (s, 3H, CH_3), 1.67 (s, 3H, CH_3), 1.66 (s, 3H, CH_3), 1.61 (s, 6H, 2×CH_3), 1.47 (s, 3H, CH_3), 1.36 (s, 3H, CH_3), 1.35 (s, 3H, CH_3) **^{13}C NMR** (125 MHz, $CDCl_3$) δ_C 176.4, 175.6, 175.1, 175.0, 172.6 (5×CO), 157.0 (CO, Cbz), 138.4, 137.6, 135.6, 134.8, 131.0, 130.9, 130.44, 130.41, 130.0, 129.9, (10×ArC), 129.7, 128.8 (2×ArCH), 128.7, 128.5 (2×ArC), 128.2, 128.0, 127.3, 127.1, 126.9, 126.8, 126.7, 126.3, 125.4, 125.3, 124.7, 124.62, 124.57, 124.5, 124.4, 123.1, 122.6 (17×ArCH), 66.6 (CH_2-Cbz), 57.1, 57.0 (2C), 56.7 (4×$^{\alpha}$C), 56.6 ($^{\alpha}$C-Phe), 55.1 (C(O)NH*C*H-Pyr) 54.5 (NH_2*C*HPyr) 35.2 ($^{\beta}$C-Phe), 27.7, 27.4, 27.1, 26.9, 23.7, 23.2, 23.1, 22.5 (8×CH_3); **MS** (ES$^+$, MeOH): 1083 (100%, [M+H]$^+$); **HRMS** (ES$^+$, MeOH) *m/z* calcd. for $C_{67}H_{68}N_7O_7$ [M+H]$^+$ = 1082.5175, found 1082.5155.

(1*S*,2*S*)-1,2-bis(4-(pyren-1-ylmethoxy)phenyl)ethane-1,2-diamine dihydrochloride 127

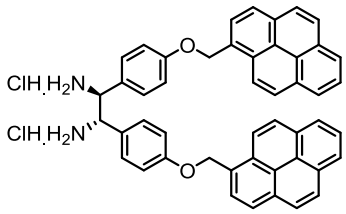

(1*S*,2*S*)-1,2-bis(4-(pyren-1-ylmethoxy)phenyl)ethane-1,2-diamine dihydrochloride was synthesised following a modification of Method B reported by Chin and Co-workers.[125] *p*-(1-pyrenylether) benzaldehyde **126** (144.5 mg, 0.43 mmol, 2.1 eq) was added to a solution of (1*R*,2*R*)-1,2-Bis(2-hydroxyphenyl)ethylenediamine **104** (50 mg, 0.21 mmol, 1 eq) in 4.25 mL of DMSO. After stirring for 24 h the mixture was poured into 12.5 mL of rapidly stirred distilled water, leading to the precipitation of a yellow solid. DCM (10 mL) was added to the mixture until the precipitate had dissolved in the organic layer which was collected. The aqueous layer was further extracted with additional DCM (2 × 10 mL). The organic layers were combined, washed with water (2×10 mL), brine (10 mL) and dried ($MgSO_4$). Removal of DCM under reduced pressure gave a 272 mg of a yellow solid. The yellow solid was dissolved in 150 mL of THF, which was concentrated to 25 mL. insoluble impurities were removed with a cotton wool plug. 4 drops of Conc. HCl were added with stirring to the solution, leading to the formation of a precipitate. The mixture was left stirring for a further 3 h. The precipitate was collected, washed with THF and dried under reduced pressure to give the title compound **127** (91 mg, 60%) as an orange solid. **mp** decomposes > 226 °C; $\mathbf{[\alpha]_D^{24}}$ = -58.0 (c = 1.0, DSMO); **IR** (ATR, cm^{-1}) 2847, 1610, 1585, 1515, 1242, 1182, 990, 844, 839, 829; **^{1}H NMR** (400 MHz, $(CD_3)_2SO$) δ_H 9.09 (s, 6H, N*H*$_3$Cl), 8.36 – 8.23 (m, 10H, PyrCH), 8.23 – 8.15 (m, 6H, PyrCH), 8.08 (t, *J* = 7.6, 2H, PyrCH), 7.32 (d, *J* = 8.7, 4H, *m*-ArCH, Ph-O-), 7.12 (d, *J* = 8.7, 4H, *o*-ArCH, Ph-O-), 5.80 (s, 4H, OC*H*$_2$), 4.99 (s, 2H, CH); **^{13}C NMR** (100 MHz, $(CD_3)_2SO$) δ_C 158.8 (*i*-ArC, Phe-O-), 130.9 (ArC), 130.8 (ArC), 130.2 (*m*-ArCH, Ph-O-), 130.1 (ArC), 128.7 (ArC), 128.0, 127.7, 127.4, 127.2, 126.5, 125.6, 125.5 (7×PyrCH), 125.4 (ArC) 124.7 (PyrCH), 124.0 (PyrCH), 123.8 (ArC), 123.3 (ArC), 113.0 (*o*-ArCH, Ph-O-), 67.9 (O*C*H$_2$), 56.2 (CH). 1 × ArC could not be located; **MS** (ES^+) 674.3 (50%, $[M-(HCl)_2+H]^+$); **HRMS** (ES^+, DMSO) *m*/*z* calcd. for $C_{48}H_{37}N_2O_2$ $[M-(HCl)_2+H]^+$ = 673.2855, found 673.2850

.

CBz-L-Phe-Aib$_4$-*S,S*-BisPhenPyrEt-NH$_2$ 127

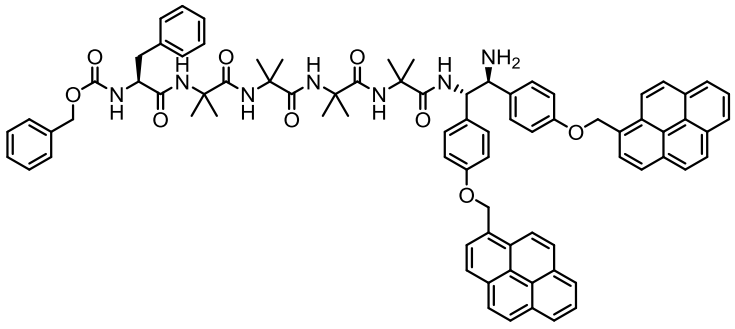

Cbz-L-Phe-Aib$_4$-OH **63** (30.0 mg 0.047 mmol, 1 eq) was coupled to (1S,2S)-1,2-bis(4-(pyren-1-ylmethoxy)phenyl)ethane-1,2-diamine dihydrochloride **127** (38.5 mg 1.1 eq) using General procedure 2. The resulting residue was purified by column chromatography (1-4% MeOH/DCM) to give 43 mg (71%) of the title compound as a white solid. mp 138-140 °C; $[\alpha]_D^{24}$ = -31.2 (C=1 in CHCl3); IR (ATR, cm-1) 3039, 2983, 2926, 2854, 2471, 1646, 1513, 1420, 1236; **^{1}H NMR** (500 MHz, D_3OD, 10% $CDCl_3$) δ_H 8.14 – 8.03 (m, 8H, PyrH), 8.02 – 7.94 (m, 7H, PyrH), 7.90 (d, *J* = 4.1, 1H, PyrH), 7.88 (d, *J* = 4.0, 1H, PyrH), 7.87 (d, *J* = 4.0, 1H, PyrH), 7.34 – 7.30 (m, 4H, ArH) 7.27 (d, *J* = 7.0, 2H, *m*-ArCH, Phe-O-), 7.26 – 7.20 (m, 6H, ArH), 7.18 (d, *J* = 8.6, 2H, *m*-ArCH, Ph-O-), 6.99 (d, *J* = 8.7, 2H, *o*-ArCH, Ph'-O-), 6.83 (d, *J* = 8.6, 2H, *o*-ArCH, Ph'-O-), 5.64 (d, *J* = 11.9, 1H, A of AB, OCH_AH$_B$-Pyr), 5.60 (d, *J* = 11.9, 1H, B of AB, OCH$_A$$H_B$-Pyr), 5.56 (d, *J* = 11.7, 1H, A' of AB', OCH_AH$_B$'-Pyr), 5.50 (d, *J* = 11.7, 1H, B' of AB', CH$_A$$H_B$'-Pyr), 5.14 (d, *J* = 12.6, 1H, A" of AB", PhCH_AH$_B$O), 5.07 (d, *J* = 12.6, 1H, B" of AB", PhCH$_A$$H_B$O), 4.22 (t, *J* = 7.6, 1H, X of ABX, $^\beta$CH_AH$_B$-Phe), 3.06 (dd, *J* = 13.7, 7.6, 1H, A of ABX, $^\beta$CH$_A$$H_B$-Phe), 2.98 (dd, *J* = 13.7, 7.6, 1H, B of ABX, $^\beta$CH$_A$$H_B$, Phe), 1.50 (s, 3H, CH_3), 1.48 (s, 3H, CH_3), 1.45 (s, 3H, CH_3), 1.38 (s, 3H, CH_3), 1.38 (s, 3H, CH_3), 1.32 (s, 3H, CH_3), 1.27 (s, 3H, CH_3), 1.26 (s, 3H, CH_3). **^{13}C NMR** (125 MHz, D_3OD, 10% $CDCl_3$) δ_C 178.6, 177.9, 176.5, 176.4, 174.0, 172.8 (6×CO), 160.5, 159.7, 158.5, 155.4, 154.9, 151.9, 137.8, 137.6, 132.7, 132.3, 131.8, 130.9 (12×ArC) 130.7, 130.3, 130.0, 129.4, 129.0, 128.9, 128.4, 128.2, 127.9, 127.0, 126.6, 126.3, 125.8, 125.4, 123.8, 116.6, 115.9 (17×ArCH), 69.7 (OCH_2Pyr), 69.5 (OCH_2Pyr), 67.7 (CH_2-Cbz), 61.7 ($^\alpha$CH, Phe), 58.7 (CH), 58.2 (CH), 57.6 57.5, 57.4, 57.3, (4×$^\alpha$C) 38.0 ($^\beta$C-Phe) 30.6 27.0, 26.7, 25.8, 24.5, 24.1, 23.6, 23.3 (8×CH_3). 8×ArC + 19×ArCH could not be located. **MS** (ES+, MeOH): 1295 (100%, $[M+Na]^+$)..

CBz-D-Phe-Aib$_4$-*S*,*S*-BisPhenPyrEt-NH$_2$ 128

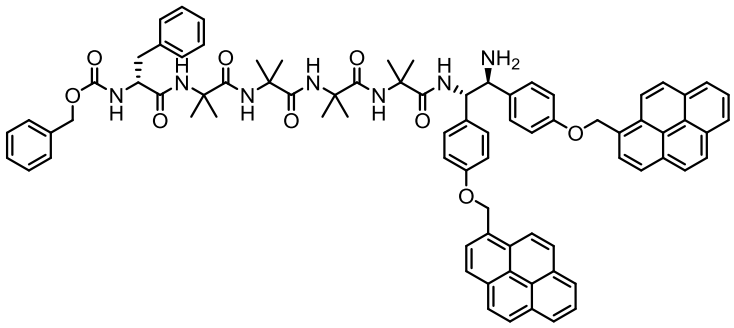

Cbz-D-Phe-Aib$_4$-OH **64** (50 mg 0.078 mmol, 1 eq) was coupled to (1S,2S)-1,2-bis(4-(pyren-1-ylmethoxy)phenyl)ethane-1,2-diamine dihydrochloride **127** (63.0 mg 1.1 eq) using General procedure 2. The resulting residue was purified by column chromatography (1-4% MeOH/DCM) to give 74.8 mg (74%) of the title compound as a white solid. **mp** 151-153 °C; **[α]$_D$** = -61.2 (C=1; $CHCl_3$); **^{1}H NMR** (400 MHz, D_3OD, 10% $CDCl_3$) δ_H 8.01 – 7.91 (m, 8H, PyrH), 7.89 – 7.75 (m, 8H, PyrH), 7.25 – 7.15 (m, 10H, C*H*CHNH$_2$, C*H*NH$_2$, 8×ArH), 7.16 (d, *J* = 6.8, 2H, *m*-ArCH, Phe-O-), 7.14 – 7.12 (m, 2H, ArH), 7.09 (d, *J* = 8.7, 2H, CH$_2$ *m*-ArCH, Phe'-O-), 6.88 (d, *J* = 8.7, 2H, CH$_2$ *o*-ArCH, Phe'-O-), 6.73 (d, *J* = 8.7, 2H, CH$_2$ *o*-ArCH, Phe-O-), 5.50 (d, *J* = 12.2, 1H, A of AB, OC*H*$_A$H$_B$-Pyr), 5.45 (d, *J* = 12.2, 1H, B of AB, OCH$_A$*H*$_B$-Pyr), 5.41 (d, *J* = 11.8, 1H, A' of AB', OC*H*$_a$'H$_b$-Pyr), 5.35 (d, *J* = 11.8, 1H, B' of AB', OCH$_a$'*H*$_b$-Pyr), 5.04 (d, *J* = 12.6, 1H, A" of AB", PhC*H*$_A$H$_B$O), 4.98 (d, *J* = 12.6, 1H, B" of AB", PhCH$_A$*H*$_B$O), 4.12 (t, *J* = 7.5, 1H, X of ABX, $^{\alpha}$CH, Phe), 2.96 (dd, *J* = 14.0, 7.5, 1H, A of ABX, $^{\beta}$C*H*$_A$H$_B$-Phe), 2.88 (dd, *J* = 14.0, 8.3, 1H, A of ABX, $^{\beta}$CH$_A$*H*$_B$-Phe), 1.41 (s, 3H, CH_3), 1.39 (s, 3H, CH_3), 1.36 (s, 3H, CH_3), 1.30 (s, 3H, CH_3), 1.29 (s, 3H, CH_3), 1.22 (s, 3H, CH_3), 1.18 (s, 3H, CH_3), 1.16 (s, 3H, CH_3). **^{13}C NMR** (125 MHz, D_3OD) δ_C 176.3, 175.2, 174.9, 172.7, 157.5, 156.8, (6×CO) 138.5, 137.3, 134.2, 133.4, 131.4, 131.1, 130.6 (7×ArC), 129.8, 129.2, 129.1 (3×ArCH), 129.0 (ArC), 128.6, 128.2, 127.9, 127.5, 127.27, 127.1, 126.8, 126.7, 126.3, 125.9, 125.2, 124.8, 124.5, 124.5, 123.0, 114.1 (16×ArCH), 68.5 (2×O*C*H$_2$Pyr), 66.4 (CH$_2$-Cbz), 60.6 ($^{\alpha}$CH, Phe) 60.3 (*C*HCHNH$_2$), 57.0 ($^{\alpha}$C), 56.9 ($^{\alpha}$C), 56.8 ($^{\alpha}$C), 56.7 ($^{\alpha}$C), 56.2 (*C*HNH$_2$), 35.2 ($^{\beta}$C-Phe), 29.7, 27.8, 27.3, 26.9, 23.8, 23.1, 23.0, 22.5 (8×CH_3). **MS** (ES$^+$, MeOH): 1295 (100%, [M+Na]$^+$).

Cbz-L-αMv-Aib$_4$-O^{t}Bu 132

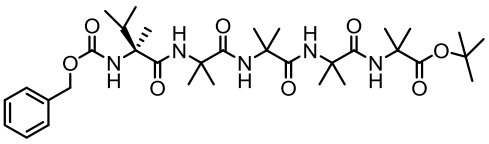

Cbz-L-αMv-OH **130** (130.17 mg, 0.49 mmol, 2 eq) was coupled to NH_2Aib_4OtBu **98** (102 mg, 0.25 mmol, 1 eq) following general procedure 3. This was purified by column chromatography (1-5% MeOH/DCM) to give the title compound **132** (60 mg, 36%) as a white solid. **^{1}H NMR** (500 MHz, $CDCl_3$) δ_H 7.45 (s, 1H, NH), 7.38 – 7.30 (m, 7H, 5×ArH + 2×NH), 6.31 (s, 1H, NH), 5.6 (s, 1H, NH), 5.17 (d, *J* = 12.2, 1H, A of AB, PhCH_AH$_B$O), 5.03 (d, *J* = 12.2, 1H, B of AB, PhCH$_A$$H_B$O), 2.01 – 1.91 (m, 1H, $^\beta$CH, αMeVal), 1.54 (s, 3H, CH_3), 1.48 (s, 3H, CH_3), 1.47 (s, 3H, CH_3), 1.46 (s, 3H, CH_3), 1.45 (s, 6H, 2×CH_3), 1.41 (s, 12H, 4×CH_3), 1.40 (s, 3H, CH_3), 1.21 (s, 3H, CH_3), 0.97 (d, *J* = 6.8, 3H, $^\beta$CHCH_3, αMv), 0.93 (d, *J* = 6.9, 3H, $^\beta$CHCH_3, αMv). **^{13}C NMR** (125 MHz, $CDCl_3$) δ_C 174.2, 174.0, 173.9, 173.8, 172.7 [5×CO], 156.2 (CO, CBz), 136.2 (ArC), 128.8 (2×ArCH), 128.7 (ArCH), 128.4 (2×ArCH), 79.8 (*C*(CH$_3$)$_3$), 67.4 (CH_2, Cbz) 63.1, 57.0, 56.78, 56.76, 56.7, 56.1 (5×$^\alpha$C), 35.5 ($^\beta$CH, αMv), 27.9, 27.3, 27.0, 26.9, 25.7, 24.1, 23.8, 23.6, 23.5, 17.7, 17.4, 17.3 (12×CH_3). Data agrees with the literature[61]

H-L-αMv-Aib$_4$-O^{t}Bu 133

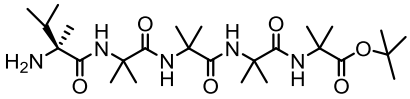

Cbz-L-αMv-Aib$_4$-O^{t}Bu **132** (58 mg, 0.8 mmol) was dissolved in 3 mL of MeOH and placed under and atmosphere of nitrogen. Pd/C (5.8 mg, 10% w/w) was added under the nitrogen atmosphere. The atmosphere was replaced with hydrogen and the mixture left to stir for 14 h. The suspension was filtered through a prepared plug of Celite® topped with activated charcoal and sand, retaining the solvent. The plug was washed thoroughly with additional MeOH and the collected solvent removed under reduced pressure to give 45 mg, (97%) of the de-protected amine **133**. **^{1}H NMR** (400MHz, D_3OD) δ_H 7.78 (s, 1H, NH), 7.53 (s, 1H, NH), 4.89 (br. s., 2H, 2×NH), 2.31 (dq, *J* = 6.9, 6.9, 6.8, 1H, $^\beta$CH, αMv), 1.56 (s, 3H, CH_3), 1.50 (s, 6H, 2×CH_3), 1.48 (s, 6H, 2×CH_3), 1.45 (s, 6H, 2×CH_3), 1.43 (s, 9H, 3×CH_3), 1.42 (s, 3H, CH_3), 1.40 (s, 3H, CH_3) 1.06 (d, *J* = 6.9 Hz, 3H, $^\beta$C(CH_3), αMv), 0.99 (d, *J* = 6.9 Hz, 3H, $^\beta$C(CH_3), αMv) **^{13}C NMR** (100MHz, D_3OD) δ_C 176.6 (CO), 176.2 (CO), 176.1

(CO), 175.7 (2×CO), 81.7 (*C*(CH_3)$_3$), 58.4 ($^{\alpha}$C), 58.1 ($^{\alpha}$C), 58.0 ($^{\alpha}$C), 57.6 ($^{\alpha}$C), 35.5 ($^{\beta}$CH, αMv), 28.3 (CH_3), 26.0 (CH_3), 25.9 (CH_3), 25.4 (CH_3), 25.3 (CH_3), 25.3 (CH_3), 25.2 (CH_3), 24.9 (CH_3), 17.6 (CH_3), 16.5 (CH_3).

Cbz-L-αMv$_2$-Aib$_4$-O^{t}Bu 134

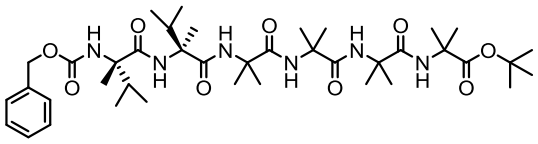

Cbz-L-αMv-OH **130** (45.0 mg, 0.17 mmol, 2 eq) was coupled to NH_2-L-αMv-Aib$_4$-OtBu **132** (45 mg, 1 eq) following General Procedure 3. Purification by silica gel column chromatography (1-5% MeOH/DCM) gave 38.5 mg (59%) of the title compound as a white solid. **^{1}H NMR** (400 MHz, D_3OD) δ_H 8.05 (s, 1H, NH), 7.78 (s, 1H, NH), 7.75 (s, 1H, NH), 7.70 (s,1H, NH), 7.44 – 7.29 (m, 5H, ArH-Cbz), 7.09 (s, 1H, NH), 5.20 (d, *J* = 12.4, 1H, A of AB, PhCH_AH$_B$O), 5.04 (d, *J* = 12.4, 1H, B of AB, PhCH$_A$$H_B$O), 1.94 (spt, 1H, $^{\beta}$CH, αMv), 1.58 (spt, 1H, $^{\beta}$CH, αMv), 1.49 (s, 6H, 2×CH_3), 1.46 (s, 9H, 3×CH_3), 1.45 (s, 6H, 2×CH_3), 1.44 (s, 3H, CH_3), 1.42 (s, 9H, 3×CH_3), 1.40 (s, 3H, CH_3), 1.39 (s, 3H, CH_3), 1.00 (d, *J* = 6.8 Hz, 3H, $^{\beta}$C(CH_3), αMv), 0.94 (d, *J* = 6.8 Hz, 3H, $^{\beta}$C(CH_3), αMv), 0.84 (d, *J* = 6.8 Hz, 3H, $^{\beta}$C(CH_3), αMv), 0.78 (d, *J* = 6.8 Hz, 3H, $^{\beta}$C(CH_3), αMv); **^{13}C NMR** (100 MHz, D_3OD) δ_C 177.4 (CO), 177.3 (CO), 176.9 (CO), 176.8 (CO), 176.4 (CO), 175.5 (CO), 175.2 (CO), 174.1 (CO), 158.3 (CO, Cbz), 138.3 (ArC), 129.6 (ArCH), 129.34 (ArCH), 129.30 (ArCH), 81.5 (*C*(CH_3)$_3$), 68.0 (CH_2, Cbz), 64.4 ($^{\alpha}$C), 63.8 ($^{\alpha}$C), 57.92 ($^{\alpha}$C), 57.89 ($^{\alpha}$C), 57.5 ($^{\alpha}$C), 57.4 ($^{\alpha}$C), 36.7 ($^{\beta}$CH, αMv), 36.5 ($^{\beta}$CH, αMv), 28.2 ((CH_3)$_3$), 27.6 (CH_3), 26.4 (CH_3), 24.0 (CH_3), 23.61 (CH_3), 23.59 (CH_3), 23.5 (CH_3), 18.8 (CH_3), 18.1 (CH_3), 17.9 (CH(*C*H_3)$_2$), 17.8 (*C*H(CH_3)$_2$), 17.5 (*C*H(CH_3)$_2$), 17.4 (*C*H(CH_3)$_2$). Data agrees with the literature.[61]

Cbz-D-αMv-Aib$_4$-O^{t}Bu 137

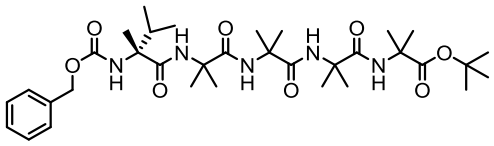

Cbz-D-αMv-OH **135** (287 mg, 1.08 mmol, 2 eq) was coupled to H-Aib$_4$-OtBu (225 mg, 0.54 mmol, 1 eq) using General Procedure 3. Purification by silica gel column chromatography (1-5% MeOH:$CHCl_3$) gave 285 mg (79%) of the title compound as a white solid. **^{1}H NMR** (400MHz, $CDCl_3$) δ_H 7.39 - 7.23 (m, 6H, Cbz + NH), 6.18 (s, 1H, NH), 5.23 (s, 1H, NH), 5.12 (d, *J* = 12.2, 1H, A of AB, PhCH_AH$_B$O), 4.96 (d, *J* = 12.2, 1H, A of AB, PhCH$_A$$H_B$O), 1.93 - 1.80 (m, 1H, $^\beta$CH, αMeVal), 1.48 (s, 3H, CH_3), 1.43 (s, 3H, CH_3), 1.41 (s, 3H, CH_3), 1.40 (s, 3H, CH_3), 1.39 (s, 3H, CH_3), 1.38 (s, 3H, CH_3), 1.35 (s, 3H, CH_3), 1.14 (s, 3H, CH_3), 0.91 (d, *J* = 6.8, 3H, $^\beta$CHCH_3, αMv), 0.87 (d, *J* = 6.8, 3H, $^\beta$CHCH_3, αMv) **^{13}C NMR** (100 MHz, $CDCl_3$) δ_C 174.1, 173.9, 173.7, 173.6, 173.6, 173.6, 172.3 (7×CO), 156.0 (CO, Cbz), 135.9 (ArC), 128.7 (2×ArCH), 128.7 (ArCH), 128.3 (2×ArCH), 79.7 (*C*$(CH)_3$), 67.4 (CH_2, Cbz) 63.0, 56.9, 56.7, 56.6, 56.0 (5×$^\alpha$C), 35.5, 27.8, 27.2, 26.9, 26.8, 25.5, 24.0, 23.7, 23.5, 23.3, 17.6, 17.2, 17.1 (12×CH_3). Data agrees with the literature.[61]

H-D-αMv-Aib$_4$-O^{t}Bu 138

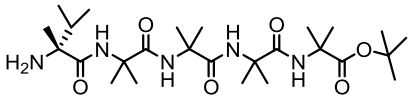

Cbz-D-αMv-Aib$_4$-O^{t}Bu **137** (130 mg, 0.19 mmol) was dissolved in 5 mL of MeOH and placed under and atmosphere of nitrogen. Pd/C (13.0 mg, 10% w/w) was added under the nitrogen atmosphere. The atmosphere was replaced with hydrogen and the mixture left to stir for 14 h. The suspension was filtered through a prepared plug of Celite® topped with activated charcoal and sand, retaining the solvent. The plug was washed thoroughly with additional MeOH and the collected solvent removed under reduced pressure to give (107 mg, 90%) of the de-protected amine **137**. **^{13}C NMR** (100MHz, $CDCl_3$) δ_C 174.3, 174.1, 173.8, 173.8, 80.4 ($C(CH_3)_3$), 57.2, 56.9, 56.6, 56. (4×$^{\alpha}$C), 34.2, 27.8, 26.2, 26.1, 25.2, 24.9, 24.6, 24.4, 24.1 (8×CH_3), 17.3 CH(CH)$_3$, 16.4 CH(CH)$_3$.

Cbz-D-αMv$_2$-Aib$_4$-O^{t}Bu 139

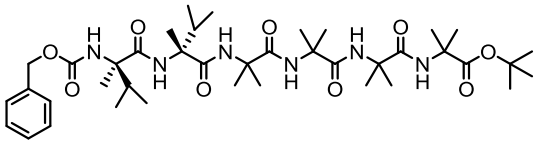

106 mg (0.4 mmol) of Cbz-D-αMv-OH **135** was coupled to H-D-αMv-Aib$_4$-O^{t}Bu **138** using General Procedure 3. The resultant residue was purified using column chromatography (1-5% MeOH/DCM) to give the title compound **139** (43.3 mg, 18%) as a white solid. **mp** 171-173 °C; **[α]$_D^{25}$** =-39.7; **IR** 3319, 2979, 2937, 1732, 1660, 1526, 1411, 1146; **^{1}H NMR** (400 MHz, D_3OD) δ_H 8.05 (s, 1H. NH), 7.78 (s, 1H, NH), 7.75 (s, 1H, NH), 7.70 (s, 1H, NH), 7.45 – 7.29 (m, 6H, NH), 7.09 (s, 1H, NH), 5.20 (d, J = 12.4, 1H, A of AB, PhCH_AH$_B$O), 5.04 (d, J = 12.4, 1H, B of AB, PhCH$_A$$H_B$O), 1.94 (sept, J = 6.6, 1H, C$^{\alpha}$H, αMv), 1.57 (sept, J = 6.9, 1H, C$^{\alpha}$H, αMv), 1.49 (s, 6H, 2×CH_3, Aib), 1.46 (s, 9H, 3 × CH_3), 1.45 (s, 6H, 2×CH_3), 1.44 (s, CH_3), 1.42 (s, 9H, 3×CH_3), 1.40 (s, 3H, CH_3), 1.39 (s, 3H, CH_3), 0.97 1.00 (d, J = 6.9 Hz, 3H, $^{\beta}$CHCH_3, αMv), 0.94 (d, J = 6.9 Hz, 3H, $^{\beta}$CHCH_3, αMv), 0.84 (d, J = 6.6 Hz, 3H, $^{\beta}$CHCH_3, αMv), 0.78 (d, J = 6.6 Hz, 3H, $^{\beta}$CHCH_3, αMv).**^{13}C NMR** (100 MHz, D_3OD) δ_C 177.4 (CO), 176.8 (CO), 176.4 (CO), 175.5 (CO), 175.2 (CO), 174.1 (CO), 158.3 (CO, Cbz), 138.3 (ArC), 129.6 (ArCH), 129.33 (ArCH), 129.30 (ArCH), 81.5 ($C(CH_3)_2$), 68.0 (CH_2, Cbz), 64.4 ($^{\alpha}$C), 63.8 ($^{\alpha}$C), 58.1 ($^{\alpha}$C), 58.0 ($^{\alpha}$C), 57.89 ($^{\alpha}$C), 57.86 ($^{\alpha}$C), 57.5 ($^{\alpha}$C), 57.4 ($^{\alpha}$C), 36.7 ($^{\beta}$$CHCH_3$), 36.5 ($^{\beta}$$CHCH_3$), 28.19

(CH_3) 28.16 ($C(CH_3)_3$), 27.6 (CH_3), 27.6 (CH_3), 26.4 (CH_3), 24.0 (CH_3), 23.62 (CH_3), 23.59 (CH_3), 23.5 (CH_3), 18.8 (CH_3), 18.1 (CH_3), 17.9 ($^{\beta}CHCH_3$), 17.8 ($^{\beta}CHCH_3$), 17.5 ($^{\beta}CHCH_3$). 17.4 ($^{\beta}CHCH_3$); **MS** (ES^+, MeOH) 775.7 (100%, $[M+H]^+$); **HRMS** (ESI^+ Micromass Q-Tof Micro) calcd for $C_{40}H_{67}N_6O_9$ 775.4970 found 775.5005.

Cbz-D-αMv-Aib$_4$-OH 141

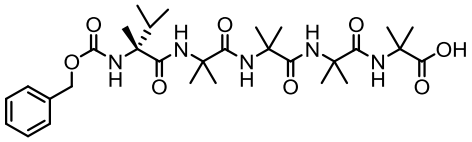

Cbz-D-αMv-Aib$_4$-O^{t}Bu (90 mg, 0.14 mmol) **137** was dissolved in 1 mL of anhydrous DCM. 1 mL of TFA was added to the stirred solution which was left for 3 h. The solvent was concentrated under reduced pressure. The Residue was azeotroped with diethyl ether (5 × 5 mL) and dried under high vacuum giving the pure product (82 mg, >99%) as a white solid. **^{1}H NMR** (400 MHz, $CDCl_3$) δ_H 9.44 (s, 1H, NH), 8.02 (s, 1H, NH), 7.70 (s, 1H, NH), 7.52 (s, 1H, NH), 7.46 – 7.24 (m, 5H, ArH), 7.01 (s, 1H, NH), 6.13 (s, 1H, NH), 5.18 (d, J = 12.5, 1H, A of AB, PhCH_AH$_B$O), 5.05 (d, J = 12.5, 1H, A of AB, PhCH$_A$$H_B$O), 2.07 (m, 1H, $^{\beta}$CH, αMeVal), 1.60 (s, 2H), 1.56 (s, 2H), 1.50 (s, 4H), 1.44 (s, 3H), 1.38 (s, 3H), 1.36 (s, 3H), 1.26 (s, 3H), 1.23 (s, 3H), 1.00 (d, J = 4.7, 3H, $^{\beta}$CHCH_3, αMv), 0.92 (d, J = 4.7, 3H, $^{\beta}$CHCH_3, αMv).**^{13}C NMR** (100 MHz, $CDCl_3$) δ_C 176.6, 176.4, 175.8, 174.7, 174.1, 156.3 (6×CO), 136.7, 128.5, 128.1, 127.6 (4 ArC), 66.9 (CH_2, Cbz), 65.8, 62.8, 57.3, 56.8, 56.6, 56.5, 34.7 ($^{\beta}$CH, αMv), 26.4, 26.3, 25.8, 24.3, 23.5, 23.1, 23.0, 17.3 17.1, 16.5, 15.2 (11×CH_3)**.**

Cbz-L-αMv$_2$-Aib$_4$-OH 142

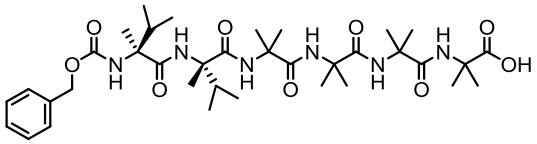

Cbz-L-αMv$_2$-Aib$_4$-OtBu **134** 43.0 mg, (0.058 mmol) was dissolved in 2 mL of DCM. 1 mL of TFA was added with stirring at 0 °C. The ice bath was removed and the solution left to stir for 3h whereupon the reaction completion was checked by TLC. The solvent was concentrated under reduced pressure leaving a white solid. Residual TFA was removed by azeotropring with Et_2O to give the title compound **142** 22 mg (53%) as a white solid. **^{1}H NMR** (400 MHz, $CDCl_3$) δ_H 11.23 (s, 1H, COOH), 7.89 (s, 1H, NH), 7.80 (s, 1H, NH), 7.62 (s, 1H, NH), 7.57 (s, 1H, NH), 7.39 – 7.34 (m, 5H, ArH, Cbz), 6.45 (s, 1H, NH), 5.48 (s, 1H, NH), 5.18 (d, J = 12.1, 1H, CH_2, A of AB, PhCH_AH$_B$O), 5.02 (d, J = 12.1 Hz, 1H, B of AB, PhCH_AH$_B$O), 1.90 (dq, J = 6.7, 6.7, 6.7, 1H, $^{\alpha}$CH, αMv), 1.63 (s, 3H, CH_3), 1.58 (s, 3H, CH_3), 1.50 (s, 3H, CH_3), 1.48 (s, 6H, 2×CH_3), 1.46 (s, 6H, 2×CH_3), 1.43 (s, 6H, 2×CH_3), 1.38 (s, 3H, CH_3), 0.99 (d, J = 6.7 Hz, 3H, $^{\beta}$CHCH_3, αMv), 0.95 (d, J = 6.7 Hz, 3H, $^{\beta}$CHCH_3, αMv), 0.79 (d, J = 3.5 Hz, 3H, $^{\beta}$CHCH_3, αMv), 0.77 (d, J = 3.4 Hz, 3H, $^{\beta}$CHCH_3, αMv); **^{13}C NMR** (100 MHz, $CDCl_3$) δ_C 176.3, 176.2, 175.2, 172.7, 172.5, 172.3 156.4 (7×CO) 136.0 (ArC), 128.82 (ArCH), 128.77 (ArC), 128.6 (ArCH), 67.7 (CH_2-Cbz), 63.54, 62.48, 57.8, 57.00, 56.97, 56.9 (6×$^{\alpha}$C), 36.0 ($^{\beta}$CH, αMv), 35.8 ($^{\beta}$CH, αMv), 29.8, 27.3, 27.1, 26.3, 24.6, 23.3, 22.94, 22.90, 18.2, 17.9 (10×CH_3), 17.4, 17.3, 17.2, 17.1 (4×$^{\beta}$CCH_3).

Cbz-D-αMv$_2$-Aib$_4$-OH 143

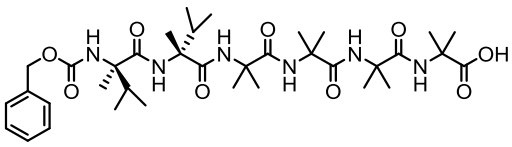

Cbz-D-αMv$_2$-Aib$_4$-OtBu **129** 43.3 mg, (0.058 mmol) was dissolved in 2 mL of DCM. 1 mL of TFA was added with stirring at 0 °C. The ice bath was removed and the solution left to stir for 3h whereupon the reaction completion was checked by TLC. The solvent was concentrated under reduced pressure leaving a white solid. Residual TFA was removed by azeotroping with Et_2O to give the title compound **143** 31.5 mg (76%) as a white solid. **mp** 214 – 217 °C; **[α]$_D^{25}$** =-67.6 (c = 1.0, $CHCl_3$); **IR** (ATR, cm^{-1}) 3292, 2981, 2927, 1742, 1655, 1530, 1455, 1385, 1316, 1262, 1231; **^{1}H NMR** (400 MHz, D_3OD) δ_H 8.04 (s, 1H, NH), 7.90 (s, 1H, NH), 7.82 (s, 1H, NH), 7.74 (s, 1H, NH), 7.68 (s, 1H, NH), 7.44 – 7.29 (m, *J* = 18.2, 7.1, 6H, ArH + NH), 7.06 (s, 1H, NH), 5.20 (d, *J* = 12.4, 1H, A of AB, PhCH_AH$_B$O), 5.04 (d, *J* = 12.4, 1H, B of AB PhCH$_A$$H_B$O), 1.94 (dq, *J* = 6.7, 6.7, 6.7, 1H, C$^\alpha$H, αMV), 1.59 (dq, *J* = 6.9, 6.9, 6.2, 1H, C$^\alpha$H, αMV), 1.52 (s, 6H, 2×CH$_3$), 1.47 (s, 6H, 2×CH$_3$), 1.46 (s, 9H, 3×CH$_3$), 1.44 (s, 3H, CH$_3$), 1.41 (s, 3H, CH$_3$), 1.39 (s, 3H, CH$_3$) 1.00 (d, *J* = 6.7 Hz, 3H, $^\beta$CHCH_3, αMv), 0.94 (d, *J* = 6.8 Hz, 3H, $^\beta$CHCH_3, αMv), 0.84 (d, *J* = 6.8 Hz, 3H, $^\beta$CHCH_3, αMv), 0.79 (d, *J* = 6.8 Hz, 3H, $^\beta$CHCH_3, αMv).**^{13}C NMR** (100 MHz, D_3OD) δ_C 178.3, 177.4, 177.0, 176.9, 175.2, 174.2, 158.4 (7×CO), 138.3 (ArC), 129.6 (ArCH), 129.32 (ArCH), 129.30 (ArC), 68.0 (CH$_2$-Cbz), 64.5, 63.78, 58.1, 58.0, 57.9, 57.1 (6×$^\alpha$C), 36.7 ($^\beta$CH, αMv), 36.5 ($^\beta$CH, αMv), 27.7, 27.6, 27.6, 26.2, 24.5, 23.6, 23.6, 23.5, 18.8, 18.1 (10×CH$_3$), 17.9, 17.8, 17.5, 17.4 (4×$^\beta$CH(CH$_3$)); **MS** (AP$^+$, MeOH): 719 (100%, [M+H]) .

Cbz-D-αMv-Aib$_4$-*S*,*S*-BisPyrEt-NH$_2$ 144

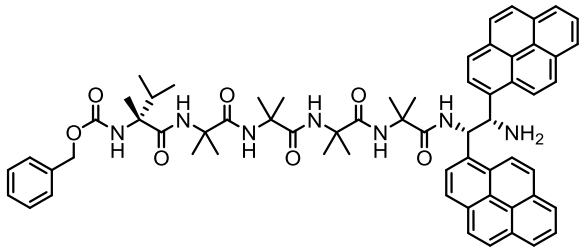

Cbz-D-αMv-Aib$_4$-OH **141** (95 mg 0.16 mmol, 1 eq) was coupled to (1*S*,2*S*)-1,2-Bis(1-pyrene)ethylenediamine dihydrochloride **120** (91.6 mg, 0.17 1.1 eq) using General Procedure 2. The resulting residue was purified by column chromatography (1-4% MeOH/DCM +0.5% NH_3(aq.)) to give 58 mg (35%) of the product as a white solid. **mp** 193 - 197 °C; **[α]$_D^{25}$** = 198.8 (c = 1.0, MeOH); **IR** (ATR, cm^{-1}) 3308, 2980, 2934, 1656,1519, 1228; **^{1}H NMR** (500 MHz, D_3OD) δ_H 8.59 (d, *J* = 7.3, 1H , PyrH), 8.45 - 8.35 (m, 2 H, PyrH), 8.32 (d, *J* = 9.2, 1H, PyrH), 7.73 - 7.95 (m, 6H, PyrH), 7.73 - 7.45 (m, 8H, PyrH), 7.43 - 7.39 (m, 2H, ArH), 7.38 - 7.33 (m, 2H, ArH), 7.31 - 7.27 (m, 1H, ArH), 6.67 (d, *J* = 8.8, 1H, C(O)NCH-Pyr), 5.96 (d, *J* = 8.9, 1H, NH_2CHPyr), 5.16 (d, *J* = 13.5, 1H, A of AB, PhCH_AH_BO), 5.16 (d, *J* = 13.5, 1H, B of AB, PhCH_AH_BO), 2.25 - 2.14 (m, 1H, $^\beta$CH, αMv) 1.70 (s, 3H, CH_3), 1.67 (s, 6H, 2×CH_3), 1.63 (s, 3H, CH_3), 1.41 (s, 3H, CH_3), 1.41 (s, 3H, CH_3), 1.38 (s, 3H, CH_3), 1.37 (m, 3H, CH_3), 0.99 (dd, *J* = 1.2, 3H, $^\beta$CHCH_3, αMv) 0.98 (dd, *J* = 1.2, 3H, $^\beta$CHCH_3, αMv); **^{13}C NMR** (125 MHz, D_3OD) δ_C 178.6 (CO), 177.6 (CO), 177.4 (CO), 177.2 (CO), 176.4 (CO), 158.3 (CO, Cbz), 138.7 (ArC), 136.3 (ArC), 135.5 (ArC), 132.4 (ArC), 132.3 (ArC), 131.8 (ArC), 131.7 (ArC), 129.8 (ArC), 129.8 (ArC), 129.8 (ArC), 129.6 (ArC), 129.2 (ArC), 128.8 (ArC), 128.3 (ArCH), 128.12 (ArCH), 128.09 (ArCH), 128.04 (ArCH), 128.02 (ArCH), 127.98 (ArCH), 126.9 (ArCH), 126.7 (ArCH), 126.6 (ArCH), 126.0 (ArCH), 126.0 (ArCH), 125.9 (ArCH), 125.7 (ArCH), 125.6 (ArCH), 125.6 (ArCH), 125.5 (ArCH), 125.5 (ArCH), 123.8 (ArCH), 123.5 (ArCH), 67.9 (CH_2-Cbz), 63.8 ($^\alpha$C), 58.7 ($^\alpha$C), 58.3 ($^\alpha$C), 58.2 ($^\alpha$C), 58.0 ($^\alpha$C), 57.7 (C(O)NH*C*HPyr), 56.5 (NH_2*C*HPyr), 35.6 ($^\beta$CH, αMv), 26.6 (CH_3), 26.3 (CH_3), 26.0 (CH_3), 25.9 (CH_3), 25.5 (CH_3), 25.3 (CH_3) 25.3 (CH_3), 18.9 (CH_3), 18.3 (CH_3), 18.1 (CH_3), 2×ArC + 4×ArCH could not be located. **MS** (ES$^+$, MeOH): 1048 (100%, [M+H]).

Cbz-L-αMv-Aib$_4$-*S,S*-BisPyrEt-NH$_2$ 145

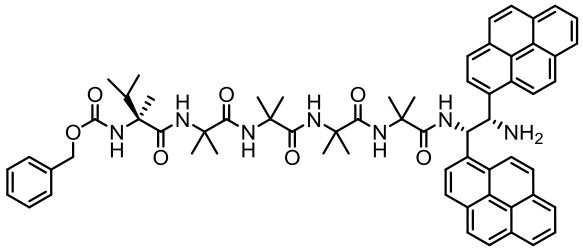

Cbz-L-αMv-Aib$_4$-OH **140** (150 mg, 0.247 mmol, 1 eq) was coupled to (1*S*,2*S*)-1,2-Bis(1-pyrene)ethylenediamine dihydrochloride **120** (145 mg, 1.1 eq) using General procedure 2. The resulting residue was purified by column chromatography (1-4% MeOH/DCM +0.5% NH_3(aq.)) to give the title compound **145** 157 mg (61%) as an off white solid. **mp** 195 - 199 °C; **IR** (ATR, cm^{-1}) 3307, 2980, 2936, 1652, 1524, 1227; **^{1}H NMR** (500 MHz, D_3OD) δ_H 8.56 (s, 1H, ArH), 8.41-8.29 (m, 3H, ArH), 7.86 – 7.69 (m, 6H, ArH), 7.49-7.63 (m, 4H, ArH), 7.48 – 7.28 (m, 9H, ArH), 6.74 (d, *J* = 9.5, 1H, C(O)NHC*H*Pyr), 6.02 (d, *J* = 9.5, 1H, NH_2C*H*Pyr), 5.26 (d, *J* = 12.7, 1H, A of AB, PhCH_AH$_B$O), 5.09 (d, *J* = 12.7, 1H, B of AB, PhCH$_A$$H_B$O), 1.99 – 1.92 (m, 1H, $^\beta$CH, αMv), 1.73 (s, 6H, 2×CH_3), 1.66 (s, 3H, CH_3), 1.63 (s, 3H, CH_3), 1.62 (s, 3H, CH_3), 1.43 (s, 3H, CH_3), 1.41 (s, 3H, CH_3), 1.36 (s, 3H, CH_3), 1.22 (s, 3H, CH_3), 0.99 (dd, *J* = 6.8, 6H, $^\beta$C(CH_3), αMv) 0.91 (dd, *J* = 6.8, 6H, $^\beta$C(CH_3), αMv); **^{13}C NMR** (125 MHz, D_3OD) δ_C 178.3 (CO), 177.6 (CO), 177.4 (CO), 177.0 (CO), 175.8 (CO), 158.2 (CO, Cbz), 138.6 (ArC), 135.9 (ArC), 135.3 (ArC), 132.2 (ArC), 132.1 (ArC), 131.6 (ArC), 131.51 (ArC), 131.49 (ArC), 129.8 (ArC), 129.6 (ArCH), 129.6 (ArC), 129.5 (ArC), 129.14 (ArCH), 128.73 (ArCH), 128.66 (ArCH), 128.59 (ArCH), 128.1 (ArCH), 128.0 (ArCH), 127.9 (ArCH), 127.83 (ArCH), 127.76 (ArCH), 127.7 (ArCH), 126.5 (ArCH), 126.4 (ArCH), 125.9 (ArCH), 125.8 (ArCH), 125.7 (ArCH), 125.52 (ArC), 125.48 (ArCH), 125.42 (ArCH), 125.37 (ArC), 125.3 (ArC), 125.2 (ArC), 123.7 (ArCH), 123.3 (ArCH), 67.8 (CH_2, Cbz), 64.2 ($^\alpha$C), 58.5 ($^\alpha$C), 58.2 ($^\alpha$C), 58.1 ($^\alpha$C), 57.8 ($^\alpha$C), 57.4 (C(O)NHCHPyr), 56.38 (NH_2CHPyr), 36.21 ($^\beta$CH, αMv), 27.89 (CH_3), 27.66 (CH_3), 27.6 (CH_3), 27.2 (CH_3), 24.2 (CH_3), 23.8 (CH_3), 23.6 (CH_3), 23.4 (CH_3), 17.8 (CH_3), 17.7 (CH_3), 17.5 (CH_3), 3×ArCH Could not be located; **MS** (ES$^+$, MeOH): 1048 (100%, [M+H]).

Cbz-D-αMv-Aib$_4$-*S,S*-BisPyrEt-NHAc 146

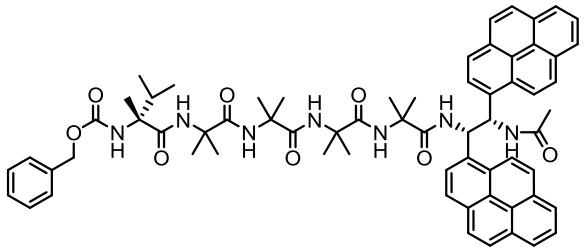

Cbz-D-αMv-Aib$_4$-(1*S*,2*S*)-1,2-*S*,*S*-BisPyrEt-NH$_2$ **144** (40 mg, 0.04 mmol) was dissolved in 1 mL of anhydrous DCM. To this was added with stirring 5.4 μL (0.03 mmol, 1.5 eq) of Ac_2O. After the mixture had stirred for 16 h the solvent was evaporated and the residue purified on a silica column (1-10% IPA:DCM) to give the title compound as a white solid (7.7 mg, 18.5%) **mp** 193 - 197 °C; **$[\alpha]_D^{25}$** = −116.8 (c = 1.0, $CHCl_3$); **IR** (ATR, cm^{-1}) 3347, 3039, 2982, 2934, 2478, 1651, 1634, 1409, 1359, 1214; **^{1}H NMR** (500 MHz, D_3OD) δ_H 8.74 (d, *J* = 9.0, 1H, NH), 8.61 (d, *J* = 9.4, 1H, PyrH), 8.58 – 8.47 (m, 2H, PyrH), 8.41 (d, *J* = 8.0, 1H, PyrH), 8.18 – 8.04 (m, 8H, PyrH), 8.00 – 7.82 (m, 8H, PyrH), 7.43 – 7.36 (m, *J* = 7.1H z, 2H, ArH), 7.36 – 7.30 (m, 2H, ArH,), 7.30 – 7.25 (m, 1H, ArH), 6.86 (d, *J* = 5.2, 1H, Aib$_4$NHC*H*Pyr), 6.80 – 6.72 (m, 1H, C*H*PyrNHAc), 5.19 (d, *J* = 12.8, 1H, A of AB, PhCH_AH_BO), 5.07 (d, *J* = 12.8, 1H, B of AB, PhCH$_A H_B$O), 2.05 (dq, *J* = 6.8, 6.8, 6.7, 1H, $^\beta$CH, αMv), 1.96 (s, 3H, CH_3), 1.70 (s, 3H, CH_3), 1.59 (s, 3H, CH_3), 1.52 (s, 3H, CH_3), 1.47 (s, 3H, CH_3), 1.45 (s, 3H, CH_3), 1.40 (s, 6H, 2×CH_3), 1.35 (s, 3H, CH_3), 1.00 (d, *J* = 6.8 Hz, 3H, $^\beta$CHCH_3, αMv), 0.95 (d, *J* = 6.9 Hz, 3H, $^\beta$CHCH_3, αMv); **^{13}C NMR** (125 MHz, D_3OD) δ_C 178.7 (CO), 177.5 (CO), 177.0 (CO), 176.3 (CO), 176.0 (CO), 172.3 (CO), 158.2 (CO, Cbz), 138.6 (ArC), 134.9 (ArC), 132.6 (ArC), 132.1 (ArC), 132.1 (ArC), 132.0 (ArC), 129.6 (ArCH), 129.5 (ArC), 129.4 (ArC), 129.1 (ArCH), 128.8 (ArCH), 128.7 (ArCH), 128.7 (ArCH), 128.4 (ArCH), 128.2 (ArCH), 128.2 (ArCH), 127.0 (ArCH), 126.89 (ArCH), 126.86 (ArCH), 126.8 (ArCH), 126.3 (ArCH), 126.2 (ArCH), 126.1 (ArCH), 126.01 (ArCH), 125.97 (ArC), 125.95 (ArC), 125.9 ArC), 125.7 (ArCH), 125.5 (ArCH), 123.6 (ArCH), 123.3 (ArCH), 67.8 (CH_2-Cbz), 58.7 ($^\alpha$C), 58.7 ($^\alpha$C), 58.3 ($^\alpha$C), 58.0 ($^\alpha$C), 57.8 ($^\alpha$C), 55.1 (*C*HPyrNHAc), 54.7 (Aib$_4$NH*C*HPyr) 36.0 ($^\beta$CH, αMv), 27.3 (CH_3), 26.9 (CH_3), 26.6 (CH_3), 24.6 (CH_3), 24.5 (CH_3), 24.1 (CH_3), 22.8 (CH_3), 19.0 (CH_3), 18.0 (2×CH_3), 17.6 (2×CH_3), 3×ArC 3×ArCH Could not be located; **MS** (ES^+, MeOH): 1113.7 ($[M+Na]^+$, 100%).

Cbz-L-αMv-Aib$_4$-*S,S*-BisPyrEt-NHAc 147

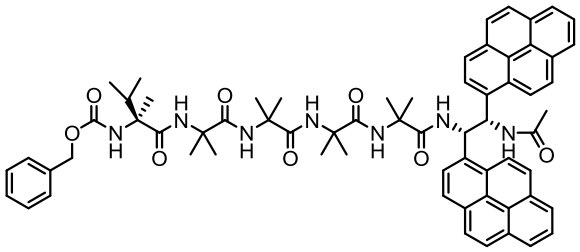

CbzαMv-Aib$_4$-(*S*,*S*)Pyr$_2$-NH$_2$ **145** (56 mg, 0.053 mmol) was dissolved 2 mL of anhydrous DCM. Ac$_2$O (7.5 μL, 0.079 mmol, 1.5 eq) was added and the solution was left to stir for 14 h. The solvent was concentrated under reduced pressure. Purification of residue by column chromatography gave the title compound (38.8 mg, 66%) as a white solid. **mp** 229-231 °C; ; **[α]$_D^{25}$** = 82.4 (c = 1.0, CHCl$_3$); **IR** (ATR, cm^{-1}) 3308, 3039, 2982, 2953, 2477, 1651, 1525, 1468, 1454, 1409, 1383, 1361, 1225, 1184, 1105, 1072, 1043; **^{1}H NMR** (500MHz, D$_3$OD) δ_H = 8.77 (d, *J* = 7.6, 1H, NH), 8.60 (d, *J* = 7.6, 1H, PyrH), 8.47 (d, *J* = 9.2, 1H, PyrH), 8.34 (d, *J* = 7.6, 1H, PyrH), 8.23 (d, *J* = 9.2, 1H, PyrH), 8.12 (s, 1H, PyrH), 8.04 (d, *J* = 9.2, 2 H, PyrH), 8.03 (d, *J* = 8.9, 1H, PyrH), 7.97 (d, *J* = 7.3, 1H, PyrH), 7.94 - 7.86 (m, 4H, PyrH), 7.84 - 7.71 (m, 7H, PyrH), 7.42 - 7.27 (m, 5H, ArH-Cbz), 6.84 - 6.76 (m, 2H, 2×C(O)NHC*H*Pyr), 5.21 (d, *J* = 12.5, 1H, A of AB, PhCH_AH$_B$O), 5.07 (d, *J* = 12.5, 1H, B of AB, PhCH$_A$$H_B$O), 2.10 (s, 3H, Ac), 2.05 – 1.94 (m, 1H, $^{\beta}$CH, αMv), 1.65 (s, 3H, CH$_3$), 1.60 (s, 3H, CH$_3$), 1.57 (s, 3H, CH$_3$), 1.50 (s, 3H, CH$_3$), 1.47 (s, 3H, CH$_3$), 1.40 (m, 3H, CH$_3$), 1.38 (s, 3H, CH$_3$), 1.33 (s, 3H, CH$_3$), 1.19 (s, 3H, CH$_3$), 0.98 (dd, *J* = 6.7, 3H, $^{\beta}$C(CH_3), αMv) 0.92 (dd, *J* = 6.7, 3H, $^{\beta}$C(CH_3), αMv); **^{13}C NMR** (125 MHz, D$_3$OD) δ_C = 178.5 (CO), 177.7 (CO), 177.6 (CO), 177.0 (CO), 176.0 (CO), 173.0 (CO,), 158.3 (CO, Cbz), 138.8 (ArC), 135.6 (ArC), 134.99 (ArC), 134.97 (ArC), 132.6 (ArC), 132.5 (ArC), 132.2 (ArC), 132.0 (ArC), 131.9 (ArC), 131.8 (ArC), 129.9 (ArC), 129.8 (ArCH), 129.3 (ArCH), 128.9 (ArCH), 128.5 (ArCH), 128.3 (ArCH), 128.22 (ArCH), 128.18 (ArCH), 126.83 (ArCH), 126.77 (ArCH), 126.72 (ArCH), 126.2 (ArCH), 126.1 (ArCH), 126.0 (ArCH), 125.91 (ArC), 125.87 (ArC), 125.83 (ArC), 125.76 (ArCH), 125.73 (ArCH), 125.68 (ArC), 123.8 (ArCH), 123.6 (ArCH), 67.9 (CH$_2$-Cbz), 58.7 ($^{\alpha}$C), 58.5 ($^{\alpha}$C), 58.4 ($^{\alpha}$C), 58.2 ($^{\alpha}$C), 57.9 ($^{\alpha}$C), 55.6 (NHC*H*Pyr), 54.8 (NHC*H*Pyr), 36.1 ($^{\beta}$CH, αMv), 27.4 (CH$_3$), 27.4 (CH$_3$), 27.0 (CH$_3$), 26.7 (CH$_3$), 24.8 (CH$_3$), 24.5 (CH$_3$), 24.0 (CH$_3$), 23.4 (CH$_3$, Ac), 18.2 (CH$_3$), 18.1 (CH$_3$), 17.8 (CH$_3$), 6×ArCH could not be located; **MS** (ES$^+$, MeOH): 1112.8 (100%, [M+Na]$^+$); **HRMS** (ESI$^+$ ORBITRAP) calcd for C$_{66}$H$_{72}$N$_7$O$_8$ 1090.5437 found 1090.5435.

Cbz-GlyAib$_4$-*S*,*S*-BisPyrEt-NH$_2$ 150

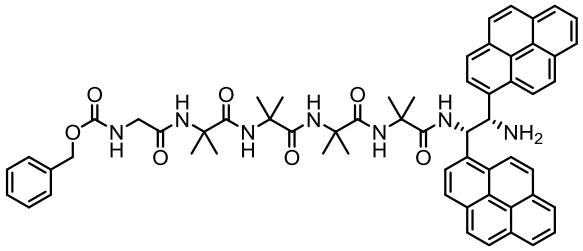

Cbz-Gly-Aib$_4$-OH **149** (85 mg, 0.15 mmol, 1 eq) was coupled to (1S,2S)-1,2-Bis(1-pyrene)ethylenediamine dihydrochloride **120** (89.6 mg, 1.1 eq) using General procedure 2. The resulting residue was purified by column chromatography (2-10% MeOH/DCM) to give 91 mg (64%) of the title compound as an off-white solid. **mp** 183-186 °C **$[\alpha]_D^{25}$** = + 48.0 (C = 1, CH_3Cl); **IR** (ATR, cm^{-1}) 3296, 3041, 2921, 2850, 2479, 1651, 1528, 1230, 1048, 1014; **^{1}H NMR** (400 MHz, $CDCl_3$) δ_H 8.59 (d, *J* = 8.9, 1H, PyrCH), 8.51 (s, 1H, PyrH), 8.46 (d, *J* = 5.8, 1H, PyrH), 8.36 (m, 2H, PyrH + C(O)N*H*CHPyr), 8.06 – 7.93 (m, 6H, PyrH), 7.92 – 7.70 (m, 14H, PyrH), 7.41 (d, *J* = 6.1, 3H, 2×ArH + NH), 7.31 (m, 5H, 3×ArH + 2×NH), 6.92 (m, 1H, NH_2CHPyr), 6.14 (d, *J* = 6.5, 1H, C(O)NHC*H*Pyr), 5.27 (d, *J* = 12.7, A of AB, PhCH_AH_BO), 5.07 (d, *J* = 12.7, 1H, B of AB, PhCH_AH_BO), 3.74 (d, *J* = 11.4, 1H, A' of AB', $^{\beta}CH_AH_B$-Gly), 3.62 (d, *J* = 15.5 , 1H, B' of AB', $^{\beta}CH_AH_B$-Gly), 2.62 (s, 2H, NH_2), 1.69 (s, 3H, CH_3), 1.62 (s, 3H, CH_3), 1.56 (s, 3H, CH_3), 1.50 (s, 3H, CH_3), 1.41 (s, 3H, CH_3), 1.32 (s, 3H, CH_3), 1.30 (s, 3H, CH_3), 1.13 (s, 3H, CH_3).**^{13}C NMR** (100 MHz, $CDCl_3$) δ_C 176.2 (CO), 175.7 (CO), 175.6 (CO), 174.6 (CO), 171.1 (CO), 158.0 (CO), 137.1, 135.8, 134.7, 131.3, 131.2, 130.6, 130.6, 130.3, 130.2 (9×PyrC), 128.8 (2C, ArCH), 128.7 (ArC), 128.3 (ArCH), 127.6 (2C, ArCH), 127.5, 127.4, 127.3, 127.3, 127.00, 126.9, 125.7, 125.6, 125.02, 124.97, 124.8, 124.7, 123.2, 122.7 (14×PyrCH) 67.0 (CH_2, Cbz) 57.3, 57.1, 57.0, 56.6 (4×$^{\alpha}$C, Aib), 55.2 (NH_2*C*HPyr), 55.1 (C(O)NH*C*HPyr), 46.1 ($^{\alpha}CH_2$), 27.3, 27.0, 26.8, 26.4, 23.8 (2C), 23.6, 23.2 (8×CH_3, Aib), 4×PyrCH 3×PyrC could not be located; **MS** (ES^+, MeOH): 992 (100%, $[M+H]^+$);

Cbz-Gly-Aib$_4$-*S*,*S*-BisPyrEt-NHAc 151

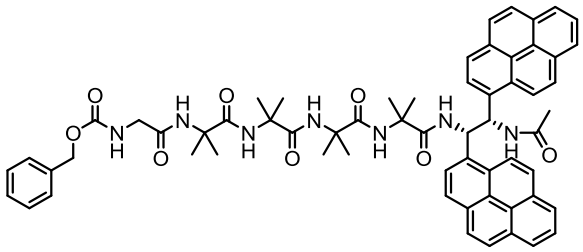

Cbz-Gly-Aib$_4$-*S*,*S*-BisPyrEt-NH$_2$ **150** 20 mg (0.02 mmol) was dissolved in 2 mL of anhydrous DCM. Ac_2O 2.8 uL, (0.03 mmol) was added and the solution was left to stir for 16 h. The solvent was concentrated under reduced pressure to give a crude residue. This was purified by silica gel column chromatography (1-10% IPA/DCM) to give the title compound **141** 5.5 mg (25%) as an off white solid. **mp** 148-153 °C; **$[\alpha]_D^{25}$** = +58.4 ($CHCl_3$, c = 1.0) **IR** (ATR, cm^{-1}) 3325, 2924, 2853, 2473, 1650, 1524, 1417, 1232; **^{1}H NMR** (500 MHz, CD_3OD) δ_H 8.75 (d, *J* = 7.3, 1H, NH), 8.55 (d, *J* = 8.0, 1H, PyrH), 8.51 (d, *J* = 9.4, 1H, PyrH), 8.37 (d, *J* = 7.9, 1H, PyrH), 8.35 (d, *J* = 9.0, 1H, PyrH), 8.11 – 8.04 (m, 5H, PyrH), 8.02 (d, *J* = 9.3, 1H, PyrH), 7.96 (d, *J* = 9.0, 1H, PyrH), 7.94 – 7.83 (m, 7H, PyrH), 7.41–7.27 (m, 5H, ArH, Phe), 6.82 (d, *J* = 6.3, 1H, CH-Pyr), 6.76 (dd, *J* = 8.7, 6.5, 1H, CH-Pyr), 5.15 (s, 2H, $PhCH_2O$), 3.76 (s, 2H, $^{\alpha}CH_2$, Gly), 2.03 (s, 3H, $C(O)CH_3$), 1.59 (s, 3H, CH_3), 1.57 (s, 3H, CH_3), 1.54 (s, 3H, CH_3), 1.50 (s, 3H, CH_3), 1.47 (s, 3H, CH_3), 1.44 (s, 3H, CH_3), 1.41 (s, 3H, CH_3), 1.36 (s, 3H, CH_3); **^{13}C NMR** (125 MHz, CD_3OD) δ_C 176.6, 176.1, 175.2 [2C], 171.2, 170.8 (6×CO), 158.0 (CO, Cbz), 136.8, 133.8, 133.6, 133.5, 131.1, 130.6, 130.4, 130.2, 130.1 (9×ArC), 128.2, 127.7, 127.3, 127.1, 126.8, 125.4, 125.3, 124.7, 124.5, 124.3, 124.1, 122.2, 122.0 (13×ArCH), 66.5 (CH_2, Cbz), 57.2, 56.9, 56.6, 56.3 (4×$^{\alpha}C$), 53.7 (CH), 53.6 (CH), 43.9 (CH_2, Gly), 29.3, 29.0, 24.5, 24.3, 24.1, 23.9, 23.8, 21.6 (8×CH_3), 6×ArC + 8× ArCH could not be located; **MS** (ES^+, MeOH): 1034.6 (100%, $[M+H]^+$).

N_3-Aib$_4$-OH 153[167]

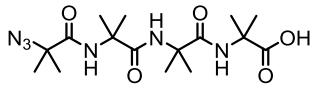

$N_3Aib_4O^tBu$ **97** (500 mg, 1.3 mmol) was dissolved in anhydrous DCM. 3 mL of TFA was added with stirring at 0 °C. The ice bath was removed and the solution left to stir for 3 h whereupon the reaction completion was checked by TLC. The solvent was concentrated under reduced pressure leaving a white solid. Residual TFA was removed by azeotroping with Et_2O to give the product as a white solid **^{1}H NMR** (400 MHz, D_3OD) δ_H 1.5 (s, 6H, 2×CH_3), 1.5 (s, 6H, 2×CH_3), 1.4 (s, 6H, 2×CH_3),

1.4 (s, 6H, 2×CH_3); **^{13}C NMR** (100 MHz, D_3OD) δ_C 178.2 (CO), 176.2 (CO), 175.6 (CO), 174.6 (CO), 64.8 ($^{\alpha}$C), 58.0 ($^{\alpha}$C), 57.7 ($^{\alpha}$C), 57.1 ($^{\alpha}$C), 25.3, 25.1, 24.9, 24.5 (4×CH_3). Data agrees with literature[167]

N_3-Aib$_4$-*S*,*S*-BisPyrEt-NH_2 154

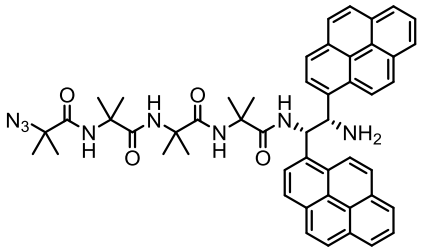

N_3-Aib$_4$-OH **153** (107 mg 0.068 mmol, 1 eq) was coupled to (1*S*,2*S*)-1,2-Bis(1-pyrene)ethylenediamine dihydrochloride **120** (165 mg, 1.1 eq) using General procedure 2. The resulting residue was purified by column chromatography (1-4% MeOH/DCM 1% NH_3(aq.)) to give 204 mg (87%) of the title compound as an off-white solid **mp** decomposes > 150 °C; **$[\alpha]_D^{25}$**= +389 (c = 1.5, DCM); **IR** (ATR, cm^{-1}) 3333, 2281, 2930, 2162, 2111, 1661, 1506, 1456 , 1383, 1362, 1220, 1169; **^{1}H NMR** (400 MHz, $CDCl_3$) δ_H 8.63 (d, *J* = 9.5, 1H, PyrH), 8.58 (d, *J* = 8.5, 1H, PyrH), 8.44 (d, *J* = 8.0, 1H, PyrH), 8.28 (d, *J* = 9.0, 1H, PyrH), 8.25 (d, *J* = 9.5, 1H, NH, C(O)N*H*CHPyr), 8.06 - 7.94 (m, 6H, PyrH), 7.93 - 7.73 (m, 7H, PyrH), 7.45 (s, 1H, NH), 7.08 (s, 1H, NH), 6.94 (t, *J* = 9.0, 1H, C(O)NHC*H*Pyr), 6.66 (br. s., 1H, NH), 5.98 (d, *J* = 9.0, 1H, NH_2C*H*Pyr), 1.69 (s, 6H, 2×CH_3), 1.55 (s, 3H, CH_3), 1.50 (s, 3H, CH_3), 1.48 (s, 3H, CH_3), 1.47 (s, 3H, CH_3), 1.35 (s, 3H, CH_3), 1.21 (s, 3H, CH_3); **^{13}C NMR** (100 MHz, $CDCl_3$) δ_C = 174.8 (CO), 173.9 (CO), 173.7 (CO), 173.0 (CO), 135.8 (PyrC), 134.7 (PyrC), 131.0 (PyrC), 130.9 (PyrC), 130.5 (PyrC), 130.4 (PyrC), 130.0 (PyrC), 129.9 (PyrC), 128.50 (PyrC), 128.48 (PyrC), 127.3 (PyrCH), 127.2 (PyrCH), 127.0 (PyrCH), 126.8 (PyrCH), 126.7 (PyrCH), 125.4 (PyrCH), 125.1 (PyrCH), 124.9 (PyrCH), 124.74 (PyrCH), 124.68 (PyrC), 124.63 (PyrCH), 124.62 (PyrC), 124.56 (PyrCH), 124.47 (PyrCH), 124.45 (PyrCH), 123.0 (PyrCH), 122.7 (PyrCH), 63.7 ($^{\alpha}$CN_3 Aib), 57.3 ($^{\alpha}$C, Aib), 56.9 ($^{\alpha}$C, Aib), 56.9 ($^{\alpha}$C, Aib), 55.5 (NH_2*C*HPyr), 55.0 (C(O)NH*C*HPyr), 27.0 (CH_3), 26.9 (CH_3), 25.7 (CH_3), 24.2 (CH_3), 23.9 (CH_3), 23.7 (CH_3), 23.7 (CH_3), 23.5 (CH_3), 3×PyrC + 3×PyrCH could not be located; **MS** (ES^+, MeOH): 827 (100%, $[M+H]^+$)..

N_3-Aib_4-*S*,*S*-BisPyrEt-NHAc 155

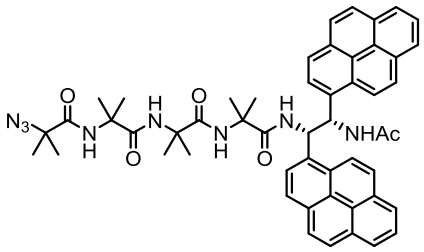

N_3Aib_4-*S*,*S*-BisPhenPyrEt-NH_2 **154** (60 mg, 0.073 mmol) was dissolved in 4 mL of anhydrous DCM. 1 mL of Ac_2O was added dropwise at 0 °C. The cooling bath was removed and the reaction left to stir for 14 h. The solvent was concentrated under reduced pressure and the resulting residue re-dissolved in 30 mL EtOAc. The organic layer was washed with aqueous $NaHCO_3$ (2 × 10 mL, Sat.), $KHSO_4$ (2 × 10 mL, 5%,), dried ($MgSO_4$) and concentratred under reduced pressure to give the title compound **155** 55.8 mg (88%) as a white solid. **mp** > 250 °C; $\mathbf{[\alpha]_D^{25}}$ = + 82.8 (C = 1; DCM); **IR** (ATR, cm^{-1}) 3343, 2927, 2481, 2111, 1635, 1512, 1414, 1381, 1362, 1263, 1224, 1184; **^{1}H NMR** ($CDCl_3$, 400MHz) δ_H 8.65 (d, *J* = 9.3, 1H, PyrCH), 8.61 (d, *J* = 7.8, 1H, PyrCH), 8.28 (d, *J* = 8.4, 1H, Aib_4N*H*CHPyr), 8.25 (d, *J* = 9.5, 1H, PyrCH), 8.13 (d, *J* = 9.3, 1H, PyrCH), 8.08 - 7.97 (m, 7H, PyrCH), 7.93 - 7.83 (m, 7H, PyrH, PyrCH), 7.60 (d, *J* = 7.0, 1H, N*H*Ac), 7.26 (br. s., 1 H, NH), 7.01 (dd, *J* = 8.4, 1H, Aib_4NHC*H*Pyr), 6.83 (dd, *J* = 7.0, 1H, AcNHC*H*Pyr), 6.78 (s, 1H, NH), 6.19 (s, 1H, NH), 2.13 (s, 3H, NHC(O)CH_3), 1.64 (s, 3H, CH_3), 1.60 (s, 3H, CH_3), 1.59 (s, 3H, CH_3), 1.46 (s, 6H, 2×CH_3), 1.40 (s, 3H, CH_3), 1.31 (s, 3H, CH_3), 1.24 (s, 3H, CH_3), 1.20 (s, 3H, CH_3); **^{13}C NMR** (100 MHz, $CDCl_3$) δ_C 175.3, 173.4, 173.10, 173.08, 170.5 (5×CO), 135.0, 133.7, 131.3, 131.2, 130.8, 130.72, 130.65, 130.6, 128.9, 128.6 (10×ArC), 127.7, 127.5, 127.5 127.3, 127.2, 127.0, 125.7, 125.6, 125.3 (9×ArCH), 125.00, 124.96 (2×ArC), 124.93, 124.86, 124.8 (3×ArCH), 124.7 (ArC) 123.3, 122.9 (2×ArCH) 64.0, 57.5, 57.2, 57.1 (4×$^{\alpha}$C, Aib) 29.9, 27.0, 25.9, 24.5, 24.3, 24.3, 24.1, 23.9 (8×CH_3), 23.6 (C(O)CH_3) **HRMS** (APCI$^+$ ORBITRAP) calcd for $C_{52}H_{53}N_8O_5$ $[M+H]^+$ 869.4133 found 869.4136.

Cbz-L-αMv$_2$-Aib$_4$-*S*,*S*-BisPyrEt-NHAc 156

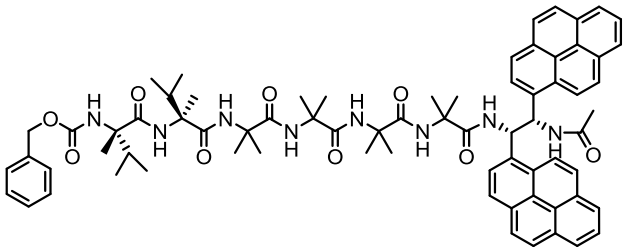

General Procedure 4 was used to synthesise Cbz-L-αMv$_2$-Aib$_4$-*S*,*S*-BisPyrEt-NHAc **156** from Cbz-L-αMv$_2$-Aib$_4$-OH **142** (23.0 mg, 0.032 mmol, 1 eq) and (1S,2S)-1,2-Bis(1-pyrene)ethylenediamine dihydrochloride **120** (18.7 mg 1.1 eq). 60 mg of crude material was returned at the first step. The acetylated residue was purified with a Phenomenex® C18-Ar preparative column. (85:15 MeOH:H_2O; 15 mL/min). The solvents were removed under reduced pressure to give 21.4 mg (56%) of a white solid **mp** 178-180 °C; **[α]$_D^{25}$** = 56.0 (c = 1.0 $CHCl_3$); **IR** (ATR) 3296, 2980, 2925, 2854 , 1655, 1527, 1260; **^{1}H NMR** (500 MHz, $CDCl_3$) δ_H 8.74 (d, *J* = 8.0, 1H, PyrH), 8.57 (d, *J* = 9.4, 1H, PyrH), 8.44 (d, *J* = 9.4, 1H, Aib$_4$N*H*CHPyr), 8.39 (d, *J* = 7.3, 1H, PyrH), 8.20 (d, *J* = 9.3, 1H, PyrH), 8.09 (d, *J* = 8.0, 2H, PyrH), 8.02 (d, *J* = 7.5, 2H, PyrH), 8.01 (d, *J* = 7.6, 2H, PyrH), 7.97 (d*J* = 7.6, 1H, PyrH), 7.94 (d, *J* = 9.5, 1H, PyrH), 7.93 – 7.90 (m, *J* = 5.0, 2H, 2 × PyrH + NH, N*H*Ac), 7.88 (d, *J* = 4.4, 2H, PyrH + NH), 7.86 (d, *J* = 3.4, 1H, PyrH), 7.84 (dd, *J* = 7.6, 3.3, 1H, PyrH), 7.78 (d, *J* = 9.4, 1H, PyrH), 7.73 (s, 1H, NH), 7.60 (s, 1H, NH), 7.52 (s, 1H, NH), 7.38 – 7.31 (m, 4H, ArH, Cbz), 7.00 – 6.94 (m, 1H, Aib$_4$NHC*H*Pyr), 6.75 (t, *J* = 6.2, 1H, AcNHC*H*Pyr), 6.34 (s, 1H, NH), 5.22 (s, 1H, NH), 5.15 (d, *J* = 12.2, 1H, A of AB, PhCH_AH_BO), 4.98 (d, *J* = 12.2, 1H, B of AB PhCH_AH_BO), 2.17 (s, 3H, CH_3, Ac), 1.82 (dq, *J* = 6.8, 6.8, 6.8, 1H, $^{\alpha}$CH, αMv), 1.69 (s, 3H, CH_3), 1.65 (s, 3H, CH_3), 1.57 (s, 3H, CH_3), 1.51 (s, 3H, CH_3), 1.53 – 1.47 (m, 1H, $^{\alpha}$CHzH, αMv), 1.42 (s, 3H, CH_3), 1.41 (s, 3H, CH_3), 1.39 (s, 3H, CH_3), 1.31 (s, 3H, CH_3), 1.30 (s, 3H, CH_3), 1.26 (s, 3H, CH_3), 0.96 (d, *J* = 6.8 Hz, 3H, $^{\beta}$CHCH_3, αMv), 0.93 (d, *J* = 6.9 Hz, 3H, $^{\beta}$CHCH_3, αMv), 0.78 (d, *J* = 4.3 Hz, 3H, $^{\beta}$CHCH_3, αMv), 0.77 (d, *J* = 4.3 Hz, 3H, $^{\beta}$CHCH_3, αMv).**^{13}C NMR** (125 MHz, $CDCl_3$) δ_C 176.2 (CO), 175.5 (CO), 175.2 (CO), 175.0 (CO), 172.5 (CO), 172.4 (CO), 170.8 (CO), 156.3 (CO, Cbz), 135.7, 135.5, 134.7, 131.4, 131.2, 130.8, 130.8, 130.50, 130.49 (8×PyrC + ArC, *Ipso*, Cbz), 128.9 (ArCH, *Para*, Cbz), 128.9 (2C, ArCH, Cbz), 128.8 (PyrC), 128.7 (2C, ArCH, Cbz), 128.4 (PyrC), 127.8, 127.5, 127.4, 127.2, 127.0, 126.6 (7×PyrCH), 126.0 (PyrC), 125.5, 125.4, 125.3 (3×PyrCH), 125.2 (PyrC), 125.1, 124.9 (2×PyrCH), 124.8

(2C, PyrC), 124.7 (2C), 124.6, 124.5, 123.3, 123.1 (6×PyrCH), 67.9 (CH_2-Cbz), 63.5, 62.4, 57.3, 57.2, 56.9, 56.9 (6×$^{\alpha}$C), 55.1 (AcNH*C*HPyr) 52.6 (Aib_4NH*C*HPyr), 36.2, 35.9 (2×$^{\beta}$CH, αMv), 29.9, 28.0, 27.6, 27.3, 27.2, 23.6, 23.4, 23.3, 22.9, 22.8, 18.1 (11×CH_3) 17.4, 17.3, 17.2, 17.1 (4×CH_3, $^{\beta}$CH(*C*H_3), αMv). **MS** (ES^+, MeOH) 1203 (100%, $[M+H]^+$).

Cbz-D-αMv$_2$-Aib$_4$-*S*,*S*-BisPyrEt-NHAc 157

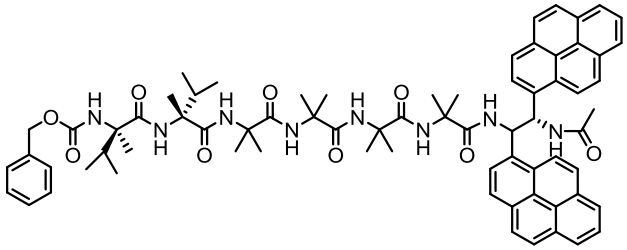

General Procedure 4 was used to synthesise Cbz-D-αMv$_2$-Aib$_4$-*S*,*S*-BisPyrEt-NHAc from Cbz-L-αMv$_2$-Aib$_4$-OH **143** (29.2 mg, 0.041 mmol, 1 eq) and (1*S*,2*S*)-1,2-Bis(1-pyrene)ethylenediamine dihydrochloride **120** (23.6 mg 1.1 eq). 60 mg of crude material was returned at the first step. The acetylated residue was purified by prep HPLC. The acetylated residue was purified with a Phenomenex® C18-Ar preparative column. (85:15 MeOH:H_2O; 15 mL/min). The solvents were removed under reduced pressure to give 14.4 mg (49%) of a white solid. **mp** 178-180 °C; **$[\alpha]_D^{25}$** = -53.2 (c = 1.0 $CHCl_3$); **IR** (ATR) 3294, 2961, 2924, 2853 , 1655, 1527, 1465, 1382, 1362 1182, 1102 1028; **^{1}H NMR** (500 MHz, $CDCl_3$) δ_H 9.01 (d, *J* = 9.5, 1H, Aib_4N*H*CHPyr), 8.77 (d, *J* = 9.4, 1H, PyrH), 8.65 (d*J* = 9.3, 1H, PyrH), 8.55 (d, *J* = 10.3, 1H, AcNH), 8.53 (d, *J* = 8.6, 1H), 8.44 (d, *J* = 8.0, 1H, PyrH), 8.26 – 8.20 (m, 3H, PyrH), 8.20 – 8.12 (m 5H, PyrH), 8.09 – 7.94 (m, 6H, PyrH), 7.90 (s, 1H, NH), 7.67 (s, 1H, NH), 7.62 (s, 1H, NH), 7.36 (s, 4H, ArH Cbz), 6.86 (d, *J* = 9.2, 1H, Aib_4NHC*H*Pyr), 6.70 (d, *J* = 8.5, 1H, AcNHC*H*Pyr), 6.35 (s, 1H, NH), 5.40 (s, 1H, NH), 5.17 (d, *J* = 12.2, 1H, A of AB, PhCH_AH_BO), 4.99 (d, *J* = 12.2, 1H, B of AB, PhCH_AH_BO), 1.88 (s, 3H, CH_3), 1.80 (s, 3H, CH_3), 1.77 – 1.68 (m, 1H, $^{\beta}$CH, αMv), 1.60 (s, 3H, CH_3), 1.56 (s, 3H, CH_3), 1.54 (s, 3H, CH_3), 1.54-1.44 (m, 1H, $^{\beta}$CH, αMv) 1.52 (s, 3H, CH_3) 1.48 (s, 3H, CH_3), 1.43 (s, 6H, 2 × CH_3), 1.38 (s, 3H, CH_3), 1.34 (s, 3H, CH_3), 0.80 (d, *J* = 5.7 Hz, 3H, $^{\beta}$CHC*H*$_3$, αMv), 0.79 (d, *J* = 5.7 Hz, 3H, $^{\beta}$CHC*H*$_3$, αMv), 0.71 (d, *J* = 6.5 Hz, 3H, $^{\beta}$CHC*H*$_3$, αMv), 0.70 (d, *J* = 6.5 Hz, 3H, $^{\beta}$CHC*H*$_3$, αMv).**^{13}C NMR** (125 MHz, $CDCl_3$) δ_C 177.0 (CO), 175.29 (CO), 175.27 (CO), 174.0 (CO), 172.7 (CO), 172.6 (CO), 169.5 (CO), 156.4 (CO, Cbz), 135.8, 135.1, 135.0, 131.6, 131.5, 131.1, 131.1, 130.7 (2C), [8 × PyrC + ArC, *Ipso*, Cbz],

128.89 (ArCH, *Para*, Cbz), 128.86 (2C), 128.7 (2C), [4×ArCH, Cbz], 128.5, 128.1 (2×PyrC), 128.0, 127.9, 127.8, 127.5, 127.2, 126.8, 126.0, 125.9, 125.7, 125.5 (10×PyrCH), 125.5 125.2 (2C), 125.2 (4×PyrC), 125.1, 125.1, 124.9, 124.9, 124.8, 124.6 123.5, 122.8 (8×PyrCH), 67.9 (CH_2-Cbz), 63.5, 62.5, 57.7, 57.5, 57.1, 57.0 (6×$^{\alpha}$C), 54.2 (AcNH*C*HPyr), 52.7 (Aib_4NH*C*HPyr), 36.1, 35.9 (2 × $^{\beta}$CH, αMv), 29.8, 28.0, 27.4, 27.4, 23.6, 23.3, 23.3, 23.1, 22.7, 18.2, 18.1 (11 × CH_3), 17.3, 17.2 (2C), 17.1 [4×CH_3, $^{\beta}$CH(*C*H_3)$_2$, αMv]); **MS** (ES^+, DCM): 1203.7 (60%, $[M+H]^+$).

2-(2-(bromomethyl)phenyl)-5,5-dimethyl-1,3,2-dioxaborinane 182

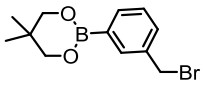

o-bromomethylphenylboronic acid **179** (430 mg, 2 mmol) and neopentyl glycol **181** (208 mg, 2 mmol) was dissolved in 5 mL of anhydrous toluene. 600 mg of activated 3Å molecular sieves was added to the solution, which was heated at reflux for 5 h. The solution was filtered through a Celite® plug. The plug was washed with further with DCM. The filtrates collected and removed under reduced pressure to give the product (510 mg, 90%) as a clear oil **^{1}H NMR** (400 MHz, $CDCl_3$) δ_H 7.80 (d, J = 7.4, 1H, ArH), 7.39 – 7.33 (m, 2H, ArH), 7.30 – 7.27 (m, 1H, ArH), 4.93 (s, 2H, CH_2Br), 3.81 (s, 4H, 2×OCH_2), 1.06 (s, 6H, 2×CH_3); **^{13}C NMR** (100 MHz, $CDCl_3$) δ_C 143.7 (2C, ArCB + Ar*C*CH_2Br), 135.7, 130.7, 130.3, 127.7 (4×ArCH), 72.53 (OCH_2), 34.71 (CH_2Br), 31.93 (*C*(CH_3)$_2$), 22.08 (CH_3). Data agrees with the literature.[171]

BQPA-3-CO-Aib$_4$-*S*,*S*-BisPyrEt-NHAc 188

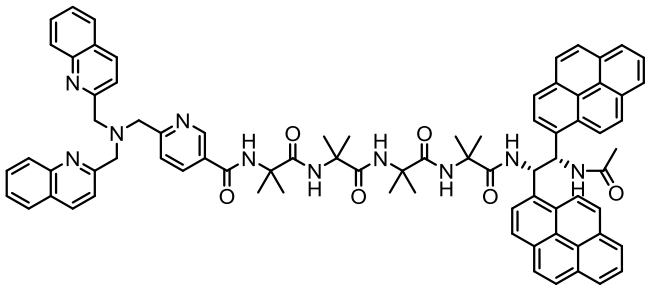

General Procedure 4 was used to synthesise BQPA-3-CO-Aib4-S,S-BisPyrEt-NHAc **188** (68mg 56%) from BQPA-3-CO-Aib$_4$OH **192** (83 mg, 0.1 mmol) and (1*S*,2*S*)-1,2-Bis(1-pyrene)ethylenediamine dihydrochloride **120** 144 mg of crude material was returned at the first step. The acetylated residue was purified on a silica column (2-10% MeOH/DCM) 68 mg 56% **mp** decomposes >190 °C; **[α]$_D^{25}$** = +85.2 ($CHCl_3$, c = 1.0); **IR** (ATR, cm^{-1}) 3306, 3042, 2979, 2928, 1648, 1597, 1523, 1505, 1382, 1362, 1224, 1172, 1139, 1132, 1026; **^{1}H NMR** (500 MHz, $CDCl_3$) δ_H 8.80 (s, 1H, PyH), 8.52 (d, *J* = 6.8, 1H, PyrH), 8.42 (s, 1H, PyrH), 8.36 – 8.23 (m, 3H, PyrH + 2×N*H*CHPyr), 8.19 (d, *J* = 6.5, 1H, PyH), 8.02 (d, *J* = 6.6, 6H, 2×QuinCH + 4×PyrH), 7.94 (d, *J* = 7.5, 2H, 2×QuinCH), 7.92 (d, *J* = 7.0, 2H, 2×QuinCH) 7.89 – 7.74 (m, 9H, PyrH) 7.72 (d, *J* = 7.3, 3H, 2×QuinCH + NH), 7.69 – 7.62 (m, 2H, PyCH + 2×QuinCH) 7.58 – 7.50 (m, 3H, 2×PyrH + NH) 7.50 – 7.43 (m, 2H, 2×QuinCH) 7.13 (s, 1H, NH), 6.84 (s, 1H, CH-Pyr), 6.68 (s, 1H, CH-Pyr), 6.44 (s, 1H, NH), 3.90 (s, 4H, 2×NCH_2Quin), 3.71 (s, 2H, NCH_2Py), 2.01 (s, 3H, NHC(O)CH_3), 1.61 (s, 3H, CH_3), 1.60 (s, 3H, CH_3), 1.55 (s, 3H, CH_3), 1.27 (s, 3H, CH_3), 1.17 (s, 3H, CH_3), 1.07 (s, 3H, CH_3), 0.99 (s, 6H, 2×CH_3); **^{13}C NMR** (125 MHz, CDCl3) δ_C 175.5 [2C], 174.7, 174.1, 170.7 (5×CO), 166.3 (CO-Py), 162.7 (PyC), 159.6 (QuinC), 148.2 (QuinC), 147.6 (PyC), 136.6 (QuinCH), 135.2 (PyCH), 134.8, 134.2, 131.2, 131.2, 130.6, 130.6, 130.5 (7×PyrC), 129.7 (QuinCH), 129.1 (PyrCH), 128.5, 128.2 (2×PyrC), 127.7 (QuinCH), 127.6 (PyCH) 127.4 (QuinCH) 127.3, 127.2, 127.0 126.9 (4×PyrCH), 126.5 (QuinCH), 125.74, 125.70 125.2, 125.07, 125.05 124.91 (6×PyrCH) 124.9 (QuinCH), 124.8, 122.8, 122.7, 122.7 122.6 (5×PyrCH), 122.5 (PyCH), 121.0 (PyrCH), 60.8 (CH_2-Quin), 59.7 (CH_2-Py), 57.3, 57.3, 57.3, 56.6 (4×C_α), 53.6 (*C*H-Pyr), 53.0 (*C*H-Pyr), 26.6, 26.8, 26.3, 26.2, 26.1, 25.1, 24.5, 23.8, 23.5 (9×CH_3) 7×PyrC, 5×PyrCH + 1×QuinC could not be located; **MS** (ES^+, MeOH): 1259.6 (100%, $[M+H]^+$) 1282.6 (90%, $[M+Na]^+$)

[Cu(BQPA-3-CO-Aib$_4$-*S*,*S*-BisPyrEt-NHAc)(ClO$_4$)$_2$(MeCN)] 193

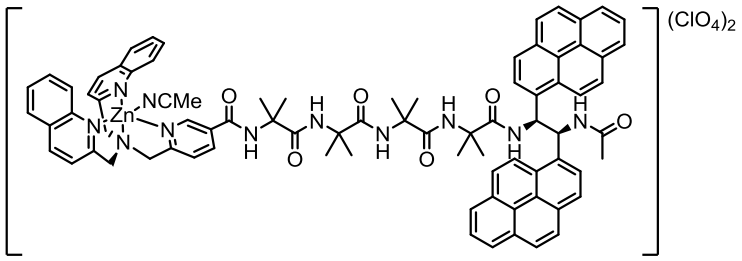

BQPA-3-CO-Aib$_4$-*S*,*S*-BisPyrEt-NHAc **188** (37 mg, 0.03 mmol) was suspended in 0.4 mL MeCN. Zinc perchlorate hexahydrate (1.9 mg, 0.03 mmol) was dissolved in 0.3 mL of MeCN and added dropwise to the suspension with stirring. After complete dissolution of the solid (~30 min) 9 mL of Et_2O was added to the solution, which was left to stir for 1 h. The newly precipitated solid was collected, washed with additional Et_2O and dried, giving the product (33 mg, 70%) **mp** Decomposes> 230 °C; $[\alpha]_D^{25}$ = −14.9 (c = 1.0, MeCN); **IR** (ATR, cm-1) 3308, 3043, 2925, 1650, 1516, 1095; **^{1}H NMR** (400 MHz, CD_3CN) δ_H 9.51 (s, 1H, PyCH), 8.82 (s, 1H, NH), 8.74 (d, *J* = 7.0, 1H, QuinCH), 8.55 (d, *J* = 8.5, 2H, PyCH), 8.44 (d, *J* = 8.4, 2H, 2×QuinCH) 8.41 – 8.35 (m, 2H, 2×QuinCH), 8.21 (d, *J* = 8.8, 2H, QuinCH), 8.17 – 7.99 (m, 9H 4×PyrH + 4×QuinCH + NH), 8.00 – 7.83 (m, 9H, 7×PyrH QuinCH + NH), 7.83 – 7.64 (m, 7H, 5×PyrH + PyCH + NH), 7.63 – 7.54 (m, 2H, 2×PyrH), 7.49 (d, *J* = 8.5, 2H, 2×QuinCH), 7.41 (s, 1H, NH), 7.35 (s, 1H, NH), 6.73 – 6.62 (m, 1H, NHC*H*-Pyr), 6.56 – 6.46 (m, 1H, NHC*H*-Pyr), 4.54 – 4.11 (m, 6H, 2×Quin-CH_2 + Py-CH_2) 2.25 (s, 3H, CH_3), 1.75 (s, 3H, CH_3), 1.72 (s, 3H, CH_3), 1.65 (s, 6H, 2×CH_3), 1.49 (s, 3H, CH_3), 1.46 (s, 3H, CH_3), 1.44 (s, 3H, CH_3), 1.22 (s, 3H, CH_3). **^{13}C NMR** (100 MHz, CD_3CN) δ_C 176.5, 175.9, 175.6, 175.2, 165.3 159.9 (6×CO), 158.9, 158.7 (2×ArC), 148.9 (ArCH), 145.6, 144.9 (2×ArC), 143.3, 142.4, 141.5 (3×ArCH), 134.8, 134.7, 134.4 (3×ArC), 133.6, 133.0 (2×ArCH), 132.0, 131.9, 131.3, 131.11 131.08, 130.8 (6×ArC), 130.2, 129.9, 129.4, 129.0 (4×ArCH), 128.8 (ArC) 128.2, 127.2, 127.1, 126.5, 126.3, 126.0, 125.9, 125.7, 125.6, 125.0, 124.9, 124.7 (12×ArCH), 124.4 (4×ArC), 123.1, 122.7, 122.6, 121.4 (4×ArCH), 59.3 (CH_2-Quin), 59.0 (CH_2-Quin), 58.7 ($^{\alpha}$C), 58.3 ($^{\alpha}$C), 58.1($^{\alpha}$C), 58.0 (CH_2-Py), 57.8 ($^{\alpha}$C), 55.1 (CH-Pyr) 53.7 (CH-Pyr) 26.6, 26.4, 26.1, 25.8, 25.2, 26.0, 24.9, 24.4, 24.0 (9×CH_3), 7 × ArCH could not be located; **MS** (ES$^+$, MeCN): 661.6 (100%, [^{64}Zn(BQPA-3-CO-Aib$_4$-(1*S*,2*S*)-BPEDA-Ac)]$^{2+}$), 663.1 (90%, [^{66}Zn(BQPA-3-CO-Aib$_4$-(1*S*,2*S*)-BPEDA-Ac)]$^{2+}$).

[Cu(BQPA-3-CO-Aib$_4$-GlyNH$_2$)(ClO$_4$)$_2$(MeOH)] 196

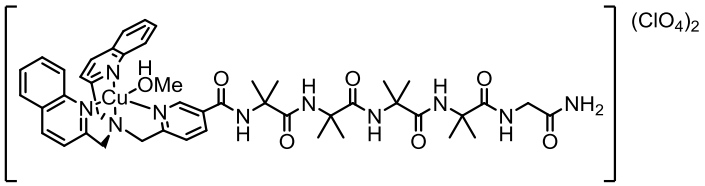

BQPA-3-CO-Aib$_4$-Gly-NH$_2$ **194** (50 mg, 0.06 mmol) was dissolved in 1.2 mL of MeOH. Copper perchlorate hexahydrate (22.3 mg, 0.06 mmol) was dissolved in 0.6 mL of MeOH and added dropwise to the suspension with stirring. After complete dissolution of the solid (~30 min) 9 mL of Et_2O was added to the solution which was left to stir for 1 h. The precipitated solid was collected, washed with additional Et_2O and dried, giving the title compound (51 mg, 80%) as a blue solid. **mp** 223-225 °C; **IR** (ATR, cm^{-1}) 3299, 2987, 2936, 1657, 1516, 1094; **MS** (ES$^+$, MeCN): 446.9 (95%, [^{63}Cu(BQPA-3-CO-Aib$_4$-Gly-NH$_2$)]$^{2+}$), 447.8 (50%, [^{65}Cu(BQPA-3-CO-Aib$_4$-Gly-NH$_2$)]$^{2+}$), 458.8 (80%, [^{63}Cu(BQPA-3-CO-Aib$_4$-Gly-NH$_2$)+Na]$^{2+}$), 459.2 (20%, [^{65}Cu(BQPA-3-CO-Aib$_4$-Gly-NH$_2$)+Na]$^{2+}$), 893.4 (100%, [^{63}Cu(BQPA-3-CO-Aib$_4$-Gly-NH$_2$)-H]$^+$), 895.4 (50%, [^{65}Cu(BQPA-3-CO-Aib$_4$-Gly-NH$_2$)-H]$^+$).

[Cu(BQPA-3-CO-Aib$_4$-*S,S*-BisPyrEt-NHAc)(ClO$_4$)$_2$(MeCN)] 197

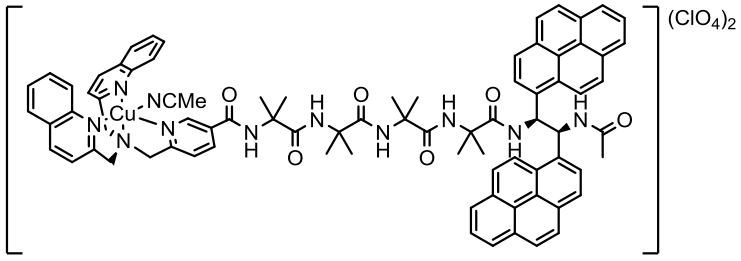

BQPA-3-CO-Aib4-*S,S*-BisPyrEt-NHAc **188** (43.9 mg, 0.03 mmol) was suspended in 1.6 ml of MeCN. Copper perchlorate hexahydrate (22.3 mg, 0.06 mmol) was dissolved in 0.3 mL of MeCN and added dropwise to the solution with stirring. After complete dissolution of the solid (~30 min) the precipitated solid was collected, washed with additional Et_2O and dried, to give the title compound **197** (32.1 mg, 70%) as green solid, **mp** decomposes > 216 °C $[\alpha]_D^{25}$ = 4.9 (c = 1.0, MeCN); **IR** (ATR, cm^{-1}) 3329, 3043, 2983, 2936, 1660, 1516, 1097 **MS** (ES$^+$, MeCN) 660.8 (95%, [^{63}Cu(BQPA-3-CO-Aib4-*S,S*-BisPyrEt-NHAc)]$^{2+}$) 662.3 (50%, 661.7543, [^{63}Cu(BQPA-3-CO-Aib4-*S,S*-BisPyrEt-NHAc)]$^{2+}$).

N_3-Aib_8-OtBu 199[59]

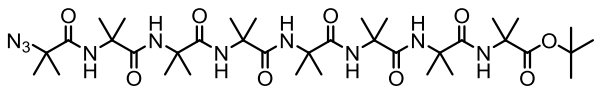

N_3AibOH_5OH **198** (1.00 g, 2.13 mmol), EDC.HCl (610 mg, 3.19 mmol, 1.5 eq) and NEt_3 (0.44 mL, 3.19 mmol 1.5 eq) were dissolved in 130 mL of anhydrous DCM and left to stir for 5 h. The reaction solution was washed with $NaHCO_3$ (2 × 40 mL) $KHSO_4$ (2 × 40 mL), dried ($MgSO_4$) and evaporated to give a crude residue. This was dried under for high vacuum for 1H r and transferred (5 mL Dry MeCN) to a solution of $H_2NAib_3O^tBu$ **88** (1.05 g, 31.8 mmol, 1.5 eq) in 20 mL dry MeCN. The solution was heated to reflux and left to stir for 7 days. The solution was then cooled to RT and evaporated to give a crude residue that was purified by column chromatography (1-5% MeOH/DCM) to give the title compound **199** 1.2 g (75%) as a white solid. **^{1}H NMR** (400 MHz, $CDCl_3$) δ_H 7.54 (s, 1H, NH), 7.50 (s, 1H, NH), 7.47 (s, 1H, NH), 7.36 (s, 1H, NH), 7.33 (s, 1H, NH), 6.92 (s, 1H, NH), 6.14 (s, 1H, NH), 1.55 (s, 6H, 2×CH_3), 1.52 (s, 6H, 2×CH_3), 1.49 (s, 6H, 2×CH_3), 1.48 (s, 6H, 2×CH_3), 1.47 (s, 6H, 2×CH_3), 1.46 (s, 6H, 2×CH_3), 1.45 (s, 6H, 2×CH_3), 1.43 (s, 9H, 3×CH_3), 1.42 (s, 6H, 2×CH_3). **^{13}C NMR** (100 MHz, CDCl3) δ_C 175.4, 174.9, 174.3, 174.22, 174.17, 174.0, 173.3, 173.2 (8×CO), 64.1, 57.0, 57.0, 57.0, 56.8, 56.8, 56.8, 56.1 (8×$^{\alpha}$C), 28.0 (4C), 25.7 (3C), 25.4 (2C), 25.3 (2C), 25.3 (2C), 25.2 (2C), 25.0 (2C), 24.5 (2C) [19×CH_3]. Data agrees with that reported in the literature.[59]

N_3-Aib_8-OMe 200

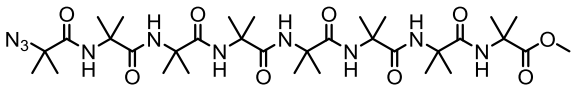

N_3-Aib_8-OtBu **199** 148 mg (0.18 mmol) was dissolved in 5 mL DCM. 1 mL of TFA was added and the mixture was left to stir for 3h until the reaction was complete. The solvent was concentrated under reduced pressure leaving a white solid. Residual TFA was removed by azeotropring with Et2O and the reaction completion was confirmed by ^{1}H NMR. The residue was re-dissolved in a mixture of 4 mL MeOH/6 mL Et_2O and placed under a nitrogen atmosphere. 250 μL of a 2 M solution of trimethylsilane-diazomethane in ether (0.51 mmol, 3 eq) was added dropwise until the the solution retained a yellow colour. The reaction was left to stir for an hour. Glacial acetic acid was added dropwise until the yellow colour dissipated (quenching any remaining trimethylsilane-diazomethane).The clear solution was left to stir for 5 mins before The solvent was concentrated under reduced pressure to give a white residue. This was purified by silica gel column chromatography (1-5% MeOH/DCM) to give the title compound **200** 16 mg (83%) as a white solid. **mp** 241-245 °C **^{1}H NMR** (400 MHz, $CDCl_3$) δ_H 7.62 (s, 2H, 2×NH), 7.55 (s, 1H, NH), 7.53 (s, 1H, NH), 7.41 (s, 1H, NH), 7.17 (s, 1H, NH), 6.49 (s, 1H, NH), 3.66 (s, 3H, OCH_3), 1.54 (s, 6H, 2×CH_3), 1.51 (s, 6H, 2×CH_3), 1.51 (s, 6H, 2×CH_3), 1.48 (s, 6H, 2×CH_3), 1.46 (s, 6H, 2×CH_3), 1.45 (s, 6H, 2×CH_3), 1.45 (s, 6H, 2×CH_3), 1.41 (s, 6H, 2×CH_3). **^{13}C NMR** (100 MHz, $CDCl_3$) δ_C 175.81, 175.78, 175.4, 175.2, 174.51, 174.46, 173.7, 173.4 (8×CO), 64.0, 57.0, 56.9, 56.8, 56.7, 56.6, 55.9, 52.1 (8×$^{\alpha}$C), 25.0 (OCH_3), 25.6-24.4 (16C, 8×CH_3)

H-Aib$_8$-OMe 201

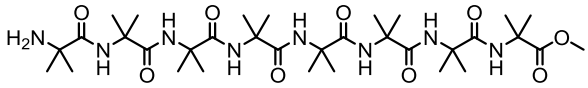

N_3-Aib$_8$-OMe **200** 50 mg (0.013 mmol) was dissolved in 2 mL MeOH and placed under a nitrogen atmosphere. 5 mg of Pd/C (10%) was added under the nitrogen atmosphere. Th atmosphere was replaced with hydrogen and the suspension left to stir vigourously for 30 mins. After the reduction was confirmed by TLC, the hydrogen atmosphere was removed and the suspension was filtered through a plug of celite®. The ssolvent was removed under reduced pressure and the residue re-dissolved in 10 mL DCM. The organic solution was washed with 1 mL of $NaHCO_3$. Dried over Na_2SO_4, filtered and removed under reduced pressure to give the title compound 46.8 mg (94%) as a white solid.**^{1}H NMR** (600 MHz, $CDCl_3$) δ_H 8.31 (s, 1H, NH), 7.81 (s, 1H, NH), 7.65 (s, 1H, NH), 7.64 (s, 1H, NH), 7.52 (s, 1H, NH), 7.44 (s, 1H, NH), 6.65 (s, 1H, NH), 3.66 (s, 3H, OCH_3), 1.50 (s, 6H, 2 × CH_3), 1.49 (s, 6H, 2×CH_3), 1.46 (s, 12H, 4 × CH_3), 1.45 (s, 12H, 4×CH_3), 1.40 (s, 12H, 4 × CH_3); **^{13}C NMR** (151 MHz, $CDCl_3$) δ_C 176.0, 175.9, 175.6, 175.2, 174.8, 174.7, 174.3 [7×CO], 56.9, 56.8, 56.71, 56.65, 56.6, 56.5, 55.8, 52.1 (8×Cα), 28.2 (OCH_3), 25.9 - 24.5 (16C, 8×CH_3). 1 × CO could not be located.

BQPA-3-CO-Aib$_8$-OMe 202

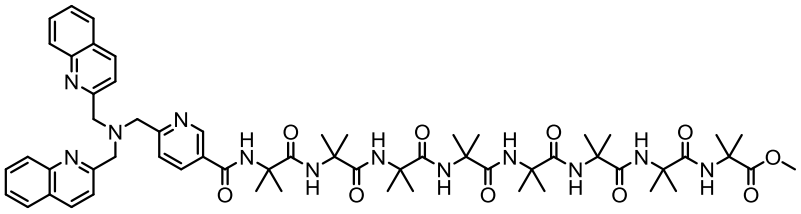

H-Aib$_8$-OMe **201** (38.7 mg, 0.054 mmol, 1 eq), BQPA-3-CO-OH **184** (28.2 mg, 1.2 eq), HOBt (11.6 mg, 1.4 eq.) EDC.HCl (13.5 mg, 1.3 eq) were added to 2 mL of DCM forming a suspension. Addition of NEt_3 (5 eq) led to dissolution of the solid. After leaving to stir for 2 days. 15 mL of additional DCM was added to the reaction mixture. This washed with distilled water (4×3 mL) and dried over Na_2SO_4. The solvent was concentrated under reduced pressure at RT to leave a crude yellow residue. The residue was purified by column chromatography (1-5% MeOH/DCM + 0.1% NH_2 (aq.)) to give the product **202** (37 mg, 60%) as a light yellow solid. **mp** 128 – 130 °C; **IR** (ATR, cm^{-1}) 2298, 2984, 2938, 1655, 1259, 1383, 1362, 1226, 1168 **^{1}H NMR** (400 MHz, $CDCl_3$) δ_H 9.09 (s, 1H, PyCH), 8.66 (s, 1H, NH), 8.30 (d, *J* = 7.9, 1H, PyCH), 8.10 (d, *J* = 8.5, 2H, 2×QuinCH), 7.98 (d, *J* = 8.4, 2H, 2×QuinCH), 7.83 (m, 2H, 2×NH), 7.81 – 7.76 (m, 6H, 4×QuinCH + PyCH + NH) 7.75-7.72 (m, 2H, 2×NH), 7.71 – 7.66 (m, 2H, 2×QuinCH) 7.54 (s, 1H, NH), 7.53 – 7.48 (m, 2H, 2×QuinCH) 7.13 (s, 1H, NH), 4.03 (s, 4H, 2×CH_2Quin), 3.96 (s, 2H, CH_2-Py),), 3.33 (s, 3H, OCH_3), 1.53 (s, 6H, CH_3), 1.49 (s, 6H, CH_3), 1.48 (s, 6H, 2×CH_3), 1.44 (s, 12H, 4×CH_3), 1.40 (s, 12H, 4×CH_3), 1.35 (s, 6H, 2×CH_3). **^{13}C NMR** (100 MHz, $CDCl_3$) δ_C 176.3, 176.2, 176.1, 176.0, 175.6, 175.4, 175.1, 175.0 (8×CO), 166.5 (CO-Py), 163.1 (PyC) 159.7 (QuinC) 149.3 (PyCH), 147.6 (QuinC), 136.8 (QuinCH), 136.1 (PyCH), 129.7, 129.2, 127.7 (3×QuinCH), 127.5 (QuinC), 126.5 (QuinCH), 123.0 (PyCH), 121.17 (QuinCH), 61.0 (CH_2-Quin), 60.0 (N*C*H$_2$Py), 57.7, 56.87, 56.9, 56.8, 56.7, 56.6 [2C], 55.9, (8×$^{\alpha}$C) 51.9 (OCH_3) 25.1 (16C, 8×CH_3) 1×PyC could not be located; **MS** (ES$^-$, MeOH): 1127.7 (100%, $[M-H]^-$).

BQPA-3-CO-Aib$_8$-OH 203

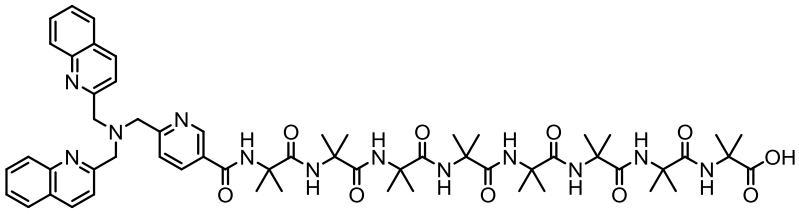

BQPA-3-CO-Aib$_8$-OMe **202** 86 mg (0.076 mmol) was dissolved in a mixture of 2.4 mL MeOH and KOH (1M, 0.8 mL). The solution was heated to 60 C and left to stir for 6 h. Afterwards the solution was allowed to cool to RT and the MeOH removed under reduced pressure. The solution was acidifed to pH 5-6 with addition of HCl and washed with DCM (3×10 mL). The organic layers were dried (Na_2SO_4) and removed at low pressure to give 61.2 mg (72%) of the pure product as a light yellow solid. **mp** Decomposes >180 °C; **IR (ATR, cm^{-1})** 3287, 2983, 2932, 1649, 1532, 1384, 1362, 1227, 1169; **^{1}H NMR** (500 MHz, CD_2Cl_2) δ_H 9.11 (s, 1H, PyCH), 8.21 (d, *J* = 7.9, 1H, PyCH), 8.18 (d, *J* = 8.3, 2H, 2×QuinCH), 8.05 (d, *J* = 8.3, 2H, 2×QuinCH), 7.98 (s, 2H, PyCH + NH), 7.85 (d, *J* = 6.8, 2H, 2×QuinCH), 7.83 (s, 2H, 2×NH), 7.80 (d, *J* = 7.8, 2H, 2×QuinCH), 7.70 (m, 6H, 2×QuinCH + 4×NH), 7.53 (t, *J* = 7.3, 2H, 2×QuinCH), 7.09 (s, 1H, NH), 4.13 (s, 4H, 2×CH_2-Quin), 4.07 (s, 2H, CH_2-Py), 1.59 (s, 6H, 2×CH_3), 1.51 (s, 6H, 2×CH_3), 1.45 (m, 30H, 10×CH_3), 1.42 (s, 6H, 2×CH_3). **^{13}C NMR** (125 MHz, CD_2Cl_2) δ_C 177.5 (CO), 176.7 (CO), 176.5 (2×CO), 176.3 (CO), 175.8 (CO), 175.5 (CO), 175.0 (CO), 167.0 (CO-Py), 159.8 (PyC), 148.8 (PyC), 147.7 (PyCH), 137.4 (QuinCH), 136.5 (PyCH), 130.25 (QuinCH), 129.18 (QuinCH), 128.35 (QuinCH), 128.2 (QuinCH), 128.0 (PyC), 127.0 (QuinCH), 123.5 (QuinCH), 121.6 (QuinCH), 61.1 (CH_2-Quin), 60.4 (CH_2-Py), 58.1 ($^{\alpha}$C), 57.5 ($^{\alpha}$C), 57.2 (3×$^{\alpha}$C), 57.2 ($^{\alpha}$C), 57.1 (2×$^{\alpha}$C), 25.4-25.21 (16×CH_3); **MS** (ES$^+$, DCM): 558.4 (100%, $[M+2H]^{2+}$) 1116.8 (20%, $[M+H]^+$).

BQPA-3-CO-Aib$_8$-S,S-BisPyrEt-NHAc 204

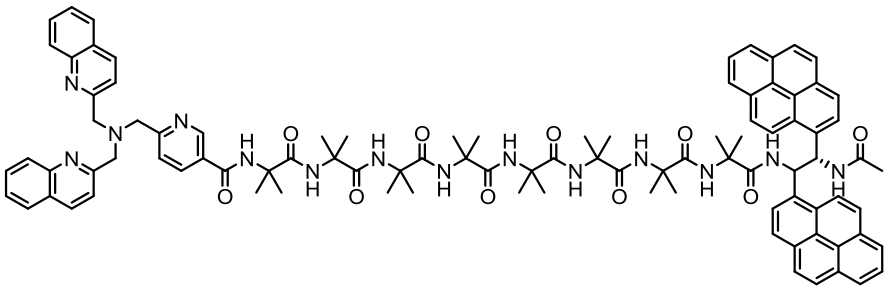

General Procedure 4 was used to synthesise BQPA-3-CO-Aib$_8$-*S*,*S*-BisPyrEt-NHAc from BQPA-3-CO-Aib$_8$-OH **203** (61.2 mg, 0.055 mmol, 1 eq) and (1*S*,2*S*)-1,2-Bis(1-pyrene)ethylenediamine dihydrochloride **120** (32.0 mg 1.1 eq). 83 mg of crude material was returned at the first step. The acetylated residue was purified on a silica column (2-10% MeOH/DCM) to give 68 mg (56%) of the title compound of a light yellow solid. **mp** decomposes >180 °C; **IR** (ATR, cm-1) 3305, 3042, 2984, 2939, 1649, 1530,1384, 1363, 1304, 1227, 1171; **^{1}H NMR** (500 MHz, D_3OD) δ_H 8.99 (s, 1H, PyCH), 8.81 (d, *J* = 8.9, 1H, PyrH), 8.57 (apparent t, *J* = 8.9, 1H, PyrH), 8.40 (d, *J* = 7.3, 1H, PyrH), 8.28 – 8.23 (m, 1H, PyCH), 8.21 – 8.18 (m, *J* = 8.5, 2H, 2×QuinCH), 8.14 – 7.99 (m, 8H, PyrH), 7.96 (d, *J* = 8.5, 2H, 2×QuinCH) 7.93 – 7.83 (m, 7H, PyrH). 7.81 (d, *J* = 8.2, 2H, 2×QuinCH), 7.78 – 7.72 (m, 3H, 2×QuinCH + PyCH), 7.73 – 7.67 (m, 2H, 2×QuinCH), 7.52 (m, 2H, 2×QuinCH), 6.84 (d, *J* = 6.2, 1H, CH-Pyr), 6.77 (dd, *J* = 8.8, 6.5, 1H, CH-Pyr), 4.07 (s, 4H, CH_2-Quin), 4.02 (s, 2H, CH_2-Py), 2.02 (s, 3H, (O)CH_3), 1.66 (s, 3H, CH_3), 1.63 (s, 3H, CH_3), 1.62 (s, 3H, CH_3), 1.60 (s, 3H, CH_3), 1.55 (s, 15H, 5×CH_3), 1.53 (s, 3H, CH_3), 1.50 (s, 3H, CH_3), 1.47 (s, 3H, CH_3), 1.47 (s, 3H, CH_3), 1.40 (s, 3H, CH_3), 1.40 (s, 3H, CH_3), 1.37 (s, 3H, CH_3).**^{13}C NMR** (125 MHz, CD_2Cl_2) δ_C 177.8, 176.5 (2C), 176.2, 175.7, 175.0, 174.3, 170.5, 166.8, 160.2 [10×CO], 148.2 (PyC), 148.1 (PyCH), 137.1 (ArCH), 136.0 (ArCH), 135.6, 131.9, 131.2, 131.0 (4×ArC), 130.1, 129.4 (2×ArCH), 128.5 (ArC), 128.1 (3C), 128.0 (2C), 127.5, 126.9 (2C), 126.3 (2C), 125.5 (2C), 125.4 (3C), 125.2 (2C), 123.7, 123.4, 123.0, 121.7 (2C) [22×ArCH], 61.4 (CH_2-Quin), 60.4 (CH_2-Py), 58.1 ($^{\alpha}$C), 57.7 ($^{\alpha}$C), 57.3 ($^{\alpha}$C), 57.3 ($^{\alpha}$C), 57.1 ($^{\alpha}$C), 32.5 (C(O)CH_3), 30.2, 30.4-29.5 (10×CH_3), 29.9 (CH_3), 29.5 (CH_3), 27.7 (CH_3), 26.0 (CH_3), 25.2 (CH_3), 23.3 (CH_3), 6×ArCH + 17×ArC + 3×$^{\alpha}$C could not be located; **MS** (ES^+, MeCN): 1600.9 (95%, $[M+H]^+$) 1623.0 (100%, [M+Na]+).

[Cu(BQPA-3-CO-Aib$_8$-*S*,*S*-BisPyrEt-NHAc)(ClO$_4$)$_2$(S)] 205

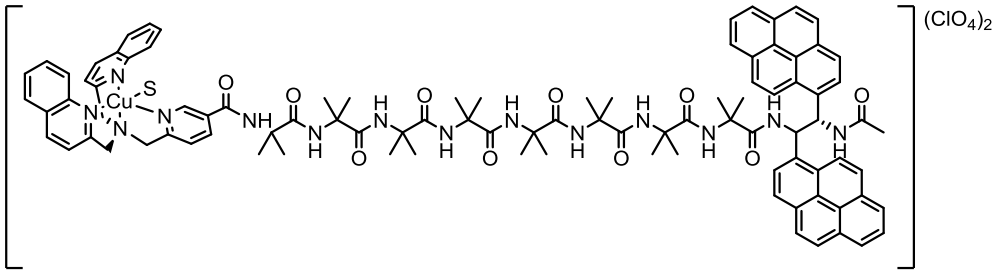

BQPA-3-CO-Aib$_8$-*S*,*S*-BisPyrEt-NHAc **204** (29.7 mg, 0.018 mmol) was suspended in 0.36 mL MeOH. Copper perchlorate hexahydrate (6.89 mg, 0.018 mmol) was dissolved in 0.2 mL of MeCN and added dropwise to the suspension with stirring. After 30 mins, with the solid now completely dissolved, 10 mL of Et_2O was added to the solution, which was left to stir for 1h. The newly precipitated solid was collected, washed with additional Et_2O and dried, affording the product (21 mg, 68%) **mp** decomposes > 220 °C**;** $[\alpha]_D^{25} = -6.0$ (c = 1.0, MeCN) **IR** (ATR, cm^{-1}) 3303, 2982, 2938, 1656, 1516, 1096. **MS** (ES$^+$, MeCN) 842.7 (100%, [^{63}Cu(BQPA-3-CO-Aib$_8$-(1*S*,2*S*)-BPEDA-Ac)+Na]$^{2+}$), 843.7 (45%, [^{65}Cu(BQPA-3-CO-Aib$_8$-(1*S*,2*S*)-BPEDA-A)+Na]$^{2+}$)

Fluorescence Experimental

Solvents:

MilliQ water, HPLC grade or above solvents were used for all experiments. Lipid stock solutions were either used as purchased (Avanti, Sigma-Aldrich) or prepared from solid lipids using spectrophotometric grade chloroform. Aliquots were added using Gilson® pipettes or Hamilton syringe for corrosive solvents.

Fluorescence:

All fluorescence experiments were performed on a Varian Cary Eclipse Spectrophotometer equipped with a temperature controller. Unless otherwise stated measurements were taken at 25 °C in a quartz cuvette, excitation wavelength of 346 nm excitation slits of 5 nm and emission slits of 5 nm or 2.5 nm depending on the fluorescent output. Em 10 Ex 2.5 used for pre-diamine compounds.

Preparation of 800 nm vesicles:

Vesicles were prepared following an extrusion protocol. Aliquots of lipid stock solutions were evaporated to give films of 0.024 mM total lipid. These films were placed under high vacuum for 1 hr to remove residual organic solvent. The films were then re-hydrated with addition of 1.2 mL of buffer solution (20 mM MOPS) vortexing until homogeneity of lipid suspension. The solution was extruded through a polycarbonate membrane (Avanti) to give a 20 mM stock solution of 800 nm vesicles. 1 mL of this solution was diluted as required to give 2 mL solutions at 5, 2.5, and 1 mM concentrations

Preparation of compound stock solutions

Stock solutions of each compound (1 mg/mL) were prepared in acetonitrile. These stock solutions were stored at 5°C in the dark between experiments. Aliquots of these stock solutions (31.3 μL for Zn^{II}-BQPA-3-CO-Aib_4-*S*,*S*-BisPyrEt-NHAc and Cu^{II}-BQPA-3-CO-Aib_4-*S*,*S*-BisPyrEt-NHAc 37.8 μL for Cu-BQPA-3-COAib_8-*S*,*S*-BisPyrEt-NHAc were added to 2 mL of each solution in a quartz fluorescence cuvette.

Addition of compounds to organic solvents

An aliquot of compound stock solution was added to 2 mL the desired organic solvent to give a 10 μM concentration of the M-BQPA-3-COAib$_X$-*S*,*S*-BisPyrEt-NHAc. The cuvette was inverted 3 times before fluorescent measurement to ensure adequate mixing.

Stock solutions of BocPro and Lutidine were prepared in acetonitrile: 21.5 mg of acid (0.1 mmol) and 12.8 mg, 13.9 μL of lutidine (0.12 mmol) was added to a 10 mL volumetric flask, giving a concentration of 0.01 M and 0.012 M respectively. This was further diluted 10 times (1 mL from stock solution 1 into a second 10 mL) to give concentrations of 0.001 M and 0.0012 M.

4 μL (0.2 equvialents vs. complex) aliquots of these amino acid stock solution were added incrementally.

Addition of compounds to Lipid mixtures:

A 2 mL solution of 800 nm lipid vesicles was prepared and added to a quartz cuvette equipped with a Teflon stirring bar. An aliquot of compound stock solution was added to this stirred solution at 25 °C within the fluorimeter and left for 1 hr. Fluorescent measurements were taken at 30 s intervals over the hour. After completion the cuvette was inverted (3×) and the fluorescence measured to confirm compound had been completely added and the system fully equilibrated (no change in fluorescence intensity).

Switching studies

To avoid addition of organic solvents and lutidine used in the solution systems carboxylic acids were converted to their sodium salts. Each amino acid was mixed with NaOH (1 eq) in MeOH and left to stir for 1 hr. The solvent was removed under pressure. The residue was placed in a vaccum oven at 80 °C for 24 h, the residue was scraped from the walls of the vessel and left for a further 24 h a 80 °C in a vacuum oven to give a free-flowing white powder.

Stock solutions of AA-Na were prepared in MilliQ water at 0.1 and 0.01 M concentrations. 2-20 equivalents of AA-Na were added with 4 μL aliquots of 0.01 M solution. 40-100 equivalents were added with 4 μL aliquots of 0.1 M solution. Where solubility in MilliQ water prevented the preparation (Leu-Enkephalin, Aspartame) of the 0.1 M stock solution, the 0.01 M stock solution was used throughout.

14.0 References

1 J. Venkatraman, S. C. Shankaramma and P. Balaram, *Chem. Rev.*, 2001, **101**, 3131–3152.

2 H. Schenkel-Brunner, *Human Blood Groups: Chemical and Biochemical Basis of Antigen Specificity*, Springer Science & Business Media, 2013.

3 S. H. Gellman, *Acc. Chem. Res.*, 1998, **31**, 173–180.

4 G. Guichard and I. Huc, *Chem. Commun. (Camb).*, 2011, **47**, 5933–5941.

5 W. S. Horne and S. H. Gellman, *Acc. Chem. Res.*, 2008, **41**, 1399–1408.

6 V. Azzarito, K. Long, N. S. Murphy and A. J. Wilson, *Nat. Chem.*, 2013, **5**, 161–173.

7 D. Seebach, D. F. Hook and A. Glättli, *Pept. Sci.*, 2006, **84**, 23–37.

8 E. A. Porter, B. Weisblum and S. H. Gellman, *J. Am. Chem. Soc.*, 2002, **124**, 7324–7330.

9 E. A Porter, X. Wang, H. S. Lee, B. Weisblum and S. H. Gellman, *Nature*, 2000, **404**, 565.

10 Y. Hamuro, J. P. Schneider and W. F. DeGrado, *J. Am. Chem. Soc.*, 1999, **121**, 12200–12201.

11 Ø. Jacobsen, H. Maekawa, N. H. Ge, C. H. Görbitz, P. Rongved, O. P. Ottersen, M. Amiry-Moghaddam and J. Klaveness, *J. Org. Chem.*, 2011, **76**, 1228–1238.

12 T. L. Raguse, E. A. Porter, B. Weisblum and S. H. Gellman, *J. Am. Chem. Soc.*, 2002, **124**, 12774–12785.

13 E. P. English, R. S. Chumanov, S. H. Gellman and T. Compton, *J. Biol. Chem.*, 2006, **281**, 2661–2667.

14 W. S. Horne, L. M. Johnson, T. J. Ketas, P. J. Klasse, M. Lu, J. P. Moore and S. H. Gellman, *Proc. Natl. Acad. Sci.,* 2009, **106**, 14751–14756.

15 J. A. Kritzer, J. D. Lear, M. E. Hodsdon and A. Schepartz, *J. Am. Chem. Soc.*, 2004, **126**, 9468–9469.

16 W. S. Horne, M. D. Boersma, M. A. Windsor and S. H. Gellman, *Angew. Chem. Int. Ed.,* 2008, **47**, 2853–2856.

17 P. Chène, *Nat. Rev. Cancer*, 2003, **3**, 102–109.

18 A. Yonath, *Angew. Chem. Int. Ed.,* 2010, **49**, 4340–4354.

19 B. Lewandowski, G. De Bo, J. W. Ward, M. Papmeyer, S. Kuschel, M. J. Aldegunde, P. M. E. Gramlich, D. Heckmann, S. M. Goldup, D. M. D'Souza, A. E. Fernandes and D. A. Leigh, *Science.,* 2013, **339**, 189–193.

20 G. Krauss, *Biochemistry of Signal Transduction and Regulation*, Wiley-VCH, Weinheim, 1999

21 S. G. F. Rasmussen, B. T. DeVree, Y. Zou, A. C. Kruse, K. Y. Chung, T. S. Kobilka, F. S. Thian, P. S. Chae, E. Pardon, D. Calinski, J. M. Mathiesen, S. T. A. Shah, J. A. Lyons, M. Caffrey, S. H. Gellman, J. Steyaert, G. Skiniotis, W. I. Weis, R. K. Sunahara and B. K. Kobilka, *Nature*, 2011, **477**, 549–555.

22 R. J. Lefkowitz, *Angew. Chem. Int. Ed.,* 2013, **52**, 6366–6378.

23 K. Palczewski, *Science.,* 2000, **289**, 739–745.

24 A. J. Vernall, S. J. Hill and B. Kellam, *Br. J. Pharmacol.*, 2014, **171**, 1073–1084.

25 D. M. Rosenbaum, S. G. F. Rasmussen and B. K. Kobilka, *Nature*, 2009, **459**, 356–363.

26 L. Birnbaumer, J. Abramowitz and A. M. Brown, *Biochim. Biophys. Acta* , 1990, **1031**, 163–224.

27 A. L. Hopkins and C. R. Groom, *Nat. Rev. Drug Discov.*, 2002, **1**, 727–730.

28 J.-P. Mazaleyrat, K. Wright, A. Gaucher, N. Toulemonde, M. Wakselman, S. Oancea, C. Peggion, F. Formaggio, V. Setnicka, T. a Keiderling and C. Toniolo, *J. Am. Chem. Soc.*, 2004, **126**, 12874–12879.

29 R. N. Zuckermann, *Pept. Sci.*, 2011, **96**, 545–555.

30 S. A. Fowler and H. E. Blackwell, *Org. Biomol. Chem.*, 2009, **7**, 1508–1524.

31 N. Ousaka and Y. Inai, *J. Org. Chem.*, 2009, **74**, 1429–1439.

32 F. Totsingan, V. Jain, W. C. Bracken, A. Faccini, T. Tedeschi, R. Marchelli, R. Corradini, N. R. Kallenbach and M. M. Green, *Macromolecules*, 2010, **43**, 2692–2703.

33 S. Sforza, G. Haaima, R. Marchelli and P. E. Nielsen, *Eur. J.O.C.*, 1999, **1999**, 197–204.

34 J. I. Yeh, B. Shivachev, S. Rapireddy, M. J. Crawford, R. R. Gil, S. Du, M. Madrid and D. H. Ly, *J. Am. Chem. Soc.*, 2010, **132**, 10717–10727.

35 S. Sforza, R. Corradini, S. Ghirardi, A. Dossena and R. Marchelli, *Eur. J.O.C.,* 2000, 2905–2913.

36 P. Wittung, M. Eriksson, R. Lyng, P. E. Nielsen, B. Norden and B. Nordcn, *J. Am. Chem. Soc.*, 1995, **117**, 10167–10173.

37 P. Wittung, P. E. Nielsen, O. Buchardt, M. Egholm and B. Nordén, *Nature*, 1994, **368**, 561–563.

38 C. Toniolo and E. Benedetti, *Macromolecules*, 1991, **24**, 4004–4009.

39 R.-P. Hummel, C. Toniolo and G. Jung, *Angew. Chem. Int. Ed.,*1987, **26**, 1150–1152.

40 G. R. Marshall, E. E. Hodgkin, D. A. Langs, G. D. Smith, J. Zabrocki and M. T. Leplawy, *Proc. Natl. Acad. Sci.*, 1990, **87**, 487-491

41 M. Crisma, F. Formaggio and C. Peggion, *Pept. Sci.*, 2001, **60**, 396-419

42 C. Toniolo, M. Crisma, G. M. Bonora, E. Benedetti, B. D. I. Blasio, V. Pavone, C. Pedone and A. Santini, *Biopolymers*, 1991, **31**, 129–138.

43 M. Kubasik, J. Kotz, C. Szabo, T. Furlong and J. Stace, *Biopolymers*, 2005, **78**, 87–95.

44 N. Berova, L. Di Bari and G. Pescitelli, *Chem. Soc. Rev.*, 2007, **36**, 914–31.

45 Y. Inai and Y. Kurokawa, *Biopolymers*, 1999, **49**, 551-564

46 M. De Poli and J. Clayden, *Org. Biomol. Chem.*, 2014, **12**, 836–843..

47 C. Toniolo, A. Polese, F. Formaggio, M. Crisma and J. Kamphuis, *J. Am. Chem. Soc.*, 1996, **118**, 2744–2745.

48 M. De Poli, L. Byrne, R. a. Brown, J. Solà, A. Castellanos, T. Boddaert, R. Wechsel, J. D. Beadle and J. Clayden, *J. Org. Chem.*, 2014, **79**, 4659–4675.

49 J. Solà, G. A. Morris and J. Clayden, *J. Am. Chem. Soc.*, 2011, **133**, 3712–3715.

50 S. P. Fletcher, J. Solà, D. Holt, R. A. Brown and Jonathan Clayden Beilstein J.O.C. 2011, **7**, 1304–1309.

51 J. Solà, S. P. Fletcher, A. Castellanos and J. Clayden, *Angew. Chemie Int. Ed.*, 2010, **49**, 6836–6839.

52 S. J. Pike, M. De Poli, W. Zawodny, J. Raftery, S. J. Webb and J. Clayden, *Org. Biomol. Chem.*, 2013, **11**, 3168–76.

53 J. Clayden, A. Castellanos, J. Solà and G. A. Morris, *Angew. Chemie Int. Ed.*, 2009, **48**, 5962–5965.

54 B. A. F. Le Bailly, L. Byrne, V. Diemer, M. Foroozandeh, G. A. Morris and J. Clayden, *Chem. Sci.*, 2015, **6**, 2313–2322.

55 Y. Inai, Y. Ishida, K. Tagawa, A. Takasu and T. Hirabayashi, *J. Am. Chem. Soc.*, 2002, **124**, 2466-2473.

56 Y. Inai, K. Tagawa, A. Takasu, T. Hirabayashi, T. Oshikawa and M. Yamashita, *J. Am. Chem. Soc.*, 2000, **122**, 11731–11732.

57 Y. Inai, H. Komori, A. Takasu and T. Hirabayashi, *Biomacromolecules*, 2003, **4**, 122–128.

58 Y. Inai, N. Ousaka and T. Okabe, *J. Am. Chem. Soc.*, 2003, **125**, 8151–8162.

59 J. Solà, M. Helliwell and J. Clayden, *J. Am. Chem. Soc.*, 2010, **132**, 4548–4549.

60 T. Boddaert, J. Solà, M. Helliwell and J. Clayden, *Chem. Commun.*, 2012, **48**, 3397-3399.

61 L. Byrne, J. Solà, T. Boddaert, T. Marcelli, R. W. Adams, G. A. Morris and J. Clayden, *Angew. Chem. Int. Ed.,* 2014, **53**, 151–155.

62 R. A. Brown, V. Diemer, S. J. Webb and J. Clayden, *Nat. Chem.*, 2013, **5**, 853–860.

63 J. Brioche, S. J. Pike, S. Tshepelevitsh, I. Leito, G. A. Morris, S. J. Webb and J. Clayden, *J. Am. Chem. Soc.*, 2015, **137**, 6680–6691.

64 J. K. Chugh and B. A. Wallace, *Biochem. Soc. Trans.*, 2001, **29**, 565-570

65 M. N. Melo, R. Ferre and M. A. R. B. Castanho, *Nat. Rev. Microbiol.*, 2009, **7**, 245–250.

66 E. N. Lyukmanova, Z. O. Shenkarev, A. S. Paramonov, A. G. Sobol, T. V Ovchinnikova, V. V Chupin, M. P. Kirpichnikov, M. J. J. Blommers and A. S. Arseniev, *J. Am. Chem. Soc.*, 2008, **130**, 2140–2141.

67 S. Wada, Y. Hitora, R. Tanaka and H. Urata, *Bioorg. Med. Chem. Lett.*, 2008, **18**, 3999–4001.

68 J. M. Sanderson, *Org. Biomol. Chem.*, 2005, **3**, 201–212.

69 B. Leitgeb, A. Szekeres, L. Manczinger, C. Vágvölgyi and L. Kredics, *Chem. Biodivers.*, 2007, **4**, 1027–1051.

70 B. V. Venkataram Prasad, P. Balaram and E. Benedetti, *Crit. Rev. Biochem. Mol. Biol.*, 1984, **16**, 307–348.

71 Lodish, *Molecular Cell Biology*, W. H. Freeman, 2008.

72 Z. O. Shenkarev, A. S. Paramonov, K. D. Nadezhdin, E. V Bocharov, I. A. Kudelina, D. A. Skladnev, A. A. Tagaev, Z. A. Yakimenko, T. V Ovchinnikova and A. S. Arseniev, *Chem. Biodivers.*, 2007, **4**, 1219–1242.

73 Z. O. Shenkarev, A. S. Paramonov, E. N. Lyukmanova, A. K. Gizatullina, A. V Zhuravleva, A. A. Tagaev, Z. A. Yakimenko, I. N. Telezhinskaya, M. P. Kirpichnikov, T. V Ovchinnikova and A. S. Arseniev, *Chem. Biodivers.*, 2013, **10**, 838–863.

74 T. P. Galbraith, R. Harris, P. C. Driscoll and B. A. Wallace, *Biophys. J.*, 2003, **84**, 185–194.

75 Z. O. Shenkarev, A. S. Paramonov, K. D. Nadezhdin, E. V Bocharov, I. A. Kudelina, D. A. Skladnev, A. A. Tagaev, Z. A. Yakimenko, T. V Ovchinnikova and A. S. Arseniev, *Chem. Biodivers.*, 2007, **4**, 1219–1242.

76 E. Fahy, D. Cotter, M. Sud and S. Subramaniam, *Biochim. Biophys. Acta*, 2011, **1811**, 637–47.

77 S. Subramaniam, E. Fahy, S. Gupta, M. Sud, R. W. Byrnes, D. Cotter, A. R. Dinasarapu and M. R. Maurya, *Chem. Rev.*, 2011, **111**, 6452–6490.

78 R. Koynova and M. Caffrey, *Biochim. Biophys. Acta - Rev. Biomembr.*, 1998, **1376**, 91–145.

79 J. N. Israelachvili, D. J. Mitchell and B. W. Ninham, *J. Chem. Soc. Faraday Trans. 2*, 1976, **72**, 1525-1568.

80 P. C. Jost, *Lipid-protein interactions, Volume 2*, Wiley, 1982.

81 J. Korlach, P. Schwille, W. W. Webb and G. W. Feigenson, *Proc. Natl. Acad. Sci.*, 1999, **96**, 8461–8466.

82 J. M. East, *Membrane structural biology with biochemical and biophysical foundations*, Taylor & Francis, 2009.

83 I. C. Pintre and S. J. Webb, *Adv. Phys. Org. Chem.*, 2013, **47**, 129–183.

84 R. G. Laughlin, *Colloids Surfaces A Physicochem. Eng. Asp.*, 1997, **128**, 27–38.

85 F. Olson, C. A. Hunt, F. C. Szoka, W. J. Vail and D. Papahadjopoulos, *Biochim. Biophys. Acta*, 1979, **557**, 9–23.

86 P. Walde, K. Cosentino, H. Engel and P. Stano, *Chembiochem*, 2010, **11**, 848–865.

87 M. I. Angelova and D. S. Dimitrov, *Faraday Discuss. Chem. Soc.*, 1986, **81**, 303-311.

88 T. Pott, H. Bouvrais and P. Méléard, *Chem. Phys. Lipids*, 2008, **154**, 115–119.

89 S. Weinstein, J. T. Durkin, W. R. Veatch and E. R. Blout, *Biochemistry*, 1985, **24**, 4374–4382.

90 B. Valeur, *Molecular Fluorescence Principles and Applications*, WILEY-VCH Verlag GmbH, 2001, vol. 8.

91 G. G. Stokes, *philisophical Trans.*, 1852, **142**, 463-562.

92 J. S. Kim and D. T. Quang, *Chem. Rev.*, 2007, **107**, 3780–3799.

93 B. N. G. Giepmans, S. R. Adams, M. H. Ellisman and R. Y. Tsien, *Science.,* 2006, **312**, 217–224.

94 J. Zhang, R. E. Campbell, A. Y. Ting and R. Y. Tsien, *Nat. Rev. Mol. Cell Biol.*, 2002, **3**, 906–918.

95 S. S. Lehrer, *Methods Enzymol.*, 1975, **278**, 286-295.

96 G. Bains, A. B. Patel and V. Narayanaswami, *Molecules*, 2011, **16**, 7909–7935.

97 M. E. Østergaard and P. J. Hrdlicka, *Chem. Soc. Rev.*, 2011, **40**, 5771–5788.

98 M. Masuko, H. Ohtani, K. Ebata and A. Shimadzu, *Nucleic Acids Res.*, 1998, **26**, 5409–5416.

99 H. W. Hellinga and J. S. Marvin, *Trends Biotechnol.*, 1998, **16**, 183–189.

100 J. K. Kalyanasundaram and K. Thomas, *J. Am. Chem. Soc.*, 1977, **99**, 2039–2044.

101 S. Cheng, J. K. Thomas and C. F. Kulpa, *Biochemistry*, 1974, **13**, 1135–1139.

102 J. D. Morrisett, H. J. Pownall, R. T. Plumlee, L. C. Smith and Z. E. Zehner, *J. Biol. Chem.*, 1975, **250**, 6969–6976.

103 J. M. Vanderkooi and J. B. Callis, *Biochemistry*, 1974, **13**, 4000–4006.

104 P. J. Somerharju, J. A. Virtanen, K. K. Eklund, P. Vainio and P. K. Kinnunen, *Biochemistry*, 1985, **24**, 2773–2781.

105 U. Koert, R. Krauss, H.-G. Weinig, C. Heumann, B. Ziemer, C. Mugge, M. Seydack and J. Bendig, *Eur J.O.C.*, 2001, 575–586.

106 H. G. Weinig, R. Krauss, M. Seydack, J. Bendig and U. Koert, *Chemistry*, 2001, **7**, 2075–2088.

107 R. Krauss and U. Koert, *Synlett*, 2003, **5**, 598–608.

108 J. Wu, Y. Zou, C. Li, W. Sicking, I. Piantanida, T. Yi and C. Schmuck, *J. Am. Chem. Soc.*, 2012, **134**, 1958–1961.

109 H. Lettre, K. Buchholz, M. Fernholz, E.Z. Phys Chem. (Leipzig), 1941, **267**, 108.

110 S. Egusa, M. Sisido and Y. Imanishi, *Macromolecules*, 1985, **18**, 882–889.

111 R. Goedeweeck and F. C. De Schryver, *Photochem. Photobiol.*, 1984, **39**, 515–520.

112 H. Mihara, Y. Tanaka, T. Fujimoto and N. Nishino, *J. Chem. Soc. Perkin Trans. 2*, 1995, 1133–1140.

113 H. Mihara, S. Lee, Y. Shimohigashi, H. Aoyagi, T. Kato, N. Izumiya and T. Costa, *Int. J. Pept. Protein Res.*, 2009, **30**, 605–612.

114 A. Szymańska, W. Wiczk and L. Lankiewicz, *Amino Acids*, 2001, **21**, 265–270.

115 I. Alves, S. Cowell, Y. S. Lee, X. Tang, P. Davis, F. Porreca and V. J. Hruby, *Biochem. Biophys. Res. Commun.*, 2004, **318**, 335–340.

116 N. Nishino, H. Mihara, Y. Tanaka and T. Fujimoto, *Tetrahedron Lett.*, 1992, **33**, 5767–5770.

117 S. Chen, L. Wang, N. E. Fahmi, S. J. Benkovic and S. M. Hecht, *J. Am. Chem. Soc.*, 2012, **134**, 18883–18885.

118 M. Sisido and Y. Imanishi, *Macromolecules*, 1985, **18**, 890–894.

119 Y. Inai, M. Sisido and Y. Imanishi, *J. Phys. Chem.*, 1990, **94**, 2734–2735.

120 M. Sisido, S. Egusa, A. Okamoto and Y. Imanishi, *J. Am. Chem. Soc.*, 1983, **105**, 3351–3352.

121 Y. Inai, M. Sisido and Y. Imanishi, *J Phys Chem*, 1990, **94**, 8365–8370.

122 M. Goedeweeck, M. Van der Auweraer and F. C. De Schryver, *J. Am. Chem. Soc.*, 1985, **107**, 2334–2341.

123 R. Goedeweeck, F. Ruttens, F. López-Arbeloa and F. C. De Schryver, *Biopolymers*, 1987, **26**, 1833–1857.

124 B. A. F. Le Bailly and J. Clayden, *Chem. Commun. (Camb).*, 2014, **50**, 7949–52.

125 H. Kim, Y. Nguyen, C. P.-H. Yen, L. Chagal, A. J. Lough, B. M. Kim and J. Chin, *J. Am. Chem. Soc.*, 2008, **130**, 12184–91.

126 J. F. Zhang, Y. Zhou, J. Yoon and J. S. Kim, *Chem. Soc. Rev.*, 2011, **40**, 3416–29.

127 K. P. Carter, A. M. Young and A. E. Palmer, *Chem. Rev.*, 2014, **114**, 4564–601.

128 H. Yuasa, N. Miyagawa, T. Izumi, M. Nakatani, M. Izumi and H. Hashimoto, *Org. Lett.*, 2004, **6**, 1489–1492.

129 F. Wang, R. Nandhakumar, J. H. Moon, K. M. Kim, J. Y. Lee and J. Yoon, *Inorg. Chem.*, 2011, **50**, 2240–2245.

130 Y.-G. Li, Q.-S. Tian, J. Zhao, Y. Feng, M.-J. Li and T.-P. You, *Tetrahedron: Asymmetry*, 2004, **15**, 1707–1710.

131 J. Spencer, A. P. Burd, C. A. Goodwin, S. A. M. Mérette, M. F. Scully, T. Adatia and J. J. Deadman, *Tetrahedron*, 2002, **58**, 1551–1556.

132 *J. Chem. Educ.*, 1994, **71**, A54.

133 L. A. Joyce, M. S. Maynor, J. M. Dragna, G. M. da Cruz, V. M. Lynch, J. W. Canary and E. V. Anslyn, *J. Am. Chem. Soc.*, 2011, **133**, 13746–13752.

134 J. M. Castagnetto and J. W. Canary, *Chem. Commun.*, 1998, 203–204.

135 N. Ousaka and Y. Inai, *J. Am. Chem. Soc.*, 2006, **128**, 14736–14737.

136 D. Bhaya, *Mol. Microbiol.*, 2004, **53**, 745–754.

137 E. C. Meng and H. R. Bourne, *TRENDS Pharmacol. Sci.*, 2001, 22, 587–593.

138 H. Smith, *Nature*, 2000, **407**, 585–591.

139 H. Durr and H. Bouas-Laurent, *Photochromism:Molecules and System.* Elsevier, 1990.

140 Y. Yokoyama, *Chem. Rev.*, 2000, **100**, 1717–1740.

141 M. Irie, *Chem. Rev.*, 2000, **100**, 1685–1716.

142 G. Berkovic, V. Krongauz and V. Weiss, *Chem. Rev.*, 2000, **100**, 1741–1754.

143 C. Renner and L. Moroder, *ChemBioChem*, 2006, **7**, 868–878.

144 E. R. Kay, D. A. Leigh and F. Zerbetto, *Angew. Chemie Int. Ed.*, 2007, **46**, 72–191.

145 B. L. Feringa, *J. Org. Chem.*, 2007, **72**, 6635–6652.

146 W. R. Browne and B. L. Feringa, *Nat. Nanotechnol.*, 2006, 1, 25–34.

147 D. Gust, J. Andréasson, U. Pischel, T. A. Moore and A. L. Moore, *Chem. Comm.*, 2012, **48**, 1947–1957.

148 I. Willner, *Acc. Chem. Res.*, 1997, 30.

149 D. D. Young and A. Deiters, *Org. Biomol. Chem.*, 2007, **5**, 999–1005.

150 G. Mayer and A. Heckel, *Angew. Chemie Int. Ed.*, 2006, **45**, 4900–4921.

151 E. Zahavy, S. Rubin and I. Willner, *J. Chem. Soc. Chem. Commun.*, 1993, 1753–1755.

152 M. Blanco-Lomas, S. Samanta, P. J. Campos, G. A. Woolley and D. Sampedro, *J. Am. Chem. Soc.*, 2012, **134**, 6960–6963.

153 A. Kocer, *Science.,* 2005, **309**, 755–758.

154 U. Al-Atar, R. Fernandes, B. Johnsen, D. Baillie and N. R. Branda, *J. Am. Chem. Soc.*, 2009, **131**, 15966–15967.

155 V. A. Lokshin, A. Samat and A. V Metelitsa, *Russ. Chem. Rev.*, 2003, **071**, 893–916.

156 V.A. Paltchkov, Patent: US005831090A, 1998.

157 V. I. Minkin, *Chem. Rev.*, 2004, **104**, 2751−2776.

158 G. S. Hartley, *Nature*, 1937, **140**, 281–281.

159 C. Zhang and N. Jiao, *Angew. Chem. Int. Ed.,*2010, **49**, 6174–6177.

160 E. Yashima, in Molecular and Supramolecular Photochemistry , eds. Y. Inoue and Ramamurthy V., Marcel Dekker, New York, 2004.

161 O. Pieroni, A. Fissi, N. Angelini and F. Lenci, *Acc. Chem. Res.*, 2001, **34**, 9–17.

162 W. Szymański, J. M. Beierle, H. a V Kistemaker, W. a Velema and B. L. Feringa, *Chem. Rev.*, 2013, **113**, 6114-6178.

163 K. Meguellati, G. Koripelly and S. Ladame, *Angew. Chem. Int. Ed.,*2010, **49**, 2738–2742.

164 M. J. Hansen, W. A. Velema, M. M. Lerch, W. Szymanski and B. L. Feringa, *Chem. Soc. Rev.*, 2015, **44**, 3358–3377.

165 V. San Miguel, C. G. Bochet and A. del Campo, *J. Am. Chem. Soc.*, 2011, **133**, 5380–5388.

166 E. Soto, J. C. MacDonald, C. G. F. Cooper and W. G. McGimpsey, *J. Am. Chem. Soc.*, 2003, **125**, 2838–2389.

167 J. Clayden, A. Castellanos, J. Solà and G. A. Morris, *Angew. Chemie*, 2009, **121**, 6076–6079.

168 W. Chen, N. B. Zuckerman, J. W. Lewis, J. P. Konopelski and S. Chen, *J. Phys. Chem. C*, 2009, **113**, 16988–16995.

169 M. Meldal, M. A. Juliano and A. M. Jansson, *Tetrahedron Lett.*, 1997, **38**, 2531–2534.

170 R. A. Brown, *Conformational Switching for Transmembrane Communication*. Thesis Univesity of Manchester, 2013.

171 D. Stones, S. Manku, X. Lu and D. G. Hall, *Chemistry*, 2004, **10**, 92–100.

Appendix I: X-ray crystal structure data

Crystal data and refinement for s3812ma **97**

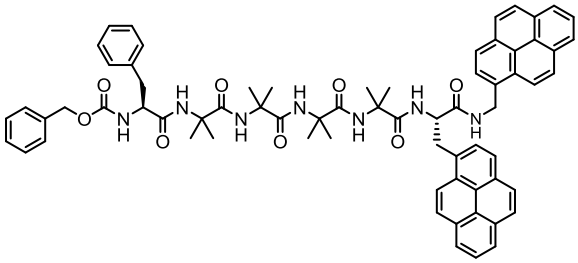

Identification code	s3812ma	
Empirical formula	C72 H72 Cl9 N7 O8	
Formula weight	1482.42	
Temperature	100(2) K	
Wavelength	1.54178 Å	
Crystal system	Orthorhombic	
Space group	P2(1)2(1)2(1)	
Unit cell dimensions	a = 13.2969(4) Å	α= 90°.
	b = 22.3943(5) Å	β= 90°.
	c = 25.1034(6) Å	γ = 90°.
Volume	7475.2(3) $Å^3$	
Z	4	
Density (calculated)	1.317 Mg/m^3	
Absorption coefficient	3.549 mm^{-1}	
F(000)	3080	
Crystal size	0.33 x 0.22 x 0.17 mm^3	
Theta range for data collection	3.87 to 70.14°.	
Index ranges	-16<=h<=12, -18<=k<=27, -30<=l<=30	
Reflections collected	35359	
Independent reflections	13829 [R(int) = 0.0414]	
Completeness to theta = 66.60°	99.8 %	
Absorption correction	Semi-empirical from equivalents	
Max. and min. transmission	0.5837 and 0.369297	
Refinement method	Full-matrix least-squares on F^2	
Data / restraints / parameters	13829 / 0 / 874	
Goodness-of-fit on F^2	1.033	
Final R indices [I>2sigma(I)]	R1 = 0.0620, wR2 = 0.1603	
R indices (all data)	R1 = 0.0732, wR2 = 0.1708	
Absolute structure parameter	-0.002(15)	
Extinction coefficient	0.00017(5)	
Largest diff. peak and hole	1.121 and -0.802 e.$Å^{-3}$	

Crystal data and structure refinement for s4270ma **157**

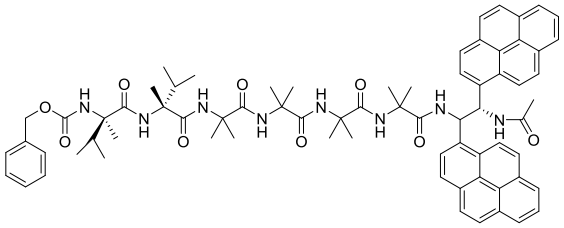

Identification code	s4270ma	
Empirical formula	C72 H82 N8 O11	
Formula weight	1235.46	
Temperature	100(2) K	
Wavelength	1.54178 Å	
Crystal system	Monoclinic	
Space group	P2(1)	
Unit cell dimensions	a = 14.2477(5) Å	α= 90°.
	b = 18.4756(7) Å	β= 114.965(3)°.
	c = 14.7030(5) Å	γ = 90°.
Volume	3508.7(2) $Å^3$	
Z	2	
Density (calculated)	1.169 Mg/m^3	
Absorption coefficient	0.642 mm^{-1}	
F(000)	1316	
Crystal size	0.24 x 0.21 x 0.01 mm^3	
Theta range for data collection	3.32 to 72.20°.	
Index ranges	-17<=h<=17, -21<=k<=22, -18<=l<=18	
Reflections collected	26086	
Independent reflections	10647 [R(int) = 0.0804]	
Completeness to theta = 67.00°	98.4 %	
Absorption correction	Semi-empirical from equivalents	
Max. and min. transmission	0.9936 and 0.809805	
Refinement method	Full-matrix least-squares on F^2	
Data / restraints / parameters	10647 / 1 / 847	
Goodness-of-fit on F^2	1.226	
Final R indices [I>2sigma(I)]	R1 = 0.1093, wR2 = 0.2889	
R indices (all data)	R1 = 0.1330, wR2 = 0.3181	
Absolute structure parameter	0.2(4)	
Extinction coefficient	0.0031(6)	
Largest diff. peak and hole	1.242 and -0.555 e.$Å^{-3}$	